NASA Tech Briefs

National
Aeronautics and
Space
Administration

Our Expanded Format Presents Approximately 250 NASA Innovations [See Page A2].

This self-contained X-ray unit developed at Goddard Space Flight Center is now marketed by an Illinois company through a NASA patent license. Tests for its approval in medical applications are underway, and it is already finding industrial uses in nondestructive testing and security. [*See the bottom of page A1.*]

Vol. 8, No. 1

Fall 1983

About the NASA Technology Utilization Program

The National Aeronautics and Space Act of 1958, which established NASA and the United States civilian space program, requires that "The Administration shall provide for the widest practicable and appropriate dissemination of information concerning its activities and the results thereof."

To help carry out this objective, NASA's Technology Utilization (TU) Program was established in 1962. Now, as an element of NASA's Technology Utilization and Industry Affairs Division, this program offers a variety of valuable services to help transfer aerospace technology to nonaerospace applications, thus assuring American taxpayers maximum return on their investment in space research; thousands of spinoffs of NASA research have already occurred in virtually every area of our economy.

The TU program has worked for engineers, scientists, technicians, and businessmen; and it can work for you.

NASA Tech Briefs

Tech Briefs is published quarterly and is free to engineers in U.S. industry and to other domestic technology transfer agents. It is both a current-awareness medium and a problem-solving tool. Potential products . . . industrial processes . .. basic and applied research . . . shop and lab techniques . . . computer software . . . new sources of technical data . . . concepts . . . can be found here. The short section on New Product Ideas highlights a few of the potential new products contained in this issue. The remainder of the volume is organized by technical category to help you quickly review new developments in your areas of interest. Finally, a subject index makes each issue a convenient reference file.

Further Information on Innovations

Although some new technology announcements are complete in themselves, most are backed up by Technical Support Packages (TSP's). TSP's are available without charge and may be ordered by simply completing a TSP Request Card found at the back of this volume. Further information on some innovations is available for a nominal fee from other sources, as indicated. In addition, Technology Utilization Officers at NASA Field Centers will often be able to lend necessary guidance and assistance.

Patent Licenses

Patents have been issued to NASA on some of the inventions described, and patent applications have been submitted on others. Each announcement indicates patent status and availability of patent licenses if applicable.

Other Technology Utilization Services

To assist engineers, industrial researchers, business executives, Government officials, and other potential users in applying space technology to their problems, NASA sponsors Industrial Applications Centers. Their services are described on page A7. In addition, an extensive library of computer programs is available through COSMIC, the Technology Utilization Program's outlet for NASA-developed software.

Applications Program

NASA conducts applications engineering projects to help solve public-sector problems in such areas as safety, health, transportation, and environmental protection. Two applications teams, staffed by professionals from a variety of disciplines, assist in this effort by working with Federal agencies and health organizations to identify critical problems amenable to solution by the application of existing NASA technology.

Reader Feedback

We hope you find the information in *NASA Tech Briefs* useful. A reader-feedback card has been included because we want your comments and suggestions on how we can further help you apply NASA innovations and technology to your needs. Please use it; or if you need more space, write to the Manager, Technology Transfer Division, P.O. Box 8757, Baltimore/Washington International Airport, Maryland 21240.

NASA Tech Briefs

National Aeronautics and Space Administration

Fall 1983
Volume 8, Number 1

COVERS: The photographs on the front and back covers illustrate developments by NASA and its contractors that have resulted in commercial and nonaerospace spinoffs. To find out more about the "Portable X-Ray Unit," Circle 207 on the TSP Request Card at the back of this issue. For more information on the "Solid-Polymer Electrolysis System," Circle 216.

About This NASA Publication

NASA Tech Briefs, a quarterly publication, is distributed free to qualified U.S. citizens to encourage commercial application of U.S. space technology. For information on publications and services available through the NASA Technology Utilization Program, write to the Manager, Technology Transfer Division, P.O. Box 8757, Baltimore/Washington International Airport, Maryland 21240.

"The Administrator of National Aeronautics and Space Administration has determined that the publication of this periodical is necessary in the transaction of the public business required by law of this Agency. Use of funds for printing this periodical has been approved by the Director of the Office of Management and Budget."

Change of Address

If you wish to have NASA Tech Briefs forwarded to your new address, use the Subscription Card enclosed at the back of this volume of NASA Tech Briefs. Be sure to check the appropriate box indicating change of address, and also fill in your identification number (T number) in the space indicated.

Communications Concerning Editorial Matter

For editorial comments or general communications about NASA Tech Briefs, you may use the Feedback card in the back of NASA Tech Briefs, or write to: The Publications Manager, Technology Utilization Office (LGT-1), NASA Headquarters, Washington, DC 20546. Technical questions concerning specific articles should be directed to the Technology Utilization Officer of the sponsoring NASA Center (addresses listed on page A4).

Expanded Format

To speed the publication of our backlog of Tech Brief items, we have increased our per-issue contents from approximately 125 to 250 items by adding short articles to the end of each subject section of NASA Tech Briefs. Titled "MiniBriefs," these short articles describe NASA innovations and reports in an abbreviated format. Most are backed up by Technical Support Packages (TSP's), which can be obtained by using the TSP Request Card at the back of this issue.

Acknowledgements

NASA Tech Briefs is published quarterly by the National Aeronautics and Space Administration, Technology Transfer Division, Washington, DC: Administrator: **James M. Beggs;** Director, Technology Utilization and Industry Affairs Division: **Ronald J. Philips;** Publications Manager: **Leonard A. Ault.** Prepared for the National Aeronautics and Space Administration by **Logical Technical Services Corp.:** Editor-in-Chief: **Jay Kirschenbaum;** Art Director: **Ernest Gillespie;** Managing Editor: **Jerome Rosen;** Chief Copy Editor: **Oden Browne;** Staff Editors: **James Boyd, Charles Gregor, Larry Grunberger, Paul Johnson, Jordan Randjelovich, Ted Selinsky, George Watson;** Graphics: **Andrew Abramoske, Ron Krause, Luis Martinez, Huburn Profitt;** Editorial & Production: **Camille McQueen, Richard Johnson, Sabrina Gibson, Stephanie Godino, Leslie Iwaskow, Henry Lai, Marion Larson, Linda Lucas, Frank Ponce, Elizabeth Texeira, Vincent Susinno, Ernestine Walker.**

NASA
TU SERVICES

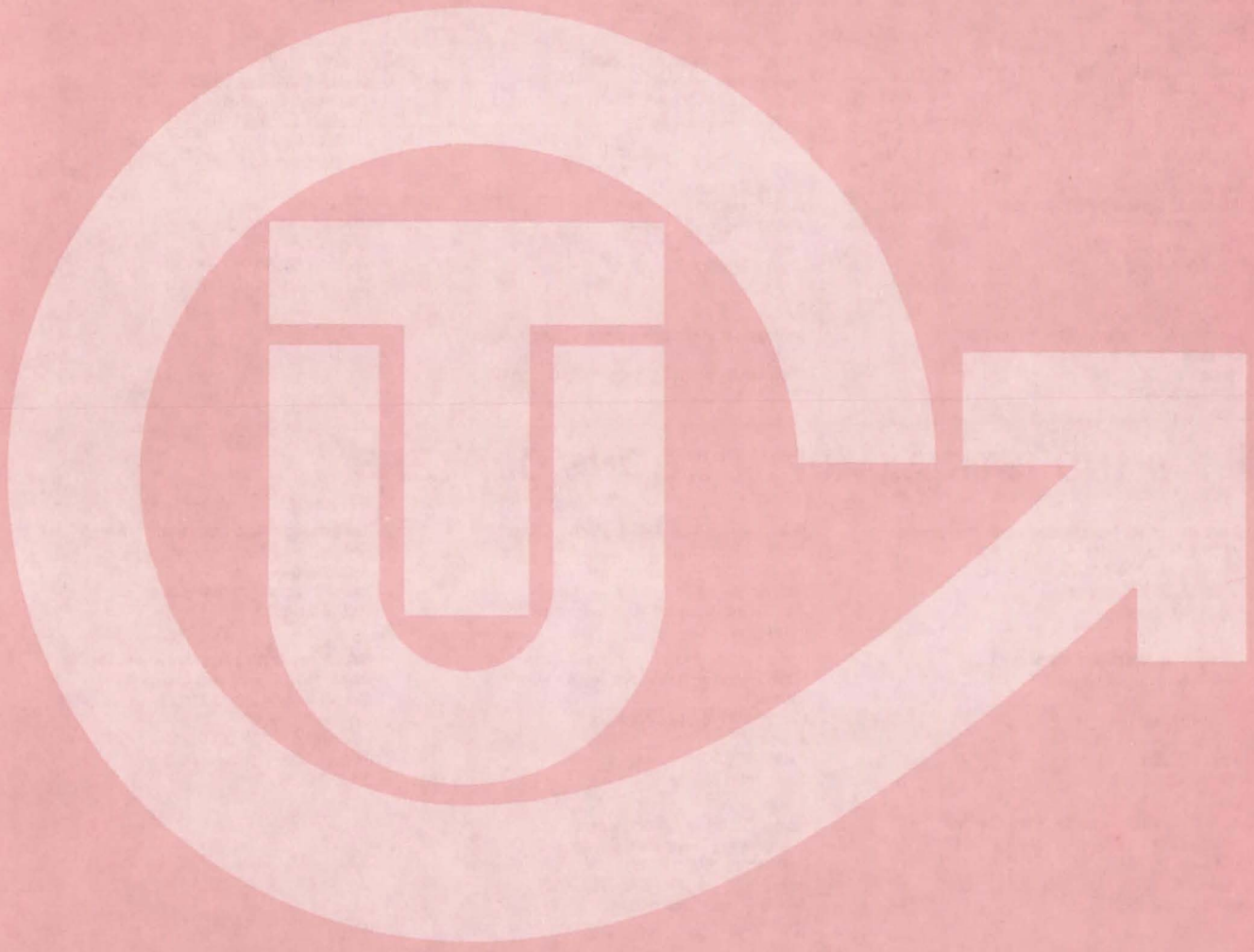

NASA TECHNOLOGY UTILIZATION NETWORK

★ TECHNOLOGY UTILIZATION OFFICERS

Stanley A. Miller
Ames Research Center
Code 240-10
Moffett Field, CA 94035
(415) 965-6471

Stanley A. Miller
Hugh L. Dryden Flight Research Center
Code 240-10
Moffett Field, CA 94035
(415) 965-6471

Donald S. Friedman
Goddard Space Flight Center
Code 702.1
Greenbelt, MD 20771
(301) 344-6242

William Chmylak
Lyndon B. Johnson Space Center
Code AL-32
Houston, TX 77058
(713) 483-3809

U. Reed Barnett
John F. Kennedy Space Center
Code PT-SPD
Kennedy Space Center, FL 32899
(305) 867-3017

John Samos
Langley Research Center
Mail Stop 139A
Hampton, VA 23665
(804) 865-3281

Harrison Allen, Jr.
Lewis Research Center
Mail Code 7-3
21000 Brookpark Road
Cleveland, OH 44135
(216) 433-4000, Ext. 6422

Ismail Akbay
George C. Marshall Space Flight Center
Code AT01
Marshall Space Flight Center, AL 35812
(205) 453-2224

Leonard A. Ault
NASA Headquarters
Code ETD-6
Washington, DC 20546
(202) 453-8424

Aubrey Smith
NASA Resident Office-JPL
4800 Oak Grove Drive
Pasadena, CA 91103
(213) 354-4849

Gilmore H. Trafford
Wallops Flight Center
Code OD
Wallops Island, VA 23337
(804) 824-3411, Ext. 201

● INDUSTRIAL APPLICATIONS CENTERS

Aerospace Research Applications Center
1201 East 38th Street
Indianapolis, IN 46205
John M. Ulrich, director
(317) 264-4644

Computer Software Management and Information Center (COSMIC)
Suite 112, Barrow Hall
University of Georgia
Athens, GA 30602
John A. Gibson, director
(404) 542-3265

Kerr Industrial Applications Center
Southeastern Oklahoma State University
Durant, OK 74701
James Harmon, director
(405) 924-0121, Ext. 413

NASA Industrial Applications Center
701 LIS Building
University of Pittsburgh
Pittsburgh, PA 15260
Paul A. McWilliams, executive director
(412) 624-5211

New England Research Applications Center
Mansfield Professional Park
Storrs, CT 06268
Daniel Wilde, director
(203) 486-4533

North Carolina Science and Technology Research Center
Post Office Box 12235
Research Triangle Park, NC 27709
James E. Vann, director
(919) 549-0671

Technology Applications Center
University of New Mexico
Albuquerque, NM 87131
Stanley Morain, director
(505) 277-3622

NASA Industrial Applications Center
University of Southern California
Denny Research Building
University Park
Los Angeles, CA 90007
Robert Mixer, acting director
(213) 743-6132

■ STATE TECHNOLOGY APPLICATIONS CENTERS

NASA/University of Florida
State Technology Applications Center
500 Weil Hall
University of Florida
Gainesville, FL 32611
J. Ronald Thornton, director

Gainesville:	(904) 392-6760
Boca Raton:	(305) 395-5100, Ext. 2292
Fort Lauderdale:	(305) 776-6645
Jacksonville:	(904) 646-2478
Orlando:	(305) 275-2706
Pensacola:	(904) 476-9500, Ext. 426
Tampa:	(813) 974-2499

NASA/University of Kentucky
State Technology Applications Program
109 Kinkead Hall
University of Kentucky
Lexington, KY 40508
William R. Strong, manager
(606) 258-4632

◆ PATENT COUNSELS

Robert F. Kempf
Asst. Gen. Counsel for patent matters
NASA Headquarters
Code GP-4
400 Maryland Avenue, SW.
Washington, DC 20546
(202) 755-3954

Darrell G. Brekke
Ames Research Center
Mail Code: 200-11A
Moffett Field, CA 94035
(415) 965-5104

Darrell G. Brekke
Hugh L. Dryden Flight Research Center
Mail Code: 201-11A
Moffett Field, CA 94035
(415) 965-5104

John O. Tresansky
Goddard Space Flight Center
Mail Code: 204
Greenbelt, MD 20771
(301) 344-7351

Marvin F. Matthews
Lyndon B. Johnson Space Center
Mail Code: AL-3
Houston, TX 77058
(713) 483-4871

James O. Harrell
John F. Kennedy Space Center
Mail Code: SA-PAT
Kennedy Space Center, FL 32899
(305) 867-2544

Howard J. Osborn
Langley Research Center
Mail Code: 279
Hampton, VA 23665
(804) 827-3725

Norman T. Musial
Lewis Research Center
Mail Code: 500-311
21000 Brookpark Road
Cleveland, OH 44135
(216) 433-4000, Ext. 346

Leon D. Wofford, Jr.
George C. Marshall Space Flight Center
Mail Code: CC01
Marshall Space Flight Center, AL 35812
(205) 453-0020

Paul F. McCaul
NASA Resident Office-JPL
Mail Code: 180-601
4800 Oak Grove Drive
Pasadena, CA 91103
(213) 354-2700

▲ APPLICATION TEAMS

Doris Rouse, director
Research Triangle Institute
Post Office Box 12194
Research Triangle Park, NC 27709
(919) 541-6980

James P. Wilhelm, director
SRI International
333 Ravenswood Avenue
Menlo Park, CA 94026
(415) 326-6200, Ext. 3520

TECHNOLOGY UTILIZATION OFFICERS

Technology transfer experts can help you apply the innovations in NASA Tech Briefs.

The Technology Utilization Officer at each NASA Field Center is an applications engineer who can help you make use of new technology developed at his center. He brings you NASA Tech Briefs and other special publications, sponsors conferences, and arranges for expert assistance in solving technical problems.

Technical assistance, in the form of further information about NASA innovations and technology, is one of the services available from the TUO. Together with NASA scientists and engineers, he can often help you find and implement NASA technology to meet your specific needs.

Technical Support Packages (TSP's) are prepared by the center TUO's. They provide further technical details for articles in NASA Tech Briefs. This additional material can help you evaluate and use NASA technology. You may receive most TSP's free of charge by using the TSP Request Card found at the back of this issue.

Technical questions about articles *in NASA Tech Briefs are answered in the TSP's. When no TSP is available, or you have further questions, contact the Technology Utilization Officer at the center that sponsored the research* [see page A4].

NASA INVENTIONS AVAILABLE FOR LICENSING

Over 3,500 NASA inventions are available for licensing in the United States — both exclusive and nonexclusive.

Nonexclusive licenses for commercial use of NASA inventions are encouraged to promote competition and to achieve the widest use of inventions. They must be used by a negotiated target date.

Exclusive licenses may be granted to encourage early commercial development of NASA inventions, especially when considerable private investment is required. These are generally for 5 to 10 years and usually require royalties based on sales or use.

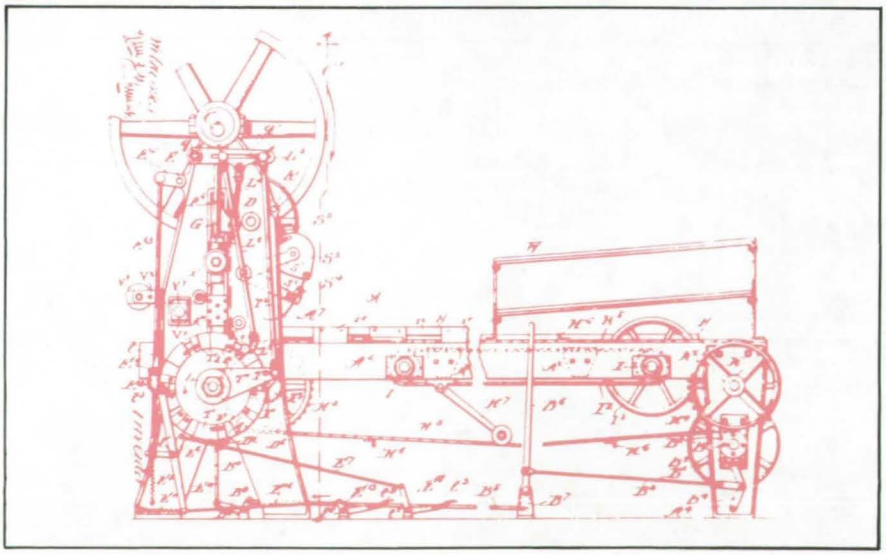

Additional licenses available include those of NASA-owned foreign patents. In addition to inventions described in NASA Tech Briefs, *"NASA Patent Abstract Bibliography"* (PAB), containing abstracts of all NASA inventions, can be purchased from National Technical Information Service, Springfield, VA 22161. The PAB is updated semiannually.

Patent licenses for Tech Briefs *are frequently available. Many of the inventions reported in NASA Tech Briefs are patented or are under consideration for a patent at the time they are published. The current patent status is described at the end of the article; otherwise, there is no statement about patents. If you want to know more about the patent program or are interested in licensing a particular invention, contact the Patent Counsel at the NASA Field Center that sponsored the research* [see page A5]. *Be sure to refer to the NASA reference number at the end of the Tech Brief.*

APPLICATION TEAMS

Technology-matching and problem-solving assistance to public-sector organizations

Application engineering projects are conducted by NASA to help solve public-sector problems in such areas as safety, health, transportation, and environmental protection. Some application teams specialize in biomedical disciplines; others, in engineering and scientific problems. Staffed by professionals from various disciplines, these teams work with other Federal agencies and health organizations to identify critical problems amenable to solution by the application of existing NASA technology.

Public-sector organization *representatives can learn more about application teams by contacting a nearby NASA Field Center Technology Utilization Office* [see page A4].

INDUSTRIAL APPLICATIONS CENTERS

Computerized access to over 10 million documents worldwide

Computerized information retrieval from one of the world's largest banks of technical data is available from NASA's network of industrial Applications Centers (IAC's). The IAC's give you access to 1,800,000 technical reports in the NASA data base and to more than 10 times that many reports and articles found in nearly 200 other computerized data bases.

The major sources include:

- *750,000 NASA Technical Reports*
- *Selected Water Resources Abstracts*
- *NASA Scientific and Technical Aerospace Reports*
- *Air Pollution Technical Information Center*
- *NASA International Aerospace Abstracts*
- *Chem Abstracts Condensates*
- *Engineering Index*
- *Energy Research Abstracts*
- *NASA Tech Briefs*
- *Government Reports*
- *Announcements*

and many other specialized files on food technology, textile technology, metallurgy, medicine, business, economics, social sciences, and physical science.

The IAC services range from tailored literature searches through expert technical assistance:

- *Retrospective Searches:* Published or unpublished literature is screened, and documents are identified according to your interest profile. IAC engineers tailor results to your specific needs and furnish abstracts considered the most pertinent. Complete reports are available upon request.
- *Current-Awareness Searches:* IAC engineers will help design a program to suit your needs. You will receive selected monthly or quarterly abstracts on new developments in your area of interest.
- *Technical Assistance:* IAC engineers will help you evaluate the results of your literature searches. They can help find answers to your technical problems and put you in touch with scientists and engineers at appropriate NASA Field Centers.

Prospective clients *can obtain more information about these services by contacting the nearest IAC* [see page A4]. *User fees are charged for IAC information services.*

STATE TECHNOLOGY APPLICATIONS CENTERS

Technical information services for industry and state and local government agencies.

Government and private industry in Florida and Kentucky can utilize the services of NASA's State Technology Applications Centers (STAC's). The STAC's differ from the Industrial Applications Centers described on page A7, primarily in that they are integrated into existing state technical assistance programs and serve only the host state, whereas the IAC's serve multistate regions.

Many data bases, including the NASA base and several commercial bases, are available for automatic data retrieval through the STAC's. Other services such as document retrieval and special searches are also provided. (Like the IAC's, the STAC's normally charge a fee for their services.)

To obtain information *about the services offered, write or call the STAC in your state* [*see page A4*].

COSMIC®

An economical source of computer programs developed by NASA and other government agencies

A vast software library is maintained by COSMIC — the Computer Software Management and Information Center. COSMIC gives you access to approximately 1,600 computer programs developed for NASA and the Department of Defense and selected programs for other government agencies. Programs and documentation are available at reasonable cost.

Available programs range from management (PERT scheduling) to information science (retrieval systems) and computer operations (hardware and software). Hundreds of engineering programs perform such tasks as structural analysis, electronic circuit design, chemical analysis, and the design of fluid systems. Others determine building energy requirements and optimize mineral exploration.

COSMIC services go beyond the collection and storage of software packages. Programs are checked for completeness; special announcements and an indexed software catalog are prepared; and programs are reproduced for distribution. Customers are helped to identify their software needs; and COSMIC follows up to determine the successes and problems and to provide updates and error corrections. In some cases, NASA engineers can offer guidance to users in installing or running a program.

Information about programs *described in NASA Tech Briefs articles can be obtained by completing the COSMIC Request Card at the back of this issue. Just circle the letters that correspond to the programs in which you are interested.*

NEW PRODUCT IDEAS

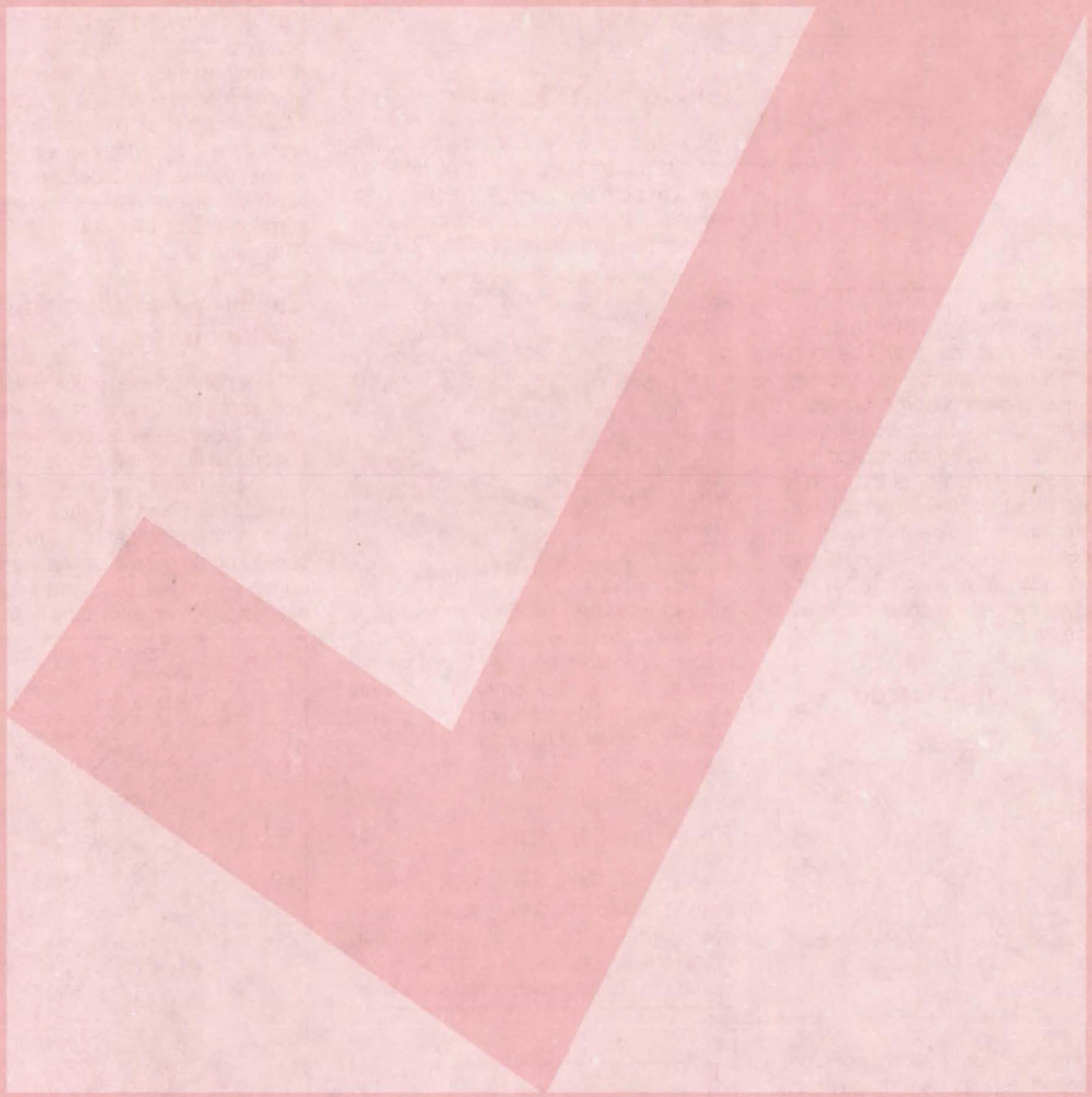

NEW PRODUCT IDEAS are just a few of the many innovations described in this issue of NASA Tech Briefs and having promising commercial applications. Each is discussed further on the referenced page in the appropriate section in this issue. If you are interested in developing a product from these or other NASA innovations, you can receive further technical information by requesting the TSP referenced at the end of the full-length article or by writing the Technology Utilization Office of the sponsoring NASA center (see page A4). NASA's patent-licensing program to encourage commercial development is described on page A6.

Surface-Moisture Monitor

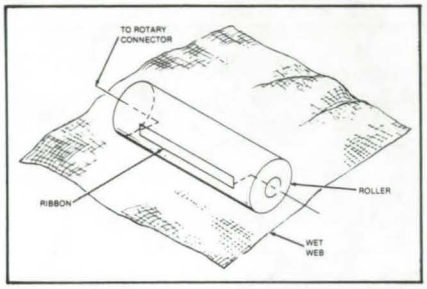

The industrial drying of sheet material, such as paper and fabric, can be monitored with a new surface-moisture sensor. A stainless-steel ribbon, mounted on a roller, periodically touches the moist sheet to gage its dampness and progress in drying. Moisture is transferred from the sheet to the ribbon, which lowers the ribbon temperature and decreases its resistance. The change in ribbon resistivity is a measure of the moisture content of the sheet material.
(See page 88.)

Latch for Stored Cargo

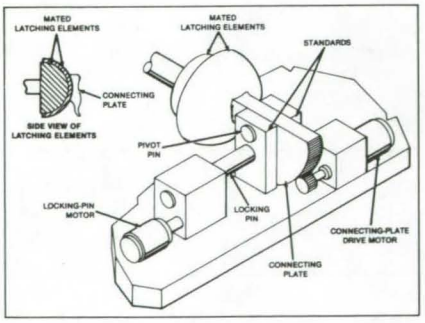

Lightweight spherical latches originally developed for spacecraft payloads can be used to secure heavy cargo. The latching elements, a convex element attached to the cargo and a concave element secured to the cargo-bay floor, automatically aline and engage with one another when the cargo is moved into storage position. Because the latch elements are spherical, the cargo weight is distributed over a broad surface area, so there are no "hotspots" when the cargo is secured. A motor-driven pin locks the latch in place.
(See page 97.)

Portable X-Y Scanner

An electromechanical scanner uses just one motor to index a probe or other fixture in both the x and y directions. Its features include low power consumption, light weight, and portability. The unit

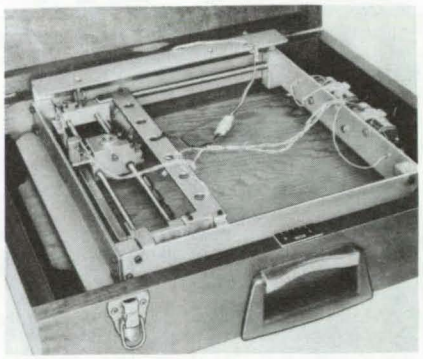

accommodates probes ranging in diameter from one-half to three-fourths inch (1.27 to 1.91 cm) and can scan an area of 60 in.^{2} (387 cm^2) in less than 4 minutes. Its 12-volt drive motor draws just 0.5 ampere at full load.
(See page 100.)

Foil Panel Mirrors

Mirrors suitable for use as infrared shields, telescope doors, solar-furnace doors, advertising displays, and other reflectors are made by bonding thick aluminum foil to honeycomb panels or other backings. The critical step in making these large, lightweight mirrors is the bonding of the foil and backing, which determines the mirror flatness and the environmental extremes that the mirror can withstand. A mirror made by this technique has a total integrated solar scatter of less than 2 percent, a surface waviness of less than 1°, and a solar absorption of less than 0.15.
(See page 122.)

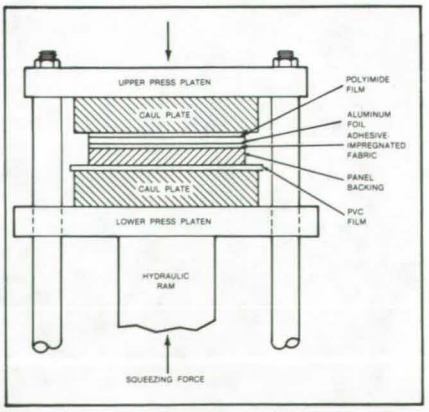

Easily-Alined Electrical Connectors

New cone-shaped multiple-wire plugs and sockets automatically aline when joined together. Rotational alinement is not critical in the new connectors, which are particularly suitable for remote manipulators and for making connections in "blind" locations. The plug and socket contain sets of mating contact rings. When the plug and socket are pushed together, each plug ring deflects

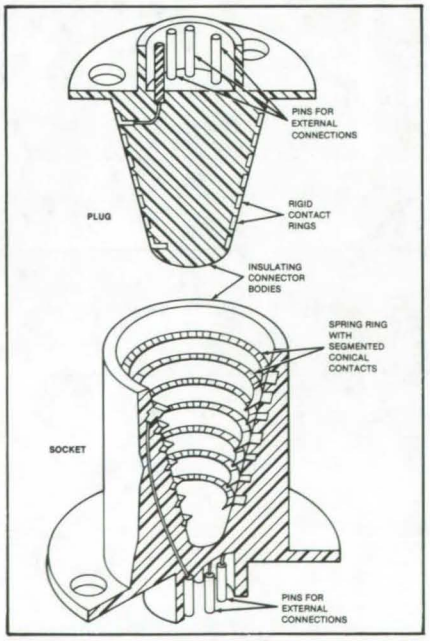

the spring segments of the corresponding socket ring. The spring connection helps push the plug out of the socket for disconnection. This protects exterior solder joints by eliminating the need to pull on the cable.
(See page 8.)

Acoustic Tooth Cleaner

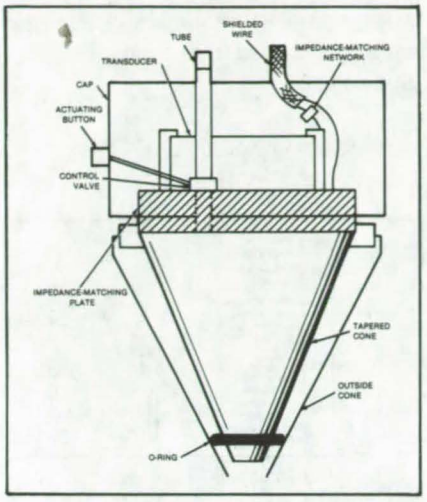

Daily dental cleaning with a new acoustic tooth cleaner may prevent calculous buildup. The tooth cleaner removes food particles and aids plaque breakdown with mild abrasive particles that are agitated in a water suspension by an acoustic wand, which is inserted in the mouth. A cap snaps over the acoustic transducer; and interchangeable outer cones maintain personal hygiene from user to user.
(See page 69.)

Adjustable Walker

Handicapped and elderly people will find getting around easier with a new adjustable walker. The user can negotiate ramps, stairs, and irregular surfaces by adjusting the two front legs of the walker.

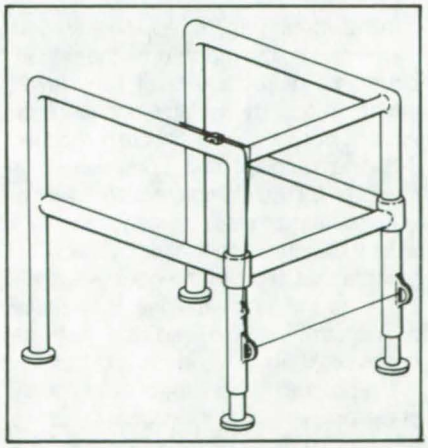

The legs are spring-loaded. When a lever is depressed, the spring pushes the legs down. The legs lock in position when the lever is released. The walker can be made from metal or from lightweight composites.
(See page 71.)

"Humanlike" Robot Hand

A manipulator hand under development has three fingers, each of which has three joints. Its fingertips are covered by a high-friction resilient material. The motor drive for the hand is mounted on the manipulator forearm,

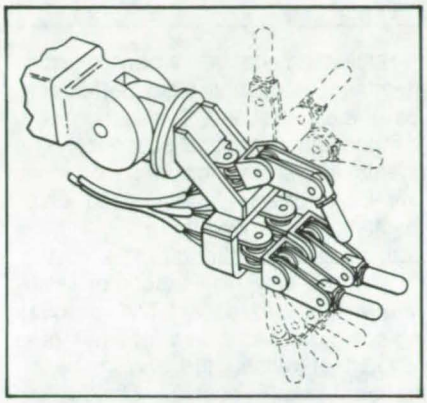

and the actuating cables run in sheaths alongside the manipulator wrist, instead of running through the wrist gimbals. The new design features rapid response to command signals and easy interchangability from forearm to forearm. The hand also has potential as a prosthesis for humans.
(See page 99.)

Lightweight Metal Mirrors

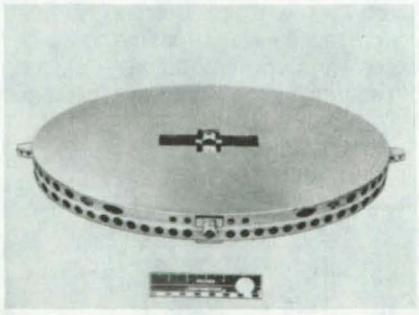

Hollow, flat mirrors fabricated by a new process are less than half the weight of previous constructions. The lightweight mirrors are fabricated by machining pockets in two plates of beryllium and then brazing the machined halves together; about 85 percent of the material is removed from the solid plates. The new mirror design is a nearly symmetrical version of the "eggcrate" structure that is often used when fabricating large, lightweight reflectors. The brazing surface is along an axis of symmetry to minimize the bimetallic effect.
(See page 121.)

Shielded Aluminum Flat-Conductor Cable

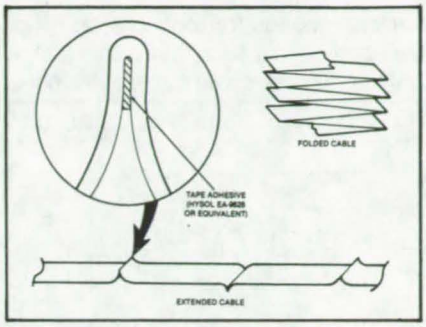

Great lengths of a new lightweight shielded flat-conductor cable can be stored by folding into relatively short stacks. To prevent the cable from fatiguing after repeated storage-and-extension cycles, the folds are glued. The cable can be used as a wiring harness for a folding photovoltaic array and as a transmission line. The cable is fabricated in a series of roll-lamination processes. Flat aluminum conductors are glued between layers of polyimide, and an aluminum shield surrounds the insulated conductors. An outer layer of polyimide protects the aluminum shield during handling and improves the thermal/optical properties of the cable for better thermal control.
(See page 7.)

Reciprocating Linear Electric Motors

Simple rugged construction, relatively low weight, and improved force control are among the advantages of a new linear reciprocating motor. Originally designed to drive Stirling-cycle cryogenic refrigerators, the motor configuration may also be applied to fuel pumps. Four coils and two magnet rings keep the current exceptionally linear,

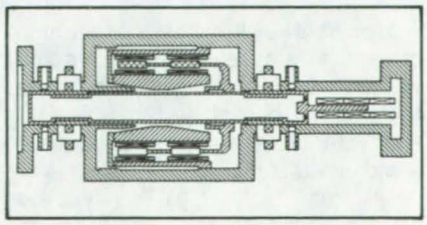

which keeps the motor force linear. As one magnet ring loads, the other unloads, keeping the average flux density in the coils constant — a decided advantage in closed-loop servosystems.
(See page 108.)

Edge Supports for Photovoltaic Modules

New supports for rooftop solar modules can be cut to length with a utility knife and installed without special tools.

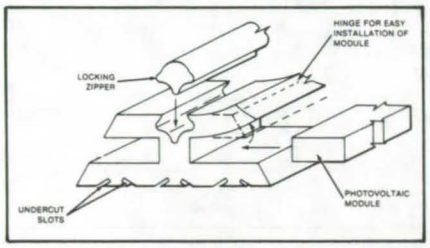

The supports, which consist of extruded rubber mullions with locking zippers, are adaptable to many different roof configurations. The mullions, made of a heat- and ultraviolet-resistant rubber, are installed on rooftops to grip the edges of the solar modules, in a manner similar to glazing gaskets. Wires, cables, and electrical connections can be molded in the mullions or installed later.
(See page 125.)

Compact Concentrators for Solar Cells

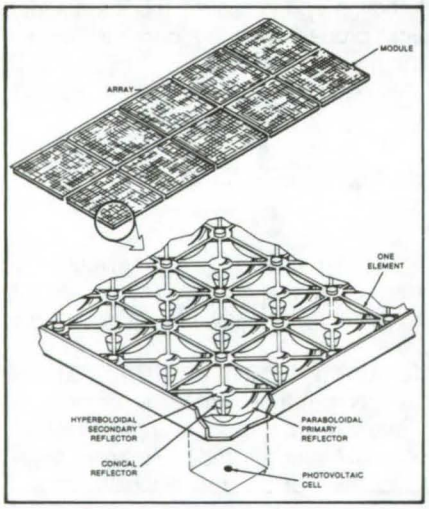

New lightweight solar concentrators provide a large electric-power output with only a small photovoltaic-cell area. Many small optical systems, one for each solar cell, gather solar energy over a wide area and direct it at a relatively small area. Each of the concentrator elements includes a paraboloidal primary mirror, a hyperboloidal secondary mirror, a conical mirror, and a photovoltaic cell. The conical mirror ensures that a substantial portion of incident light is utilized even when the concentrator axis is not pointed directly at the Sun.
(See page 35.)

Improved Polyimide Intumescent Coating

Ingredient	Proportion by Weight
Polyimide Precursor Resin Powder (Monsanto Skybond RI-7271 or Equivalent)	1.00
Methanol	1.67
Titanium Dioxide	0.044
Glass Microballoons	0.022

Nucleating agents in a new polyimide intumescent coating yield better char foam when fire strikes. The titanium dioxide and glass-microballoon nucleating agents trigger the formation of many smaller, more uniformly sized cells, resulting in improved thermal-insulating and mechanical-strength characteristics for the polyimide precursor resins with which they are used. The new coating could be used in aircraft interiors to retard heat transfer, fire, and smoke formation. A solution containing the coating ingredients is brushed onto metal and other surfaces. By applying successive coats, a tenacious continuous film is formed.
(See page 60.)

Heat-Pipe Thermal Switch

A new heat-pipe thermal switch connects and disconnects a heat source and a heat sink. The heat pipe lengthens to connect the two elements and contracts when cooling is no longer needed. Since the heat pipe isolates the heat source mechanically from the heat sink, except when cooling is actually required, the source is protected from vibrations.

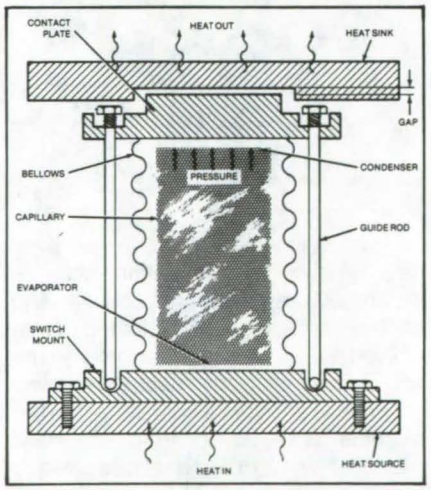

Ball-and-socket guide rods and a bellows allow relative motion of the source and heat sink. When the working fluid begins to evaporate, the pressure buildup lengthens the bellows until the heat-pipe condenser contacts the heat sink. When the source is sufficiently cooled, the pressure decreases, the bellows contract, and the heat source and heat sink are again isolated from each other.
(See page 83.)

Variable-Conductance Heat-Transfer Module

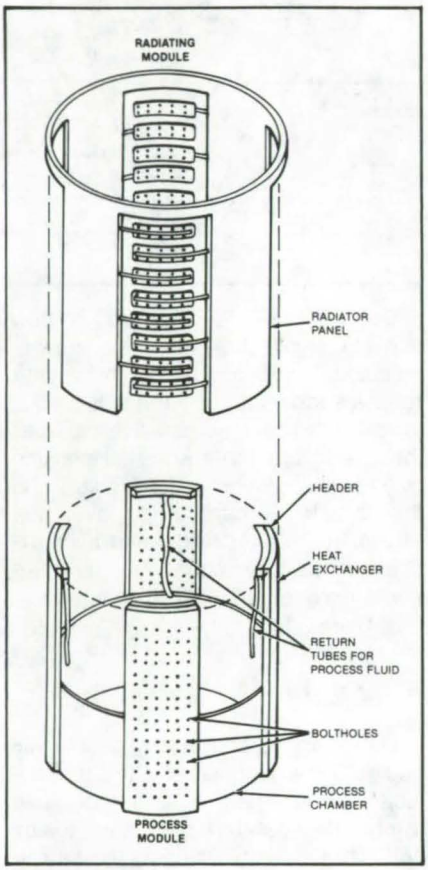

A new heat-transfer apparatus cools gases and fluids and returns them to instruments or processes at fixed lower temperatures. The variable-conductance system consists of a process module, radiating module, and controller. It is modular for quick connection, disconnection, and process isolation. The rate of heat transfer is controlled by electrical heaters that shorten the effective working lengths of the heat pipes. For service or adjustment, the radiator can be removed without disturbing the integrity of the process containment or the purity of the process fluid. If a process module must be repaired or replenished, the radiator module can be connected to another process module in the interim, thus reducing the required number and cost of radiator modules.
(See page 98.)

Electronic Components and Circuits

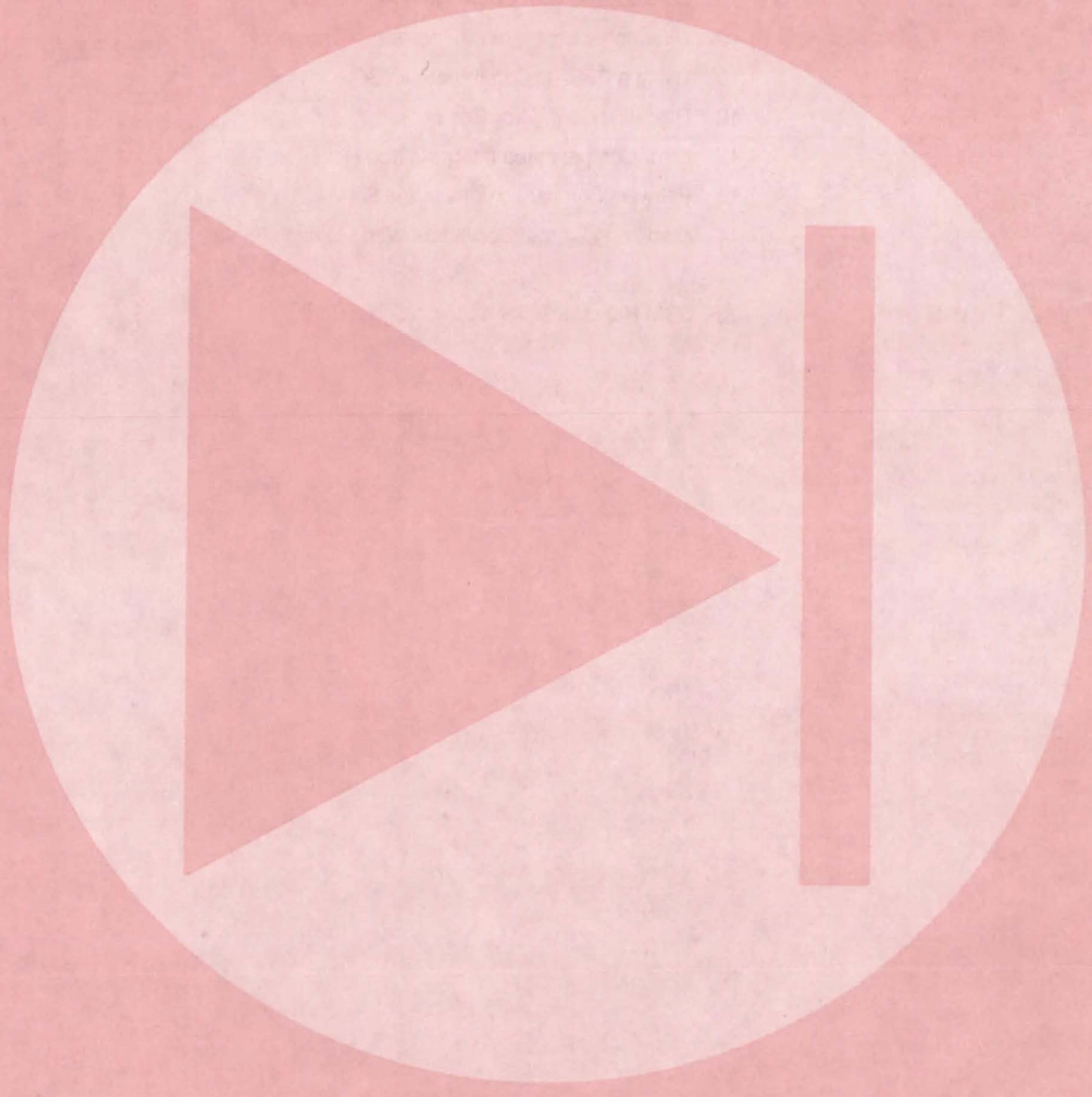

Band-Pass Amplifier Without Discrete Reactance Elements

Inherent or "natural" device capacitance is exploited.

Goddard Space Flight Center, Greenbelt, Maryland

Two pairs of operational amplifiers and eight resistors are the only discrete devices used to construct a novel band-pass amplifier. Although band-pass and resonant circuits with active elements and feedback are not new, earlier approaches usually require at least one type of discrete reactive element (either capacitive or inductive) among the outboard components.

The circuit is based on the reactive component inherent in the gain/bandwidth behavior of integrated operational amplifiers due to irreducible device capacitances. The gain of a typical unit varies with frequency according to

$$A(f) = \frac{A_O}{1 + jf/f_3}$$

where A_O = the open-loop dc voltage gain, f = frequency, and f_3 = the characteristic −3-dB or "rolloff" frequency.

The amplifiers are paired in feedback circuits as shown in the figure. Two types of amplifiers are used: Units A_2 and A_3 have equal gain/bandwidth products and rolloff frequencies, while units A_1 and A_4 have much higher gain/bandwidth products and rolloff frequencies than those of A_2 and A_3. The resonant behavior of this arrangement is best visualized in terms of the admittance "seen" by a signal source connected to the input terminals. At frequencies greater than about 10 times the rolloff frequency f_3 but less than the unity-gain frequency $f_g = A_O f_3$ of amplifiers A_2 and A_3, the input admittance is given approximately by

$$Y = \frac{1}{R_i - j\dfrac{f_g R_S R_i}{(R_5 + R_6)f}} + \frac{1}{R_O} - \frac{jf_g(R_1 + R_2)R_4}{fR_O R_1(R_3 + R_4)}$$

(continued on next page)

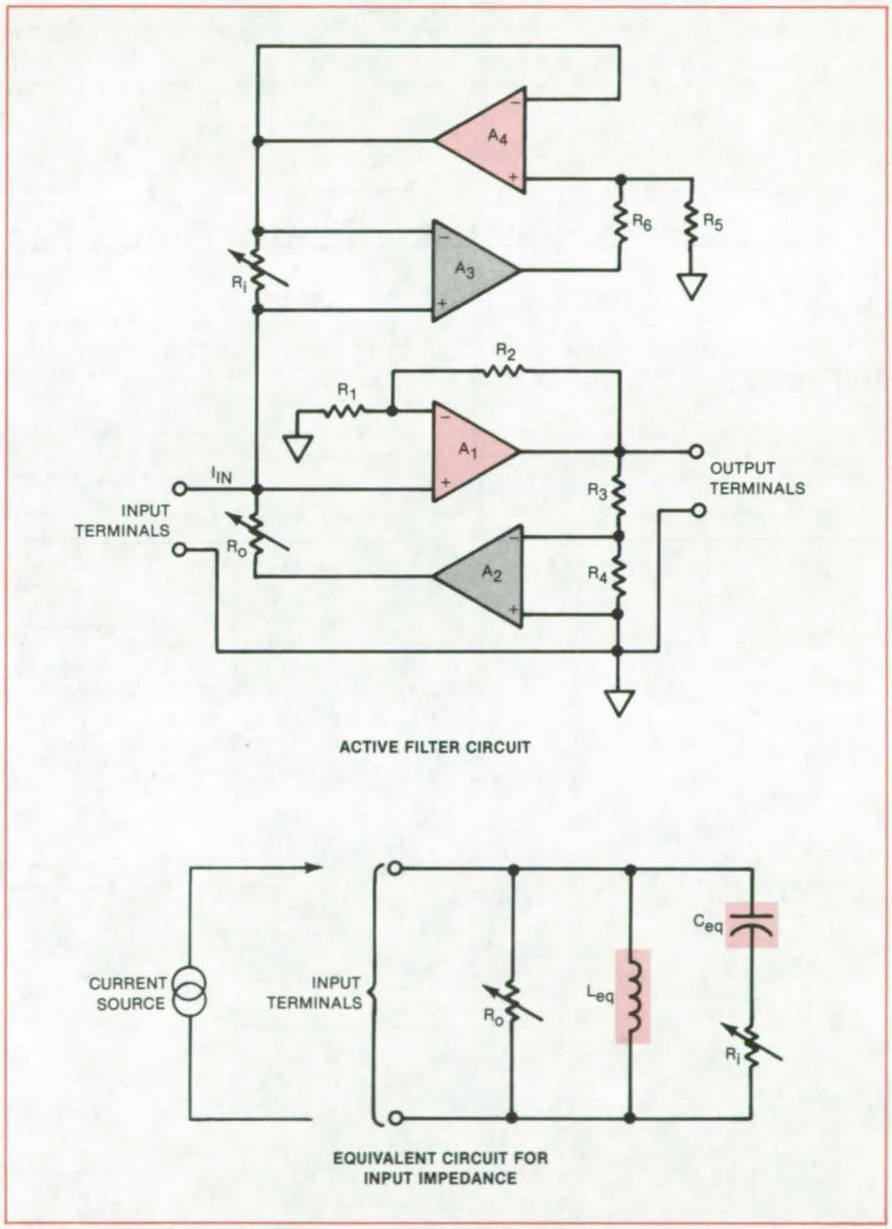

The **Band-Pass Circuit** (above) has the input impedance of the equivalent circuit (below) at frequencies much greater than the operational-amplifier rolloff frequency. The apparent inductance and capacitance arise from the combined effects of feedback and the reactive component of amplifier gain in that frequency range.

This is the same as the admittance of the equivalent circuit at the bottom of the figure, with

$$C_{eq} = \frac{R_5 + R_6}{2\pi f_g R_S R_i} \text{ and}$$

$$L_{eq} = \frac{R_1(R_3 + R_4)R_o}{2\pi f_g R_4(R_1 + R_2)}$$

At the input terminals, the circuit looks like a resonant circuit with an inductor, a capacitor, and resistances. The resonant frequency and the damping ratio ("Q factor") are adjusted by varying R_i and R_o. The band-pass output is taken from the output terminal of A_1.

An example of the range of available operating frequencies is provided by one type of commercial operational amplifier that has $f_3 = 1$ Hz and $f_g = 500$ kHz. If the design calls for a fixed resonant frequency, then R_i and R_o can be miniaturized, and the entire circuit can be fabricated on a single chip. Other design variations are possible, such as eliminating one or more of the lumped resistances to achieve a particular gain characteristic.

This work was done by Leonard Kleinberg of **Goddard Space Flight Center.** *For further information, Circle 1 on the TSP Request Card.*

This invention is owned by NASA, and a patent application has been filed. Inquiries concerning nonexclusive or exclusive license for its commercial development should be addressed to the Patent Counsel, Goddard Space Flight Center [*see page A5*]. *Refer to GSC-12788.*

Phase Detector for Power-Factor Controller

Positive feedback assures reliable switching.

Marshall Space Flight Center, Alabama

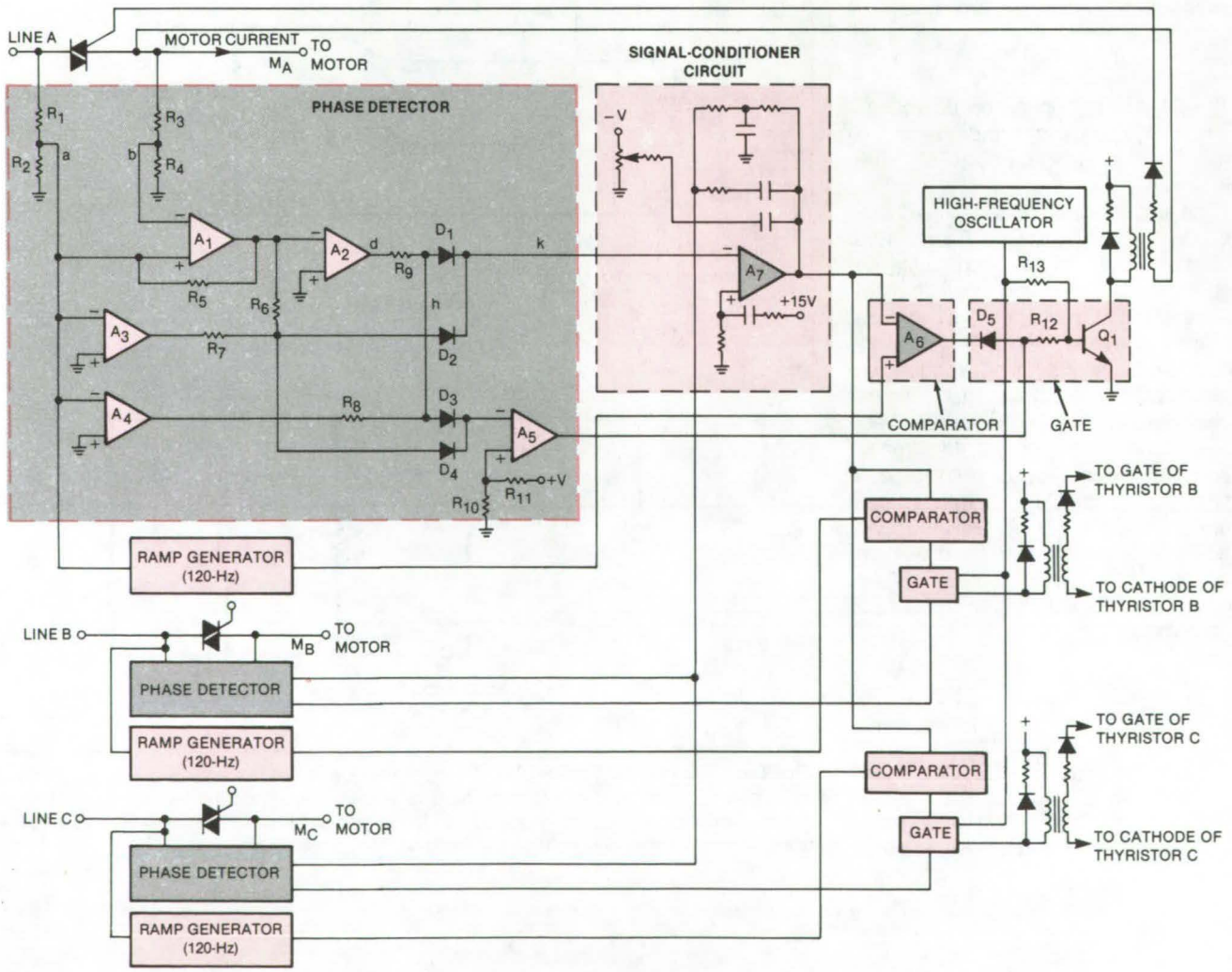

A **Three-Phase Power-Factor Controller** includes three phase detectors, one of which is shown in detail. Each phase detector produces rectangular waves of duration approximately equal to the lag time between the line voltage and the motor current.

The three-phase power-factor motor controller in the figure includes a phase detector (portion inside colored dashed box) in each leg of the powerline. Each phase detector generates rectangular pulses that repeat at the powerline frequency and have durations approximately equal to the time lag between the line voltage and the motor current.

As described in earlier articles on power-factor motor controllers, the phase-detector output is combined with a manually- or automatically-set power-factor command voltage and compared with a line-synchronous ramp voltage. The comparator output is then used to control the thyristor that feeds power to the motor.

In each leg, or phase, of the powerline, the line and motor voltages are sampled by resistive voltage dividers R_1,R_2 and R_3,R_4, respectively. These reduce the usual 240-V line voltage by a nominal factor of 20 to a level compatible with the solid-state circuitry. The zero crossings of the sampled line voltage are detected by operational amplifiers A_3 and A_4, which produce inverted and noninverted square waves, respectively, in synchronism with the line voltage. The sampled line voltage also triggers the ramp generator.

To detect the phase lag of the motor current, the output of amplifier A_1 must switch in synchronism with the zero crossing of the motor current. Operating as a comparator, A_1 samples this current in terms of the voltage across the thyristor.

The sampled voltage difference across the thyristor includes a common-mode error due to the imprecision of the voltage-divider resistors. During the thyristor "on" period, typical resistor tolerances can cause the magnitude of voltage at point "b" to exceed erroneously that at point "a" by as much as 0.4 V, thus preventing A_1 from switching when it is supposed to or making it switch when it is not supposed to. To overcome the common-mode error, resistor R_5 introduces about 0.5 V of positive feedback that latches A_1 at the proper polarity as long as the current flows.

When the motor current reaches zero, the thyristor turns off, and the potential drop across it rises rapidly to a typical magnitude of 50 V and polarity opposite that of the current during the immediately-preceding "on" period. This causes a 2.5-V difference at the inputs of A_1 sufficient to overcome the 0.5-V positive feedback and make the A_1 output switch polarity.

The voltage samples are thus converted into rectangular waveforms with leading edges at the zero crossings of the line voltage and motor current. These waveforms are combined in the network consisting of R_6 through R_{11}, D_1 through D_4, A_2, and A_5 to produce two output waveforms: The voltage at point "k" is a positive rectangular wave that is on during the interval between the zero crossing of the line voltage and the next zero crossing of the current; that is, during a period equal to the lag between the voltage and the current. The output of A_5 is a rectangular wave that is negative while the point "k" voltage is on and positive at other times.

Both waveforms are used in the thyristor-triggering portion of the system. Due to the finite switching speeds of the amplifiers, the interval of negative output of A_5 is actually about 10 to 20 μs longer than the positive-output interval at point "k." At full motor load, this slight difference is needed to keep the thyristors nonconducting for a short period after the zero crossing of current so that the thyristor voltage will rise enough to overcome the latching bias and allow switching to occur.

This work was done by Frank J. Nola of **Marshall Space Flight Center.** *For further information, Circle 2 on the TSP Request Card.*

This invention is owned by NASA, and a patent application has been filed. Inquiries concerning nonexclusive or exclusive license for its commercial development should be addressed to the Patent Counsel, Marshall Space Flight Center [see page A5]. Refer to MFS-25854.

Power-Factor Controller With Fast Load Response

Sudden changes in induced emf are sensed.

Marshall Space Flight Center, Alabama

In a refinement of the soft-starting three-phase power-factor motor controller, a few additional components enable the circuit to respond quickly to a sudden increase in motor load. The soft-start characteristic is also improved. The earlier versions of this circuit are described in "Three-Phase Power-Factor Controller" (MFS-25535), page 3, *NASA Tech Briefs*, Vol. 6, No. 1 (Spring 1981), and "Soft-Starting Power-Factor Motor Controller" (MFS-25586), page 4, *NASA Tech Briefs*, Vol. 7, No. 1 (Fall 1982).

The added circuitry (see figure) senses the induced electromotive force of the motor during the nonconducting period of the thyristor in phase A. When the motor is idling and operating at a controlled low power factor, the sudden application of a large load causes this voltage to have a polarity opposite that of the line voltage in phase A. This opposite voltage is used to derive a fast-reaction control voltage to bring the motor quickly up to full power.

The line and motor voltages in phase A are sampled through resistive voltage dividers. Operational amplifier A_1 converts the sample of phase A line voltage to a square wave: When line A is positive (negative) with respect to neutral, the output of A_1 is positive (negative), causing transistor Q_1 to go on (off) and transistor Q_2 to go off (on). This prevents the sample of motor voltage from reaching the negative (positive) input of A_2. Thus, the amplified sample of motor voltage at the output of A_2 is always positive with respect to neutral if the motor voltage has the same polarity as that of the line

(continued on next page)

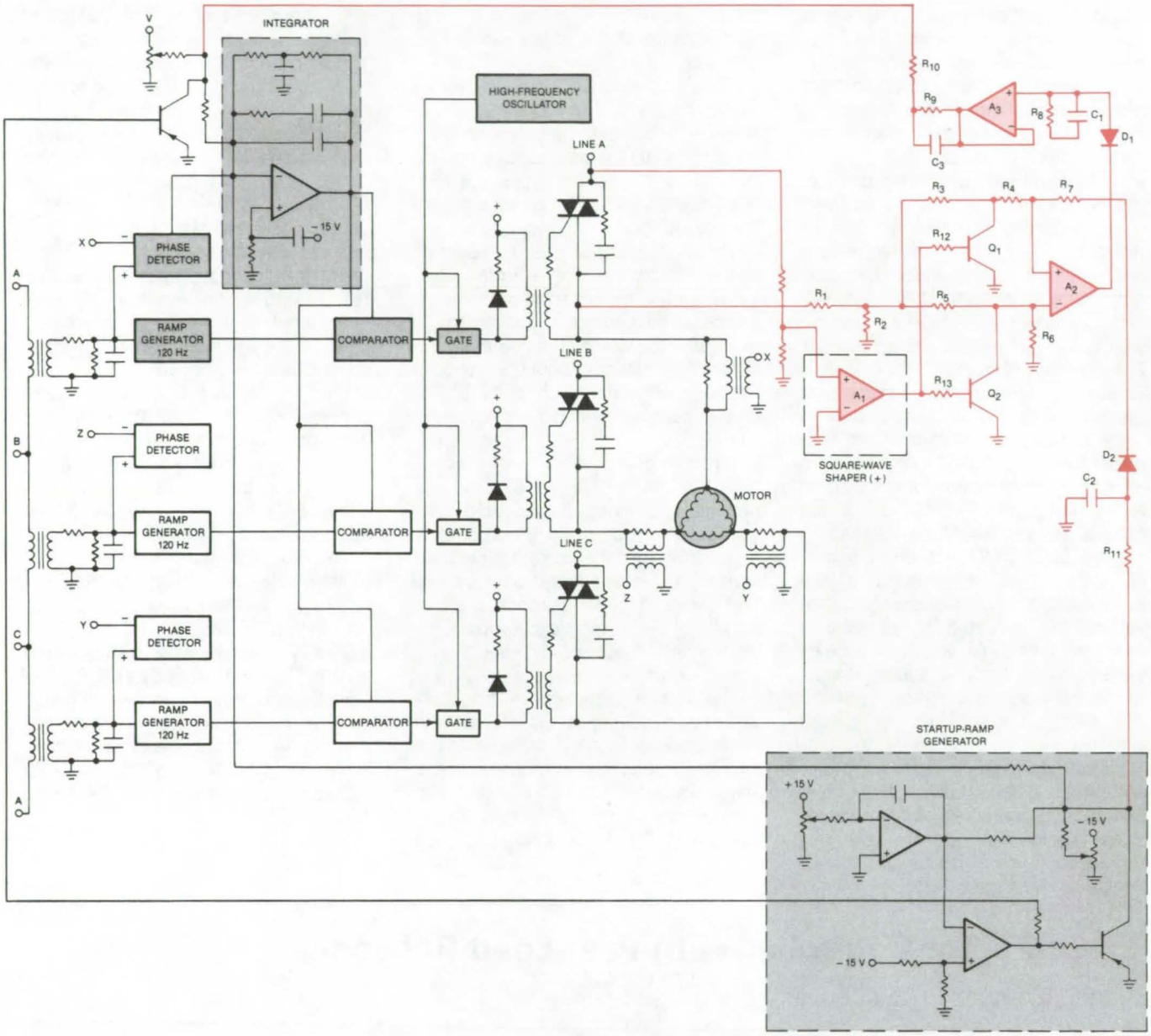

The **Rapid-Load-Response Addition** (part in color) senses the induced motor emf to detect a sudden load increase and generates a command signal to increase the applied power in response.

voltage and is always negative with respect to neutral if the motor voltage has the opposite polarity as in the case of a suddenly applied load.

Diode D_1 blocks the positive output of A_2 but passes the negative output to the noninverting input of A_3, charging capacitor C_1 in the process. A_3 is connected as a voltage follower to present a high impedance to C_1 and permit it to discharge through R_8 with a time constant of several seconds. This feature assures fast attack and slow decay, thus avoiding control instability. The output of A_3 is fed through C_3, R_9, and R_{10} to the integrator shown in dashed outline as a power-factor command signal that supersedes other command signals (except that of the soft-start ramp) until the voltage on C_1 decays.

The negative output of A_2 is fed through the network of D_2, C_2, and R_{11} to be added to the soft-start ramp signal. During startup, the magnitude of the added signal decays, making the ramp more nearly linear and thereby effecting a softer start.

The additional circuitry makes further energy saving possible: The motor can be operated at a higher phase angle (lower power factor) during idle than it could without the rapid-load-response addition. Motors previously had to be operated at a higher power factor during idle to retain the ability to respond quickly to load increases.

This work was done by Frank J. Nola of **Marshall Space Flight Center.** *For further information, Circle 3 on the TSP Request Card.*

This invention is owned by NASA, and a patent application has been filed. Inquiries concerning nonexclusive or exclusive license for its commercial development should be addressed to the Patent Counsel, Marshall Space Flight Center [see page A5]. Refer to MFS-25852.

Shielded Aluminum Flat-Conductor Cable

Thin wiring harness stores compactly.

Marshall Space Flight Center, Alabama

A lightweight shielded flat-conductor cable has been developed as a wiring harness for a folding solar photovoltaic array and as a transmission line for instrumentation signals. The cable is thin, allowing long lengths to be stored by folding into relatively short stacks.

The cable is fabricated in a series of roll-lamination processes. Aluminum conductors are embedded in an adhesive layer between Kapton (or equivalent) polyimide insulating sheets (see Figure 1). Aluminum shields are held by adhesive on the outsides of the polyimide sheets. The upper and lower aluminum shields are electrically connected at both edges by aluminum tape secured with a conductive contact cement. An outer polyimide layer protects the aluminum shield during handling and improves the thermal/optical properties of the cable for better thermal control.

The aluminum shield reduces the flexibility of the cable, and the cable can withstand only a limited number of repetitions of sharp bending at the same spot. To prevent severe local stress cycling at the folds during extension and storage operations, the folds are glued in place (see Figure 2).

This work was done by S. G. Farina of Flexible Circuits, Inc., and Lockheed Missiles & Space Co., Inc., for **Marshall Space Flight Center.** *No further documentation is available.*
MFS-25899

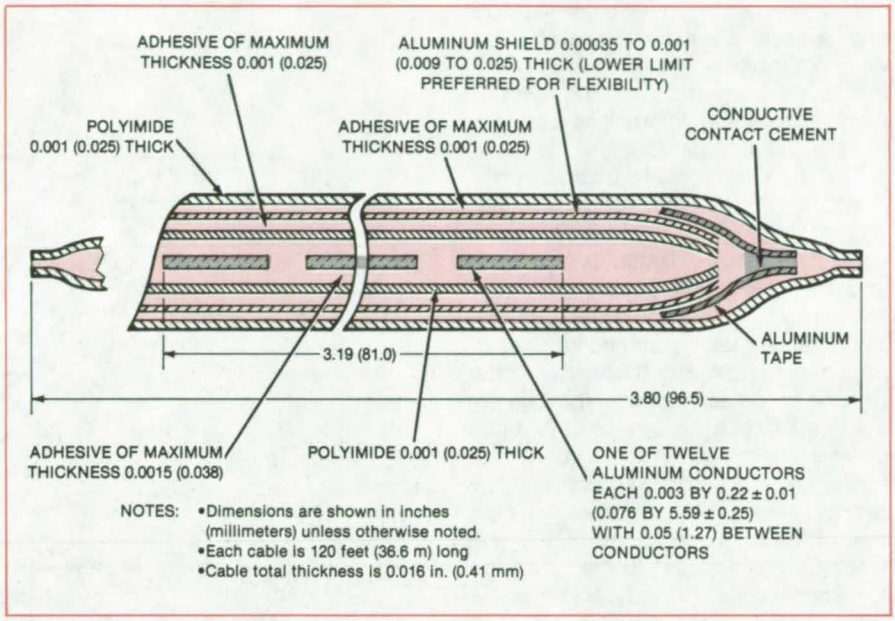

Figure 1. **Flat Aluminum Conductors** are glued between layers of polyimide. An aluminum shield surrounds the insulated conductors. The outer layer is polyimide.

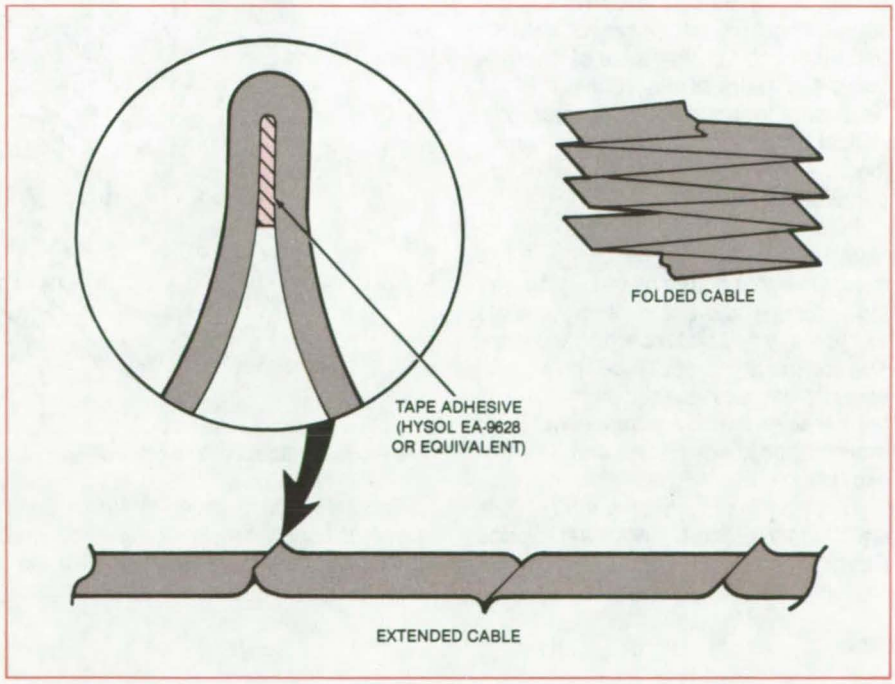

Figure 2. **Great Lengths of Thin Cable** are stored by folding it into a stack. The folds are glued to prevent fatigue after repeated storage-and-extension cycles.

Conical Electrical Connectors Aline Easily

Rotational alinement is not critical in a design useful for remote manipulators.

Marshall Space Flight Center, Alabama

New cone-shaped multiple-wire plugs and sockets automatically aline with each other when joined together. They are particularly suitable for remote manipulators and for making connections in "blind" locations.

The plugs and sockets are made from phenolic or other insulating materials commonly used for connectors. Metal contact rings (see figure) are molded into the plug cone either flush with the conical surface or slightly protruding. The segmented contacting spring rings are molded into the socket cone with the spring segments protruding into the interior space. Wires or other conductors are molded into the connector bodies, leading from the contact rings to sets of standard contact pins at the outside of the plug and socket. Wires are electrically connected to the pins with standard multiple-pin connectors or by soldering.

When the plug and socket are pushed together, each plug ring deflects the spring segments of the corresponding socket ring. This assures alinement and electrical contact. Because of the rotational symmetry of the cones, it is not necessary to rotate the connectors to a critical angular orientation before mating. The spring compression makes disconnection easy.

In remote locations or where connectors are ganged, it may be helpful to mount the connectors on panels. Mounting screws would allow the connectors to slide a small distance on the panel. The connectors would be given just enough slack to enable them to aline themselves, thereby compensating for mounting-position errors and thermal expansion.

This work was done by Keith H. Clark and Donald R. Scott of **Marshall Space Flight Center.** *For further information, Circle 4 on the TSP Request Card.*

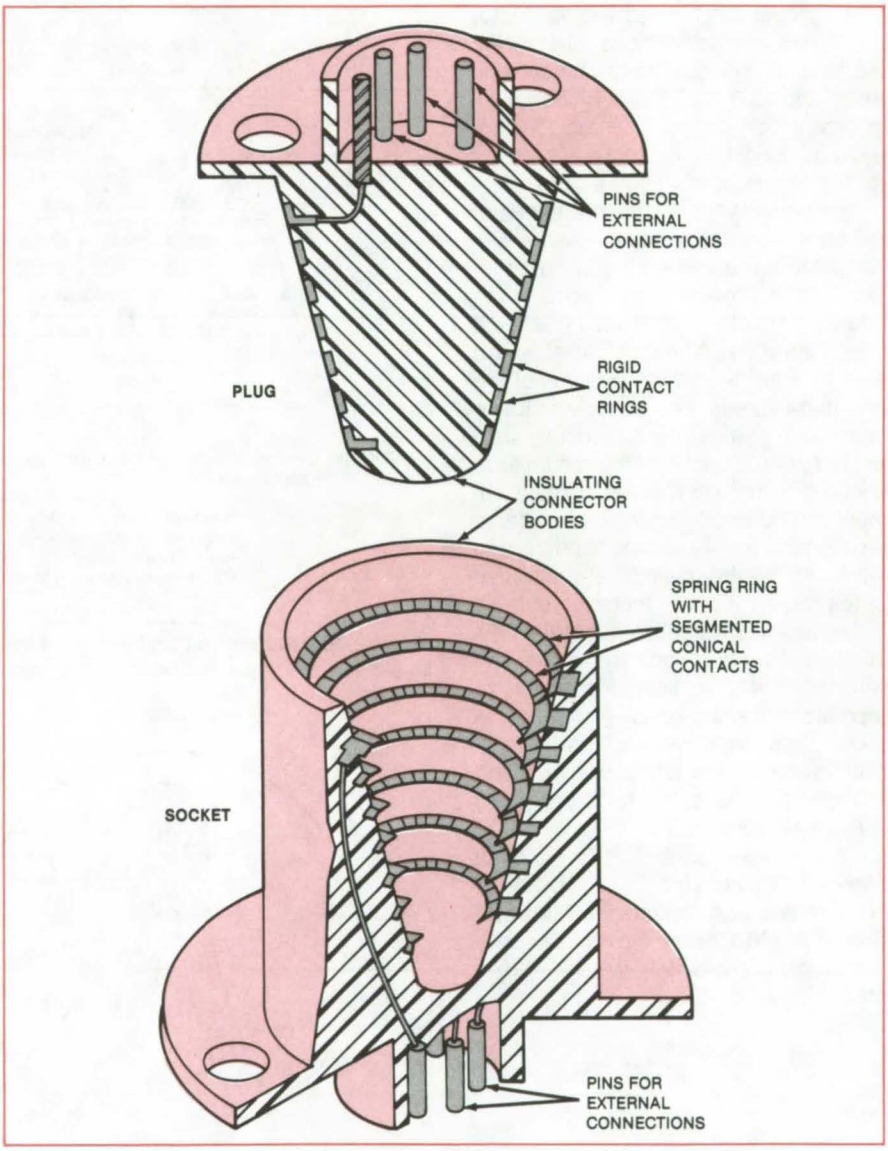

The **Plug and Socket** have conical bodies with sets of mating contact rings.

This invention is owned by NASA, and a patent application has been filed. Inquiries concerning nonexclusive or exclusive license for its commercial development should be addressed to the Patent Counsel, Marshall Space Flight Center [see page A5]. Refer to MFS-25211.

Directional Coupler With Increased Directivity

Diffraction loss is reduced by curving one reflector.

NASA's Jet Propulsion Laboratory, Pasadena, California

A new design for a four-port directional coupler promises to improve directivity while reducing diffraction loss. Intended primarily for use in local-oscillator diplexers (first-mixer inputs), the new design will increase the signal-to-noise ratios and therefore the ranges of millimeter and submillimeter heterodyne receivers.

In an older version of the diplexer, two parallel plates serve as reflectors in a ring resonator (see Figure 1). The system operates as a four-port broadwall waveguide hybrid junction. At millimeter and submillimeter wavelengths the system operates in a quasi-optical manner. The distance between the plates is adjusted for laserlike or quasi-optical input of a local-oscillator signal through one port, quasi-optical input of the received signal through another port, and directional coupling of the combined signals through the output port to the mixer.

The parallel-plate resonator is subject to diffraction loss since the top and bottom of the cavity are open. In the improved version, one of the parallel-plate reflectors is replaced by a reflector with a slight toroidal curvature (see Figure 2). With the help of diffraction theory the horizontal and vertical radii of curvature are chosen to minimize the unwanted diffraction of signal energy out of the cavity and to increase the directivity [which is defined as (power coupled out to the mixer) ÷ (power coupled back out through the received-signal input port)].

The new design was tested successfully at 100 GHz. Future developments will include a more complete presentation of the diffraction theory of the system and further experimental refinements.

This work was done by Herbert M. Pickett and Arthur E. Chiou of Caltech for **NASA's Jet Propulsion Laboratory.** *For further information, Circle 5 on the TSP Request Card.*
NPO-15892

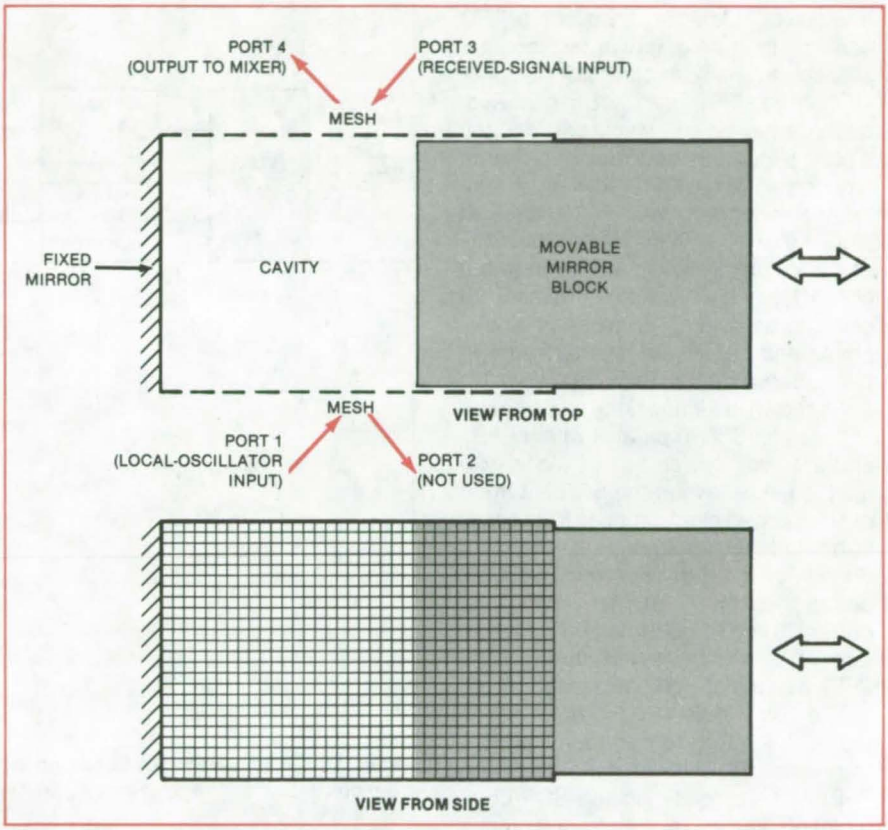

Figure 1. The **Basic Diplexer Design** involves an adjustable four-port ring resonator in a folded Fabry-Perot cavity.

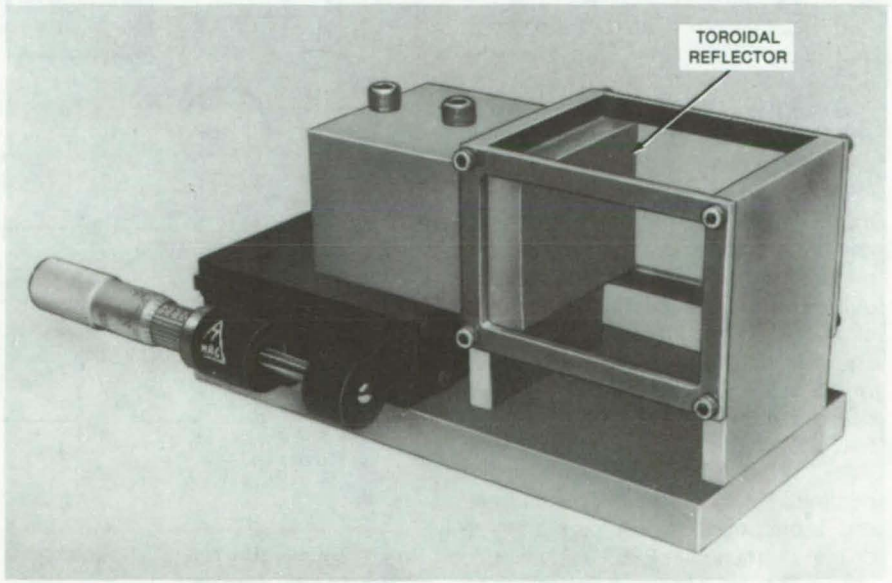

Figure 2. In the **Improved Diplexer** the adjustable reflector has toroidal curvature (separate horizontal and vertical cylindrical curvatures) to reduce diffraction loss through the open cavity ends.

Using a PFET To Commutate an SCR

Accidental turn-on is prevented.

NASA's Jet Propulsion Laboratory, Pasadena, California

A power field-effect transistor (PFET) can limit the rate of forward voltage application to a silicon-controlled rectifier (SCR). The PFET does not exhibit secondary breakdown, which can destroy bipolar transistors performing the same function. It is desirable to limit the increase of forward voltage because at higher than specified values, the SCR can accidentally switch on, even in the absence of the firing signal. The new circuit can be used in all types of single-phase and polyphase inverters and in buck-, boost-, and flyback regulators.

As shown in Figure 1, the basic circuit includes an SCR in parallel with a PFET and a 10-volt power supply, along with drive sources. When the SCR is turned on (by a drive voltage applied to its gate), current flows through it to the load. Shortly (of the order of a microsecond) before the time for turning off the load current, the PFET is turned on. The load current is thus diverted through the PFET and the 10-volt power supply.

The 10-volt power supply back-biases the SCR, forcing the current in the SCR to reverse and then become zero. The PFET is held on during the SCR commutation time and is then turned off at a controlled rate so as to limit the rate of forward voltage reapplication to the SCR. The maximum current that the PFET must carry is equal to the load current plus the recovery current of the SCR.

Since the SCR commutation time is small in comparison with the switching period, the power dissipated in the PFET is low. The low power dissipation allows the PFET to handle currents higher than its continuous rating and to commutate a number of SCR's. Topologies that utilize one PFET to commutate a number of SCR's are economically attractive. The concept is illustrated in Figure 2, where one PFET is used to commutate SCR's S1A through SNA. When commutation of a particular switch SiA (where i = 1 . . . N) is desired, the corresponding commutation SCR switch SiB is turned on. The current in SiA can then be diverted through the PFET as described above. The result is controlled switching

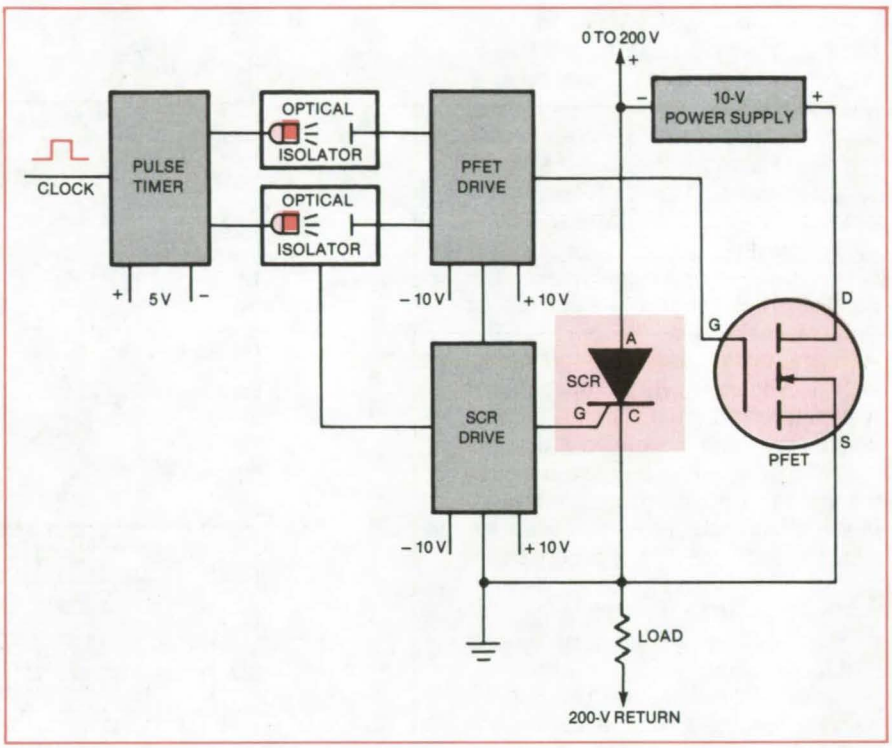

Figure 1. A **PFET Diverts the Load Current** around an SCR to prevent false SCR triggering from current and voltage switching transients.

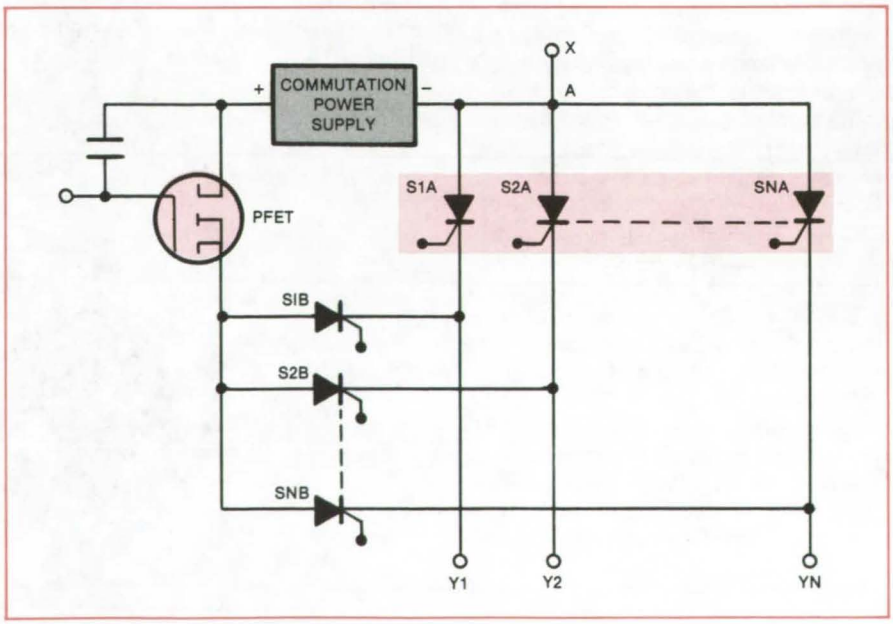

Figure 2. **One PFET** acts in cooperation with SCR's S1B through SNB to commutate SCR's S1A through SNA.

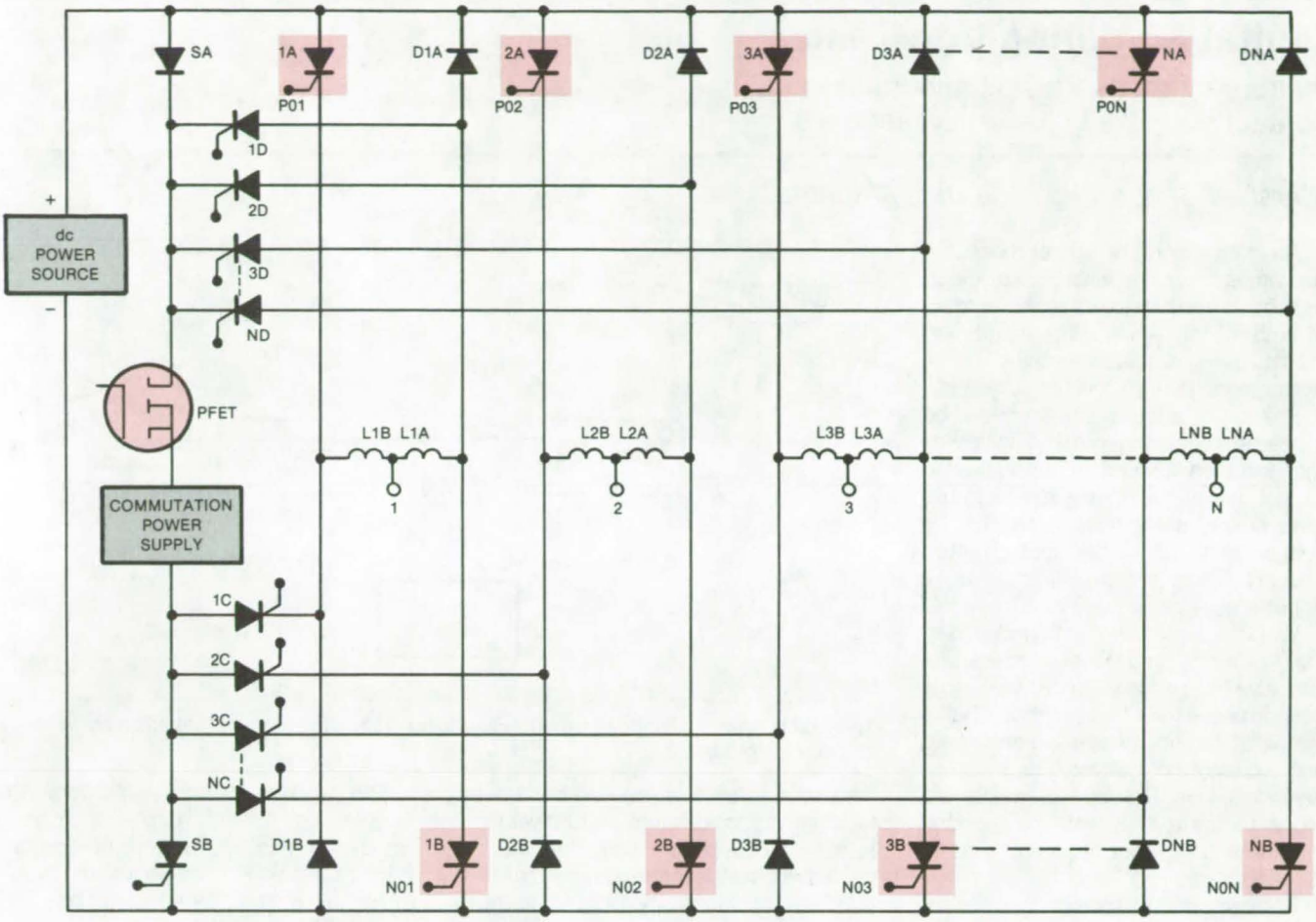

Figure 3. A **Polyphase Bridge Inverter** employs the single-PFET commutation technique.

of unidirectional current from an input terminal X to selected output terminals Y1 through YN.

The techniques of using a PFET to commutate a number of SCR's can also be extended to polyphase bridge inverters, as shown in Figure 3. The circuit achieves commutation of SCR iA by diverting its current through SCR SA, the PFET, and the commutation SCR iC. Similarly, the commutation of SCR iB is achieved by diverting its current through the commutating SCR iD, the PFET, and SCR SB. The inductors L1A through LNA prevent large circulating currents from flowing through the antiparallel diodes D1A through DNA during the commutation interval of SCR's S1A through SNA, respectively. The inductances L1B through LNB serve a similar purpose for the diodes D1B through DNB during the commutation of SCR's S1B through SNB. A 10-kW version of the inverter shown in Figure 3 was fabricated and tested.

This work was done by Dean B. Edwards and Wally E. Rippel of Caltech for **NASA's Jet Propulsion Laboratory.** *For further information, Circle 6 on the TSP Request Card.*

Inquiries concerning rights for the commercial use of this invention should be addressed to the Patent Counsel, NASA Resident Office-JPL [see page A5]. Refer to NPO-15282.

"Fuel Gage" for Electric Vehicles

The equivalent of a "fuel gage" for electric-powered vehicles would monitor the state of charge of lead/acid batteries at any stage in the charging cycle by measuring the charging current and either gas evolution or electrode potential. The system would display the remaining useful charge, analogous to the indication of a gasoline-tank gage.

(See page 26.)

Cryogenic Pressure Seal for Wires

Polyurethane is the sealant in a high-pressure feedthrough for use at cryogenic temperatures. A fitting filled with the sealant passes electrical leads through a wall between high- and low-pressure chambers. The sealant is a two-part polyurethane. Various elastomers or polymers may work, depending on the pressure differential and the fluid to be contained.

(See page 77.)

Membrane Switches Check Seal Pressure

An array of flexible membrane switches can indicate the closure of a seal. A membrane switch responds to the pressure exerted by a rigid surface on a compliant sealing medium. The switch contacts can be monitored electronically. The principle can be used to ensure the integrity of seals on refrigerator and oven doors and hatches on airplanes or submarines.

(See page 75.)

Digital Soldering-Iron Tester

Instrument reads the tip temperature and contact potential in just a few seconds.

Marshall Space Flight Center, Alabama

An instrument (see figure) measures the temperature and voltage of a soldering-iron tip and provides a digital readout of both measurements. The instrument thus quickly gives assurance that conditions are correct for reliable soldering.

Previously, a thermocouple had to be brazed in a soldering-iron tip. The tip was then installed in an iron, the iron heated to full temperature, the temperature read on an analog meter, and the tip voltage read on another analog meter. The procedure required from 6 to 10 minutes per iron.

With the new tester, a tinned soldering tip is touched to a temperature-sensitive button for 4 seconds and to a voltage probe for 1 to 3 seconds. The tip temperature (in degrees Fahrenheit) and voltage (in millivolts) appear on digital displays. The measurements are more accurate than with the previous method and together require only 15 to 20 seconds per iron.

The instrument is compact. It is contained in a 9- by 12-inch (22.9- by 30.5-cm) package. The temperature sensor to which the soldering-iron tip is touched is a columbium button welded to a thermocouple junction. The columbium prevents the thermocouple materials from contaminating the soldering-iron tip and vice versa.

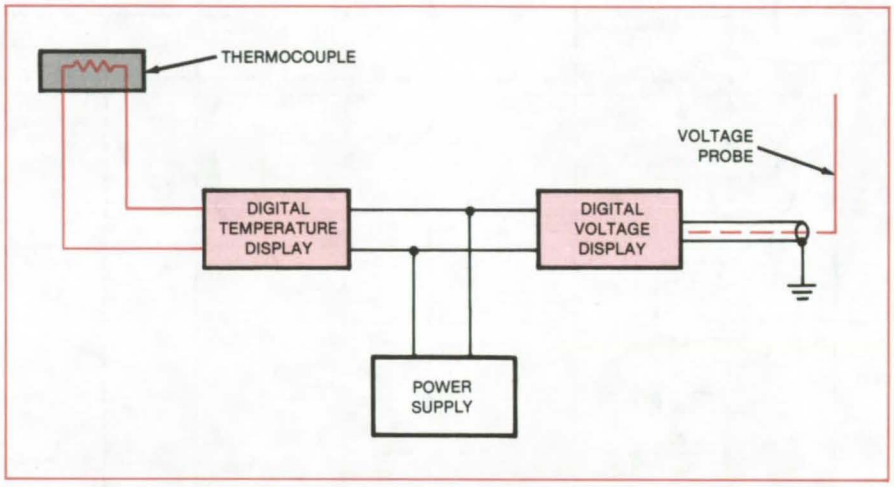

The Test Instrument includes a thermocouple for measuring temperature and a probe for measuring voltage.

This work was done by Richard N. Buggle and William H. Metka, Jr., of Honeywell, Inc., for **Marshall Space Flight Center.** *For further information, Circle 7 on the TSP Request Card.*
MFS-25863

Error-Compensated Integrate and Hold

Differencing circuit cancels the error caused by switching-transistor capacitance.

Ames Research Center, Moffett Field, California

Differential compensation reduces the error in an improved integrate-and-hold circuit. A prototype developed for the Galileo Probe Project has less outout voltage error (by a factor of 5) than a comparable conventional circuit. The new configuration could be applied in systems where very low voltages are sampled or where there are many integrate-and-hold cycles before the circuit is reset.

A conventional integrate-and-hold circuit (see figure, top) consists of an operational amplifier with a feedback capacitor. The output voltage is proportional to the integral of the input voltage over the time during which the input switch is closed. When the switch is opened, the output remains constant until the integrator is reset by a short circuit across the capacitor.

When a junction field-effect transistor (JFET) is used as the input switch, the transistor gate-to-source capacitance C_1 couples charge from the gate input pulse to the integrating capacitor C_2, introducing an error voltage at the output.

To compensate for the error, a second JFET is added, as shown in the circuit at the bottom of the figure. When the input switch of that circuit is opened, C_1 couples charge into C_2 as before and produces an error voltage through the inverting input port of the operational amplifier. However, C_4 (the gate-to-source capacitance of the second JFET) couples charge into C_3 to produce an error voltage of opposite polarity through

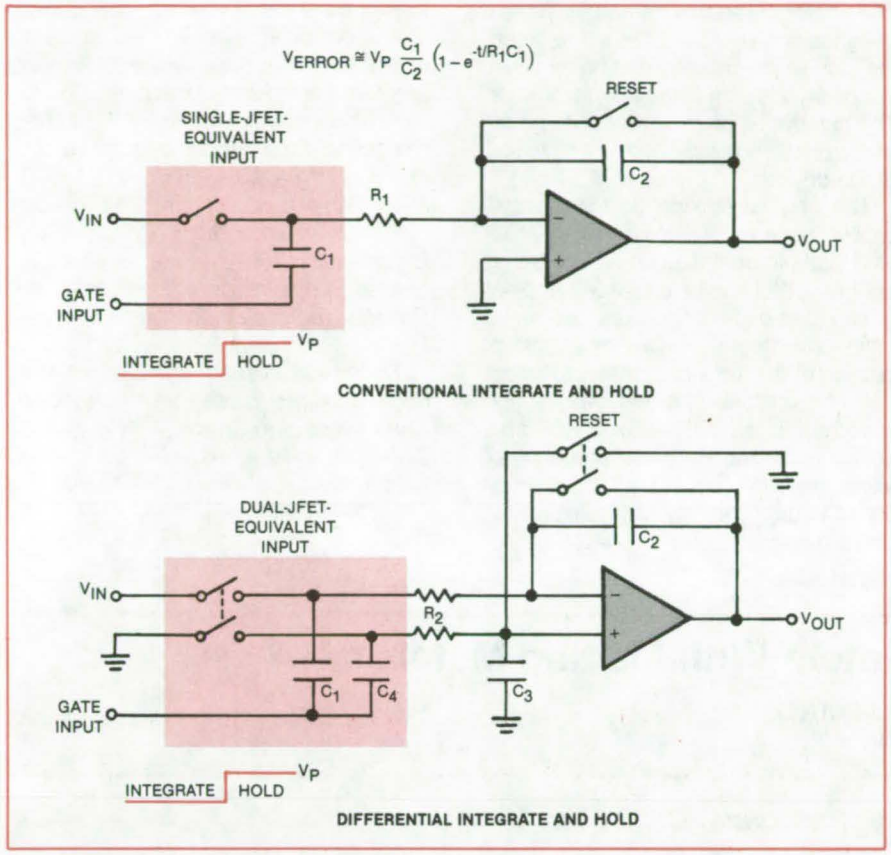

In a conventional **Integrate-and-Hold-Circuit** using a JFET switch (top), the gate-to-source capacitance causes an error in the output voltage. The differential connection shown at the bottom cancels out the error.

the noninverting input port. With proper choices of components, the differential error can be made to approach zero.

Another advantage of this differential integrate-and-hold circuit is the cancellation of the operational amplifier bias currents in C_3 and C_2. This cancellation further reduces output error voltage. The improved circuit requires only four additional parts; and if quad JFET switches are used (instead of dual switches), no additional IC packages are required.

This work was done by M. D. Matlin of Martin Marietta Corp. for **Ames Research Center.** *For further information, Circle 8 on the TSP Request Card.*

Inquiries concerning rights for the commercial use of this invention should be addressed to the Patent Counsel, Ames Research Center *[see page A5].* *Refer to ARC-11303.*

Pairwise Comparison of Voltage Sets

Optical preprocessor compares 16 incoming signals with reference voltages.

Langley Research Center, Hampton, Virginia

A prototype 16-channel integrated optical data preprocessor performs pairwise comparison of two sets of analog voltages. It uses optical interferometry to compare N analog voltages from remote sensors with N reference voltages. The device is capable of functioning in a "screening" mode where the input data are compared to the reference data set, and only signal differences are detected; or the input data are compared to many reference sets to permit classification.

The device consists of an $LiNbO_3$ substrate (see figure) containing a complex but symmetric Ti-indiffused waveguide pattern, two symmetrically-dis-

(continued on next page)

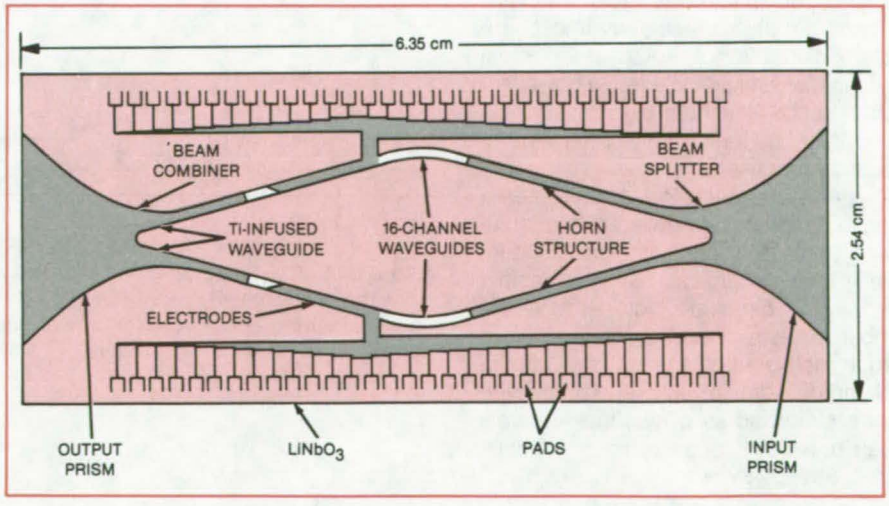

The **Integrated Optical Data Preprocessor** uses optical subtraction to take a "vector difference" of two sets of analog voltages.

posed electrode structures, and two As_2S_3 surface gratings, which act as a beam splitter and beam combiner, respectively. The overall configuration is that of a Mach-Zehnder interferometer with each arm divided, over a portion of its length, into 16 separate channels.

Each of the 7-μm-wide channels passes through a gap between a pair of electrodes. Because of the electro-optic effect, the light undergoes a phase shift that is proportional to the difference between the voltages on the members of each electrode pair. The phase difference is converted to an amplitude difference by optical interference at the beam combiner.

Each channel gives rise to a signal, the intensity of which is proportional to the scalar difference in analog voltages. The vector difference comes from summing the scalar differences at the detector. All electrical information is introduced on one arm of the interferometer. The electrodes on the other arm are for gross phase adjustment and fine tuning of the device.

The original application for the preprocessor is in satellite onboard processing of pictorial data so that data that are not useful can be discarded and not transmitted back to the base station. Its main advantages are a significant reduction of the amount of meteorological data of negligible value and the very high speed intrinsic to optical devices. Such a device could recognize the presence of excessive cloud cover and could signal a halt to data transmission. Similarly, it could recognize clear seawater and interrupt data transmission if only departures from clear water were of interest.

This work was done by Carl M. Verber and Richard P. Kenan of Battelle Columbus Laboratories for **Langley Research Center.** *Further information may be found in NASA CR-165636 [N81-19900/NSP], "An Investigation for the Development of an Integrated Optical Data Preprocessor" [$9]. A copy may be purchased [prepayment required] from the National Technical Information Service, Springfield, Virginia 22161.*

Title to this invention has been waived under the provisions of the National Aeronautics and Space Act (42 U.S.C. 2457(f)), to the Battelle Columbus Laboratories, Columbus, OH 43201.
LAR-12929

Stabilizing Crystal Oscillators With Melting Metals

Heat of fusion provides an extended period of constant temperature and frequency.

NASA's Jet Propulsion Laboratory, Pasadena, California

A quartz crystal can be kept at a constant temperature — and hence constant oscillating frequency — by exploiting the heat of fusion of an immersion material. In the new technique, the crystal is surrounded by a metal in a spherical container. As the outside temperature rises to the melting point of the metal, the metal starts to liquefy; but the temperature stays at the melting point until no solid metal remains.

The immersion technique is being developed as a way of stabilizing the frequency of spacecraft radio transmissions from the surface and atmosphere of the planet Venus. Potential terrestrial applications might include low-power environmental telemetering transmitters and instrumentation transmitters for industrial processes.

The requirements for a useful stabilizing material are a large latent heat of fusion, high density, high heat conductivity, and chemical stability against autotropic decomposition. Among the most suitable materials are therefore such metals as potassium, sodium, tin, bismuth, cadmium, lead, and zinc. In the pure state and as alloys, these metals can provide a range of melting points from 60° to 427° C.

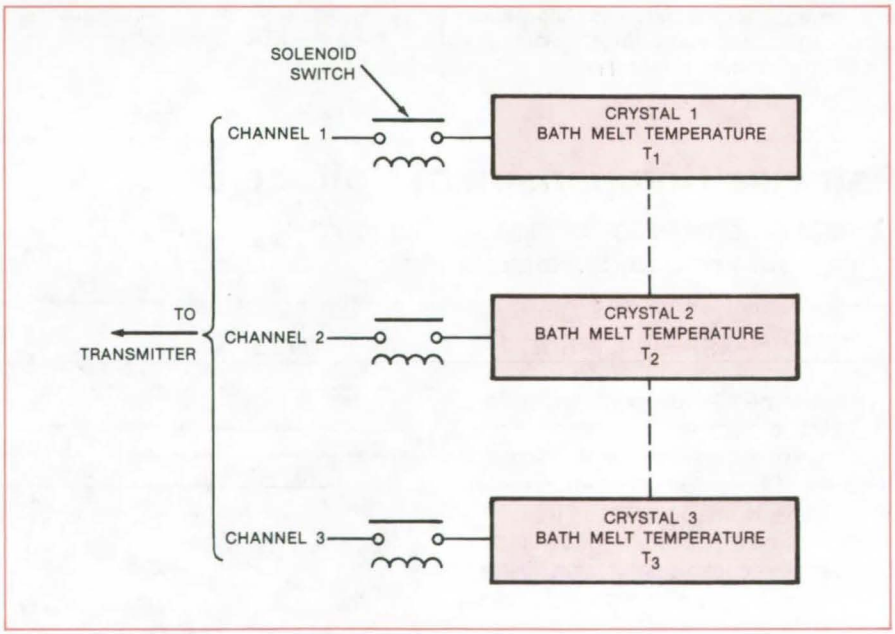

A Crystal Unit Is Selected for operation when its metal is melting and absorbing heat from the environment without changing temperature. The phase of a unit — liquid, solid, or melting — can be determined from a resistivity measurement, so that the units can be switched on automatically.

In tests on developmental models, a quartz crystal can filled with cadmium metal (melting point 320° C) was placed on a 1-inch (2.54-cm) container with a total mass of 60 grams. Such a unit maintains the crystal temperature within a few tenths of a degree for 10 minutes if the outside temperature changes sharply by 108° F (60°C) above the metal melting point. If the temperature excursion is 68° F (37.8° C), the crystal stays at the melting-point temperature for 30 minutes. The technique stabilizes the crystal temperature against temperatures below the melting point as well as against rises above it.

The transmission period can be extended by using many crystals, each immersed in a different alloy (see figure). The alloy compositions can be selected to provide a range of melting points so that the radio can transmit continuously as the ambient temperature changes. The alloy that is melting at any given moment is detected by measuring its electrical resistance: The bulk resistivity of the solid and liquid phases of many alloys differs by a factor of about 2. The crystals would be switched on in succession automatically so that at any given time, only the crystal under the best temperature control would be transmitting.

This work was done by James B. Stephens and Charles G. Miller of Caltech for **NASA's Jet Propulsion Laboratory.** *For further information, Circle 9 on the TSP Request Card.*
NPO-15641, NPO-15642, and NPO-15643

Books and Reports

These reports, studies, and handbooks are available from NASA as Technical Support Packages (TSP's) when a Request Card number is cited; otherwise they are available from the National Technical Information Service.

SCM Handbooks for dc-to-dc Converters

Two documents aid in the design of control modules for dc-to-dc converters.

A dc-to-dc regulated converter can be divided into two parts: a power circuit and a control circuit. The power circuit handles the energy transfer from the source to the load. The control circuit manages the rate of the source/load energy transfer as a function of load. During transient operations, the control circuit provides protection against catastrophic failure to all converter elements.

The electrical performance of a dc-to-dc converter depends heavily on the quality of its control system. The incentive of performance improvement prompted the initial development of a multiple loop control concept at NASA in the late sixties. Since then, the control concept has undergone several major program efforts, culminating in the development of a standardized control module (SCM). Three power-stage configurations were utilized: buck, boost, and buck/boost.

Features of the SCM include:

- Adaptive stability: The multiple loop control used in the SCM will accommodate changes in power/control parameters, including those due to reactive loading, and adaptively maintain the converter-load system stability.
- Power component stress limiting: The SCM limits the instantaneous electrical stresses in all converter power components, ensuring orderly and predictable steady-state and transient operations.
- Implementation of various control laws: The SCM is capable of implementing a large number of control laws through minimal circuit changes.
- Unified design approach: The SCM involves a design procedure that enables the designer to select the control circuit parameters so that for an arbitrarily-chosen power stage, prescribed performance characteristics for parameters like stability, audiosusceptibility, and transient response can be met concurrently.

Application and User's Handbooks (two volumes) now available were developed for the Lewis Research Center under NASA Contract NAS3-20102 with TRW Defense and Space Systems and Virginia Polytechnic Institute and State University. The objective of this contract was to provide concise analysis and design guidelines for the SCM. The analysis and guidelines, which are contained in the two handbooks, should enable an engineer to readily design the SCM circuit best suited to his or her specific needs and to confidently predict the resulting overall converter performance.

This work was done by F. C. Lee and M. F. Mohmoud of Virginia Polytechnic Institute and State University and Y. Yu of TRW Defense and Space Systems Group for **Lewis Research Center.** *Further information may be found in:*

NASA CR-165172 [*N81-10301/NSP*], *"Application Handbook for a Standardized Control Module (SCM) for DC to DC Converters Volume I"* [*$20.50*], *and*

NASA CR-165173 [*N81-11314/NSP*], *"User's Design Handbook for a Standardized Control Module (SCM) for DC to DC Converters Volume II"* [*$16*].

Copies of these reports may be purchased [prepayment required] from the National Technical Information Service, Springfield, Virginia 22161.
LEW-13886

MiniBriefs describe NASA innovations and reports in an abbreviated format. Readers desiring additional information on these items should request the Technical Support Packages (TSP's), available in most cases, which can be obtained by using the TSP Request Card at the back of this issue.

Solid-State Crossbar Switch

It combines analog and digital circuits for multiline/multiport switching.

A bidirectional solid-state crossbar switch provides interfacing and switching for 16 × 24 coordinate ports for 16 parallel signal lines. It is intended for rapid manual-controlled or computer-controlled reconfiguration of distributed computing systems.

The switch allows for the connection of any one port, of a set of 16 ports, to any one of another set of 24 ports. Any one of the remaining 15 of the first set may be connected to any one of the remaining 23 of the second set, and so on. A total of 16 data paths are thus possible.

This work was done by Tage O. Anderson of Caltech for **NASA's Jet Propulsion Laboratory.** *For further information, Circle 10 on the TSP Request Card.*

This invention has been patented by NASA (U.S. Patent No. 4,331,956). Inquiries concerning nonexclusive or exclusive license for its commercial development should be addressed to the Patent Counsel, NASA Resident Office-JPL [see page A5]. Refer to NPO-15066.

Detecting Defective Solder Bonds

The method is noncontact and nondestructive.

A technique detects defective solder bonds in a solar array or other large circuit board, using a thermal-imaging camera. The board is placed between a heat lamp and the camera. Poor joints are indicated by "cold" spots on the infrared image. This technique does not require any physical contact with the board, which is heated only a few degrees centigrade. The thermal images can be stored on a videotape.

This work was done by Roy Paulson, Jesus Barney, and Herman J. Decker of Lockheed Missiles & Space Co., Inc., for **Marshall Space Flight Center.** *For further information, Circle 11 on the TSP Request Card.*
MFS-25507

Blowing Dust Away With Electrostatic Wind

Ionized air molecules drive away contaminants.

An electrostatic "wind" sweeps dust away from the vicinity of high-voltage equipment. The wind is generated by a sharply pointed needle held at a voltage in the range from 10 to 25 kilovolts. The high electric field near the needle point releases electrons, which ionize air molecules (primarily oxygen). Repelled by the electrostatic field, the ions sweep dust molecules away.

The electrostatic wind prevents dust buildup and subsequent electrical breakdown in powerlines, transformers, switchgears, Van de Graaff generators, electrostatic precipitators, and other high-voltage equipment. It makes periodic cleaning or air blasting unnecessary.

This work was done by Merwyn G. Utter of the University of Arizona for **NASA Headquarters.** *For further information, Circle 12 on the TSP Request Card.*
HQN-10936

Improved Coil for Hydrogen Dissociators

The flat coil has a rigid printed-circuit substrate.

A printed-circuit substrate provides a rigid support for the flat spiral coil used to apply a radiofrequency (RF) field to a hydrogen plasma. Coupling coils for hydrogen dissociators must be supported mechanically to withstand vibration and shock.

The new coil structure also minimizes the RF electric field near the glass walls of the plasma vessel and therefore reduces direct electron bombardment of the glass. The design lends itself well to high production and standardized dimensions.

This work was done by R. F. Vessot of the Smithsonian Institution for **Marshall Space Flight Center.** *For further information, Circle 13 on the TSP Request Card.*

Inquiries concerning rights for the commercial use of this invention should be addressed to the Patent Counsel, Marshall Space Flight Center [see page A5]. Refer to MFS-25638.

The Effect of Cosmic Rays on MSI Devices

Low-power logic devices are susceptible to cosmic-ray particles.

Five MSI (medium-scale-integration) device technologies, including TTL, low-power TTL, Schottky, CMOS, and low-power Schottky, were subjected to a 120-MeV krypton-ion beam from a cyclotron and monitored for single-event upsets. The test results show that low-power TTL and low-power Schottky devices are affected by cosmic-ray nuclei, with the Schottky devices being the most sensitive. The results could find terrestrial application for radiation-hardening of electronic devices and systems. The tests were undertaken because galactic cosmic rays were suspected to be the cause of some anomalous single-bit changes in volatile data stored onboard satellites.

This work was done by Donald K. Nichols and William E. Price of Caltech and John P. Woods of MIT for **NASA's Jet Propulsion Laboratory.** *For further information, Circle 14 on the TSP Request Card.*
NPO-15779

Cooling Waveguide Flanges in Microwave Transmitters

Flange appendage circulates coolant for conductive heat removal.

Waveguides are normally cooled by water tubes, the cooling passages of which bypass the flanges that hold the guides together. During operation, the

sharp temperature rise in the flange reduces power transmission and can result in breakdown or plasma arcing. To conductively cool the flange, it can be modified by adding an appendage through which coolant would circulate.

The flange appendage includes a bore that accommodates the coolant tube. An O-ring surrounds the bore so that when adjacent waveguide sections are bolted together, a continuous conduit is formed for the coolant. A pressure-release groove in the modified flange prevents coolant from entering the waveguide should an O-ring seal fail.

This work was done by Bill C. J. Chen and Robert W. Hartop of Caltech for **NASA's Jet Propulsion Laboratory.** *For further information, Circle 15 on the TSP Request Card.*

This invention has been patented by NASA (U.S. Patent No. 4,382,239). Inquiries concerning nonexclusive or exclusive license for its commercial development should be addressed to the Patent Counsel [see page A5]. Refer to NPO-15401.

Uncooled IR Detector

Detector combines a liquid-crystal film with a light-sensitive solid-state array.

An infrared (IR) image detector consists of a heat-responsive liquid-crystal film between a visible-light source and a light-sensitive solid-state array. The combination detects IR images with continuous readout and potential for image storage. It requires no cooling, unlike most solid-state IR detectors that must be cooled to reduce background noise.

The liquid-crystal film acts as an IR detector when maintained just below the temperature of transition from opacity to transparency. When IR radiation is absorbed by this film, the resultant heating changes its visible-light transmission, thereby modulating the uniform visible-light beam as it passes through the film. The variation in light intensity is then read by the detector array.

This work was done by Paul J. Shlichta of Caltech for **NASA's Jet Propulsion Laboratory**. *For further information, Circle 16 on the TSP Request Card.*
NPO-14832

Transmitting Electromagnetic Energy into Liquids

A rough liquid surface enhances coupling.

Agitating the surface of a liquid-nitrogen bath with periodic or aperiodic excitation enhances the electromagnetic coupling between a microwave horn and a blackbody temperature standard immersed in the liquid. A possible 2 K error in the brightness temperature of the source, caused by surface reflections, is overcome by the agitation. The rough liquid surface provides a gradual and improved impedance transition between the atmosphere and the liquid nitrogen.

The impedance transformation may be useful in other interfaces between electromagnetic radiation and liquids. Biomedical, radar, and meteorological applications are examples.

This work was done by Edward J. Johnston of Caltech for **NASA's Jet Propulsion Laboratory.** *For further information, Circle 17 on the TSP Request Card.*
NPO-15868

Improved Two-Phase Switching Regulator

The coupled-inductor polyphase regulator has better efficiency and lower inductor losses.

An improved two-phase switching regulator employs negative coupling between the inductors to achieve a better power-to-weight ratio while reducing peak switching currents and inductor losses. Although conventional two-phase switching regulators generate significantly-lower input and output ripple compared with their single-phase counterparts, they do not improve inductor or switching-device utilization. Design equations and tables were developed and measured results were obtained for several breadboard systems. Inductor utilization was shown to improve by about 35 percent using the new technique.

This work was done by Wally E. Rippel of Caltech for **NASA's Jet Propulsion Laboratory.** *For further information, Circle 18 on the TSP Request Card.*

Inquiries concerning rights for the commercial use of this invention should be addressed to the Patent Counsel, NASA Resident Office-JPL [see page A5]. Refer to NPO-15172.

Ti/Pd/Cu Contacts for Semiconductor Devices

Copper systems are equivalent in performance to silver or gold systems.

Titanium/palladium/copper contacts for semiconductor devices perform as well as the more expensive silver and gold systems now used. A 300-Å titanium layer and a 200-Å palladium layer are deposited on the semiconductor device by electron-beam evaporation. The desired contact pattern is etched using photoresist. A thin layer of copper is plated on the contact pattern from a cyanide solution. The copper layer is then built up to 4 to 8 microns by electroplating from an acid solution.

This work was done by Robert B. Campbell and Ajeet Rohatgi of Westinghouse Electric Corp. for **NASA's Jet Propulsion Laboratory.** *For further information, Circle 19 on the TSP Request Card.*
NPO-15043

Improved High-Current Drive Circuit

It uses a VMOS field-effect power transistor.

A high-current drive circuit, such as those used for solar-panel loads, employs an n-channel enhancement-mode VMOS field-effect power transistor to eliminate the problem of oscillation at high power encountered in conventional circuits with bipolar transistors. The drive voltage required is typically 1 to 3 V for a load current of 10 A.

The circuit is fast because the low input capacity of the VMOS transistor keeps the RC time constant in the low millisecond range even with a 10-kΩ drive resistance. In addition, there are no current-storage problems such as those associated with the bipolar transistors.

This work was done by Steven W. Cole of Caltech for **NASA's Jet Propulsion Laboratory.** *For further information, Circle 20 on the TSP Request Card.*
NPO-14938

Programable Power Conditioner

It accepts a range of inputs and produces a range of outputs.

A versatile power conditioner can be programed to handle power from a wide range of sources such as solar arrays, fuel cells, and electrochemical batteries. It can also be programed to regulate voltage over the range of 20 to 180 volts dc, maintain a constant current at any value between 0 and 100 amperes, provide impedance matching between sources and loads, and provide changing voltages and currents on the basis of sensor measurements (for battery charging, for example).

The conditioner consists of two parts. The power stage is a switching regulator. A controller stage uses a microprocessor to generate an analog control signal for the power stage.

This work was done by John R. Lanier, Robert E. Kapustka, James R. Graves, John R. Bush, and Eugene Perry of **Marshall Space Flight Center.** *For further information, Circle 21 on the TSP Request Card.*
MFS-25531

Antenna for Imaging Sea Ice

An antenna for imaging of the polar regions could have terrestrial applications.

A synthetic-aperture-radar antenna operates at X-band and provides a 360-km-wide continuous-image swath from a 700-km orbit. The antenna consists of four horizontally-polarized 19.0-by 0.6-m planar waveguide arrays and appropriate feed networks mounted on a single aluminum supporting structure. The arrays are arranged in a "W" configuration to point the antenna beams at the proper crosstrack angles.

Each antenna array is made of eight sections approximately 2.4 m long and 0.6 m wide, uniformly fed by an eight-way corporate feed. Each array is composed of slotted half-height, thin-wall copper-plated graphite/epoxy waveguides. The antenna is suitable for high-quality imaging of sea ice in polar regions above 60° latitude and should be of interest to designers of similar antenna systems.

This work was done by Frank T. Barath and Rolando L. Jordan of Caltech for **NASA's Jet Propulsion Laboratory.** *For further information Circle 22 on the TSP Request Card.*
NPO-15352

Electronic Systems

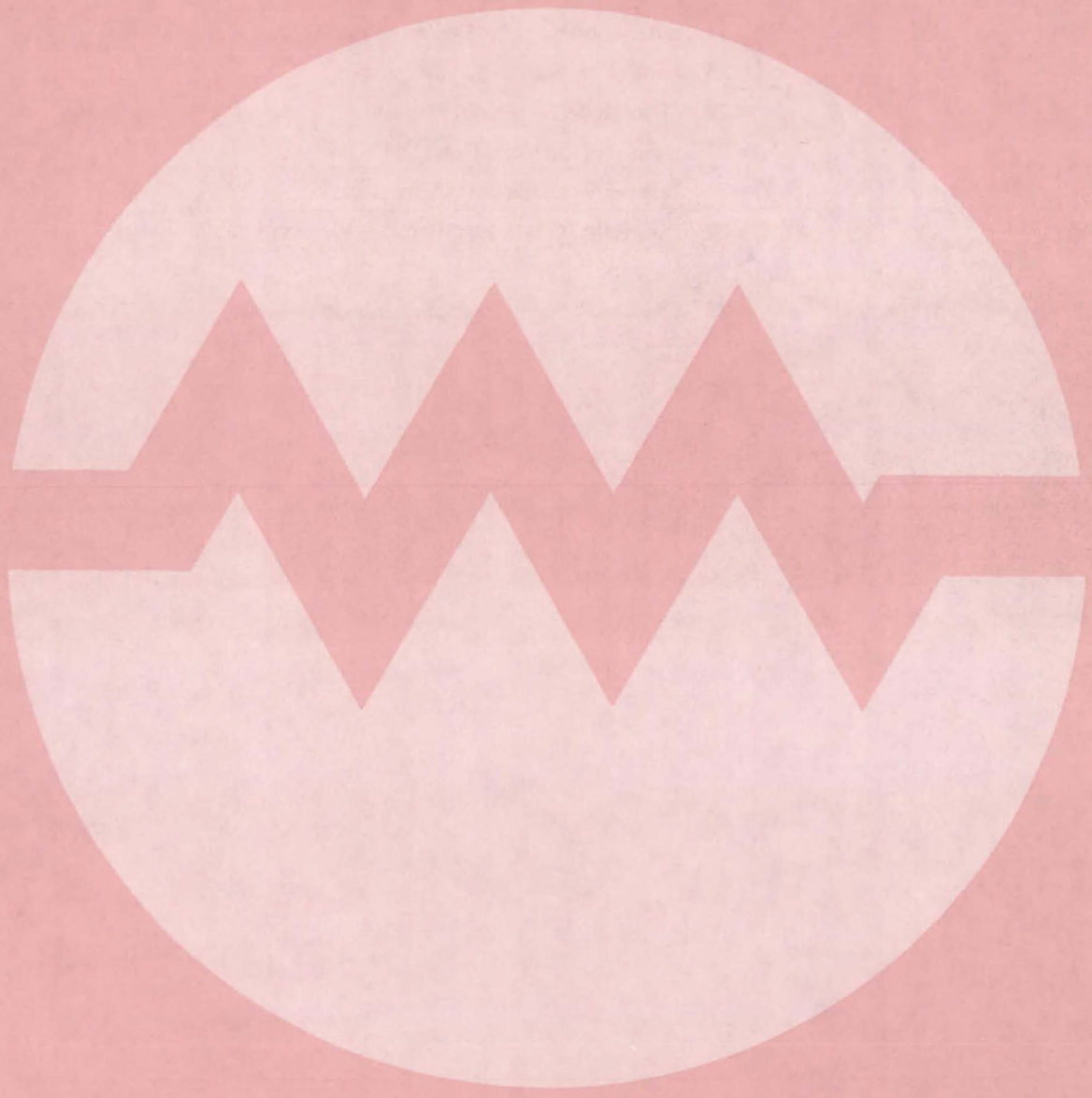

Lightning-Transient Recorder

A battery-powered system operates for more than a year.

NASA's Jet Propulsion Laboratory, Pasadena, California

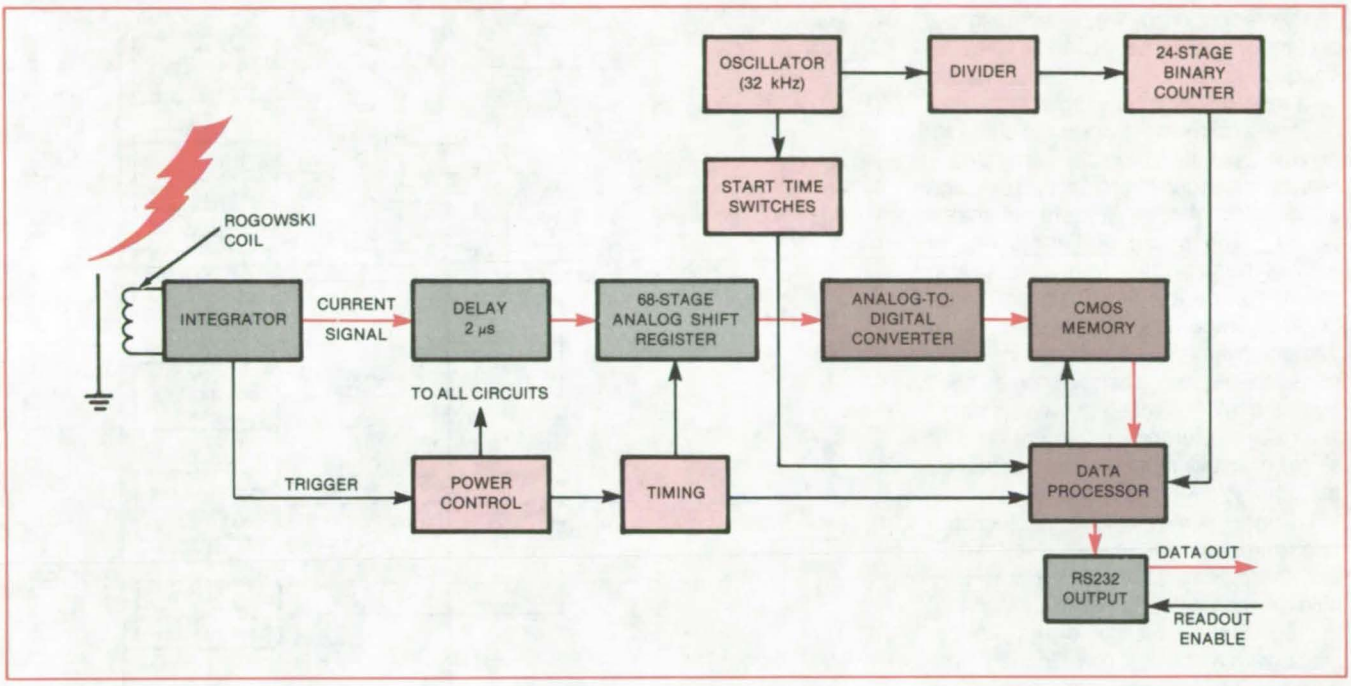

The **Lightning-Transient Recorder** digitizes and records up to 146 current samples at selected intervals during a lightning stroke. The system operates unattended on battery power for more than a year.

Currents induced by lightning are recorded automatically by the system diagramed in the figure. Powered by 23 alkaline C-cells and 5 D-cells, the unit can be left unattended in the field until read out and reset by a portable data collector.

In the new system, the rate of change of current in a lightning arrester is sensed by a Rogowski coil (a coil wound around a toroidal core that surrounds the current-carrying wire). The coil output is integrated to produce a current signal. The current signal is passed through a 2-μs delay line while a trigger signal derived from the coil output initiates the power-control and timing functions.

At the end of the 2-μs delay, the analog shift register is ready to process data. During the 109 μs before the first data sample emerges from the analog shift register, the analog-to-digital converter and the microprocessor are initialized. The analog-to-digital converter has 256 quantization levels from −75.00 to 74.41 kA.

After digitization, the data are stored in a static complementary-metal-oxide/semiconductor (CMOS) memory. Battery power is supplied to the memory at all times to preserve the data. Data output is initiated by momentarily closing the output-request switch.

Several features are included to prevent the loss of data: Readout will not take place unless the data collector is plugged into the output connector, as indicated by a "readout enable" signal. The data are read out twice, then the memory clears automatically. The readout stops and the data are preserved in the memory if the "readout enable" signal is interrupted during data collection.

The system employs a varying sample rate that provides the highest time resolution at the beginning of the stroke, when it is needed most. The sampling sequence is as follows: 1 at 0.1 μs, 14 at 0.2 μs, 1 at 1 μs, 52 at 2 μs, 1 at 20 μs, 67 at 40 μs, and finally 10 at 40 μs taken at 400-μs intervals. The processing and storage of all 146 samples require about 10 ms.

To save memory space the processor works backward through the stored data to delete all values within 0.6 kA of zero. The first 18 samples are always saved, however, regardless of their magnitudes. This editing is not completed if another stroke triggers the unit during the process.

The system includes a clock to label the data according to time. A 32,568-Hz oscillator output is divided down to provide a ½-Hz clock counted by a 24-stage binary counter with a full range of about 1.06 years. Up to 50 time tags for separate lightning strokes can be recorded. The memory can store the full 146 samples of 15 strokes. The system will continue to store time tags of lightning strokes even if the transient-current memory is full.

This work was done by Richard L. Grumm of Caltech for **NASA's Jet Propulsion Laboratory.** *For further information, Circle 23 on the TSP Request Card.*

NPO-15895

Virtual-Center Antenna-Arraying System

Separate signals are averaged to produce a reference frequency and phase.

NASA's Jet Propulsion Laboratory, Pasadena, California

The reception of weak radio signals and the measurement of the source location or direction would be enhanced by a new way of combining signals from multiple antennas. The outputs of the receivers associated with the separate antennas are added to produce an average signal from which a reference signal is derived. The phase and frequency of each of the separate antennas relative to the reference are then tracked by the separate receivers. This system is expected to have lower phase jitter with consequently higher signal/noise ratios than the older "master/slave" system where the reference is generated at a single (master) antenna and tracked by the other (slave) antennas.

Using a geometric analogy, the separate antennas are called "vertexes," and the place where the separate signals are combined is called the "virtual center." The center may or may not coincide with a physical point in the antenna array. As shown in the figure, the system includes a number of long feedback loops, running between the vertexes and the center, and short loops at the vertexes, by which the local oscillators in the receivers track their local offset from the reference phase and frequency.

The output of each receiver is band-pass-filtered to eliminate the data portion of the signal. The remaining signal S_k of the kth receiver includes the received carrier of frequency ω_0 and phase ϕ_k, plus noise n_k. This is fed to a first mixer, the other input of which is the center (reference) signal of frequency ω_1 and the estimated carrier phase $\hat{\theta}_0$. The low-pass-filtered mixer output L_k consists of a sinusoid of frequency $\omega_0 - \omega_1$ and phase $\theta_k - \hat{\theta}_0$, plus a noise-modulated version of the reference signal. L_k is fed to a second mixer. The other second-mixer input is the output W_k of the voltage-controlled oscillator of the kth vertex loop, which has frequency $\omega_0 - \omega_1$ and phase $\hat{\theta}_k$, the phase estimate of the kth vertex.

After the second mixer and low-pass filtering, the resulting signal X_k is a sinusoid of phase $\phi_k(t) = \theta_k(t) - \hat{\theta}_k(t) - \theta_0(t)$, plus a narrow-band Gaussian noise $N_k(t)$ (where t = time). Each X_k is passed through the vertex filter F_k, the output Y_k of which controls the oscillator of the kth vertex loop. The X_k are also summed with relative weights β_k to produce $Z(t) = \Sigma\beta_k X_k$ at the summing junction. Z is filtered by F_0 to produce Y_0, which controls the reference oscillator.

With the vertex-loop bandwidth set at about one one-hundreth that of the center-loop bandwidth, the phase jitter is made nearly equal to that of an ideal combined-carrier-reference array. The performance is essentially the same as that of a single antenna having an aperture equal to the sum of the individual antenna apertures. The virtual-center arraying system should be useful in applications requiring accurate phase estimates; for example, in reception of weak telemetry signals, in transmitter or reflector locating, nondestructive testing of structures, or geophysical exploration.

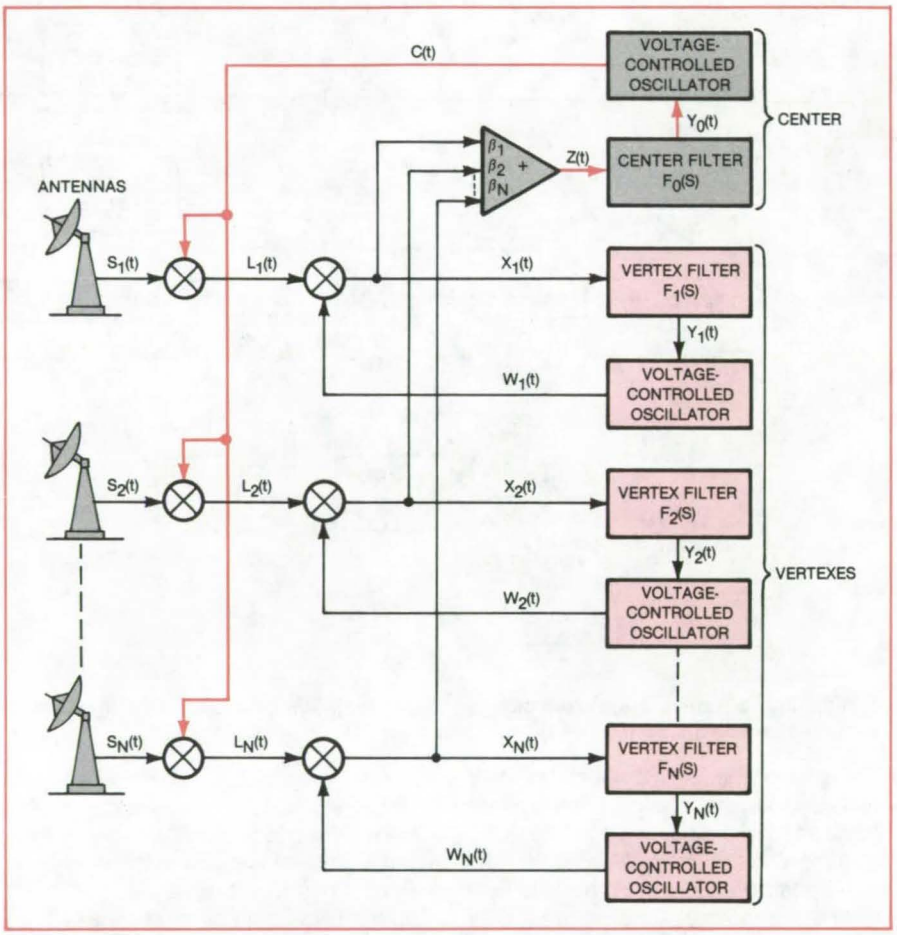

The **Virtual-Center Antenna-Arraying System** develops a reference carrier from the separate received signals. The phase of the signal at each receiver is determined by comparison with the reference phase.

This work was done by Leslie J. Deutsch, James W. Layland, Richard G. Lipes, and Robert L. Miller of Caltech for **NASA's Jet Propulsion Laboratory.** *For further information, Circle 24 on the TSP Request Card.*

NPO-15874

Phased-Antenna-Array Conical Scanning

Antenna pointing is faster than in mechanical scanning.

NASA's Jet Propulsion Laboratory, Pasadena, California

A proposed technique for pointing the beam of a phased-array antenna system would combine the advantages of single-antenna conical scanning and dual-beam phased-array scanning. Fine antenna pointing with the new technique would be much faster than is possible by mechanical rotation. The technique should have many uses in military and civilian radar, principally in tracking aircraft, balloonborne weather instruments, and other moving signal sources or reflectors.

In its simplest form, the new technique would employ three antennas (see figure), though more could be used. The sharp central lobe (the beam) of the phased array points in a direction that depends on the relative phase shifts of the signals received or transmitted by the three antennas. This system uses two sets of phase shifters so that the array simultaneously receives signals from two independently controllable beams that point in slightly different directions.

One of the beams (the scanning beam) operates in the conical-scanning mode; that is, it revolves at a small difference in pointing angle around the estimated line of sight to the target. When there is a pointing error, the power at each receiver varies at the scanning frequency, and corrections are made to the estimated line of sight in response to these variations. When the estimated line of sight is correct, the power is relatively constant in all three receivers.

The other (tracking) beam is directed along the estimated line of sight so that tracking or data reception or both can continue without the interfering effects of excessive offcenter attenuation and conical-scan-rate flutter. The tracking beam thus maintains the highest-available signal-to-noise ratio at all times.

Electronic beam-rotation rates of several kilohertz should be possible in telemetry systems having data rates of hundreds of kilobits per second and in tracking systems without data transmission. This contrasts with rates as low as 10^{-2} Hz for mechanical conical scanning of large antennas. With the faster electronic scanning the antenna system easily continues to track the target during wind gusts and follows target motion. Furthermore, scanning rates of several kilohertz would grant some immunity to received-signal amplitude variations caused by target rotation, weather changes, or ionospheric effects, all of which would be slower than the conical-scan flutter.

The dual-beam technique would ordinarily be used in conjunction with a mechanical antenna-pointing system that performs the slow, gross pointing adjustments. The new technique would save the energy that would otherwise be expended in mechanical conical scanning.

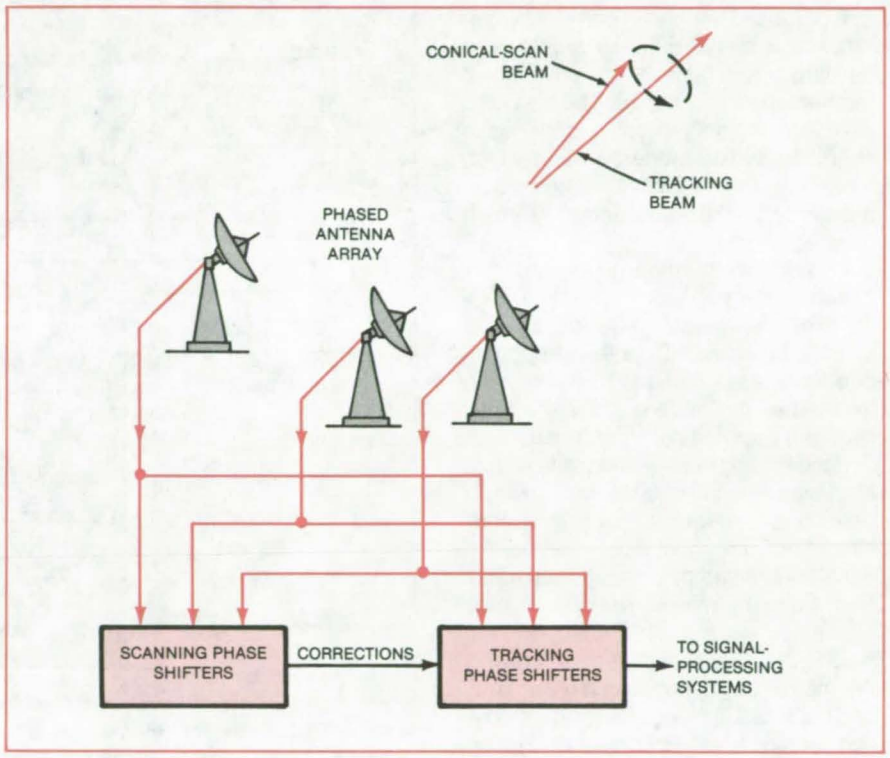

A **Three-Antenna Phased Array** is connected to the receiving signal-processing system through two phase-shifting networks. The two networks simultaneously steer the phased array in two slightly-different beam directions: one for scanning and one for tracking.

This work was done by James R. Lesh of Caltech for **NASA's Jet Propulsion Laboratory.** *For further information, Circle 25 on the TSP Request Card.*

This invention is owned by NASA, and a patent application has been filed. Inquiries concerning nonexclusive or exclusive license for its commercial development should be addressed to the Patent Counsel, NASA Resident Office-JPL [see page A5]. Refer to NPO-15899.

Binary Correlator for Electromagnetic Signal Patterns

Modulation patterns are recognized without extensive calculations.

Goddard Space Flight Center, Greenbelt, Maryland

A proposed method of correlating digitized radio-signal patterns promises to be simpler and faster than conventional mathematical techniques. The new concept was originally developed for use in search-and-rescue operations in which a passing satellite picks up a frequency-modulated distress signal from a downed aircraft.

In addition to the modulation produced by the transmitter, the frequency shift of the signal received by the satellite includes a Doppler component due to satellite motion. To identify the transmitter, the receiving system must separate the modulation component.

If the signal frequency is digitized and displayed in matrix form with rows of time bins and columns of frequency bins, then the modulation component can be identified as a recognizable pattern within the matrix. The matrix is implemented with a set of shift registers (see figure). Each shift register (row of the matrix) corresponds to a given time, and each cell in a register (column position within a row of the matrix) corresponds to a given frequency. Corresponding cells in the registers represent the same frequencies.

When a particular frequency is detected at a particular time, the appropriate cell contains a 1. The collection of 1's in all the cells in the shift registers forms a pattern that represents the time/frequency pattern of the total received signal, and the subpattern of the expected distress signal may be embedded somewhere within the pattern.

To determine whether the expected subpattern is present, the correlator compares the total pattern with the expected pattern: First, the individual registers are shifted to the right. Each register is shifted by the number of cells that the expected 1's would have to be shifted to form a column of 1's in the rightmost cells. These last cells provide input to an analog resistive summing network. If there is a perfect match to the expected pattern, then all inputs will equal 1 and the analog output will have the large value that indicates correlation.

In practice, a few end cells will contain 0's even with the pattern present because of noise and lost bits. The analog output level that is considered to indicate correlation will therefore depend on the anticipated noise level and the desired confidence level.

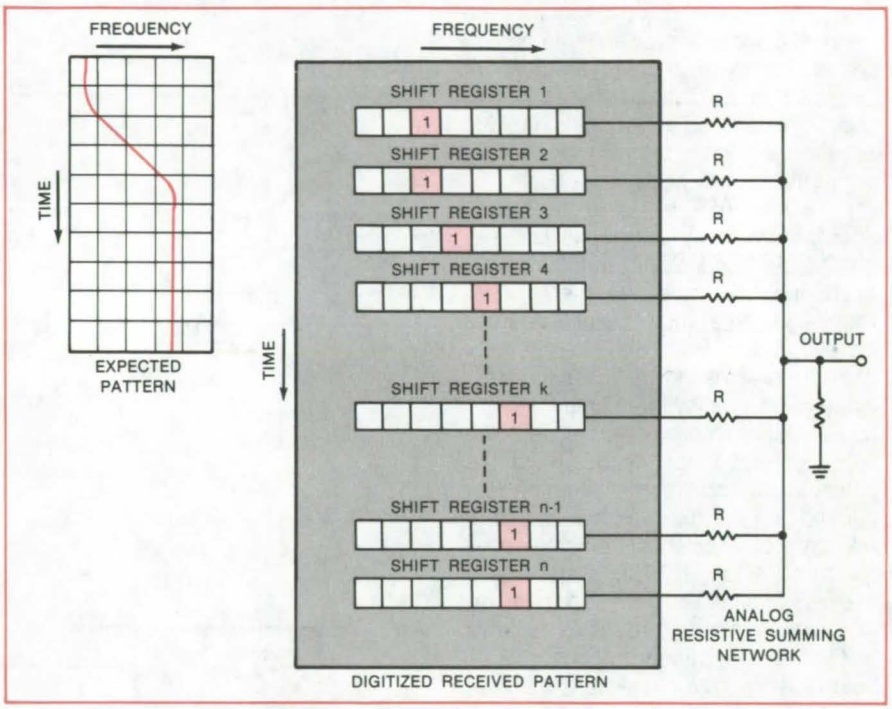

A Set of Shift Registers contains the pattern of 1's and 0's representing the presence or absence of a received signal in the designated time/frequency bins. The pattern in the shift registers is correlated with the pattern of the expected signal by first shifting the bit in each cell to the right according to the expected pattern and then summing the shift-register outputs in the analog summing network.

Once a particular submatrix has been searched, a new submatrix is searched. This can be done in two ways:

- When the individual registers have each been individually shifted according to the expected pattern, they can be shifted to the right and left together, one column at a time, so as to scan across the matrix. This would be equivalent to removing an unknown frequency bias caused by local oscillator offset.
- The horizontal scans described above can be repeated after a vertical shift of all data from each cell to the corresponding cell in the next shift register. This would be equivalent to a search over time to remove clock bias or along-track position uncertainty.

In addition to beacon recognition, the new technique may be useful in other applications requiring the identification of a smaller pattern of 1-bit data within a larger matrix of such data. One example might be the detection of expected features in synthetic-aperture-radar scans. With current VLSI capability, an array of several hundred elements on a side could be placed on a single chip. Also, the horizontal axis could represent a signal feature other than frequency for different applications.

This work was done by John B. Garrison and Robert E. Jenkins of Johns Hopkins University for **Goddard Space Flight Center.** *For further information, Circle 26 on the TSP Request Card.*

This invention is owned by NASA, and a patent application has been filed. Inquiries concerning nonexclusive or exclusive license for its commercial development should be addressed to the Patent Counsel, Goddard Space Flight Center [see page A5]. Refer to GSC-12714.

Radar Cuts Subsoil Survey Costs

Soil features are located with minimum time and labor.

John F. Kennedy Space Center, Florida

A ground-penetrating radar (GPR) system supplements manual and mechanical methods in performing a subsurface soil survey. The mobile system obtains a graphic profile of soil discontinuities and interfaces as a function of depth. Only one or two test borings may be necessary to substantiate the soil profile.

The GPR is an impulse radar system operating within a frequency range of 80 to 1,000 MHz. An antenna coupled to the ground surface radiates repetitive electromagnetic pulses that penetrate from as little as 3 m to as deep as 20 m. The depth of penetration depends on the kind of soil, water content, and salt content. Radar is ineffective in high-salt-content soils, but water-saturated soils having low conductivity respond well to radar pulses.

The transmitted radar signals are reflected from underground discontinuities and are picked up by the radar receiver. These reflectors may be different soil horizons, soil/rock interfaces, artificial objects, or other materials with contrasting dielectric properties. Organic matter, salt content, clay mineralogy, particle size, and moisture content are some soil properties affecting dielectric properties.

The GPR signals are processed and displayed by a graphic recorder (see figure). As the antenna is moved along the surface, the recorder prints the vertical scan for each horizontal position: The strength of the instantaneous reflection is proportional to the degree of blackness printed for the corresponding depth. This produces a continuous profile resembling a cross section found at a roadcut.

The antenna can be towed at speeds up to 8 km/h for rapid exploratory work. Detailed studies can be performed by hand towing at very slow speed (0.5 km/h) or by placing the antenna at specific locations.

(continued on next page)

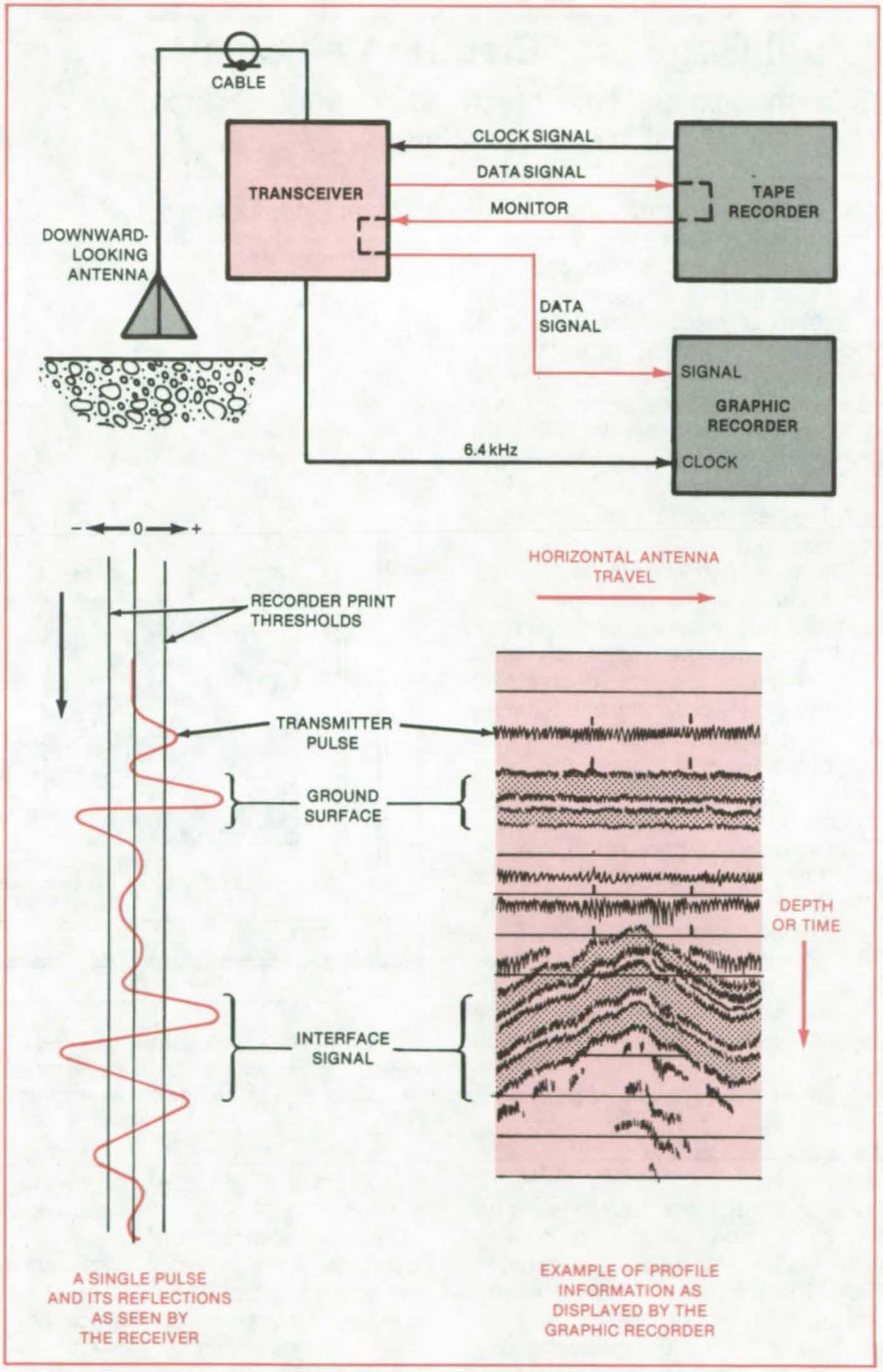

A mobile **Ground-Penetrating Radar System** antenna sends repetitive pulses into the ground to probe soil discontinuities and interfaces. The reflected pulses are displayed on a graphic recorder. The three-band display is a characteristic of the radar system.

The GPR-received pulse-stream pattern has three main components: the transmitted pulse that serves as a ground and time reference, a surface reflection, and the interface reflection. The vertical depth scale can be calculated if the soil dielectric constant is known or if the pulse travel time is measured for an interface of known depth.

GPR should prove useful as a reconnaissance tool. After a preliminary survey by GPR, a few borings can be made for more-detailed soil analysis at known depths.

This work was done by R. Wojtasinski of **Kennedy Space Center,** *R. W. Johnson of the U.S. Department of Agriculture, and R. Glaccum of Technos, Inc. For further information, Circle 27 on the TSP Request Card.*
KSC-11227

"Fuel Gage" for Electric Vehicles

Gas-emission and time-integrated-current measurements may indicate battery charge state.

NASA's Jet Propulsion Laboratory, Pasadena, California

The equivalent of a "fuel gage" for electric-powered vehicles may be an outgrowth of research at NASA's Jet Propulsion Laboratory. Tests there indicate the possibility of monitoring the state of charge of lead/acid batteries at any stage in the charging cycle by measuring the charging current and either gas evolution or electrode potential. The data would be processed by a microcomputer.

The system would combine data from these measurements (see figure) to give a readout of remaining useful charge, analogous to the indication of a gasoline-tank gage. The decrease in energy-delivery capability of the battery with increased discharge rate would be computed automatically.

The theoretical indicator of the state of charge is the time-integrated charging/discharging current, which would be monitored by an ammeter. However, this baseline must be corrected for losses due to gas generation. Thus, experiments were done to find a reliable indicator of the losses. Two parameters — the rate of gas evolution and the positive-electrode potential — were investigated.

Current readings were continuously taken from charging and discharging batteries and fed to a computer. Gas-flow meters were installed in the cell vents and their readings also fed to the computer. In some cases a probe electrode was used to measure plate potentials. The decrease in stored energy calculated by time-integrating the current reading was corrected by including the portion of the stored battery energy consumed in generating gas during the charge.

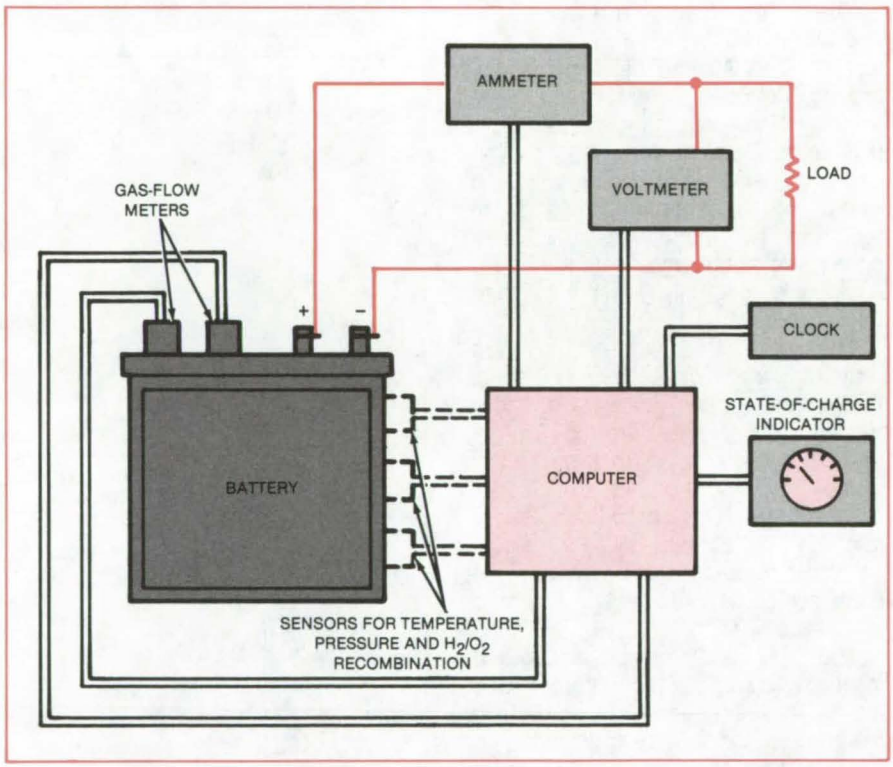

Current and Gas Evolution are monitored to obtain an indication of the remaining useful charge. Other potentially useful indications include cell voltage, cell pressure, cell temperature, and the rate of gas recombination on a catalyst.

Tests were performed on several different types of lead/acid batteries in various conditions of previous use, at various standardized charge and discharge rates. Despite some anomalies and statistical fluctuations, the measurements generally showed a correlation between the cell capacity estimated by the computer and the true capacity as measured by the actual energy delivered during the subsequent discharge.

For the development of a commercially viable system, it will be necessary to have a convenient method of continuously monitoring the rates of gas evolution. This would be difficult in practice and might be impossible for sealed batteries. A possible solution may be the measurement of the potential of positive electrodes with respect to that of reference electrodes: There appears to be a relationship between such measurements and the onset of gassing

in cells that have no antimony in the lead electrodes. Other possibilities may include monitoring the gas pressure in sealed cells or the temperature of a catalyst at which hydrogen and oxygen recombine into water.

This work was done by John J. Rowlette of Caltech for **NASA's Jet Propulsion Laboratory.** *For further information, Circle 28 on the TSP Request Card.*

Inquiries concerning rights for the commercial use of this invention should be addressed to the Patent Counsel, NASA Resident Office-JPL [see page A5]. Refer to NPO-15759.

Measuring Software-Execution Time

Test circuit times routines even during multiprogram operation.

John F. Kennedy Space Center, Florida

A test circuit measures software-execution time. The circuit generates a pulse that is started by a signal at the beginning address of the program under test and is ended by a signal at the ending address. The pulse duration is measured with a logic analyzer to determine the execution time.

Simple software routines can be timed by counting the number of instructions and calculating the total execution time. However, this method may be inaccurate when the program is running under an operating system in which other programs and input/output devices contend for CPU time.

The input signals for the tester are obtained from a memory-controller circuit board of the CPU. The input lines to the tester are well buffered to assure minimal loading of the CPU. The tester has its own power supply, so that no demand is made on the CPU power supply.

The circuit is built around two sets of comparators that trigger on the starting and stopping addresses. These addresses for a given routine are manually set with rows of switches on the front panel (see figure), each switch serving to connect or disconnect one of the bit lines of a comparator. Irrelevant ("don't-care") bits in an address are excluded from processing by setting switches in the bit masks — rows of switches similar to those of the address lines.

When an address signal (ignoring the "don't-care" bits) matches the address-switch settings, the normally-low comparator output goes high. Such a transition in the starting-address comparator causes one of the outputs of a J-K flip-flop to go high. When the stopping address is reached, a similar transition takes place in the stopping-address comparator, causing the J-K comparator to reset, with the output returning to the low state. The duration of the high output state is the pulse duration corresponding to the execution time. In case the stopping address is not reached, a switch on the panel allows the circuit to be reset manually.

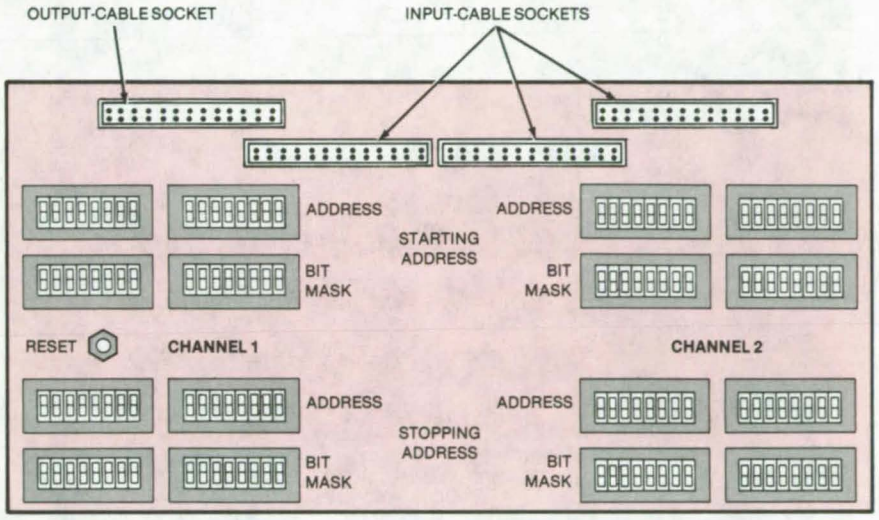

The **Front Panel** of the test circuit contains receptacles for three input cables and one output cable, a reset switch, and sets of address switches. The starting address for a channel is selected by a top cluster of switches, while the stopping address is selected by a bottom cluster of switches. Corresponding sets of bit-mask switches select "don't-care" (irrelevant) address bits.

This work was done by Carlos Pinera of International Business Machines Corp. for **Kennedy Space Center.** *For further information, Circle 29 on the TSP Request Card.*
KSC-11267

Telemetry Speeds Forest-Fire Control

An airborne system rapidly delivers hard copy to firefighters.

Ames Research Center, Moffett Field, California

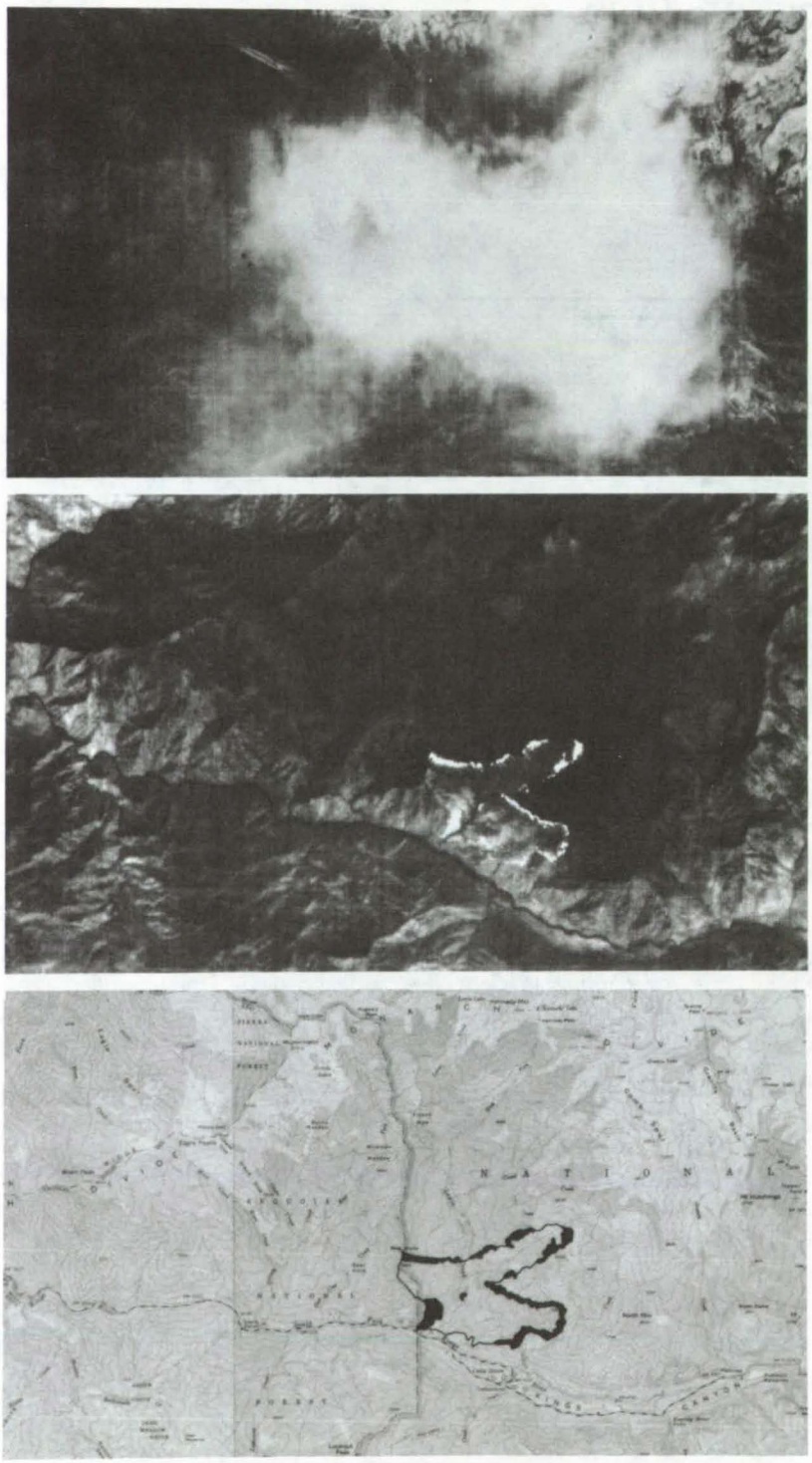

Real-Time Data-Link Images like these can be placed in the hands of firefighters 10 minutes after the airborne sensors scan the scene. At the top is the infrared image. The visible image is at the center, and a USGS map of the area is on the bottom.

Hard-copy images that show conditions along the complete perimeter of a forest fire are supplied quickly to firefighting teams by airborne electronics. Sensors in an airplane send data to a ground station for image processing, and the imagery is immediately transferred to U.S. Geologic Survey (USGS) maps by a photo interpreter. The maps are then transmitted by telecopier directly to the fire-control camps.

The total elapsed time from acquisition of data in the airplane to receipt by the fire camp is less than 10 minutes. The information therefore can be used to aid in decisions involving the deployment of firefighters and equipment. The same technique could be used in flood control, monitoring oilspills, observing thermal currents, and pollution monitoring.

In the forest-fire application in California, two complementary airborne sensors are used: a multispectral scanner operating in the infrared channel (8 to 14 microns) and a charge-coupled-device linear scanner with a far-red filter (0.8 to 1.1 microns). These spectral ranges provide good smoke penetration and burn-area definition.

Data from the scanners are transmitted in either digital or analog format via an L-band data link to a ground station and there processed into hard-copy imagery. The U-2 airplane carrying the sensors operates at an altitude of 21 kilometers, allowing line-of-sight transmission to a distance of 500 km. With the ground station at Ames Research Center (near San Francisco), virtually all forested lands in California can be observed. Additional ground stations or direct transmission to a geostationary satellite would allow real-time observations without geographic limitations.

The figure shows the visible image and the thermal infrared image of a fire in Kings Canyon National Park, as those images appeared in the data-link copy. The corresponding 1:62,500 USGS map is also shown.

This work was done by John C. Arvesen and James W. Cherbonneaux of **Ames Research Center.** *For further information, Circle 30 on the TSP Request Card.*

Inquiries concerning rights for the commercial use of this invention should be addressed to the Patent Counsel, Ames Research Center [see page A5]. Refer to ARC-11438.

Dual-Rate Transmission Reduces Weather Effects

Scheme ensures that maximum data are received on the average.

NASA's Jet Propulsion Laboratory, Pasadena, California

A dual-rate scheme for maximizing the data returned during a spacecraft mission, may be adaptable, as is or with modifications, to high-frequency terrestrial data transmission. The dual-rate scheme includes a minimum data rate for essential information, such as spacecraft "health" data and minimal image coverage. The scheme also includes a higher rate for "bonus" data that can only be received in good weather.

Telemetry rates must be set as high as possible to send all the data accumulated during a mission. Yet the higher the data rate, the worse the interference by adverse local weather conditions. Spacecraft operating near the outer planets and beyond are so far away that transmission times are too long to permit altering data rates to the momentary optimal values in accordance with receiver weather conditions. By the time the rate is changed in response to a command and the data received on Earth, the weather may have changed completely. A similar problem is presented by a terrestrial data transmitter that is not under the control of the receiving station.

If the data rate is fixed in advance at that minimum value that guarantees a reasonable prospect of success during bad weather, the total data transmitted may be too small to take full advantage of the mission. On the other hand, if too high a rate is chosen, there is a risk of losing all the data in bad weather.

The dual-rate transmission scheme puts the data into two channels. In one example of the dual-rate scheme, 47.8 percent of the power, containing the bonus data, would be at a rate of 0.5388 times the channel bandwidth. The code words for the base data would be assigned the remaining 52.2 percent of the average power and sent at a rate of one-eighth the channel bandwidth. The base code words would be centered as a "cloud" around the bonus code words. In bad weather, the bonus code words would look like Gaussian noise to a receiver: They could not be decoded; but if the weather were good, the bonus code words could be decoded and removed as noise by subtraction. The base code words could then be decoded.

Although the data rate in bad weather for the dual-rate strategy would be only half that of the traditional scheme, the enormous gain in clear weather would more than make up for this on the average. The dual-rate strategy would yield a net data rate 2.5 times the best achievable with a single transmission rate. This improvement is equivalent to a power gain of 4.6 dB.

This work was done by Edward C. Posner of Caltech for **NASA's Jet Propulsion Laboratory.** *For further information, Circle 31 on the TSP Request Card.*

NPO-15807

Books and Reports

These reports, studies, and handbooks are available from NASA as Technical Support Packages (TSP's) when a Request Card number is cited; otherwise they are available from the National Technical Information Service.

Charge Efficiency Tests of Lead/Acid Batteries

Current, voltage, and gas evolution were measured during charge/discharge cycles.

A series of standardized tests for evaluating the charging efficiency of lead/acid storage batteries is described in a new report. The purpose of these tests was to provide information for the design of a battery charger that will allow maximum recharge efficiency for electric-vehicle batteries consistent with other operating parameters, such as range, water loss, and cycle life.

After suitable development, more-exotic battery types may eventually dominate in electric vehicles; but in the near future the widely-available lead/acid type will be used. Extensive data are available on the use of lead/acid batteries in automotive-starter and telephone-system applications but relatively little on their use as primary energy sources in electric vehicles. The tests described in the report were run to improve the understanding of specific processes during charging and of their effects on charging efficiency.

(continued on next page)

The report contains numerous graphs of cycle tests and other data concerning the performance of lead/acid batteries in electric vehicles. Six battery samples were tested with various charge/discharge cycling procedures. The six batteries were divided into two groups of three, with one group being designated "new" and the other "aged." The aged group was put through 200 deep cycles before beginning the testing phase. The current and voltage of the batteries were recorded at temperatures of 0°, 20°, and 49° C. Oxygen concentration was monitored continuously during charging. The total gas-evolution rate was determined many times during charge. Although the results pertain to one model of a proprietary battery, the general conclusions on charge/discharge are expected to be the same for other lead/acid batteries considered for electric vehicles.

Recommendations are presented both for charging and for measuring the state of charge. The report cautions that the charge-acceptance characteristics of lead/acid batteries may vary significantly from one manufacturer to another or among different models from one manufacturer.

This work was done by John J. Rowlette of Caltech for **NASA's Jet Propulsion Laboratory.** *To obtain a copy of the report, "Electric and Hybrid Vehicle's Charge Efficiency Tests of ESB EV-106 Lead-Acid Batteries," Circle 32 on the TSP Request Card.*
NPO-15869

MiniBriefs describe NASA innovations and reports in an abbreviated format. Readers desiring additional information on these items should request the Technical Support Packages (TSP's), available in most cases, which can be obtained by using the TSP Request Card at the back of this issue.

Extending the Memory of Microcomputers

Memory is increased while retaining real-time capabilities.

Extra memory capacity can be added to a microprocessor without increasing the memory address length and without special transfer instructions. It is done by dedicating a block of space in the main memory to hold the addresses of locations in the extra memory. A special circuit added to the microcomputer recognizes commands that signify the use of the extra memory. The extra memory block is then substituted on the address bus for the base memory. The commands are then executed on the contents of the extra memory, rather than on the contents of the main memory.

This work was done by Gordon A. Wiker of Caltech for **NASA's Jet Propulsion Laboratory.** *For further information, Circle 33 on the TSP Request Card.*

Inquiries concerning rights for the commercial use of this invention should be addressed to the Patent Counsel, NASA Resident Office-JPL *[see page A5].* *Refer to NPO-15295.*

Radio-Frequency and Wideband Modulation Arraying

The summing network receives coherent signals from all the receivers in an array.

A method sums the narrow-band radio-frequency (RF) carrier powers and wide-band spectrum powers of an array of separate antenna/receiver systems designed for phase-locked-loop or suppressed-carrier operation. The group delay of the separate antennas and RF systems is equalized by settable acoustic surface-wave delay lines in the intermediate-frequency stage of each receiver and vernier controlled by delay servo loops, each operating from a digital controller. The controlled delay is thus adjusted to provide phase-correlated signals at the spectrum summing junction, which combines the spectrum power outputs of all the receivers in the array.

This work was done by Milton H. Brockman of Caltech for **NASA's Jet Propulsion Laboratory.** *For further information, Circle 34 on the TSP Request Card.*
NPO-15030

Improved Coal-Thickness Measurement

Summed signals and a dielectric-filled antenna improve the measurement.

An improved FM radar for measuring the thickness of a coal seam eliminates spectrum splitting and reduces the magnitude of the echo from the front coal surface. To eliminate spectrum splitting, which produces two apparent echoes and reduces the operator's ability to determine target range, the FM signal is produced by combining the usual frequency ramp with a lower frequency signal. The return signals are mixed with a sample of the transmitted signal to create difference-frequency signals for a spectrum analyzer.

The echo problem is solved by reducing dielectric mismatch. The horn antenna and its waveguide are filled with a material having a dielectric constant close to that of coal and the mouth of the horn is placed against the coal face.

This work was done by Thomas A. Barr of **Marshall Space Flight Center.** *For further information, Circle 35 on the TSP Request Card.*

This invention has been patented by NASA (U.S. Patent No. 4,161,731). Inquiries concerning nonexclusive or exclusive license for its commercial development should be addressed to the Patent Counsel, Marshall Space Flight Center *[see page A5].* *Refer to MFS-23721.*

Pulse Response Yields Battery Charge State

Response to an input pulse could characterize the state of charge of a battery.

An instrument is proposed that would indicate the state of charge of a battery and would be particularly useful as a fuel indicator for electric vehicles. The instrument electronically measures the input and response of a forcing-function pulse that periodically modulates the charge or discharge current. It then analyzes the input and response by time-series analyses to indicate the changes to the functions that characterize the changing state of charge of a battery during charge and discharge.

For any battery state of charge, there is some unique response such that the ratio of the response to the input completely characterizes that state. A periodic measurement of the results of the process indicates how much charge remains or has to be put back in the battery.

This work was done by Carl P. Chapman and Thomas A. Barber of Caltech for **NASA's Jet Propulsion Laboratory.** *For further information, Circle 36 on the TSP Request Card.*
NPO-14882

Automatic Control of Multimedia Shows

An audiovisual program is synchronized digitally.

A digital controller synchronizes the events in a multimedia simulation of a rocket firing at Kennedy Space Center. The presentation employs two movie projectors, four slide projectors, an audio tape player, countdown clocks, and lights, consoles, and segmented display boards. The controller synchronizes over 60 events to the two 16-millimeter movies regardless of speed variations in the movie projectors.

A serial time code is recorded on the tape with the show narration, which is electrically synchronized with the movie films. Events are controlled by the time code and thus start and stop at the proper time in relation to the movies.

This work was done by Larry D. Holley and James P. Strode of **Kennedy Space Center**. *For further information, Circle 37 on the TSP Request Card.*
KSC-11080

Digital SAR Processor

It produces real-time, single-look, high-resolution imagery.

A proposed digital synthetic-aperture-radar (SAR) processor achieves a rate of 4×10^6 samples per second. The system combines frequency-domain and time-domain processing for a two-dimensional azimuth correlation.

A control processor in the SAR provides reference functions and timing circuitry. A range correlator, performs the synthetic-aperture processing. It is a straightforward match filter consisting of a pipelined fast Fourier transform (FFT) followed by two reference-function multipliers and a pieplined inverse FFT. An azimuth correlator consists of a block-pipelined FFT followed by two transversal filters and azimuth-reference multipliers for range-migration correlations. Target-response interpolations and range-migration corrections are performed in a time-domain transversal filter.

This work was done by Chialin Wu and Kuang Y. Liu of Caltech for **NASA's Jet Propulsion Laboratory.** *For further information, Circle 38 on the TSP Request Card.*

Inquiries concerning rights for the commercial use of this invention should be addressed to the Patent Counsel, NASA Resident Office-JPL [see page A5]. Refer to NPO-15519.

Electric-Power System Simulator

It shows different combinations of generation, storage, and load components.

A simulator gives a quick overview of power system operation. It is useful in viewing total system performance for 1 day, as it shows different combinations of generation, storage, and load components and their effects on an electric utility.

The simulator hardware consists of a display, a video monitor with keyboard input to a microprocessor, and a video monitor for the display of load curves and power generation. Situations with both conventional and unconventional power-generation options are created and demonstrated, and the characteristics of each generation and storage unit, as well as load curves, can be selected and keyboarded into the system. The simulator is a useful planning tool for electric utilities, regulatory agencies, and laymen interested in understanding the basics of electric-power system operation.

This work was done by Ralph W. Caldwell, Richard L. Grumm, and Brian L. Biedebach of Caltech for **NASA's Jet Propulsion Laboratory**. *For further information, Circle 39 on the TSP Request Card.*

Inquiries concerning the rights for the commercial use of this invention should be addressed to the Patent Counsel, NASA Resident Office-JPL [see page A5]. Refer to NPO-15515.

Connecting Separate Computers to a Common Bus

A network bus adapter handles protocols for computer-to-commputer communications.

Individual network bus adapters (NBA's) connect computers, microprocessors and minicomputers, and terminals to a common global bus, a twin-axial cable. Communication is in accordance with the standard protocol, even though the host devices operate at different rates and under different protocols.

An NBA does all the protocol handling and communcation with the bus for its host computer, such that processors of different speeds can send data to each other continuously at their maximum speed. Any host processor can communicate with any other, or with several or with all. At least 64 processors can be connected, with an expected maximum of 256, providing the capability of building a large computer network for distributed processing.

This work was done by Anil K. Agrawan, Philip G. Mullen and Vivatvong V. Vadakan of Caltech for **NASA's Jet Propulsion Laboratory.** *For further information Circle 40 on the TSP Request Card.*

This invention is owned by NASA, and a patent application has been filed. Inquiries concerning nonexclusive or exclusive license for its commercial development should be addressed to the Patent Counsel, NASA Resident Office-JPL [see page A5]. Refer to NPO-15433.

Frequency-Diversity Reception for Phase Modulation

Signal-to-noise ratio would be improved.

A proposed system would receive phase modulation transmitted simultaneously on different carrier frequencies. It could be used for carriers received through different antennas or through the same antenna. The system would normally be used for digital signals. Fixed or variable delay lines, as needed, would be inserted in the channels to equalize the group delays. The signals could be combined at baseband, but are preferably combined by coherent summing at the intermediate frequency for improved signal-to-noise ratio.

The transmitted modulation may be gated on or off among the various carriers. After coherent intermediate-frequency summing at the receiver, the total modulation would be recovered.

This work was done by Milton H. Brockman of Caltech for **NASA's Jet Propulsion Laboratory.** *For further information, Circle 41 on the TSP Request Card.*
NPO-15040

Eliminating Doppler Effects in Synthetic-Aperture Radar Optical Processors

A pair of photodetectors generates correction signals.

An instrument detects Doppler shifts in radar data and corrects processing parameters so that ambiguities caused by the shifts are not manifested as double or overlapping images. Developed for synthetic-aperture radar, the instrument uses spatial shifts in the optical Fourier transform of a target scene to actuate servomechanisms for optical centering of images during processing.

A pair of photodetectors are stationed in a plane behind the Fourier transform lenses so that the intensity of the optical Fourier transform impinges equally on both detectors when there is no Doppler shift. When Doppler shift is present, however, light is distributed unequally on the detectors and a bipolar voltage is generated. The voltage actuates motors on the optical-correlator elements to balance out the effects of the Doppler shift.

This work was done by Nicholas J. Constantinides and Thomas J. Bicknell of Caltech for **NASA's Jet Propulsion Laboratory.** *For further information, Circle 42 on the TSP Request Card.*

This invention has been patented by NASA (U.S. Patent No. 4,371,946). Inquiries concerning nonexclusive or exclusive license for its commercial development should be addressed to the Patent Counsel, NASA Resident Office–JPL [see page A5]. Refer to NPO-14998.

Electronically-Scanned Fourier-Transform Spectrometer

Instrument is efficient, lightweight, and stable.

A proposed Fourier-transform spectrometer configuration uses electronic, instead of mechanical, scanning. This makes the configuration insensitive to vibration-induced sampling errors that are introduced into mechanically scanned systems.

The interferometer of the instrument forms the Fourier transform of a spectrum on an array of photodetectors. The array is scanned electronically, and the output data is Fourier-transformed into a visible or infrared spectrum.

The proposed configuration requires no moving parts, is compact, and will inherently be much harder to misaline than existing mechanically scanned types, particularly in applications where the whole interferometer must be cooled to cryogenic temperatures, as in long-wavelength infrared spectroscopy.

This work was done by James B. Breckinridge and Fred G. O'Callaghan of Caltech for **NASA's Jet Propulsion Laboratory.** *For further information, Circle 214 on the TSP Request Card.*

Inquiries concerning rights for the commercial use of this invention should be addressed to the Patent Counsel, NASA Resident Office-JPL [see page A5]. Refer to NPO-15844.

Physical Sciences

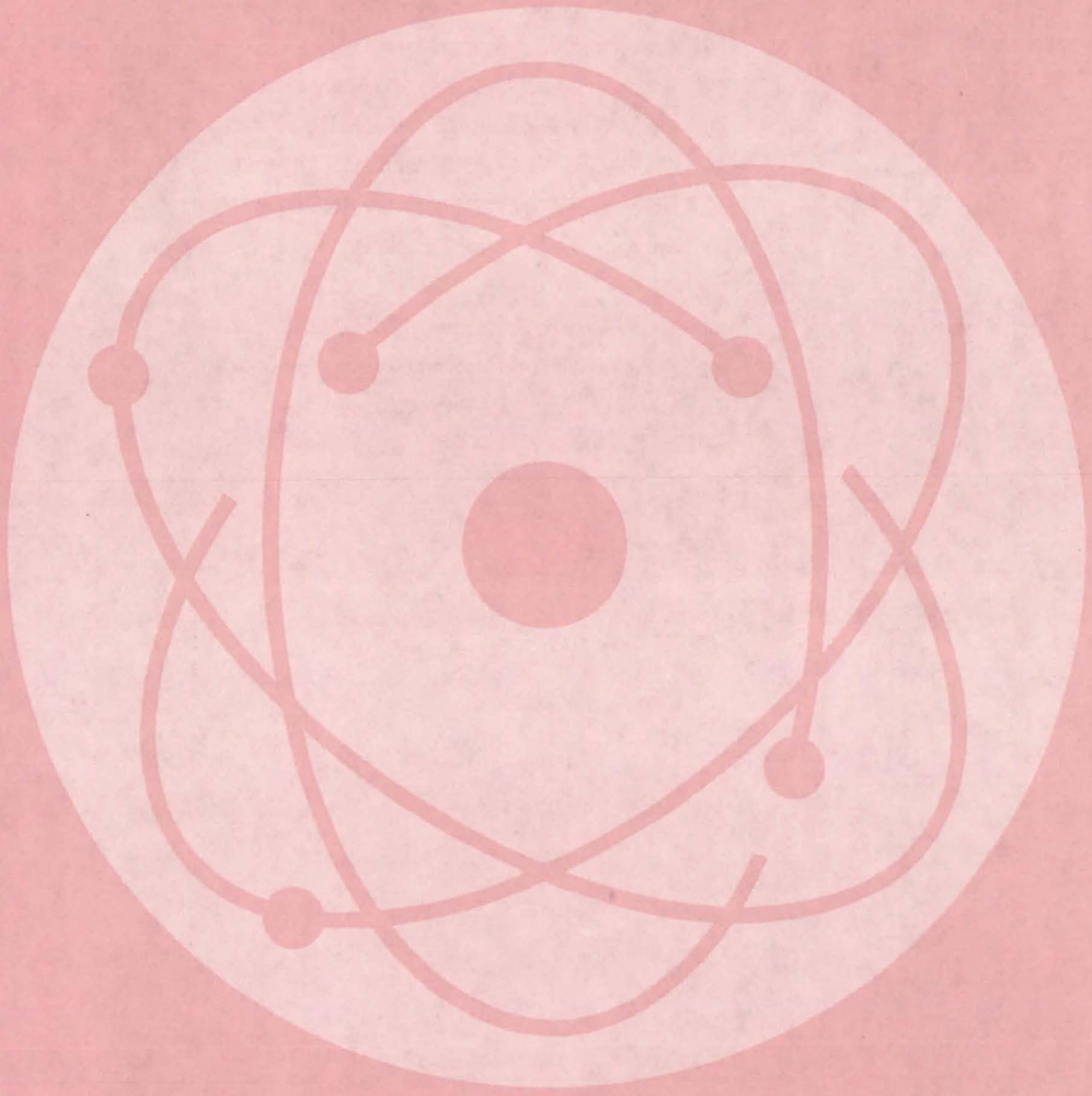

Hardware, Techniques, and Processes

Books and Reports

MiniBriefs

Compact Concentrators for Solar Cells

Each cell in an array has its own concentrator.

Marshall Space Flight Center, Alabama

A lightweight solar concentrator accepts energy from the Sun over a relatively wide range of pointing-angle error. Unlike older designs that call for a single large optical system to gather solar energy over a wide area and direct it at a relatively small area of photovoltaic cells, the new concentrator uses many small optical systems for this purpose — one optical system for each solar cell. The new concentrator therefore requires far less height than its predecessors.

The concentrators are mounted on a panel along with solar-cell modules (see figure). A panel might contain 10 modules, each module comprising 256 solar cells, for example. Typical dimensions for such a panel might be 12 feet (3.66 m) long by 4.8 feet (1.46 m) wide. With the new concentrator design, it would be only 0.5 inch (1.27 cm) thick.

Each of the 2,560 concentrator-and-cell elements in the panel includes a paraboloidal primary mirror, a hyperboloidal secondary mirror, a conical mirror, and a photovoltaic cell. Sunlight falling on an element is first reflected by the paraboloidal mirror to the reflective undersurface of the hyperboloid. The hyperboloidal mirror reflects light into the open-ended conical mirror to the photovoltaic cell. All of the light that is incident parallel to the concentrator axis — and a portion of the nonparallel light — passes through the conical mirror directly, without striking the side of the cone.

A large portion of the nonparallel light, however, falls on the inner surface of the conical mirror. Much of this light is reflected by the cone onto the photovoltaic cell. The cone thus ensures that a substantial portion of incident light is utilized even when the concentrator axis is not pointed directly at the Sun.

The concentration ratio is somewhat less than the ratio of the entrance-aperture area of the paraboloidal mirror to the area of the solar cell. For a solar-cell radius of 2 mm, the 12.7-mm-thick concentrator has a concentration ratio of 150.

(continued on next page)

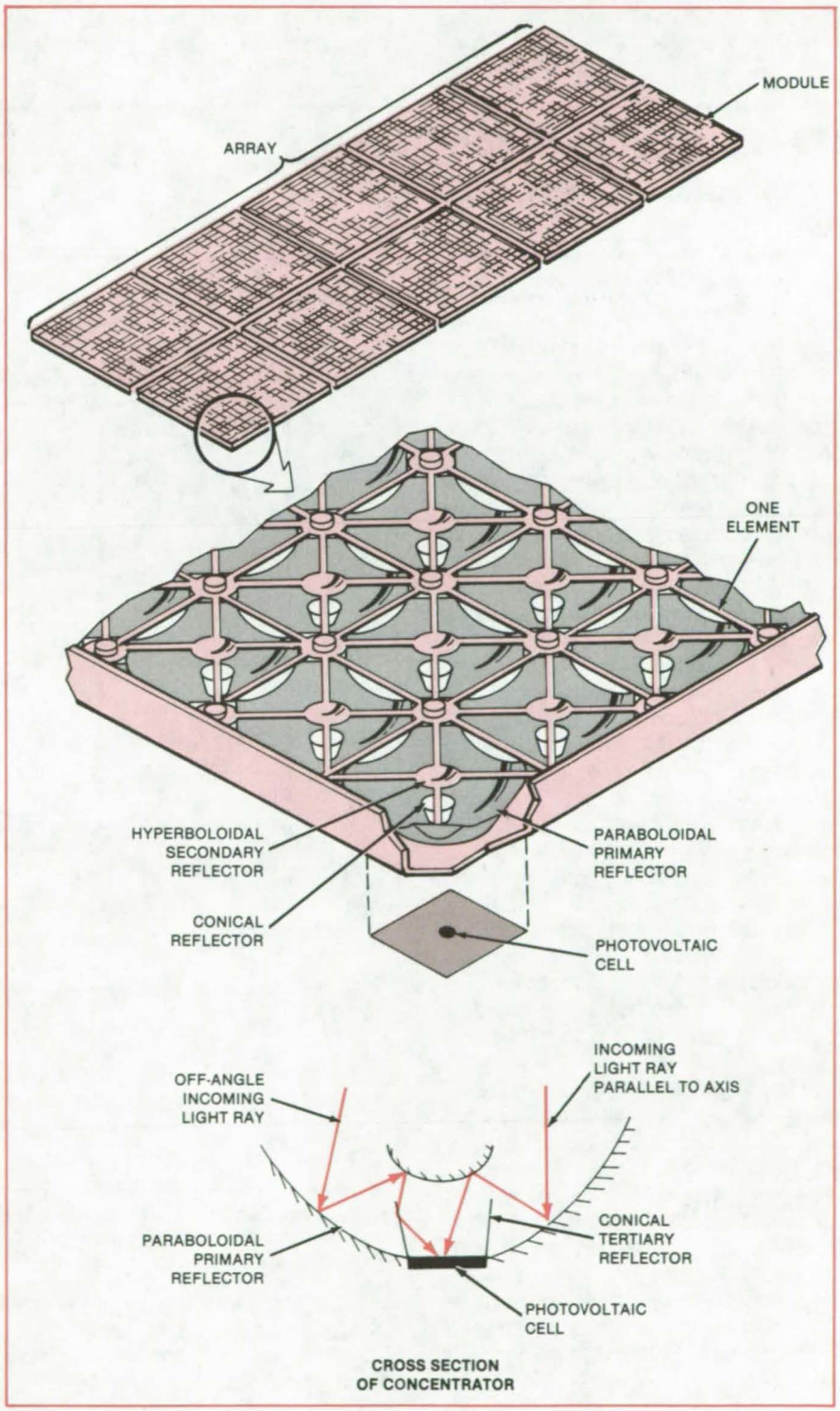

A **Cassegrain Reflector** — a combination of paraboloidal and hyperboloidal mirrors — is used with a conical reflector at each element of the array. The three components direct light to a small solar cell.

The concentrator need not be precisely alined with the Sun: This feature simplifies the design of tracking mechanisms. For example, for a 1° offset between the concentrator axis and the line to the Sun, the solar radiation falling on cells is about 97 percent of that at zero offset. At 2° offset, the relative energy flux drops to about 93 percent. At 3° offset, the energy flux is still about 80 percent that at zero offset. Beyond 3°, however, the incident energy drops off sharply with increasing offset.

The new concentrator provides a large electric-power output with only a small photovoltaic-cell area. At the same time, the concentrator does not present any serious heat-dissipation problems. The cells can be mounted on a thin aluminum base and maintained at a temperature no higher than 200° C. The base, which serves as a heat sink, need be no thicker than structural integrity requires. No cooling fins, fans, pumps, or heat pipes are needed, not even in a vacuum.

This work was done by Voo Sung Whang of TRW, Inc., for **Marshall Space Flight Center.** *For further information, Circle 43 on the TSP Request Card.*
MFS-25511

Testing Large Solar Mirrors

Mirror figure is evaluated in terms of imaging properties.

NASA's Jet Propulsion Laboratory, Pasadena, California

A modified solar simulator functions as the collimator in an inexpensive system for testing large paraboloidal solar-collector mirror segments (gores). The equipment includes a scanner for measuring the irradiance distribution in the solar image produced by the gore and a camera equipped with special apertures for determining the magnitude and location of figure errors on the gores.

A lens forms an image of the arc-lamp source at the focal point of the main mirror in the solar simulator (see Figure 1). The main solar-simulator mirror converts the light from this source into a collimated beam, 19 ft (5.8 m) in diameter, directed downward onto the gore. The gore is oriented with its optic axis along the beam. The beam diverges from parallelism by no more than 1.5°, a value low enough to permit realistic evaluation of the gore under test.

To determine the irradiance distribution in the image in the focal region, a photodiode detector is scanned through the beam. The distribution is mapped by recording the detector output on an x-y plotter.

The magnitude of figure errors (deviations from proper surface shape) is recorded using a photographic technique related to the Foucault knife-edge test. A converging field lens is placed near the focal point of the gore. It forms a real image of the gore on a white screen (see Figure 2). In turn, each of a series of annular apertures of various inner and outer diameters is then placed adjacent to the field lens. If the figure of the gore were perfect, most of the light reflected from the gore would pass through the center of the field lens, and the screen would be dark for every aperture except the smallest one (which has a full circular opening).

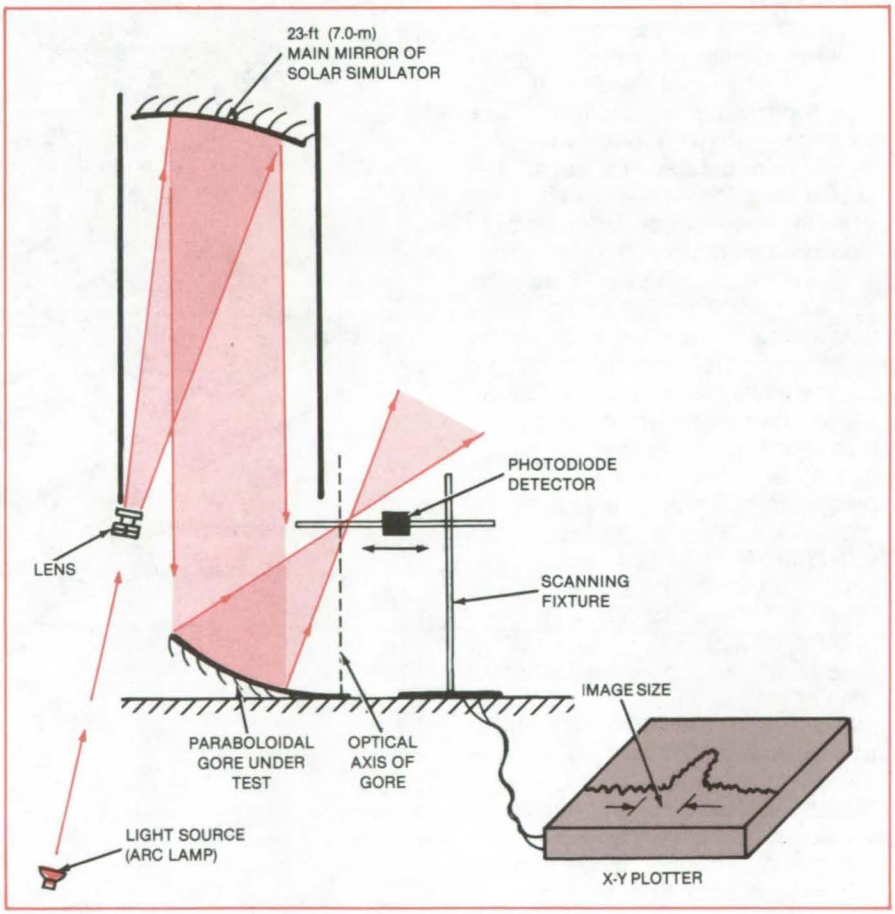

Figure 1. The **Paraboloidal-Mirror-Gore Test Facility** uses the main mirror and one of the light sources of an existing solar simulator as a collimator. The setup for measuring the image-irradiance distribution is shown.

Light from a misfigured region on the gore would arrive at the field lens at too

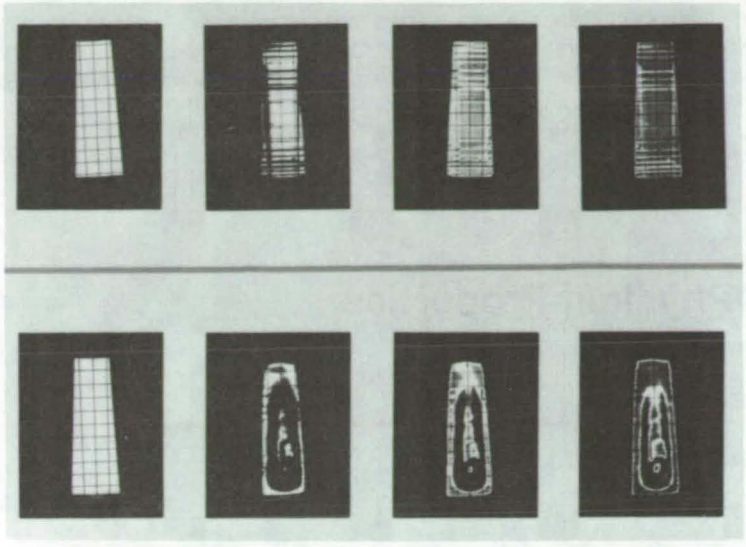

Figure 2. **Photographs of Gore Surfaces** made in collimated light with annular apertures show bright spots for areas having surface-slope deviations with magnitudes corresponding to the aperture sizes. Sample photographs are shown for two gores. The grid pattern is included on the imaging screen as a coordinate reference.

large a radius to pass through the smallest aperture. That portion of the gore image on the screen would be dark when the smallest aperture is used, but would be bright when using whatever aperture passes light at the radius corresponding to that particular surface-figure deviation. Thus, a series of photographs made with each aperture in turn gives a series of maps of areas on the gore having figure errors of similar magnitude.

This work was done by Maurice J. Argoud, Walter L. Walker, Robert S. Leland, Lloyd V. Butler, and Edwin W. Dennison of Caltech for **NASA's Jet Propulsion Laboratory.** *For further information, Circle 44 on the TSP Request Card.*
NPO-15404

Two-Stage Off-Axis Cylindrical Solar Concentrator

The reflector for a photovoltaic power supply uses off-axis geometry for efficient uniform illumination.

NASA's Jet Propulsion Laboratory, Pasadena, California

A two-stage off-axis parabolic cylindrical concentrator has been designed for the illumination of photovoltaic cells. Nonimaging secondary concentrators in combination with focusing primary elements achieve maximum concentration for an acceptance angle of ±4.25° while maintaining relatively uniform illumination of the cell plane. The cylindrical geometry permits easy furling and unfurling of the mirrors for transport and deployment.

The figure shows how solar rays, if incident within ±4.25° of the concentrator axis, are collected and directed to the photovoltaic cells. The aperture of the first stage is 10 m wide, and the focal length is 5 m, with the result that the concentration of the first-stage off-axis cylindrical paraboloid alone is 5.74. The concentration of the second stage is 1.60, giving an overall concentration of 9.2. By contrast, a symmetrical parabolic cylindrical arrangement with the same input angle and relative aperture would have a first-stage concentration of 6.45 and a second-stage concentration of 1.25, for

(continued on next page)

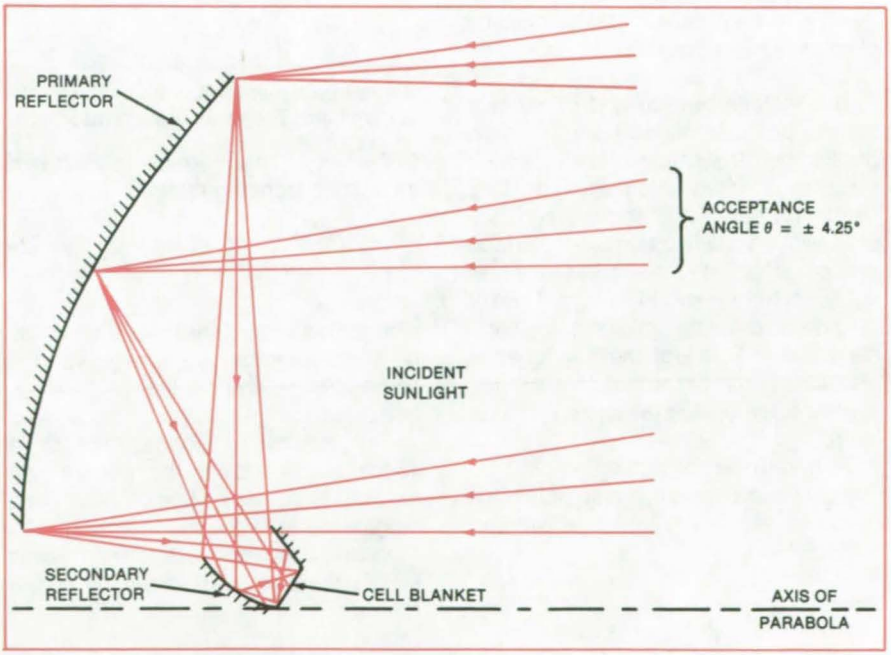

This **Two-Stage Solar-Energy Concentrator** uses off-axis geometry to achieve efficient uniform illumination of photovoltaic cells. The primary reflector is a parabolic cylinder and therefore is readily adaptable to rolling up for transport and unrolling for deployment.

an overall concentration of only 8.05, neglecting obstruction by the second stage.

This design satisfies the requirements for concentration and uniform power density, in addition to having the advantage of the two-dimensional (cylindrical) geometry. The foldable cylindrical structure has potential for both terrestrial and space applications.

This work was done by Roland Winston and Joseph J. O'Gallagher of the University of Chicago, Walter T. Welford of the University of London, and Donald E. Rockey of Caltech for **NASA's Jet Propulsion Laboratory.** *For further information, Circle 45 on the TSP Request Card.*
NPO-15484

Contactless Measurement of Physical Properties

Surface tension and other properties are determined from measurements of the resonant frequency.

NASA's Jet Propulsion Laboratory, Pasadena, California

The surface tension and other physical properties of molten and liquid samples that are excited at resonance can be measured by observing their photographic or TV image and noting the resonant frequency and its rate of change. Conventional methods of measuring surface tension use loops and rods to measure the breakaway force from the liquid. However, these methods can introduce contaminants into the sample.

The new contactless measurement technique determines sample surface tension, outgassing, viscosity, contamination, and the rate of change of these properties. From these properties, the purity of a sample can be determined. The technique can be used in normal gravity and in low gravity in either a vacuum or a gaseous environment, where the sample is positioned by electrostatic, acoustic, or magnetic forces.

The surface tension and purity of a sample are determined from its shape oscillations. The shape of a suspended sample oscillates when excited at its resonant frequency, and the frequency of oscillation is a function of the surface tension. The rate of increase or decrease of frequency indicates the rate of outgassing or contamination of the sample volume. Some of the fundamental modes of oscillation of an excited spherical sample are shown in the figure.

To determine the purity and physical properties of a sample, the sample is excited into resonance. From the observed

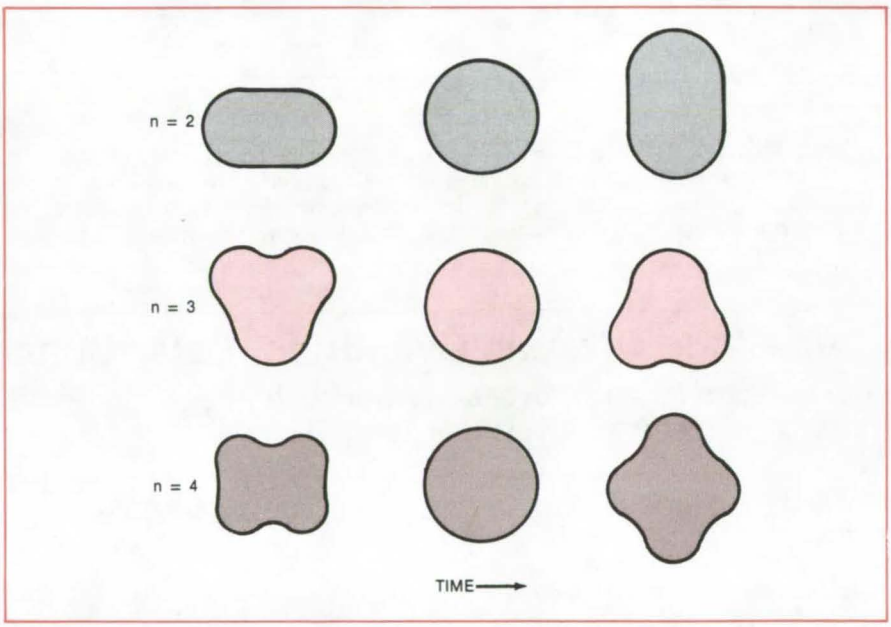

Some **Fundamental Modes of Oscillation** of a liquid sample excited at resonance are shown here. The value of n corresponds to the number of degrees of freedom excited.

frequency, f, the surface tension σ is calculated from the relation

$$\sigma = \frac{(2\pi f)^2 \varrho\, a^3}{8}$$

where σ is surface tension, ϱ is the density, a is the radius of a sphere with the same volume, and f is the frequency in hertz.

The sample is observed for a 15-minute period. If the surrounding medium becomes haloed or discolored, outgassing is probably occurring. The resonant frequency is then rechecked and the frequency and direction of drift rate computed. If the drift rate is positive, outgassing has occurred.

The change in image volume is related to the outgassing rate and to the change in frequency. If the resonant frequency decreases, then nucleation has taken place, and there are probably contaminants in the sample. Nucleation is related to the change in surface tension.

This work was done by Daniel D. Elleman, Taylor G. Wang, Eugene H. Trinh, and Arvid Croonquist of Caltech for **NASA's Jet Propulsion Laboratory.** *For further information, Circle 46 on the TSP Request Card.*
NPO-15839

Drying Milk With Boiler Exhaust

Considerable energy could be saved in the powdered-milk industry.

NASA's Jet Propulsion Laboratory, Pasadena, California

In a proposed modification of the customary process for making powdered skim milk, boiler flue gas would be recycled to the milk-spray drier instead of vented to the exhaust stack. Because the milk-processing industry consumes large amounts of heat, this simple economy measure could be a substantial energy saver.

The only special requirement is that the boiler be fired with natural gas or other clean fuel, so that the combustion products will not contaminate the milk. This approach should be adaptable to existing plants with minimal investment because most are already equipped with natural-gas-fired boilers that generate large quantities of flue gas.

The modified drying process is shown schematically in the figure. Boiler flue gas at 300° to 450° F (150° to 235° C) is channeled through an insulated duct from the boiler exhaust outlet through an auxiliary combustion system to the gas-inlet port of the spray drier. The hot flue gas is injected directly into the milk spray, drying the spray by efficient direct-contact heat exchange. The auxiliary combustion system supplies additional heat during reduced boiler output.

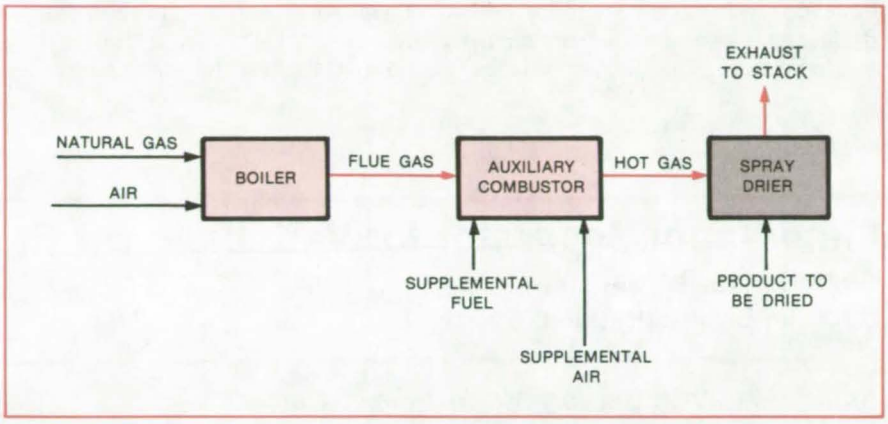

The **Boiler Flue Gas** is fed to the spray drier where it directly contacts the product to be dried. Additional heat is supplied by the auxiliary combustor when the boiler output is low.

The precise energy saving depends on the steam requirements of other processes during drier operation. For a representative plant that produces 10,000 lb (4,500 kg) of skim-milk powder per hour, it has been estimated that boiler exhaust could supply 42 to 100 percent of the drying-heat requirement.

This work was done by Mark R. Broussard of Caltech for **NASA's Jet Propulsion Laboratory.** *For further information, Circle 47 on the TSP Request Card.*

NPO-15923

Hydrogen Masers as Time and Frequency Standards

They track each other with 100 times more precision than do cesium standards.

NASA's Jet Propulsion Laboratory, Pasadena, California

NASA's need for precisely-synchronized frequency sources at several deep-space tracking stations around the globe has turned up evidence that the hydrogen maser may be superior to the conventional cesium-133 source for such applications. Cesium devices can be used to set geographically separated clocks to a few parts in 10^{12}, whereas hydrogen masers may be set to within a few parts in 10^{14}. Moreover, geographically separated hydrogen masers have tracked each other for more than a year to within a few parts in 10^{15}.

The 13th General Conference of Weights and Measures, held in Paris in 1970, adopted the spectral line splitting of cesium as the basis for determining Universal Coordinated Time. Nonetheless, early workers in the field tried to use the hyperfine hydrogen spectral line for a frequency standard because of its potential for smaller bandwidth and higher-precision. They encountered problems, however, when they tried to measure the line-separation frequency of $1{,}420{,}405{,}751.769 \pm 0.002$ hertz. They believed that hydrogen masers had a life expectancy of only 6 months, a period that did not promise the requisite long-term stability, especially in contrast to the extremely long lifetime of cesium atomic clocks. Further, it was difficult for them to keep a hydrogen maser operating for the million seconds needed for one sampling period. There was also confusion about measuring residual magnetic fields, to which the hydrogen maser is particularly sensitive. The net result is that there were few consistent long-term data.

(continued on next page)

It is known, however, that the frequency offset of a hydrogen-maser output from its hyperfine line frequency is a function of the ambient magnetic field, cavity mistuning, thermal motion of the atoms in the cavity, and collisions of the atoms with the walls of the cavity. Cavity mistuning is the major contributor: If it is corrected, the remaining frequency deviations will be quite small. These deviations depend on the manufacturer's design and the geographic location of the maser. Thus, if a maser remains at one location, some of the small offsets in frequency will remain constant throughout the life of the maser. In addition, if geographically separated masers have the same manufacturer, the design-dependent factors will tend to cancel.

Three hydrogen masers — in Australia, Spain, and the United States — have been calibrated with a traveling cesium standard traceable to the National Bureau of Standards and operated for an extended period to evaluate their suitability as standards. The units track each other within 7 parts in 10^{15}, even though they were retuned at least twice during an interval of 15 months and the Spanish unit was out of service for 60 days.

This work was done by Samuel C. Ward of Caltech for **NASA's Jet Propulsion Laboratory.** *For further information, Circle 48 on the TSP Request Card.*
NPO-15858

Fluid/Vapor Separator for Variable Flow Rates

A shutter varies the gas throughput of a porous plug.

Ames Research Center, Moffett Field, California

A porous plug with an adjustable shutter accommodates variations in the rate of vapor flow from a helium II storage vessel. The plug blocks the passage of liquid but adjusts in exposed area to allow the passage of gas over a range of throughputs. It is currently being studied as the phase separator in the vent line of the coolant reservoir for a spaceborne infrared telescope. On Earth, the variable plug could have applications in refining operations, industrial chemistry, and steam-powered equipment.

The figure illustrates the plug in a test setup, where the porous plug separates the bath from the vent line. It is covered by a flow-control plate, half of which is solid and half of which contains access holes. A shutter with a semicircular opening is rotated to block some of the access holes to vary the working area of the plug. During the tests, a motor slowly rotated the shutter.

The tests demonstrated the effectiveness of variable-area devices for handling the variations of mass and entropy flow required for He II systems subjected to variable heat inputs. Flow changes of up to ±60 percent of the mean value can be tolerated. No liquid breakthrough occurs as long as the adjustable cross-sectional area is within the range established for the pumping rate.

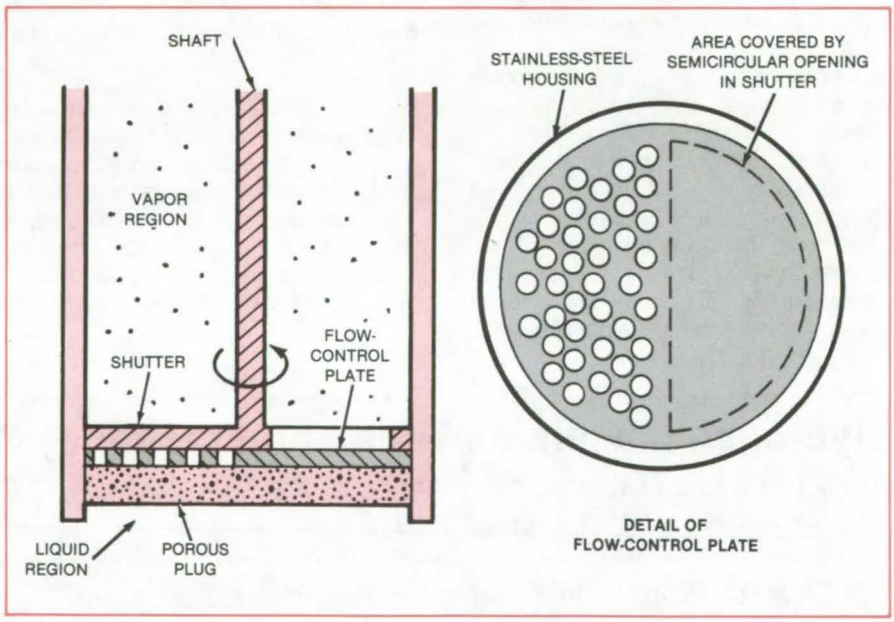

The **Variable Area** exposed on the porous plug allows it to pass varying rates of vapor flow while blocking flow of the liquid helium II from the cryogenic bath.

This work was done by John W. Vorreiter of **Ames Research Center** *and Jeffrey M. Lee, Chiang Chuang, Traugott H. K. Frederking, Gregory S. Brown, and Yasuharu Kamioka of UCLA. For further information, Circle 49 on the TSP Request Card.*
ARC-11401

Computation of Bragg Reflection for Layered Microstructures

Bragg diffractors are analyzed for use in X-ray mirrors and other applications.

NASA's Jet Propulsion Laboratory, Pasadena, California

Multilayered thin-film structures are efficient diffractors for X-rays and extreme ultraviolet radiation. These synthetic layered microstructures (SLM's) have potential applications as glancing-incidence mirrors or as filters for wavelengths of a few to a few hundred angstroms. Calculations based on an "optical" model of multilayers show how the design can be modified to take into account the scattering, absorption, and refractive properties of the layers.

Recent vapor-deposition techniques produce multilayered structures with layer thicknesses of the order of tens of angstroms. An SLM can be tailored to a specific application by varying the layer thicknesses and the number of layers to control the reflectivity (see figure), diffraction width, and wavelength resolution.

A principal design concern for a multilayer reflector is the wavelength range in which it must function. For a structure with a sufficiently large number of layers (a few hundred to a few thousand), the contrast between the scattering-amplitude densities of the two materials must be as large as possible to achieve the highest reflectivity integrated over the range of glancing angles around the diffraction peak. On the other hand, this contrast must be as small as possible to achieve the highest wavelength resolution.

Compatibility is another important factor in choosing materials for an SLM: The materials must not react chemically or interdiffuse after fabrication, or else the diffraction properties will change and degrade with time. One promising material combination is tungsten and carbon. Other candidate pairs include Al/Be, B/Be, Be/Mg, and B/LiH; but their chemical stability in thin-layer stacks remains to be investigated.

Imperfections in the layers can lead to deviations from the performance of a mathematically ideal structure. Sharp interfaces made gradual by partial interdiffusion, variations in layer thicknesses, and layer roughness leading to scattering all affect diffraction intensities.

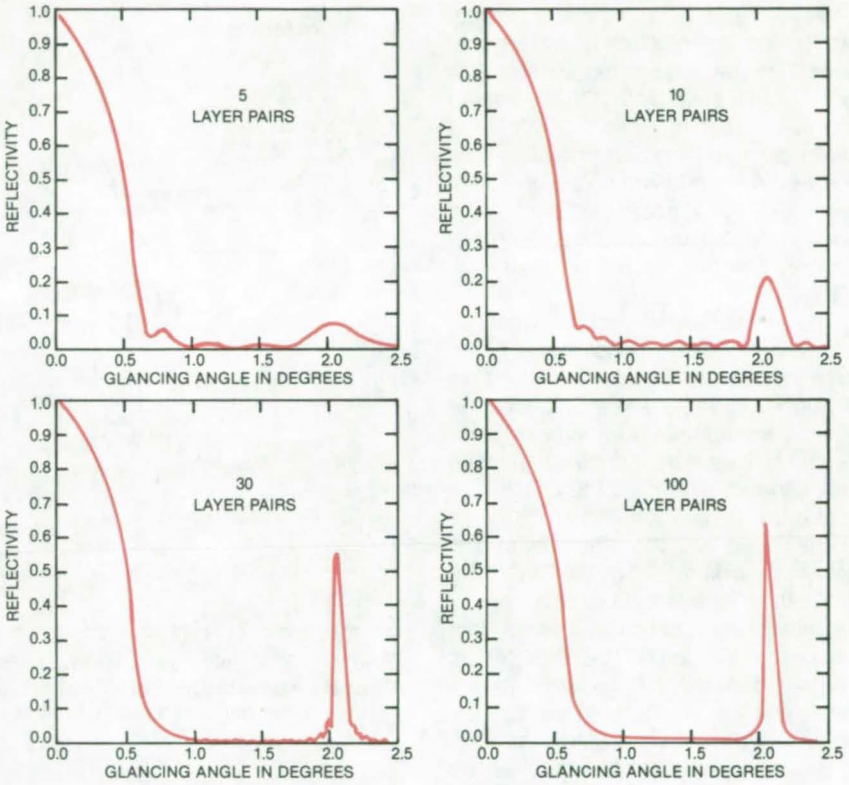

Reflectivity Versus Glancing Angle was calculated for 2.632-Å radiation diffracting from a stack of 12.4-Å tungsten layers alternating with 20.0-Å carbon layers. Note that the subsidiary interference peaks diminish as the number of layer pairs increases.

This work was done by James W. Underwood and Troy W. Barbee of Caltech for **NASA's Jet Propulsion Laboratory.** *For further information, Circle 50 on the TSP Request Card.*
NPO-15880

Antivortex Inlet Ribs for Fluid Seals

Flow straightening ribs in the inlets of annular cross-section fluid-pressure seals can reduce turbine-rotor instability. The ribs are easy to manufacture and are usually easy to install in existing equipment. The rib concept offers a relatively inexpensive solution to some lateral-instability problems in many other systems with rotating pressure seals.
(See page 113.)

Predicting Moisture Absorption in Composite Materials

Heat-transport computer programs can be adapted to solve the problem of predicting moisture absorption by composite materials, such as graphite-fiber-reinforced epoxy. Manufacturers and users of composites could benefit from the abundance of software available for solving heat-transport problems.
(See page 60.)

Improved Radiative Control of Ribbon Growth

Improvements in an apparatus for growing dendritic-web silicon crystals increase the growth rate and reduce the formation of silicon oxide. Both the crucible lid and the radiation shields were modified. The improvements provide for the precise control of the web temperature profile.
(See page 128.)

Holographic Twyman-Green Interferometer

An off-axis Fresnel zone plate is used to obtain fringe visibility close to unity.

NASA's Jet Propulsion Laboratory, Pasadena, California

Mirrors and other optical elements are tested for quality by a Twyman-Green interferometer that uses an off-axis Fresnel zone plate (OFZP) instead of the conventional beam splitter and beam diverger. The 50-percent diffraction efficiency of this type of zone plate utilizes energy almost as efficiently as a conventional Twyman-Green interferometer, and the theoretical fringe visibility is unity.

The new optical configuration is shown in Figure 1. The collimated beam from the laser is divided into two beams, U and D, by the off-axis Fresnel zone plate. The undiffracted beam, U, is reflected by the reference mirror and then split into two beams by the OFZP. The zero-order beam, denoted UU, returns to the laser; and the other beam, denoted UD, is diffracted by the OFZP. The first diffracted beam, D, is reflected by the mirror under test and is also split into two beams by the OFZP: The diffracted portion, denoted DD, returns to the laser; and the undiffracted portion, denoted DU, passes parallel to beam UD.

Beam UD, reflected by the reference mirror, serves as a reference beam; whereas beam DU, reflected by the mirror under test, is the aberrated test beam. The interferogram (created by the interference of UD and DU) shows the surface error of the mirror under test. The lens relays an image of the mirror onto the interferogram plane.

If the test element is refractive, then an additional flat mirror is required. The front focal point of the test refractive element should coincide with the center, O, of the diffractive beam; otherwise, the interferogram will show an array of concentric fringes caused by the defocus. A null test of an aspherical mirror is performed by replacing the unaberrated OFZP with an aberrated OFZP that functions as a diverger, a beam splitter, and a conventional null lens.

The configuration shown in Figure 2 is used to fabricate such an OFZP. High-quality optical elements are required beyond the pinholes. The zone plate is made by exposing a dichromated gelatin hologram plate that has a uniform frequency response from 100 lines/mm to 5,000 lines/mm.

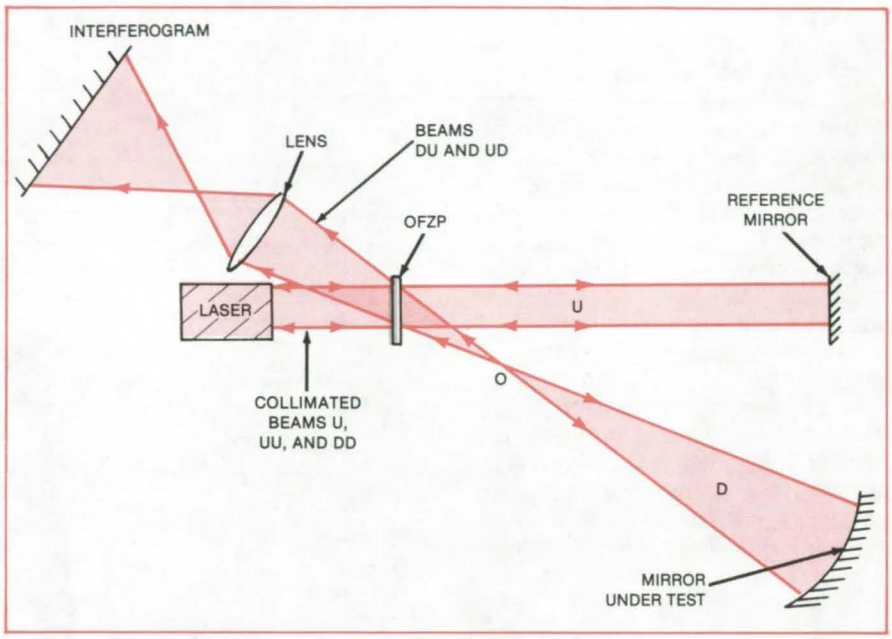

Figure 1. The **Holographic Twyman-Green Interferometer** (HTGI) employs an off-axis Fresnel zone plate (OFZP) as the beam splitter and beam diverger in place of two separate elements that perform those functions in a conventional Twyman-Green interferometer.

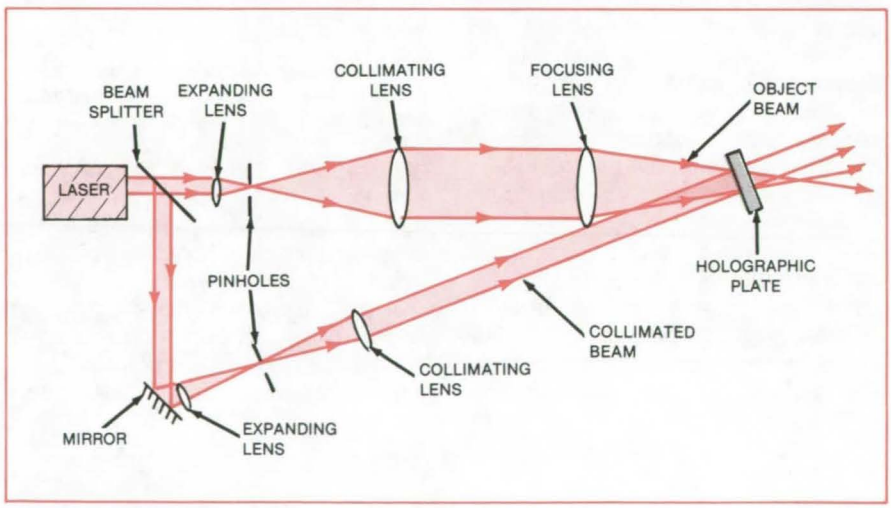

Figure 2. The **Off-Axis Fresnel Zone Plate** is formed holographically in a dichromated gelatin plate by the interference between a diverging object beam and a collimated reference beam.

The wave-front quality of a dichromated OFZP was evaluated by a double-exposure holography technique. The wave-front distortion of the hologram after processing is about 0.1 wave peak-to-valley and 0.041 wave rms.

This work was done by Chungte W. Chen, James C. Wyant, and James B. Breckinridge of Caltech for **NASA's Jet Propulsion Laboratory.** *For further information, Circle 51 on the TSP Request Card.*
NPO-15754

Improved Electrostatic Optical System

The device is suitable for molecular epitaxial formation of semiconductor components.

NASA's Jet Propulsion Laboratory, Pasadena, California

A chromatically- or spherically-corrected electrostatic lens focuses a molecular beam down to a spot the size of 1 micron. The beam is suitable for drawing doping patterns on semiconductor crystals and for fine-line etching of microelectronic patterns. The beam energy is only about 1 percent of implantation energy, so substrate damage is minimal.

The improved electrostatic lens system uses a cylindrical mirror as the central element between two tubular lenses. Aberrations introduced by the mirror tend to cancel those introduced by the tubular lenses. The result is an order-of-magnitude improvement in chromatic or spherical compensation.

In some electrostatic lens systems, screens are put in the path of particles to control focusing. However, the problem with this type of lens is that the focusing depends on the energy of the particles. In addition, ions sputter away the screens, changing the electrical properties of the system and transferring the screen material onto the target.

The three-section lens shown in the figure uses conventional electrostatic optical components arranged in a new configuration with appropriate voltage differentials. The cylindrical mirror, between two tubular lenses, has a metal rod at the center on the axis. The rod is supported on thin metal struts in a field-free region.

The first tubular lens bends the charged particles from a point source toward the axis, except that aberration effects cause the higher energy particles to remain further from the axis than the slower particles. The field in the gap of the second tubular lens focuses the particles at the image point, however, some aberration inevitably remains.

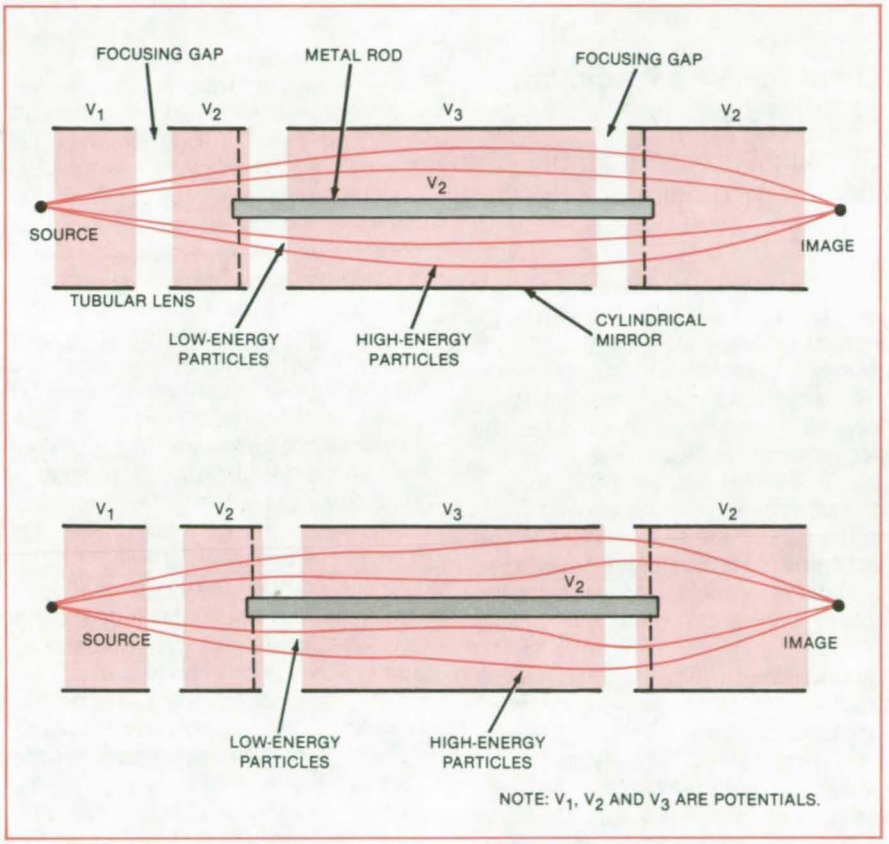

The **New Electrostatic Optics System** has a cylindrical mirror analyzer (CMA) between two conventional tubular lenses with appropriate voltage differences. The tubular lenses bend the slower particles toward the axis more than the faster particles as shown at the top. However, when the fields in the CMA portion are applied, the slower particles are bent away from the axis more than the faster particles, as shown at the bottom. Chromatic and spherical compensations are obtained by the proper balance of voltage differences between the lens sections.

The tube lenses in this optical system bend the slower particles toward the axis more than the faster particles. However, the radial field in the cylindrical mirror can compensate for this effect, so that the net bending of slower particles is the same as that of faster particles, providing for chromatic and/or spherical compensations. The type and degree of compensation are controlled by the voltage differences between the lens sections.

This work was done by Blair F. Lewis of Caltech for **NASA's Jet Propulsion Laboratory.** *No further documentation is available.*
NPO-15774

Books and Reports

These reports, studies, and handbooks are available from NASA as Technical Support Packages (TSP's) when a Request Card number is cited; otherwise they are available from the National Technical Information Service.

Least-Squares Prediction of Solar Activity

Statistical procedures for long-range prediction of solar activity are compared.

Studies of statistical methods for predicting future solar activity are described in a 47-page report containing extensive graphical and tabular presentations of the analyses. The Lagrangian-least-squares method, which gives the best predictions, is presented in detail. The FORTRAN source code for the method is given in an appendix.

The goal of the analyses was to find an improved method for predicting solar activity for a period up to one full solar-activity cycle (approximately 11 years) into the future using all solar-activity data available up to the date at which the prediction is calculated. Direct measurements of 10.7-cm solar flux ($F_{10.7}$) and geomagnetic activity (A_p) are available from 1947 and 1932 on, respectively. The $F_{10.7}$ data base was extended back over a total of 20 solar-activity cycles to the year 1747 by using an equation relating Sunspot data (Zurich-smoothed Sunspot number R) to the smoothed solar flux, $F_{10.7}$. The equation was obtained by a regression analysis of the two sets of data since 1947. Similarly, the A_p data base was extended back to 1884 using other geomagnetic data (C_i).

The six steps in the Lagrangian-least-squares method are as follows:

1. Select the maximum (or minimum) points of each solar cycle.
2. Determine the periods, P_j, in months.
3. Determine the average period, P, in months.
4. Compute the ratios $\tau_j = P_j/P$.
5. Using a conventional interpolation method, read off 132 solar-flux values in each cycle j at intervals of τ_j months.
6. When all the cycles have been blocked in this manner, the McNish-Lincoln method (which is based on a mean approximation of all past solar cycles with a correction for the departure of the current value from the mean) is applied to produce predictions of the mean and $\pm 1\sigma$, $\pm 2\sigma$, and $\pm 3\sigma$ values of $F_{10.7}$ for the next cycle, assuming that the distribution of values is Gaussian with standard deviation σ.

In the trials of various modifications of the Lagrangian-least-squares method, data for cycles 1 through j were used to predict values for cycle j + 1. The goodness of fit to the actual data for cycle j + 1 was judged using the Pearson chi-square statistic. In predicting $F_{10.7}$, the Lagrangian-least-squares technique gave better chi-squares than the straight McNish-Lincoln procedure on most solar cycles, but it was still not within the 95th percentile level of confidence.

The improved performance of the Lagrangian-least-squares method over that of the McNish-Lincoln method is considered to be due to the "lining up" of the maximums (or minimums), cycle by cycle as described above. A further analysis of the variation in the solar-cycle period and amplitude shows evidence supporting the existence of an aperiodic variation in both.

This work was done by Robert L. Holland, C. A. Rhodes, and Harold C. Euler, Jr., of **Marshall Space Flight Center.** *Further information may be found in NASA TM-82462 [N82-27211/NSP], "Lagrangian Least-Squares Prediction of Solar Activity" [$10]. A paper copy may be purchased [prepayment required] from the National Technical Information Service, Springfield, Virginia 22161. The report is also available on microfiche at no charge. To obtain a microfiche copy, Circle 52 on the TSP Request Card.*
MFS-25870

Solar Heating and Cooling Development Program

Heating is practical now, but cooling needs more development.

A final report describes a program for the design and development of solar heating and cooling systems having high performance, low cost, and modular application. The contractors for the program provided a full range of system and subsystem design, fabrication, installation, maintenance, and evaluation.

The following solar-energy systems were delivered:

- Two single-family residential space-heating systems,
- Heating and Rankine-cycle cooling systems in several sizes for multifamily residential or commercial use, and
- A 16-kVA Rankine-cycle power-generation unit.

The systems were installed in a variety of locations, ranging from Arizona to Minnesota. All systems have performed well.

The report describes the main technical features of each of the systems. It discusses subsystems, including the collectors, header-and-collector-interconnecting hardware, collector support structure, purge coil (excess-heat-rejection) unit, storage unit, heating and cooling units, energy transport, controls, and hot-water subsystem. It presents a summary of performance and costs.

In addition, the contractors fully qualified a solar collector according to interim performance criteria; developed a pumping module for transporting energy between components and subsystems; developed a high-performance, low-cost heat exchanger; developed a low-cost collector support structure; defined and tested several Rankine-cycle air-conditioner improvements; analyzed Rankine-cycle power generation; and studied advanced Rankine-cycle air cooling.

One major finding of the program is that solar space-heating and hot-water systems are effective, practical, and potentially competitive with future fuel prices. Rankine-cycle cooling systems perform as designed, but are uneconomical on account of fundamental thermodynamic limitations and system operating energies. Advanced research and development on Rankine-cycle air-conditioning systems — hardware, configuration, and controls — are essential.

This work was done by Robert Aaen and Albert Gossler of Honeywell Technology Strategy Center for **Marshall Space Flight Center.** *To obtain a copy of the report, Circle 53 on the TSP Request Card.*
MFS-27015

Designing Flat-Plate Photovoltaic Arrays

Different approaches to designing solar modules and arrays for terrestrial applications are summarized.

A nine-page report presents an overview of the state of the art in design techniques for flat-plate solar photovoltaic modules and arrays. The paper discusses the design requirements, design analyses, and test methods that have been identified and developed for this technology over the past several years in an effort to reduce cost and improve the utility and reliability for a broad spectrum of terrestrial applications.

First, the requirements at the subsystem level are addressed where system, application, and user needs are most easily defined and judged. Next, array support structures and modular design requirements are reviewed. Emphasis is focused on the engineering aspects of array and module design, including system interface concerns, structural support, thermal design, safety, electrical circuit design, reliability, and environmental endurance.

Integrated into the discussion are references to available analytical tools and test methods that have been found useful in designing array elements. Those techniques that work are identified, and areas where techniques are presently lacking are indicated.

This work was done by Ronald G. Ross, Jr., of Caltech for **NASA's Jet Propulsion Laboratory.** *To obtain a copy of the report, "Design Techniques for Flat-Plate Photovoltaic Arrays," Circle 54 on the TSP Request Card.*
NPO-15729

MiniBriefs describe NASA innovations and reports in an abbreviated format. Readers desiring additional information on these items should request the Technical Support Packages (TSP's), available in most cases, which can be obtained by using the TSP Request Card at the back of this issue.

Multiple-Wavelength Metal/Halide Laser

A single device produces multiple lasing lines.

A laser capable of producing many lasing lines has several reservoirs of halide lasant mixed with the chlorides of copper, manganese, and iron. Existing metal/halide systems, in contrast, produce significant energy output at only one or two transitions.

In the new laser, each of the separately heated reservoirs contains a single halide. The vapor density of the individual halides is controlled by a metered flow of neon carrier gas. A convection-control technique makes it possible to rapidly change from one metal halide to another at maximum energy.

This work was done by Noble M. Nerheim of Caltech for **NASA's Jet Propulsion Laboratory.** *For further information, Circle 55 on the TSP Request Card.*
NPO-15256

Scanning XeCl Laser

Potential applications of the narrow-bandwidth laser include remote sensing and high-resolution spectroscopy.

A scanning XeCl oscillator/ring-laser amplifier produces a narrow spectral bandwidth (<0.003 nm) over a tuning range of 307.5 to 308.5 nm. The ring configuration has the following advantages: (a) The oscillator is decoupled from the amplifier, (b) the output is unidirectional, (c) the output beam is uniform, and (d) the inexpensive optics allow variable output coupling and cavity length.

Fluorescence excitation spectra of OH radicals produced in a methane/oxygen flame were recorded using the new laser. Other potential applications include remote sensing of atmospheric OH radicals, chemical processing, isotope separation, and high-resolution spectroscopy.

This work was done by James B. Laudenslager, Thomas J. Pacala, and I. Stuart McDermid of Caltech for **NASA's Jet Propulsion Laboratory.** *For further information, Circle 56 on the TSP Request Card.*
NPO-15692

Simplified Laser Tuning

Tuning arrangement employs a single grating and two planar mirrors.

An arrangement of front-surface mirrors and a single holographic grating significantly reduces the spectral bandwidth and simplifies the tuning of a laser output. The laser can be used to induce fluorescence in measuring concentrations of trace species, such as the OH radical, in the atmosphere.

The grating is used in both grazing incidence and Littrow orientations. By using a suitable grazing angle, an incident laser beam illuminates more of the grooves of the grating. The diffracted beam is expanded only in one dimension, simplifying the alinement of tuning optics and allowing for the use of a long, thin grating that is both inexpensive and compact.

This work was done by I. Stuart McDermid and Thomas J. Pacala of Caltech for **NASA's Jet Propulsion Laboratory.** *For further information, Circle 57 on the TSP Request Card.*

Inquiries concerning rights for the commercial use of this invention should be addressed to the Patent Counsel, NASA Resident Office-JPL [see page A5]. Refer to NPO-15690.

Obtaining Pulses From a CW Laser

Two acousto-optic modulators operate in tandem.

A proposed system would generate pulses from the output of a continuous-wave laser. The duration and repetition rate of the pulses could be controlled.

The laser beam is fed through an acousto-optic modulator, which is driven by a sum of harmonically related frequencies and which diffracts portions of the beam through small angles and shifts these diverging waves through frequencies equal to the frequencies of the traveling acoustic waves. The diverging waves are recombined into a parallel output beam in a second modulator that is driven by the same signal source that drives the first one.

This work was done by Jack S. Margolis of Caltech for **NASA's Jet Propulsion Laboratory.** *For further information, Circle 58 on the TSP Request Card.*

This invention has been patented by NASA (U.S. Patent No. 4,332,441). Inquiries concerning nonexclusive or exclusive license for its commercial development should be addressed to the Patent Counsel, NASA Resident Office-JPL [see page A5]. Refer to NPO-15111.

Controlling Metal-Halide Vapor Density in Lasers

Streams of buffer gas convect and dilute the metal-halide vapor.

The energy per pulse and peak power per pulse of a copper-halide or other metal-halide laser depend upon the vapor density inside the laser tube. A new technique uses the flow of buffer gas through the reservoir, which contains heated metal halide, to convect the vapors into the discharge tube. A second stream of buffer gas dilutes the vapor. The final vapor density in the laser tube is controlled and changed by adjusting either one or both of the buffer-gas flow rates.

The buffer gas—for example, neon—is injected into the top of the vaporizer and flows down and then up in the reservoir, where it mixes with the copper halide vapors. The mixture then flows through an outlet into the laser tube and is diluted by the second stream of buffer gas injected into the laser tube.

This work was done by Thomas J. Pivirotto of Caltech for **NASA's Jet Propulsion Laboratory.** *For further information, Circle 59 on the TSP Request Card.*

This invention has been patented by NASA (U.S. Patent No. 4,347,613). Inquiries concerning nonexclusive or exclusive license for its commercial development should be addressed to the Patent Counsel, NASA Resident Office-JPL [see page A5]. Refer to NPO-15021.

Fluorine Mixer/Vaporizer for Chemical Lasers

The fluorine is vaporized by a flow of helium.

A mixer/vaporizer chamber gasifies liquid fluorine before it is injected into the lasing cavity of a hydrogen fluoride/deuterium fluoride laser. The fluorine is vaporized by a flow of helium. Hot helium gas is injected into the chamber and the liquid fluorine is introduced into the chamber as droplets. Because the laser already uses helium to absorb heat, the addition of hot helium to vaporize the liquid fluorine does not affect the subsequent use of the fluorine.

This work was done by Anthony Giandomenico of Caltech for **NASA's Jet Propulsion Laboratory.** *For further information, Circle 60 on the TSP Request Card.*
NPO-15552

Improved Laser Velocimeter

It can monitor fluid motion in three dimensions.

A self-alining laser velocimeter uses simple lenses and Doppler-frequency shift by a scattering disk to monitor fluid motion in three dimensions. The instrument includes a continuous-wave laser, a phase shifter, a drive-frequency oscillator, a phase-shift detector, and two synchronous output detectors.

The synchronous detectors use the detected light signal and the fundamental component and the second harmonic of the phase-shifter drive frequency to determine the fluid velocity. Three separate optical systems can be operated simultaneously with the same laser and the same phase-shift detector. Thus, x, y, z position and velocity can be monitored.

This work was done by Lee Opert Heflinger of TRW, Inc., for **Marshall Space Flight Center.** *For further information, Circle 61 on the TSP Request Card.*
MFS-25465

Solar-Collector Radiometer

Unit measures up to 30,000 solar constants with 1 percent accuracy.

A water-cooled Kendall radiometer measures the output of solar energy concentrators. The unit measures irradiance up to 30,000 solar constants with 1 percent accuracy. It responds to wavelengths from ultraviolet to far infrared.

The radiometer aperture intercepts only a small portion of the total incident radiation. This radiation enters a blackened cavity where it is converted into heat. The heat flows through a thermal resistor upon which the hot junctions of a thermopile are mounted. The heat flux through the thermal resistor is an accurate measure of the amount of radiation passing through the radiometer aperture. An electrical heater winding, located on the cavity, provides electrical heating that is accurately equivalent to radiation heating and thereby gives an accurate calibration of the radiometer.

This work was done by James M. Kendall, Sr., of Caltech for **NASA's Jet Propulsion Laboratory.** *For further information, Circle 62 on the TSP Request Card.*
NPO-14986

Ceramic Solar Receiver

Matrix concept offers efficient heat transfer at high temperatures.

A proposed solar receiver would use a ceramic honeycomb matrix to absorb heat from the Sun and transfer it to a working fluid at temperatures of 1,095° to 1,650° C. The receiver could drive a gas-turbine engine or provide heat for industrial processes.

Solar radiation from a concentrator would enter the receiver through a

fused-silica dome and impinge on the ceramic matrix. The gaseous working fluid would enter the receiver through a sealed joint, cool the fused-silica dome, and flow through the matrix, which transfers heat to the gas. The heated gas would leave the receiver through another sealed joint.

This work was done by C. S. Robertson, Jr., of General Electric Co. for **NASA's Jet Propulsion Laboratory.** *For further information, Circle 63 on the TSP Request Card.*
NPO-15769

Bricks and Cans for Thermal Storage

Water-filled cans and bricks provide efficient thermal storage for solar space and hot-water heating.

Water-filled cans and bricks containing voids of various sizes may be superior to rocks as the heat-storage medium in a solar-energy storage tank. Tests were conducted to determine the effect of size and stacking orientation of standard 10-hole bricks and water-filled soup cans on heat storage, heat transfer, and pressure drop in a water-filled thermal storage bed. The test results indicate that these thermal storage mediums are suitable for use in both passive and active solar heating systems.

This work was done by Hrishikesh Saha of Alabama A & M University for **Marshall Space Flight Center.** *For further information, Circle 64 on the TSP Request Card.*
MFS-25625

Two-Fluid Solar Pond

Proposed insulated covered cavity would absorb and store solar energy in its lower heavier layer.

An insulated plastic-covered solar pond is proposed that would use two immiscible liquids of different densities to collect and store solar energy. The lighter density fluid, which is transparent to short-wavelength solar radiation, passes the radiation to the higher density fluid and minimizes upward ultraviolet-radiation losses. Adding a black dye to the bottom fluid enhances the absorption of the pond and its collection and storage efficiency. The small aperture of the pond cavity gives the pond the radiation-retention properties of a blackbody.

This work was done by Fikry L. Lansing of Caltech for **NASA's Jet Propulsion Laboratory.** *For further information, Circle 65 on the TSP Request Card.*

This invention is owned by NASA, and a patent application has been filed. Inquiries concerning nonexclusive or exclusive license for its commercial development should be addressed to the Patent Counsel, NASA Resident Office-JPL [see page A5]. Refer to NPO-15419.

Effects of Outdoor Soiling on Photovoltaic Modules

Airborne contaminants degrade module performances.

A report describes experiments to understand the effects of airborne contaminants on the sensitive surfaces of photovoltaic modules. Comparative electrical and optical performance data at field-test sites throughout the United States were collected and examined. The results show significant time and site dependence. During periods when natural removal processes, especially rain, do not dominate, the rate of particulate contamination appears to be largely material-independent. Glass and acrylic top-cover materials retain fewer particles than does silicone rubber. Side-by-side long-duration outdoor testing is the most effective way of evaluating soiling differences between materials.

This work was done by Alan R. Hoffman and Carl R. Maag, Jr., of Caltech for **NASA's Jet Propulsion Laboratory.** *To obtain a copy of the report, Circle 66 on the TSP Request Card.*
NPO-15186

Effect of Temperature on Fiber-Optic Delay

Fiber/jacket interactions affect performance.

Attenuation and phase measurements have been made to assess the effect of temperature on signal delay and attenuation in two fiber-optic cable samples. The signal source was a laser diode operating at a carrier wavelength of 0.817 microns.

In one of the cables (a loose-fiber type) the change of phase delay with temperature was 6.7 ppm/° C, independent of temperature in the range from −50° to +60° C. A virtually identical phase-delay change was observed in a bare, uncabled fiber. The attenuation increased with lower temperatures. In a solid-jacket fiber cable, a much higher change in phase delay with temperature is observed, ranging from 15 ppm/°C at +50° C to 47 ppm/°C at −50° C. The difference is believed to be due to the larger strain coupling between fiber and cable in the solid-jacket fiber cable. Loose-tube fiber cables are therefore considered more stable with respect to temperature.

This work was done by Larry A. Bergman, Sverre T. Eng, Alan R. Johnston, and George F. Lutes of Caltech for **NASA's Jet Propulsion Laboratory.** *For further information, Circle 67 on the TSP Request Card.*
NPO-15148

Stabilizing Fiber-Optic Transmission Lines

A voltage-controlled optical phase shifter is the key.

An optical phase shifter stabilizes the propagation delay of a fiber-optic transmission line by compensating for temperature and pressure effects. The technique is also applicable to phased array antenna systems and very-long-baseline interferometer distribution systems.

The change in the delay is determined by sending a signal to the far end of the optical fiber, where it is reflected and sent back down the same fiber. The two signals are compared, and the detected phase error signal drives a voltage-controlled optical phase shifter to reduce the error. This system also makes it possible to synchronize the phase of the references at different remote locations.

This work was done by George F. Lutes and Kam Y. Lau of Caltech for **NASA's Jet Propulsion Laboratory.** *For further information, Circle 68 on the TSP Request Card.*

This invention has been patented by NASA (U.S. Patent No 4,287,606). Inquiries concerning nonexclusive or exclusive license for its commercial development should be addressed to the Patent Counsel, NASA Resident Office-JPL [see page A5]. Refer to NPO-15036.

Ionic Refrigerator

With no moving parts, a proposed refrigerator would have a long life.

A refrigerator is proposed that would have a long lifetime because it would have no moving parts. The thermal energy of the refrigeration process would be transported by hydrogen ions that go through three phase changes in absorbing heat and three phase changes in dissipating heat.

Hydrogen would be vaporized, dissociated, and ionized on the anode side of a solid polymer electrolyte, where it would absorb heat from its surroundings. The ions then conduct through the electrolyte to the cathode side, where they are deionized, recombined, and condensed, giving off heat. The energy released on the cathode side is then conducted to a heat sink or radiated away.

This work was done by Robert Richter of Caltech for **NASA's Jet Propulsion Laboratory.** *For further information, Circle 69 on the TSP Request Card.*
NPO-15288

Estimating the Solubility of Gases in Battery Electrolytes

The estimates are in excellent agreement with experimental values.

A simple method is proposed for estimating the solubility of gases in electrolytes of lithium batteries, using expressions for the energy of vaporization and for the molar volume. An equation derived from solution theory relates the mole fraction of a gas in a solution to the mole fraction of the solvent, the average partial molar volumes, and the solubility parameters.

The method gives estimates that are in excellent agreement with experimental values when applied to nonpolar gases dissolved in nonassociated liquid electrolytes, such as $SOCl_2$, SO_2Cl_2, $POCl_3$, 2MTHF, and propylene carbonate.

This work was done by Daniel David Lawson and Harvey A. Frank of Caltech for **NASA's Jet Propulsion Laboratory.** *For further information, Circle 70 on the TSP Request Card.*
NPO-15610

Evaporation Tower With Prill Nozzles

A tower could be more efficient than conventional evaporation equipment.

Liquids such as milk and fruit juice could be concentrated by passing them through a tiny nozzle to form droplets, then allowing the droplets to fall through an evacuated tower with cooled walls. Because of the uniformity and small size of the droplets, a greater percentage of water would be removed than might be possible with conventional evaporation equipment.

The liquid would be formed into small uniform droplets by passing it through a "prill" nozzle, which can be an elliptical hole in a thin film. Depending on the temperature difference between the liquid and the tower wall, a percentage of water would evaporate on each pass through the tower; that is, for larger temperature differences, more water would be removed.

This work was done by Eugene R. du Fresne of Caltech for **NASA's Jet Propulsion Laboratory.** *For further information, Circle 71 on the TSP Request Card.*

Inquiries concerning rights for the commercial use of this invention should be addressed to the Patent Counsel, NASA Resident Office-JPL [see page A5]. Refer to NPO-15609.

Accelerated Solar-UV Test Chamber

Medium-pressure mercury-vapor lamps provide a high ratio of ultraviolet to total power.

A chamber for evaluting solar-ultraviolet (UV) radiation damage permits accelerated testing without overheating the test specimens. It uses a water jacket as a filter for medium-pressure mercury-vapor lamps, which concentrate about three times as much of their total radiation in the UV as do xenon-arc lamps. The chamber allows accelerated UV testing up to 30 Suns with specimen surface temperatures of 85° to 267° F (30° to 130° C).

This work was done by Amitava Gupta and Eric G. Laue of Caltech for **NASA's Jet Propulsion Laboratory.** *For further information, Circle 72 on the TSP Request Card.*
NPO-15063

Imaging Bubble Formation In a Drop Tube

The entire process is under control of a computer.

A computer-controlled image-acquisition system tracks an object, such as a water bubble, as it moves in a drop tube. Ultimately, such a tracking system will be used to observe fusion-pellet formation in a drop furnace.

To observe the formation/deformation of a bubble in a drop tube, the bubble is illuminated by xenon flashlamps and imaged by video cameras at 26 points along its path. The cameras are turned on automatically after the bubble is detected by photodetectors. All imaging data are stored on a video disk. By placing the entire process under the control of a computer, individual frames can be accessed quickly and efficiently, either in sequence for a single droplet or drop-to-drop at a single station.

This work was done by Roger Helizon and Mark C. Lee of Caltech for **NASA's Jet Propulsion Laboratory.** *For further information, Circle 73 on the TSP Request Card.*
NPO-15114

Microwave Radiation Detector

A direct photon detector responds to microwave frequencies.

A method based on trapped-ion frequency-generation standards is proposed to detect radio-frequency (RF) radiation at 40.5 GHz. The technique could be used for direct-detection (RF) communication, radar, and radio astronomy.

In the new direct quantum detector, laser pumping of trapped mercury ions causes them to emit photons when irradiated with 40.5-GHz microwave energy. The photons could be detected by a photomultiplier tube and counted to assess the level of the incident microwave radiation. The structure is thus a laser-pumped direct photon detector for the 40.5-GHz radiation. The technique can be extended to other radiation frequencies by using other species of trapped ions.

This work was done by James R. Lesh of Caltech for **NASA's Jet Propulsion Laboratory.** *For further information, Circle 74 on the TSP Request Card.*
NPO-15932

Materials

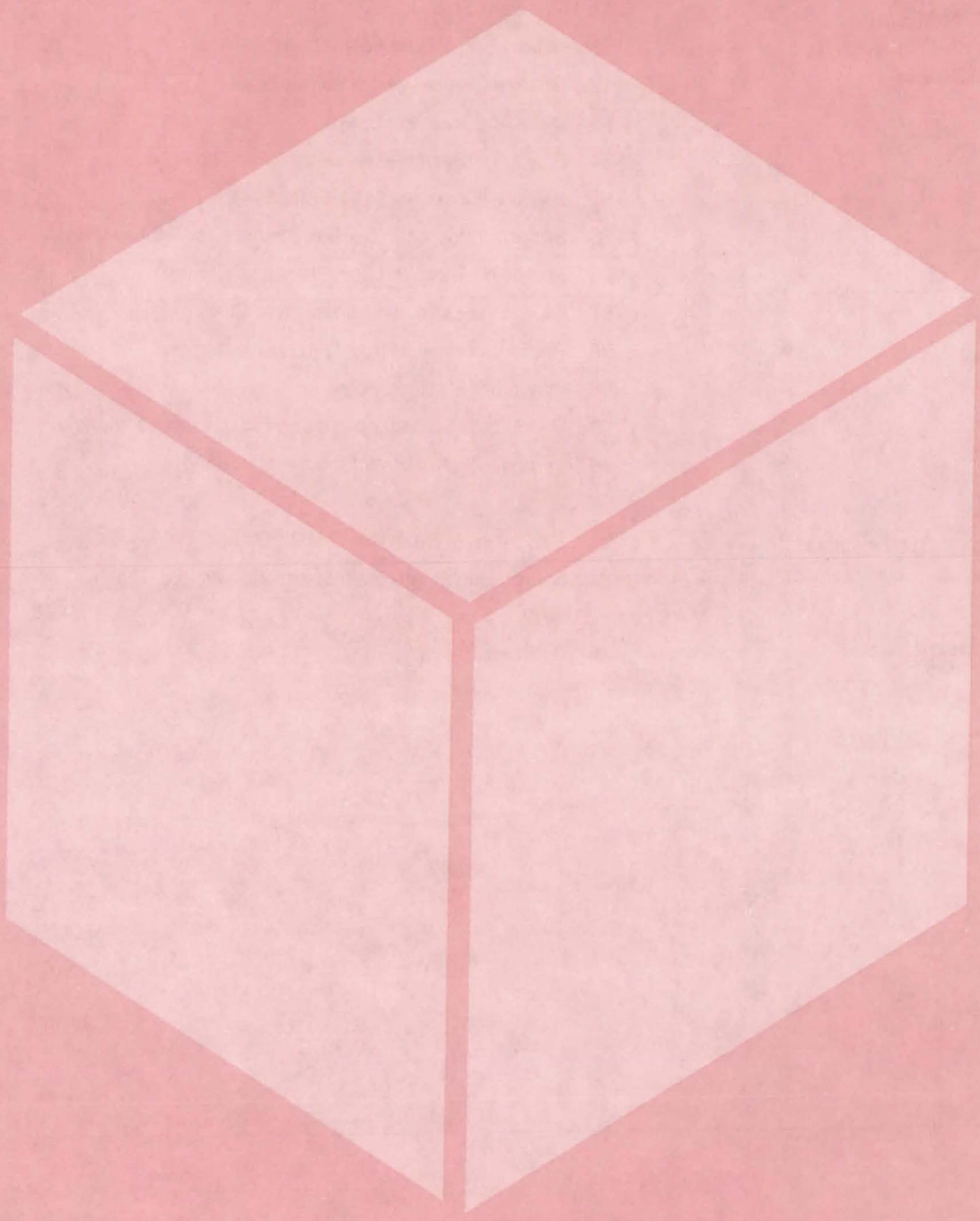

Hardware, Techniques, and Processes

Books and Reports

MiniBriefs

One-Step Coal Liquefaction

Steam injection improves yield and quality of product.

NASA's Jet Propulsion Laboratory, Pasadena, California

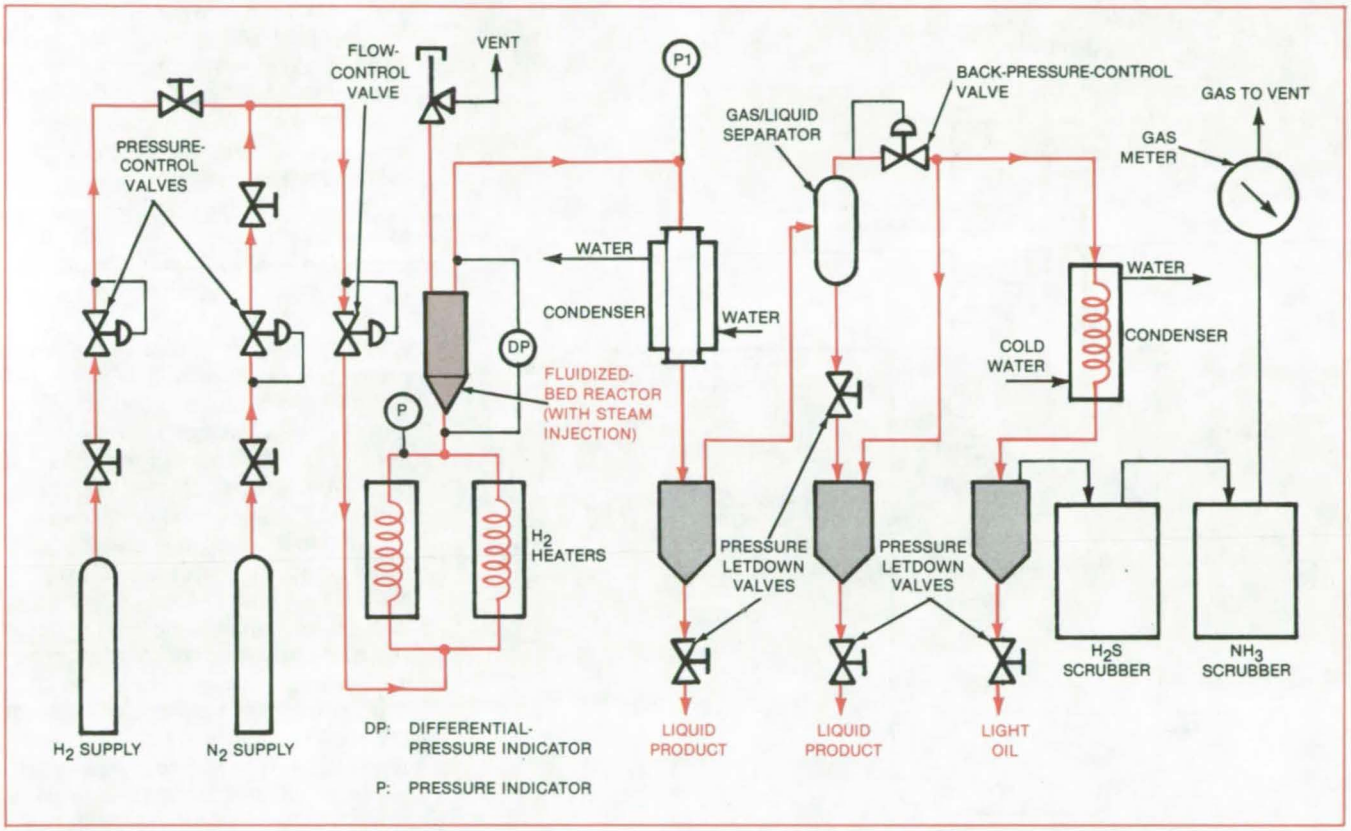

Crushed Coal Is Liquefied in a single step in a fluidized-bed reactor through which hydrogen and other gases flow.

A single-step process for liquefying coal increases liquid yield and reduces hydrogen consumption. The principal difference between this and earlier processes is that it includes the injection of steam into the reactor. The steam lowers the viscosity of the liquid product, so that further upgrading is unnecessary.

In older processes, the liquefaction product was highly viscous. It was therefore difficult to handle the product and to separate it from the catalyst. A second step had to be added to reduce viscosity and form the desired distillates, such as heating oil, jet fuel, and diesel fuel.

The new one-step process has been tested in a laboratory-scale fluidized-bed reactor system (see figure). The fluidized-bed reactor was 1.5 inches (3.8 cm) in inside diameter and 4 feet (1.2 m) high. A maximum liquid-product yield of about 33 percent (by weight of coal) was obtained from subbituminous coal at a temperature of about 1,000° F (540° C) and a pressure of 1,500 lb/in.^{2} (10 MPa). An increase in pressure to 2,000 lb/in.^{2} (14 MPa) did not increase the yield. However, the injection of steam into the reactor increased the liquid yield to 38 percent. In addition, steam injection slightly reduced hydrogen consumption.

In tests with bituminous coal (without steam injection), liquid yield increased with an increase of pressure from 1,500 to 2,000 lb/in.^{2}. A yield of 43 percent was obtained at a temperature of 1,000° F under a pressure of 2,000 lb/in.^{2}. The hydrogen consumption was 3.8 percent, versus 4.5 to 5 percent consumption in other processes. With optimized process conditions and steam injection, the liquid yield rose to about 50 percent, as compared with 40 to 45 percent for conventional liquefaction processes.

The liquid product from the subbituminous coal had 75 percent distillate boiling at temperatures up to 850° F (454° C) with a sulfur content of 0.38 percent. The injection of steam increased the distillate yield to 79 percent. The liquid product from the bituminous coal had 86 percent distillate boiling up to 850° F with a sulfur content of 0.41 percent. The concentration of asphaltenes was also low, indicating a high-quality liquid product.

This work was done by Shaik A. Qader of Caltech for **NASA's Jet Propulsion Laboratory.** *For further information, Circle 75 on the TSP Request Card.*

This invention is owned by NASA, and a patent application has been filed. Inquiries concerning nonexclusive or exclusive license for its commercial development should be addressed to the Patent Counsel, NASA Resident Office-JPL [see page A5]. Refer to NPO-15891.

Molten Slag Would Boost Coal Conversion

A proposed reactor would increase the residence time of unconverted char.

NASA's Jet Propulsion Laboratory, Pasadena, California

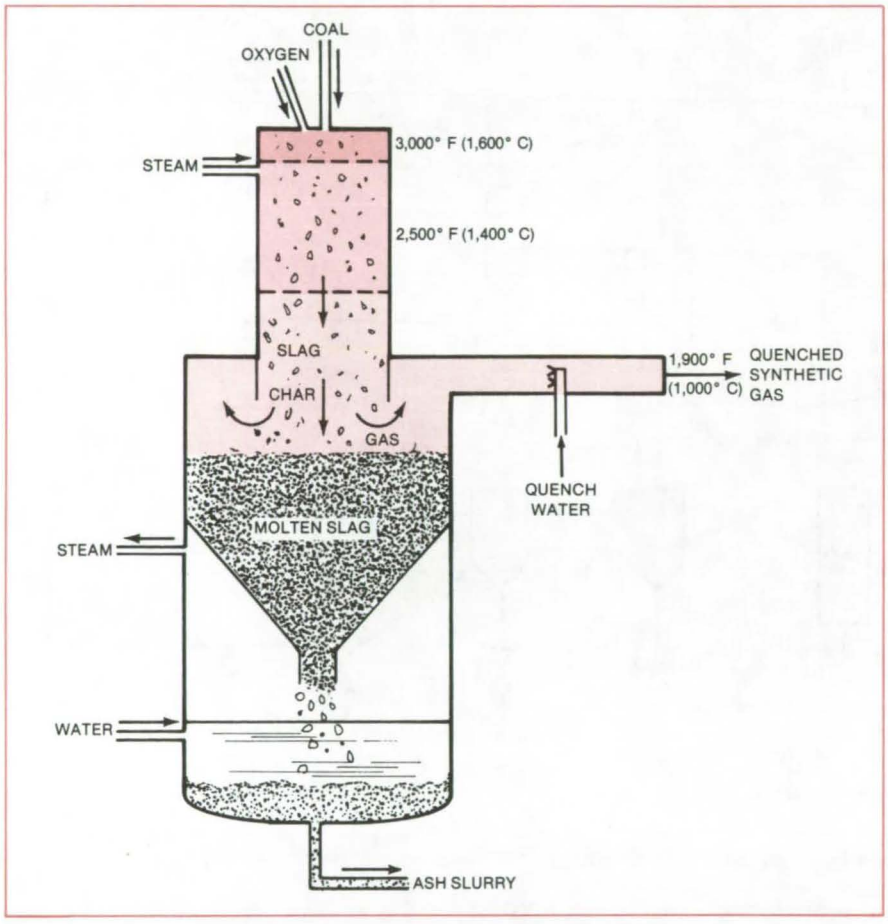

Near-100-Percent Carbon Conversion may be achievable in this reactor incorporating a molten-slag bath. The slag maintains the unconverted carbon impinging on its surface at high temperatures for a longer period of time, thus enhancing conversion.

A proposed single-stage coal gasifier uses a molten-slag bath to increase carbon conversion without increasing oxygen consumption. The slag would increase the effective residence time of unconverted char by providing an oxygen-transfer medium.

The improved gasifier was conceived to eliminate the problems presented by unreacted coal or char. Currently, this char must be recycled or burned in a boiler. This may be difficult and costly when the reactor is incorporated in a coal-conversion facility.

The molten slag is added at the bottom of the reactor (see figure). It is produced from the coal-ash minerals. Unconverted carbon particles land on the surface of the slag and continue to be exposed to the high-temperature gases of the reactor. The unreacted carbon thus has a better chance of converting to gas by reacting with such other gases as water, carbon dioxide, or hydrogen or with an oxygen-transfer medium such as ferric oxide. The synthetic gas (mostly CO and H_2) is quenched with a water spray. Ash is removed as a water slurry.

This work was done by Joseph F. Ferrall of Caltech for **NASA's Jet Propulsion Laboratory.** *For further information, Circle 76 on the TSP Request Card.*

NPO-15711

Silicone Cerenkov-Radiator Material

Dyes enhance visible output.

Goddard Space Flight Center, Greenbelt, Maryland

Three fluorescent dyes combine to increase the output of a silicone material that would normally have a low yield of visible Cerenkov radiation by converting the large amount of available ultraviolet photons into visible light. The dyes are zone-refined paraterphenyl, scintillation-grade bis[o-methyl styryl]benzene (bis-MSB), and scintillation-grade polyphenylene oxide (PPO).

The base material is RTV-615, a commercial silicone rubber. This material is desirable as a Cerenkov radiator because it is solid, easily molded at room temperature, and transparent to visible light. It has a refractive index, n, of 1.406, as compared to that of such other Cerenkov radiators as water (n = 1.33) and glass or plastics of $n \geq 1.5$. The intermediate refractive index results in an intermediate Cerenkov threshold speed (speed of light ÷ n), thus enabling the detection of charged particles traveling at speeds between those detectable

with the other Cerenkov-radiator materials.

In the silicone, charged particles at and near the threshold speed generate Cerenkov radiation at ultraviolet wavelengths. Since the material is a strong ultraviolet absorber, it is necessary to convert the radiation to visible light at the source: This allows a substantial amount of radiation to escape from the material to be detected by a photomultiplier or other device sensitive to visible light. The dye mixture, dispersed throughout the RTV-615, efficiently converts ultraviolet Cerenkov radiation of wavelengths from 210 through 400 nm into visible light in the 400- to 530-nm blue region. All three dyes are necessary to effect the conversion. The ultraviolet energy is absorbed by the paraterphenyl and PPO, then radiatively transferred to the bis-MSB that emits in the blue.

The dyes are incorporated into the silicone just before molding. First, the dye powders are dissolved in a volatile solvent, such as grain alcohol. The solution is mixed with the uncured silicone-rubber liquid, and the mixture is placed in a vacuum to remove the solvent. After evaporation of the solvent, the mixture is poured into a mold and cured for several hours at room temperature.

Final compositions are generally in the range of 0.01 to 0.1 gram of paraterphenyl, 0.02 to 0.2 gram of bis-MSB, and 0.08 to 0.8 gram of PPO per 100 grams of RTV-615. Sheets are typically molded 1 m square and up to 2 cm thick. The cured sheet is wrapped with an opaque material to exclude unwanted visible light and other background radiation.

This work was done by V. K. Balasubrahmanyan, Jonathan F. Ormes, and Robert E. Streitmatter of **Goddard Space Flight Center.** *For further information, Circle 77 on the TSP Request Card.*

This invention is owned by NASA, and a patent application has been filed. Inquiries concerning nonexclusive or exclusive license for its commercial development should be addressed to the Patent Counsel, Goddard Space Flight Center [see page A5]. *Refer to GSC-12805.*

Detecting Methane Leaks

A remote sensor uses laser radiation backscattered from natural targets.

NASA's Jet Propulsion Laboratory, Pasadena, California

An improved laser system for detecting methane (CH_4) concentrations in air uses natural topographic targets without reflecting mirrors. Previous systems had lower sensitivity and thus required mirrors to be placed on the targets to obtain sufficiently strong return signals. The new remote sensor, which is capable of scanning areas of up to 100 m in radius, could also be used for remote detection of natural-gas leaks, and the location of methane emissions in landfill sites.

In the system shown in the figure, two He/Ne lasers generate the required wavelengths for measuring CH_4 concentrations by differential absorption. One laser operates at 3.3913 microns, the other is modified to operate at 3.3903 microns by inserting a cell containing CH_4 into the optical cavity to quench the favored line at 3.3913 microns. The chopper wheel is operated at 2 kHz.

Laser radiation backscatterred from a topographic target is collected by a 30-cm-diameter spherical mirror near the transmitter. The beam is then imaged onto a 2-mm-diameter InSb detector cooled to 77 K. A narrow-band optical filter in front of the detector is also cooled to 77 K. The signal is amplified and sent to a phase-sensitive detector for analysis.

With a pine wall as a natural reflecting target, sensitivity of the system was measured at about 5 ppm-m in 1 second. The sensitivity falls off as $1/R^2$, where R is the distance to the target. A commercial version of this system is under development.

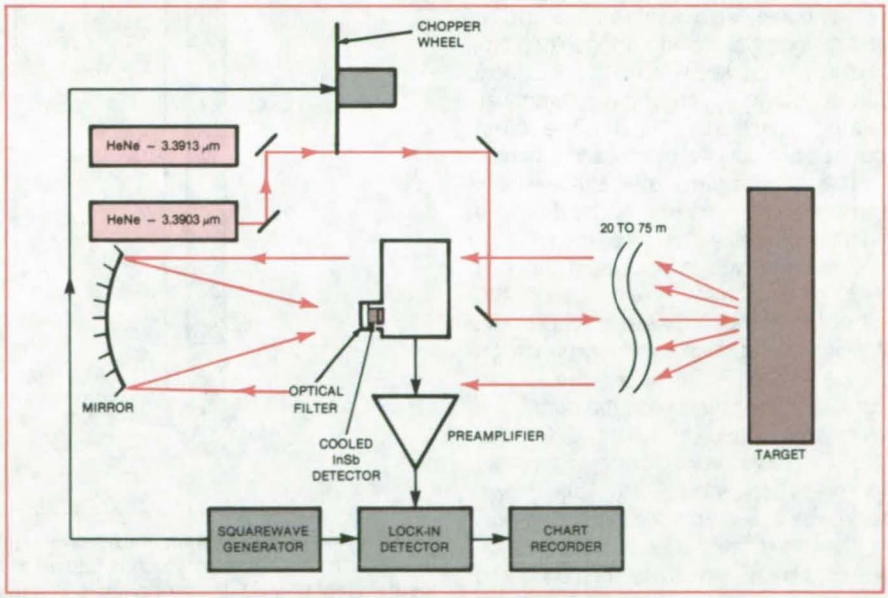

The **He/Ne Laser System for Remote Scanning of Methane Leaks** employs a topographic target to scatter light to a receiver near the laser transmitter. The apparatus, which is powered by a 1.5-kW generator, can be transported to field sites and pointed at suspected methane leaks.

This work was done by William B. Grant and E. David Hinkley of Caltech for **NASA's Jet Propulsion Laboratory.** *For further information, Circle 78 on the TSP Request Card.*

This invention is owned by NASA, and a patent application has been filed. Inquiries concerning nonexclusive or exclusive license for its commercial development should be addressed to the Patent Counsel, NASA Resident Office-JPL [see page A5]. *Refer to NPO-15790.*

Polycarbosilazane-Resin Polymerization Process

Process is suitable for production of silicon nitride/silicon carbide fibers.

Marshall Space Flight Center, Alabama

The polymerization of polycarbosilazane resin from the monomer tris(N-methylamino)methylsilane has been demonstrated at laboratory scale. High-tensile-strength silicon carbide/silicon nitride ($Si_xN_yC_z$) fibers are prepared by pyrolyzing fibers drawn from a melt of polycarbosilazane resin. Such fibers show promise as replacements for carbon fibers in high-strength composites for automotive, aerospace, and other applications where the high electrical conductivity of the carbon fibers makes them unsuitable. The resistivity of $Si_xN_yC_z$ fibers prepared from polycarbosilazane is 7×10^8 ohm-cm, which is 10^6 times greater than that of carbon fibers.

The new polymerization process was demonstrated using the reflux distillation apparatus shown in the figure. It consists of a 250-ml round-bottom boiling flask or pot, a condenser, a drying tube, and a 6-ft (1.8-m) long glass column 1 inch (2.5 cm) in diameter packed with glass rings. Most of the packed region of the column was heated by a cylindrical heater. The boiling pot was surrounded by a heating mantle.

The tris(N-methylamino)methylsilane monomer was prepared by the dropwise addition of methyltrichlorosilane to liquefied methylamine in petroleum ether at $-30°$ C. To achieve polymerization, 100 ml of the monomer were placed in the boiling pot and refluxed at polymerization temperatures: For 2 hours, the heated portion of the column and the boiling pot were maintained at about 520° and 475° C, respectively. After being cooled to room temperature, the light brown resin was collected from the boiling pot.

The resin is soluble in conventional solvents such as methylene chloride and chloroform. The average molecular weight was determined to be 11,500 by gel-permeation chromatography. The softening point of the resin was about 210° F (100° C). The chemical structure (see right side of figure) was inferred in part from infrared spectroscopic data, which showed features corresponding to $N-H$, $C-H$, $N-CH_3$, and $Si-CH_3$ bonds, and from nuclear magnetic resonance spectroscopy, which showed peaks corresponding to $N-CH_3$ and $Si-CH_3$.

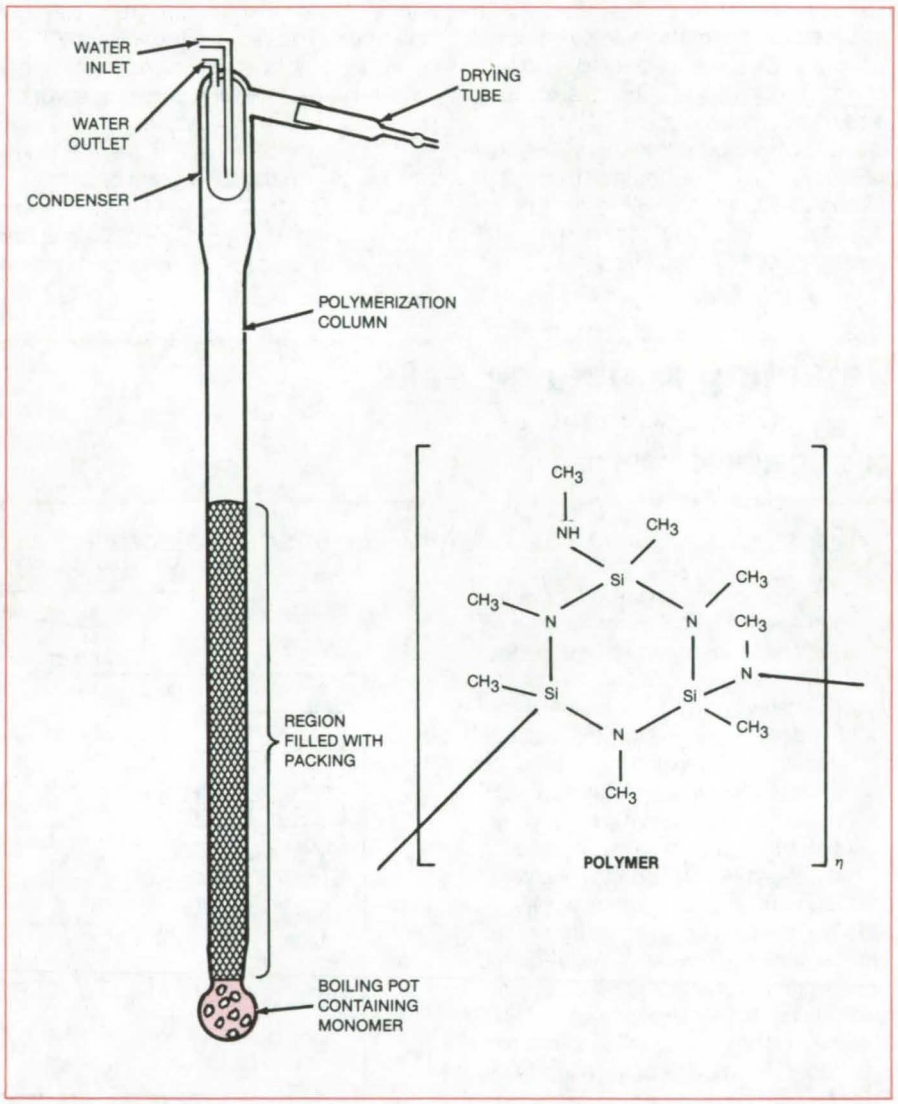

The **Polymerization System** shown on the left is used to produce polycarbosilazane resin, the inferred structure of which is shown at the right. The packed region is surrounded by heaters (not shown). The monomer is placed in the boiling pot and heated for 2 hours during which time polymerization gradually takes place.

This work was done by B. G. Penn, F. E. Ledbetter III, and J. M. Clemons of **Marshall Space Flight Center.** *For further information, Circle 79 on the TSP Request Card.*

Inquiries concerning rights for the commercial use of this invention should be addressed to the Patent Counsel, Marshall Space Flight Center [see page A5]. *Refer to MFS-25758.*

$Si_xN_yC_z$ Fibers for Safer Composites

High-strength, high-electrical-resistance fibers are proposed in place of graphite to make safer composites.

Marshall Space Flight Center, Alabama

Graphite fibers are widely used to construct fiber-reinforced composites. However, because of the high electrical conductivity of graphite fibers, there are potential hazards during the manufacture, application, and disposal of reinforced composites made with them.

Silicon nitride/silicon carbide ($Si_xN_yC_z$) fibers prepared by the pyrolysis of polycarbosilazanes are a proposed substitute for carbon fibers. Tests show the new fibers to have physical properties comparable to graphite but with a lower conductivity.

The electrical resistivity of the silicon nitride/silicon carbide fibers is about a million times greater than that of graphite. The average resistivity value obtained for the new fibers, which is about 7×10^8 ohm-cm, lies within the range of semiconductors (10^{-3} to 10^{10} ohm-cm) and approaches the value of true insulators.

The mechanical properties of the fibers are comparable to those of carbon fibers. For example, the tensile modulus [29×10^6 psi (2.0×10^{11} N/m^2)] for a fiber 0.4 mil (0.1 mm) in diameter is of the same order of magnitude as that of graphite, which is 55×10^6 psi (3.8×10^{11} N/m^2). The figure shows the decrease in the tensile rupture modulus of the fibers with increasing diameter. The prepyrolyzed fibers also exhibit the same characterstic, which means that the amount of tension applied to the precursor fiber to orient the molecular chains during pyrolysis and increase the strength of the silicon nitride/silicon carbide fiber is limited by the fiber diameter.

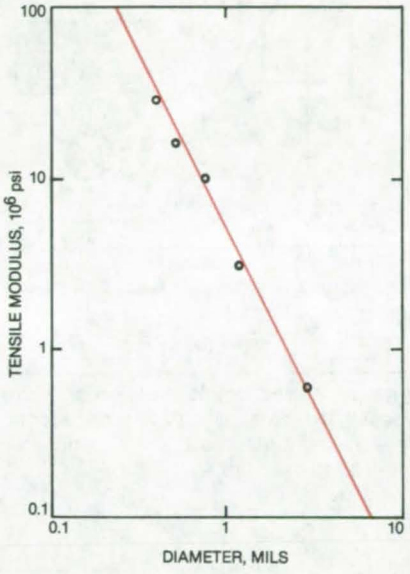

The **Tensile Rupture Modulus** of the silicon carbide/silicon nitride fibers decreases with increasing diameter. This trend will affect the properties of composite materials constructed from the fibers since high-modulus fibers serve as constraints to deformation of the composite matrix.

Polycarbosilazanes can be prepared from various monomers. The silicon nitride/silicon carbide fibers tested were pyrolyzed from polycarbosilazanes prepared from tris(N-methylamino) methylsilane. Polycarbosilazane resin was drawn into fibers from a melt and subsequently treated and pyrolyzed. The pyrolyzed fibers are shiny black.

This work was done by F. E. Ledbetter III, B. G. Penn, and J. M. Clemons of **Marshall Space Flight Center.** *For further information, Circle 80 on the TSP Request Card.*

This invention is owned by NASA, and a patent application has been filed. Inquiries concerning nonexclusive or exclusive license for its commercial development should be addressed to the Patent Counsel, Marshall Space Flight Center *[see page A5].* *Refer to MFS-25721.*

Silicon Nitride Antireflection Coatings for Photovoltaic Cells

Chemical-vapor deposition is adapted to yield a graded index of refraction.

Ames Research Center, Moffett Field, California

Antireflection coatings that increase the efficiency of silicon solar cells are formed by the plasma-enhanced chemical-vapor deposition (PECVD) of silicon nitride coatings. The silicon nitride is deposited in layers, the refractive index of which decreases with distance away from the cell/coating interface. The changing index of refraction allows adjustment of the spectral transmittance for the wavelengths at which the cell is most effective at converting light to electric current.

The silicon nitride layers are deposited on the cells in a reactor between resistance-heated stainless-steel electrodes in an atmosphere of silane, argon, and ammonia with a total pressure of 27 Pa (see figure). The cells rest on the grounded lower electrode, which is heated to 300° C. A signal generator operating at 13.56 MHz and 10 watts is connected to the electrodes to establish the plasma. The plasma enhances the reaction of silane and ammonia, which deposits solid silicon nitride on the cell surface.

Silane makes up 10.63 percent of the total silane/argon flow, which is held constant at 23 stdcm^3/min. The flow of ammonia is doubled every 510 s. Increasing the nitrogen periodically creates layers of increasingly-nitrogen-rich

(continued on next page)

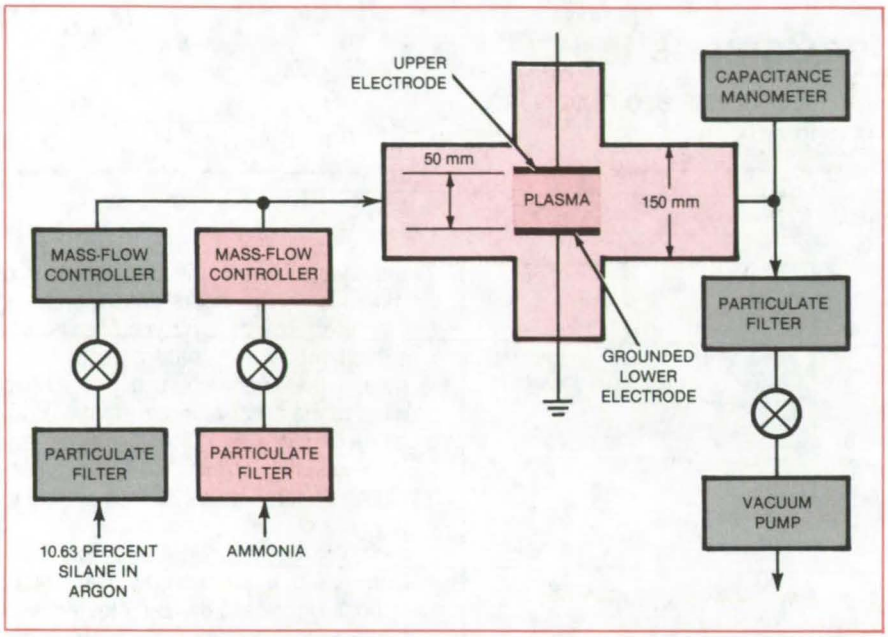

Plasma-Enhanced Chemical-Vapor Deposition is performed in this reaction chamber. The flow of ammonia is increased during the process, to increase the nitrogen content of the silicon nitride outer layers. The total gas pressure is maintained at 27 Pa by means of the throttling valve. The power density is adjusted to 127 mW/cm^2.

material on the cell. The refractive index decreases as the nitrogen content of a layer increases. In a four-layer coating, for example, the refractive index may vary in steps from 3.1 at the cell/coating interface to 1.83 at the outer coating surface as the ammonia flow is varied from 0.18 to 1.5 stdcm^3/min.

The new PECVD technique is the first to vary nitrogen concentration to control the index of refraction. In one instance, multiple layers of PECVD silicon nitride decreased the total reflectance of polished silicon from 35 percent to 3 percent over the wavelength range of 0.4 to 1.0 μm. The average conversion efficiency of solar cells was increased from 8.84 percent to 12.63 percent.

This work was done by C. C. Johnson and T. Wydeven of **Ames Research Center** *and K. Donohoe of Tegal Corp. For further information, Circle 81 on the TSP Request Card.*

Inquiries concerning rights for the commercial use of this invention should be addressed to the Patent Counsel, Ames Research Center [see page A5]. *Refer to ARC-11447.*

Improving Trace-Ion Sensitivity

Background noise is reduced by some special precautions.

Marshall Space Flight Center, Alabama

Special precautions minimize contamination in trace-ion detection systems, improving quality control in a host of production operations, including integrated-circuit fabrication, lens fabrication, and vacuum-tube assembly. When used with one commercial contamination detector, the procedures increase sensitivity by 25 percent overall and nearly double it for small samples.

The new technique — really a way of reducing background noise — applies to a standard setup for measuring the contamination of integrated circuits and other components, in which a "clean" solution is passed over the component, and the solution resistance is monitored. As ions are picked up, the solution resistance decreases, thus providing a measure of ionic contamination. In these measurements, a high baseline resistance, before a component is inserted, is desirable since it allows lower levels of contamination to be detected.

The commercial system used by a NASA contractor (Alpha Ionograph system) gave a maximum baseline resistance of 50 megohms. Contamination picked up from the air and flow-line components prevented the attainment of higher baseline resistances.

The new procedures routinely yield a baseline resistance of 62.5 ohms. Three specific changes were made:

1. A blanket of argon flows over the solution so that there is no chance for contamination from the air to creep in,
2. A conventional pump is replaced with one made of polytetrafluoroethylene components, and
3. All metal couplings are eliminated from flow lines.

These provisions allow the requisite increase in solution baseline resistance. For small samples, the resistance increases to 100 megohms — double the maximum value with the old method.

The conventional test tank is fitted at its top with a rectangular funnel gate. A tank of argon gas with a regulator and flowmeter is connected to the funnel gate by a vinyl tube. The tank is connected by vinyl tubing to the new recirculating pump with a polytetrafluoroethylene piston.

This work was done by Richard N. Buggle of Honeywell Inc. for **Marshall Space Flight Center.** *No further documentation is available.*
MFS-25766

Discharge Extracts Oxygen From CO_2

Process under development could supply oxygen for life support in hazardous environments.

Ames Research Center, Moffett Field, California

A process for electrically decomposing carbon dioxide could supply oxygen for life support in undersea research, mines, and other hazardous environments. Developed at NASA's Ames Research Center, the process for reducing CO_2 gas occurs in a special high-voltage-discharge reactor. Tests of a prototype reactor have identified the important process variables. Conversion efficiency is now only about one-half that of chemical reduction of CO_2, but it is expected to improve as the process is optimized.

The figure shows the prototype reactor used in laboratory tests. It consists of concentric glass cylinders, sealed together at the ends. One end of the double-walled vessel has a gas inlet; a gas outlet is fused into the other end. Electrodes are silverplated onto the reactor external surfaces — one on the inside diameter of the inner wall, the other on the outside diameter of the outer wall.

A "silent" electric discharge occurs in the approximately-1.3-millimeter space between the cylinders when an alternating potential above 3,200 volts is impressed across the electrodes. CO_2 pressure is 40 kN/m^2, or 300 mm of mercury. Under those conditions, the CO_2 gas becomes partially ionized and conductive, and a portion (up to about 12 percent) is reduced to O_2 and CO.

The tests show that the current in the discharge plasma is the primary variable responsible for the reduction of carbon dioxide. Current density and gas-flow rate are related directly to the rate of reduction, while voltage and frequency have little effect other than to establish current levels. Temperature and pressure also have little effect.

Power consumption is high because the reactor vessel, which behaves as a capacitor, has a low power factor. The addition of an inductive element to create a resonant circuit improves the power factor and reduces power consumption. The power factor and carbon dioxide reduction rate are optimized when the voltage is only slightly greater than that required to induce the discharge. The maximum efficiency with the present design is 1 liter of carbon dioxide reduced per 100 watt-hours.

In contrast to chemical reduction, the silent-electric-discharge method of carbon dioxide reduction operates at near-ambient temperature and pressure. The energy cost, using the present design, is twice that of the solid electrolyte method. However, the design can be improved and the cost reduced.

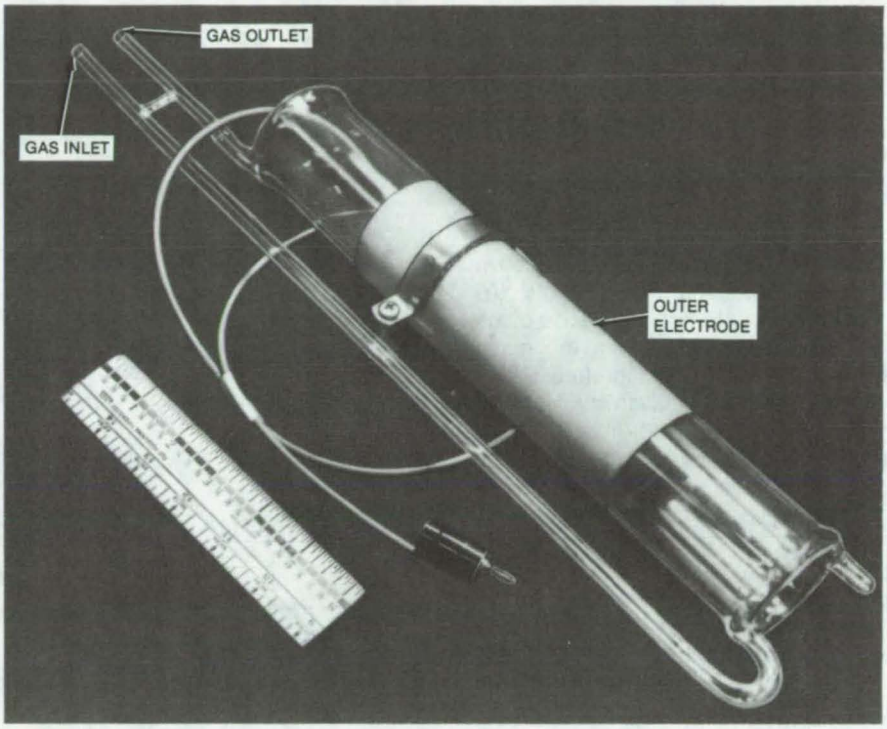

The Prototype CO_2 Reactor Vessel produces oxygen from carbon dioxide at an expense of about 100 watt-hours of electricity per liter of gas reduced. Suggested design changes to improve efficiency include narrowing the gap between the walls to operate at lower voltages and increasing the area of one electrode while decreasing the area of the other to reduce the capacitance.

This work was done by Robert S. Luce of Lockheed Missiles & Space Co. for **Ames Research Center.** *Further information may be found in NASA CR-152146 [N78-25767/NSP], "An Investigation of the Reduction of Carbon Dioxide in a Silent Electric Discharge" [$10]. A copy may be purchased [prepayment required] from the National Technical Information Service, Springfield, Virginia 22161.*

ARC-11305

Perfluoroalkylene-Ether Triazine Elastomers

New process yields a product that resists heat and the action of oxygen and water.

Ames Research Center, Moffett Field, California

The end-product physical properties are carefully controlled in a new synthesis procedure for perfluoroalkylene-ether triazine elastomers. The elastomers are highly resistant to heat, oxidation, and hydrolysis.

The starting material is perfluoroalkylene-ether dinitrile, which is reacted rapidly with ammonia to form the corresponding diamidine. In the reaction, it is essential that a large excess of liquid ammonia and a low concentration of the fluoroether dinitrile reactant be maintained. The dinitrile is therefore added drop by drop as a solution in Freon-113 (1,1,2 trichloro-1,2,2-trifluoroethane) and the reaction mixture stirred rapidly during the addition.

The diamidine reaction product dissolved in Freon-113 is converted to perfluoroalkylene-ether (imidoylamidine) dinitrile by reaction with perfluoroalkylene-ether dinitrile. The dinitrile, dissolved in Freon-113, is reacted with perfluoroalkylether acid anhydride to yield perfluoroalkylene-ether (triazine) dinitrile, the linear triazine prepolymer. The final elastomer is prepared by reacting the prepolymer with liquid ammonia, then heating it at 150° C. The polymerization reactions are summarized in the figure.

All reactions are stepwise — that is, reactant is added to the mixture only after previously added reactant has been consumed. Emphasis on a stepwise process to achieve reproducibility is underscored by the uniform thermal and physical properties of the final cross-linked polymers. Indeed, efforts to develop a batch, rather than stepwise, process produced highly erratic results and were abandoned.

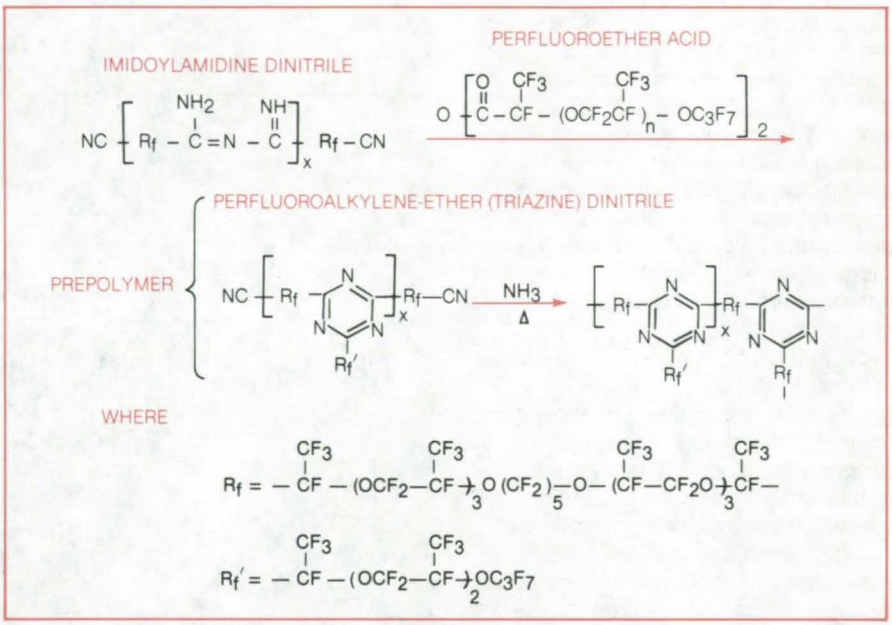

In the Ring-Closing Step, which gives the elastomer its stability, imidoylamidine dinitrile reacts with perfluoroether acid, yielding prepolymer. The prepolymer is then treated with ammonia and cured by heating to form the polymer.

A perfluoroalkylene-ether triazine elastomer with a molecular weight of about 6,200 has a light-tan color and highly desirable properties. It remains flexible at low temperatures, having a glass-transition temperature of −45° C. It survives boiling in water for 2 weeks without weight loss or deterioration of physical properties. Weight loss after exposure to air or nitrogen at 300° C is less than 5 percent.

This work was done by Robert W. Rosser of **Ames Research Center** *and Timothy S. Chen and Chungheng Cheng of San Jose State University. For further information, Circle 82 on the TSP Request Card.*

Inquiries concerning rights for the commercial use of this invention should be addressed to the Patent Counsel, Ames Research Center [*see page A5*]. *Refer to ARC-11402.*

Elastomer-Modified Polyimides

New resins yield laminates with improved mechanical properties.

Ames Research Center, Moffett Field, California

Phosphorus-containing imide resins have now been toughened by the inclusion of elastomers. The inclusion of phosphine oxides has been known to increase fire retardance in this and other polymer systems, while the incorporation of elastomers in other polymer systems has been observed to increase toughness.

A thermosetting resin is prepared by reacting an N-N′-bisimide of an unsaturated dicarboxylic acid of formula 1 (see figure) with an amine-terminated butadiene-acrylonitrile elastomer (ATBN) or with an amine-terminated

perfluoroalkylene ether. The amine-terminated elastomers are added in amounts up to 10 percent by weight of the imide resins. The reaction may be carried out in an inert polar solvent such as dimethylformamide, N-methyl pyrrolidone, or dimethylacetamide. A solution of the solvent and the reactants can be used for fabricating fiber-reinforced structures or as an adhesive. The following procedure is typical:

Bisimide from tris(m-aminophenylphosphine oxide) was prepared by reacting 24.225 g of amine (0.075 mole) with 15.68 g of maleic anhydride (0.16 mole) in dimethylformamide. The solution was stirred at room temperature for 1 hour and then refluxed for 1 to 2 hours. The solution was then cooled, and 2.6 g of ATBN were added. It was stirred at room temperature overnight.

Eight plies of graphite cloth were brush-coated with this solution, and these prepregs were dried at 125° ± 5° C for 20 to 30 minutes. After stacking together, curing was done at 180° C at a pressure of 140 psi (9.7×10^5 N/m^2) for 2½ hours. Postcuring was done at 218° ± 2° C for 16 hours.

Shear strength of a laminate containing 26.6 percent resin was 5.85×10^3 psi (4.03×10^7 N/m^2), tensile strength was 61.91×10^3 psi (4.269×10^8 N/m^2), flexural strength was 149.62 psi (1.032×10^6 N/m^2), and flexural modulus was 25.21×10^6 psi (1.738×10^{11} N/m^2). These indicate an improvement of 98.9, 35.2, 96.8, and 17.7 percent, respectively, over the unmodified resin.

For composites made with the modified polymers, environmental effects upon performance have yet to be determined. In particular, some embrittlement may occur at temperatures below 0° C and some softening above 75° C. Moisture absorption may also cause some degradation of properties.

This work was done by George M. Fohlen, John Parker, and Indra K. Varma of **Ames Research Center.** *No further documentation is available.*

Inquiries concerning rights for the commercial use of this invention should be addressed to the Patent Counsel, Ames Research Center [see page A5]. Refer to ARC-11400.

N-N′-BISIMIDE OF AN UNSATURATED DICARBOXYLIC ACID

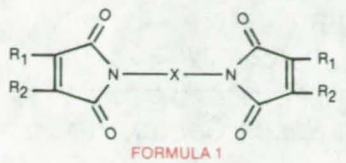

$R_1, R_2 = H-, CH_3-, Cl-$

FORMULA 1

WHERE X IS a, b, c, or d

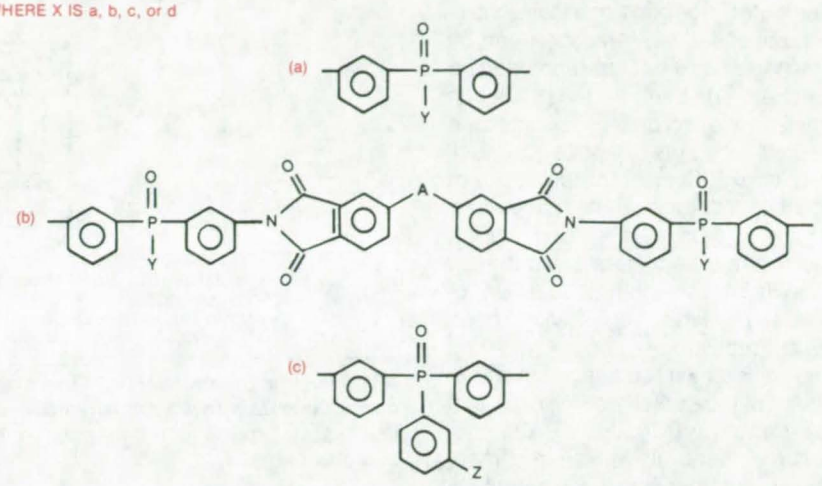

$Y = CH_3-, C_2H_5-, C_6H_5-$

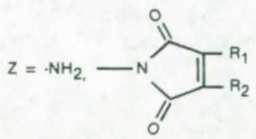

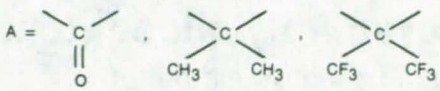

AMINE-TERMINATED ELASTOMERS

AMINE-TERMINATED PERFLUOROALKLENE ETHER

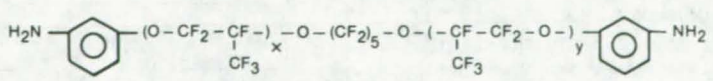

x + y = 2 OR 3

AMINE-TERMINATED BUTADIENE-ACRYLONITRILE ELASTOMER (ATBN)

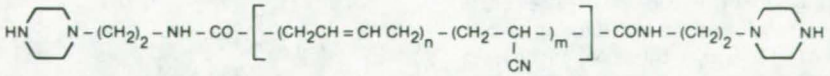

Ingredients of the Modified Polymer include a bisimide of formula 1 and an amine-terminated elastomer of a type shown below. The cure is effected by heating to a temperature that is suited to the particular ingredients used and is generally in the range of 200° to 300° C.

Predicting Moisture Absorption in Composite Materials

Heat-transport programs are adaptable for absorption analysis.

Lyndon B. Johnson Space Center, Houston, Texas

Computer programs that solve complex problems in heat transport can be adapted to solve what may appear to be an unrelated problem — the prediction of moisture absorption by composite materials, such as graphite-fiber-reinforced epoxy. Since moisture content seriously affects the strength and other mechanical properties of composites, manufacturers and users could benefit substantially from the abundance of software available for solving heat-transport problems.

The differential equations that describe heat transport by conduction and mass transport by diffusion (the mechanism of water absorption in composites) are of the same mathematical type. Moreover, thermal-analysis computer programs for conductive heat transport have received much attention since the late 1950's and have been highly refined. Thus, instead of starting over and creating new programs to compute water absorption, designers can often simply adapt thermal-analysis programs.

In an application of the technique by a NASA contractor, moisture absorption predicted by an adapted heat-transport program for a graphite/epoxy sandwich panel (see figure) accurately matched data for an isothermal moisture-absorption test on the panel. However, moisture content was a strong function of specimen temperature, indicating that serious errors could be introduced if average specimen temperature were used to determine diffusion coefficients when a significant temperature gradient exists in the specimen. The thermal-analysis-based program avoids such errors because it simultaneously calculates temperatures and concentrations and can use the temperature-dependent properties.

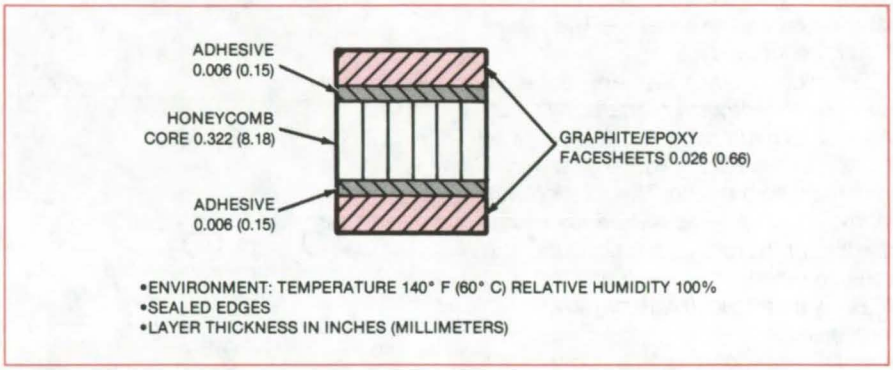

A **Lightweight Sandwich Panel Specimen** was used for a comparison of water absorption measurements with program predictions. In the program model, the moisture — like heat in a heat-transport problem — moves through a variety of materials and structures along complex paths.

This work was done by John R. Haines of McDonnell Douglas Corp. for **Johnson Space Center.** *For further information, Circle 84 on the TSP Request Card.*
MSC-20109

Improved Polyimide Intumescent Coating

Nucleating agents yield better char foam when fire strikes.

Ames Research Center, Moffett Field, California

A new polyimide intumescent coating (see table) uses titanium dioxide (TiO_2) and glass microballoons as nucleating agents to improve the foaming characteristics of a commercially-available polyimide precursor resin.

The polyimide precursor resin is a partially-polymerized, low-molecular-weight, resin formed by reacting a half ester of an aromatic tetracarboxylic acid (e.g., from benzophenone dianhydride) with an aromatic diamine. In the further polymerization/curing step, the small

Ingredient	Proportion by Weight
Polyimide Precursor Resin Powder (Monsanto Skybond RI-7271 or Equivalent)	1.00
Methanol	1.67
Titanium Dioxide	0.044
Glass Microballoons	0.022

In the **Thermal-Protection Coating Formulation,** ingredient proportions are not critical and can vary somewhat from those shown here.

esterifying alcohol (e.g., ethanol) molecule is split out and functions as a pneumatogen (blowing agent) to form the foam. At the same time, a ring closure reaction takes place between the freed carboxyl group and remaining hydrogen on the aromatic diamine to form the polyimide structure.

Without the nucleating agents, the resin forms a low-density foam with large irregular cells or bubbles when a flame is applied. The nucleating-agent particles trigger the formation of many smaller, more uniformly sized cells, resulting in improved thermal-insulating and mechanical strength characteristics.

A solution containing the improved coating can be brushed onto metal and other surfaces. By applying successive coats (with intermediate drying), a tenacious film up to 0.03 in. (0.8 mm) thick can be formed. When a flame is applied to the surface of the coating, it forms a thick, low-density insulating foam that emits little smoke or noxious fumes and is only slowly ablated away. Depending on initial film thickness, the substrate temperature can remain below 400° F (204° C) for 15 to 45 minutes when subjected to a flame with a temperature of of about 1,000° F (540° C) capable of supplying heat (to a cool surface) at the rate of 8 Btu/s-ft^2 (90 kW/m^2).

One use proposed for the new formulation is coating interior surfaces in commercial aircraft. If there were a fuel fire outside the plane, inside air temperatures might be kept low enough to allow the fire to be put out and the passengers to escape. Also, combustible overhead racks and ceiling panels with intumescent polyimide surface coating would not overheat, burst into flames, and add their fuel and smoke to an inside fire.

This work was done by Ival O. Salyer and B. Lawrence Fox of the University of Dayton for **Ames Research Center.** *For further information, Circle 85 on the TSP Request Card.*
ARC-11369

Books and Reports

These reports, studies, and handbooks are available from NASA as Technical Support Packages (TSP's) when a Request Card number is cited; otherwise they are available from the National Technical Information Service.

Evaluation of Structural Cellular Glass

Preliminary design information is presented.

The use of cellular (foamed) glass in substrates for solar mirrors is evaluated in a collection of two reports and a technical paper. Cellular glass is commercially available, having been used for over 40 years as thermal insulation. Its low cost makes it a likely candidate for large solar-mirror supports. Cellular glass may also come to have other structural uses outside the solar-energy field.

The first report discusses the state of the structural-cellular-glass programs as of June 1979. It includes a survey of the field with a summary of the technology up to that time. Possible future developments in the program are outlined. A section on design considerations includes the results of preliminary mechanical-property tests and is presented as a guide to design engineers.

The second report gives further details of a program to develop improved cellular glasses and to characterize the properties of these glasses and of commercially available materials. Conventional testing techniques were adapted to these materials. The methods of linear fracture mechanics were applied to develop two theoretical models of fracture behavior. The time-dependent slow-crack-growth behavior was found to be more complex than in dense glass and ceramics. The technical paper, entitled "Fracture Mechanics of Cellular Glass," refines the models and uses linear elastic fracture mechanics to relate the microstructure to the macroscopic mechanical behavior.

This work was done by Marc A. Adams and James G. Zwissler of Caltech for **NASA's Jet Propulsion Laboratory.** *To obtain a copy of the documents described in this article, Circle 86 on the TSP Request Card.*
NPO-15680

Microfissuring in Nickel-Based-Alloy Welds

Cracking mechanisms are proposed.

An investigation of the physical metallurgy of near-solidus intergranular cracking, or microfissuring, in Inconel® 718 alloy welds is described in a report. (Inconel® is a registered trademark of the Inco family of companies). Castings made from this nickel-based alloy are particularly sensitive to microfissuring when they are welded. The cracks occur in the heat-affected zone of the weld and reduce the life expectancy of engines and other equipment in which the castings are used. The investigation sought to identify the cause of the microfissuring and quantify its behavior.

The data, although inconclusive, suggest at least two mechanisms that might explain intergranular cracking in the heat-affected zone of several high-temperature alloys. One theory is based on the separation of intergranular liquid, while the other involves mechanical failure of solid ligaments surrounded by intergranular liquid. Both mechanisms concentrate strain in the grain boundaries, causing intergranular brittleness at low strain (less than 1 percent). These mechanisms may also pertain to the physical metallurgy of casting, powder metallurgy sintering, and hot isostatic pressing.

In the investigation, samples of the alloy were plastically strained at various temperatures near the solidus. The plastic strain was varied between that needed to cause fracture and that needed to initiate a few small cracks. This was done at several temperatures so that the degree of cracking could be plotted against the plastic strain for each temperature of interest. This plot was used to extrapolate the degree of cracking to the incipient cracking strain. The incipient cracking strain thus obtained was plotted against temperature to give an incipient cracking envelope in strain-versus-temperature coordinates. This plot can be used to predict microfissuring.

With the aid of photomicrographs and energy-dispersive X-ray analysis, it was found that niobium-rich phases are redistributed in the heat-affected zone during welding. These phases, in the

(continued on next page)

form of stringers and randomly distributed particles, can be transformed into a low-ductility intergranular network. However, the formation of such networks can probably be suppressed by control of the alloy microstructure through suitable modifications of the temperature, speed, atmosphere, and other parameters of the welding process.

It was also found that the near-solidus cracking behavior exhibits several distinct phases. These are (a) intergranular crack closure at approximately 120° C below the bulk solidus, (b) multiple intergranular crack growth between 90° and 40° C below the bulk solidus, (c) single intergranular crack growth 40° C below the bulk solidus, and (d) fluid flow at and above the bulk solidus.

This work was done by Raymond G. Thompson of Clemson University for **Marshall Space Flight Center.** *To obtain a copy of the report, "Hot Tensile Tests of Inconel 718," Circle 87 on the TSP Request Card.*
MFS-25815

MiniBriefs describe NASA innovations and reports in an abbreviated format. Readers desiring additional information on these items should request the Technical Support Packages (TSP's), available in most cases, which can be obtained by using the TSP Request Card at the back of this issue.

Improved Thermosetting Imide Resins

The modified resins have a lower curing temperature.

Imide monomers can be chemically modified to lower their cure temperature by 90°, at the least, without compromising the flame resistance of the cured resins made from them. The imide monomers are prepared by reacting tris (m-aminophenyl phosphine oxide) with an unsaturated cyclic anhydride in dimethyl formamide or glacial acetic acid. The properties of the imide monomers are altered by substituting benzophenone tetracarboxylic acid dianhydride for some of the cyclic anhydrides. Cured imide resins and composites with high heat and flame resistances are obtained by heating the imide monomers or graphite fibers impregnated with them to curing temperatures of 180° C and postcuring temperatures of 220° C.

This work was done by George M. Fohlen and John A. Parker of **Ames Research Center** *and Indra K. Varma of NRC. For further information, Circle 88 on the TSP Request Card.*

Inquiries concerning rights for the commercial use of this invention should be addressed to the Patent Counsel, Ames Research Center [see page A5]. *Refer to ARC-11368.*

Stress-Corrosion Cracking in Martensitic PH Stainless Steels

Precipitation-hardening alloys are evaluated in marine-environment tests.

A report describes marine-environment stress-corrosion cracking (SCC) tests of three martensitic precipitation-hardening (PH) stainless-steel alloys. Specimens with various grain orientations were stressed at 25 to 100 percent of their yield strength during the tests. The SCC resistance of the alloys ranged from low to high among specimens from various mill heats.

For each test condition, the report lists the number of failed specimens (ones that fractured), the elapsed time to failure, and the total number of specimens tested. Photomicrographs and scanning electron microscope micrographs generally show more stringers and carbide precipitates in specimens from heats more susceptible to SCC. Tables of the mechanical properties and chemical analyses of the steels are also included.

This work was done by T. S. Humphries and E. E. Nelson of **Marshall Space Flight Center**. *To obtain a copy of the report, "Stress Corrosion Cracking Evaluation of Martensitic Precipitation Hardening Stainless Steels," Circle 89 on the TSP Request Card.*
MFS-25400

Nitrogen Supply Uses Hydrazine

Liquid hydrazine is dissociated and residual gas removed to produce almost pure nitrogen.

A nitrogen generation module catalytically dissociates liquid hydrazine and then dissociates and separates the product gases to yield almost pure nitrogen. Designed for cabin nitrogen replenishment during space flight, the module performs three functions: hydrazine dissociation, ammonia dissociation, and hydrogen removal.

The product gases flow in a cylindrical annular housing concentric with a central hydrazine feed tube. Three ammonia dissociation stages, each of which consists of two side-by-side tubes packed with an ammonia dissociation catalyst, are located in the central core around the outside of the hydrazine dissociation stage. Four hydrogen removal stages, consisting of palladium /silver tubes, are located around the outside of the module. By serially arranging alternate ammonia dissociation and hydrogen removal stages, the concentrations of ammonia and hydrogen in the product nitrogen stream are drastically reduced beyond initial equilibrium levels.

This work was done by Dennis B. Heppner of Life Systems, Inc., for **Ames Research Center.** *For further information, Circle 90 on the TSP Request Card.*
ARC-11464

Walnut Hulls Clean Aluminum

Hulls inflict minimal substrate damage.

Walnut hulls were found to be the best abrasive for cleaning aluminum surfaces prior to painting. Samples blasted with walnut hulls showed no compressive stress of the surface. Samples blasted with abrasives such as silicon carbide, silica sand, or garnet showed average compressive stresses of 23.6 to 33.1 ksi (163×10^6 to 228×10^6 N/m^2). Walnut-hull blasting resulted in the least amount of warpage and gave the smoothest surface.

The quality of the repainted surfaces was very similar to a first-time painted surface. When purchased in quantity, walnut hulls were the least expensive abrasive.

This work was done by Wendell R. Colberg, Gail H. Gordon, and Charles H. Jackson of **Marshall Space Flight Center.** *For further information, Circle 91 on the TSP Request Card.*
MFS-27012

Low-Pressure Alcohol Distillation

Heat requirements are lowered for the process.

Vacuum distillation allows the use of low-temperature waste energy to produce alcohol for fuel. The temperature requirements are lowered enough to make solar heat absorbed by flat-plate collectors a feasible energy source. The alcohol is produced without adding other solvents, eliminating the need for dehydration or hydrocarbon stripping as a final step. Distillation at reduced pressure can be used for products other than alcohol.

This work was done by Donald O. Frazier, Frederick W. zur Burg, and Joe C. Cody of **Marshall Space Flight Center.** *For further information, Circle 92 on the TSP Request Card.*

This invention is owned by NASA, and a patent application has been filed. Inquiries concerning nonexclusive or exclusive license for its commercial development should be addressed to the Patent Counsel, Marshall Space Flight Center [see page A5]. Refer to MFS-25516.

Diesel Particulate Destruction

A pulsed electrical discharge eliminates particulates in diesel exhaust.

Particulates in diesel exhaust gas can be destroyed by passing them through an agglomerator and a series of high-voltage-biased grids. The particulates, being semiconductive, initiate spark discharges along the grid/gas interface. The sparks have high temperature (>5,000 K) and high plasma density. Thus they can erode or induce combustion of the particulates. The technique also offers a way of instantaneously measuring the particulate mass in diesel exhaust.

This work was done by Lien C. Yang of Caltech for **NASA's Jet Propulsion Laboratory.** *For further information, Circle 93 on the TSP Request Card.*

This invention has been patented by NASA (U.S. Patent No. 4,376,637). Inquiries concerning nonexclusive or exclusive license for its commercial development should be addressed to the Patent Counsel, NASA Resident Office-JPL [see page A5]. Refer to NPO-15426.

Dissolving Bubbles in Glass

An analytical expression calculates the changes of bubble radius with time.

An analytical expression is used to calculate the time it takes for stationary bubbles of oxygen and carbon dioxide to dissolve from a glass melt. It is part of a model of the glass-refining process. The technique ignores bubble motion and treats a stationary single bubble composed of one gas in an infinite glass melt.

The technique is based on an analytical expression for bubble radius as a function of time, without the consequences of surface tension included. The dissolution rates, which include surface-tension effects, are calculated by numerical integration of the quasi-stationary governing equation.

This work was done by Michael C. Weinberg of Caltech, Paulette I. K. Oronato of GTE Corp., and Donald R. Uhlmann of MIT for **NASA's Jet Propulsion Laboratory.** *For further information, Circle 94 on the TSP Request Card.*
NPO-15105

Packaging Nuclear and Chemical Waste for Disposal

Waste would be encapsulated in hollow silicon spheres.

In a proposed method, nuclear and chemical waste would be quickly encapsulated in hollow silicon spheres by forming, filling, and sealing the sphere. The process can be entirely automated.

As the glass spheres are formed by nozzles they are filled by a pulsing injection of the waste material. The glass spheres then seal themselves and drop from the nozzles into a contactless coating facility where a lead coating is applied. After coating with lead, an additional coating of molten glass is applied to protect the lead coating. An alternate procedure is to incorporate lead in the glass-formation step, thus forming lead/glass spheroids. After cooling, the spheres roll down a channel to be packaged in a primary container for storage.

This work was done by Taylor G. Wang of Caltech for **NASA's Jet Propulsion Laboratory.** *For further information, Circle 95 on the TSP Request Card.*

Inquiries concerning rights for the commercial use of this invention should be addressed to the Patent Counsel, NASA Resident Office–JPL [see page A5]. Refer to NPO-15454.

Extracting Oil From Tar Sands

Oil can be extracted using solar energy.

The recovery of oil from tar sands is possible by a batch process, using steam produced by a solar heater. In the extraction process, a solar heater provides steam for heating a solvent boiler. The boiling solvent removes the oil from the tar sands in a Soxhlet extractor. Because the solar heater is off during the night, the Soxhlet extractor can be emptied and recharged for the next day.

This work was done by Larry B. Ford and David Daly of Caltech for **NASA's Jet Propulsion Laboratory.** *For further information, Circle 96 on the TSP Request Card.*
NPO-15760

Monitoring Lignin Content in Paper Processing

Feedstock and finished pulp can be analyzed and controlled automatically.

A proposed microprocessor-based system would control the digestor in paper processing automatically and in real time. The system acquires samples from the feed hopper, the digestor, and the blow tank. The sample is homogenized, washed, and dried while it is conveyed to a flash pyrolyzer. In the pyrolyzer, the material is converted into its basic constituents — mostly compounds of molecular weight less than 200.

A mass spectrometer produces a spectrum of the pyrolysis products and records the peaks caused by cellulose and lignin. The microprocessor calculates the lignin content, and feeds this information to the control system for adjustment of such parameters as pressure, temperature, and white-liquor flow.

This work was done by Heinz G. Boettger of Caltech for **NASA's Jet Propulsion Laboratory.** *For further information, Circle 97 on the TSP Request Card.*
NPO-15796

Ceramics for Solar Receivers

Materials for high-temperature use are reviewed.

A report discusses the characteristics of ceramics and assesses the potential of candidate materials in solar receivers. Design requirements are presented, including those for a receiver with fluid exit temperatures up to 1,425° C.

Structural ceramics are being considered for solar applications because of their high-temperature capability, availability, and low cost. Ceramics that are of potential interest for solar receivers may be classified into three major categories: oxides, aluminosilicates, and the carbide and nitride families. Each category is discussed, and the ceramics are compared in a table.

This work was done by Alvydas A. Kudirka of Caltech for **NASA's Jet Propulsion Laboratory.** *To obtain a copy of the report, Circle 98 on the TSP Request Card.*
NPO 15763

Sialon Electrodes and Insulators for MHD Device

A proposed MHD channel structure uses conducting and insulating sialon ceramics.

A rectangular magnetohydrodynamic (MHD) channel structure for electrical power generation has been designed using pure sialon ceramic for the insulating portion of the structure and metal-bearing sialon cermet for the conducting portion.

The ceramic and the cermet materials share important properties:

- They are stable and show excellent oxidation resistance to at least 2,730° F (1,500° C).
- Their thermal characteristics are nearly identical; both have high thermal conductivity and a low thermal-expansion coefficient.
- They are compatible with molten metals.

The electrical resistivity of the ceramic is similar to that of alumina. The conducting material molybdenum silicide could be used in the cermet.

This work was done by Wayne M. Phillips of Caltech for **NASA's Jet Propulsion Laboratory.** *For further information, Circle 99 on the TSP Request Card.*
NPO-14945

Removing Images From Microfilm

The film is softened, scraped, and then dried.

Unwanted images can be removed from microfilm by softening the base film with hot water, scraping the film, and drying it with isopropyl alcohol. The method is simple, and there is no visible damage to the film.

To remove unwanted images from microfilm, the base film first is softened with hot water heated to 80° C. Then, the film is gently scraped with a blunt metal spatula or a tetrafluoroethylene policeman and dried.

This work was done by Lois L. Taylor of Caltech for **NASA's Jet Propulsion Laboratory.** *For further information, Circle 100 on the TSP Request Card.*
NPO-15146

Glass for Solar Concentrators

A survey evaluates engineering parameters of commercial glasses.

A report identifies four commercially available glasses as promising reflectors for solar concentrators. They have properties of high reflectance (80 to 96 percent), lower cost than first-surface silver metalization, and resistance to environmental forces.

The four superior glasses mentioned in the report include two fusion glasses, one sheet glass and one float glass. The investigation on the efficiency of solar concentrators included data from Jet Propulsion Laboratory in-house measurements and vendor-supplied information. Anodized aluminum surfaces are also possible candidates for solar concentrators.

This work was done by Frank L. Bouquet of Caltech for **NASA's Jet Propulsion Laboratory.** *To obtain a copy of the report, Circle 101 on the TSP Request Card.*
NPO-14923

Reducing Soot in Diesel Exhaust

Electrically charged fuel improves oxidation.

A proposed fuel-injection system would reduce the amount of soot formed in diesel engines. A spray injector electrically charges the fuel droplets as they enter the cylinder. The charged droplets repel each other, creating a dilute fuel mist that is easily penetrated by the oxygen in the cylinder. This encourages more complete combustion and hinders soot formation.

A mathematical model describes the expansion of the cloud of identically charged droplets. The required electrical power has been computed in terms of the fuel, spray, and engine characteristics. Despite the high voltage needed to charge the droplets, sparking will not occur before compression-induced ignition if the droplet-expansion time is properly chosen.

This work was done by Josette Bellan of Caltech for **NASA's Jet Propulsion Laboratory.** *For further information, Circle 102 on the TSP Request Card.*
NPO-15715

Three-Zone Catalyst Resists Sulfur Poisoning

Zone configuration and composition increase efficiency.

A three-zone catalyst bed uses different types of nickel catalysts to convert sulfur-containing hydrocarbon fuels to hydrogen and carbon monoxide. The zones are designed to achieve the conversion with a minimal residue of unconverted hydrocarbon, no soot, and minimal sulfur contamination.

The first zone allows the reaction of fuel with air on the nickel catalyst while maintaining inlet heat requirements and producing enough hydrogen to prevent sulfur from deactivating the catalyst. The second zone continues the air-oxidation reaction and initiates the steam-hydrocarbon reaction. It prevents soot formation by not allowing the flow to stagnate, unreacted, in this critical, high-temperature zone. The third zone provides enough activity and surface area to complete the steam reforming reaction. The hydrogen partial pressure and the retention of catalyst temperature prevent sulfur poisoning of the catalyst.

This work was done by Gerald E. Voecks, Maria F. Stephanopoulos, and John Houseman of Caltech for **NASA's Jet Propulsion Laboratory.** *For further information, Circle 103 on the TSP Request Card.*
NPO-14827

Combined Silane Pyrolysis and Silicon-Particle Melt

Melter directly coupled to pyrolyzer would eliminate difficulties of transport.

The fine silicon particles produced when silane is pyrolyzed are light, fluffy masses that have almost no ability to flow, making it difficult to transport them to a melter. A proposed coupling of a free-space silane pyrolyzer and a melter without intervening steps would produce molten silicon with no problems of fine-particle movement, storage, contamination in transport, or oxide formation.

The combined processes could use the free-space reactor of an already-operational silane pyrolyzer that could be coupled with the crucible heater of an operational furnace as the melter section. A graphite-connector transition zone passes the rain of silicon from the pyrolyzer to the melter section.

This work was done by Harry Levin of Caltech for **NASA's Jet Propulsion Laboratory.** *For further information, Circle 104 on the TSP Request Card.*
NPO-15510

Epoxy Grout With Silica Thickener

Grout cures quickly, even in the presence of hydraulic oil.

An epoxy grout lasts long, does not sag, and cures quickly, even in the presence of hydraulic oil. Within several hours after mixing, the grout can bear a load. It can replace portland cement dry-pack grout, which stops curing in the presence of hydraulic oil.

The grout is a mixture of aggregate particles, finely-divided silica, epoxy resin, and triethylenetetramine curing agent, with the mixture containing about 85 percent silica and aggregate particles and 15 percent resin and curing agent. The silica is a thickening agent and keeps the grout from sagging. The surface of a sample tested only one and a half hours after mixing had a load-bearing strength of over 700 psi (4.8×10^6 N/m^2).

This work was done by Charles E. McClung of Monsanto Research Corp. for **NASA's Jet Propulsion Laboratory.** *For further information, Circle 105 on the TSP Request Card.*

This invention has been patented by NASA (U.S. Patent No. 4,395,503). Inquiries concerning nonexclusive or exclusive license for its commercial development should be addressed to the Patent Counsel, NASA Resident Office-JPL [see page A5]. Refer to NPO-15202.

Measuring Trace Hydrocarbons in Silanes

The technique is rapid and uses standard analytical equipment.

A chromatographic method includes a standard flame-ionization detector (FID) to measure low-level concentrations of hydrocarbons in silane. The presence of such hydrocarbons as methane, ethane, and ethylene causes carbon deposits in high-purity silicon resulting from silane pyrolysis.

Silane gas containing traces of hydrocarbons is injected into a carrier gas of moist nitrogen having about 0.2 percent water vapor. The carrier, water, and silane pass through a short column packed with powdered sodium hydroxide, which combines with the moisture and silane to form a nonvolatile sodium silicate. The carrier gas, free of the silane, but containing the nonreactive hydrocarbons, pass to a silica-gel column where a chromatographic separation takes place. The individual hydrocarbons are then measured by the FID.

This work was done by Louis A. Lesser of Union Carbide Corp. for **NASA's Jet Propulsion Laboratory.** *For further information, Circle 106 on the TSP Request Card.*
NPO-15273

Plated Metal Powders for Electrode Pastes

Metal grains to be sintered are precoated with frit metal.

Improved coated metal powders are used to make the ink-like electrode pastes for the printing and sintering electrode-fabrication process. The grains of the base metal (for example, copper) are coated with a low-melting-point metal — for example, lead or tin — by electroless deposition.

The electroless process plates each grain over its entire surface without the need for electrical contact to each grain. Due to agitation during plating, there is no agglomeration of the powder. Since the grains are already coated with frit metal, no special effort is needed to protect them from oxidation or to assure the wetting of the grains by the frit metal during sintering.

This work was done by Donald B. Bickler of Caltech for **NASA's Jet Propulsion Laboratory.** *For further information, Circle 107 on the TSP Request Card.*

This invention has been patented by NASA (U.S. Patent No. 4,388,346). Inquiries concerning nonexclusive or exclusive license for its commercial development should be addressed to the Patent Counsel, NASA Resident Office-JPL [see page A5]. Refer to NPO-15161.

Rhenium Prevents Corrosion

Thrust chamber is protected from corrosive fuel during burns.

A rhenium layer inside a carbon-composite thrust chamber prevents corrosion when a liquid fluorine/hydrazine rocket engine is fired. This type of liner may also eliminate erosion of solid-propellant carbon nozzles.

The rhenium is vapor deposited inside the thrust chamber. It acts as a barrier between the ammonia and the carbon during chamber operation. The rhenium layer was tested in a 200 second test. No corrosion was noted at posttest inspection.

This work was done by Marshall A. Appel of Caltech for **NASA's Jet Propulsion Laboratory.** *For further information, Circle 108 on the TSP Request Card.*
NPO-15011

Hydrogen Production From Heavy Fuels

Better heat-transfer properties may avoid sulfur poisoning of the catalyst.

A monolithic supported catalyst allows the initiation of steam reforming to take place more rapidly at the inlet section of a reactor. This is due to the improved heat-transfer properties associated with this type of continuous-wall support, intimately in contact with the reactor wall. This advantage, coupled with a greatly reduced pressure drop in comparison to a conventional packed-bed catalyst, will permit the reforming of hydrocarbon fuels without requiring an increase in tube-wall temperatures and a change in tube materials. Because of the heat transfer benefits, steam reforming of sulfur-containing fuels heavier than the conventional naphtha (for example, No. 2 fuel oil) may be possible without higher tube-wall temperatures and sulfur poisoning.

This work was done by Gerald E. Voecks and Maria F. Stephanopoulos of Caltech for **NASA's Jet Propulsion Laboratory.** *For further information, Circle 83 on the TSP Request Card.*
NPO-14826

Making Thermoplastics Flame-Resistant

Elastomer-coated hydrate salts are added.

An inorganic hydrate-salt filler coated with an elastomer containing acidic groups imparts flame and smoke retardancy to thermoplastics while preventing the degradation of impact resistance that usually results from high filler loadings in thermoplastics. The elastomer forms a well-bonded elastomeric interphase between the filler and the resin. The elastomer-filled composite fails by shearing or crazing rather than by fracture.

This work was done by William A. Mueller, John D. Ingham, and William W. Reilly of Caltech for **NASA's Jet Propulsion Laboratory**. *For further information, Circle 110 on the TSP Request Card.*

This invention has been patented by NASA (U.S. Patent No. 4,373,039). Inquiries concerning nonexclusive or exclusive license for its commercial development should be addressed to the Patent Counsel, NASA Resident Office-JPL [see page A5]. Refer to NPO-14857.

Radiation Improves Materials Bonding

Bonds with fluorocarbons are made without surface preparation.

Irradiating rubber-based adhesives produces a strong adhesive bond with fluorocarbons without extensive surface preparation. In test runs, cloth tape with rubber-based adhesives adhered strongly to fluorocarbon surfaces after the tape was exposed to cobalt-60 radiation.

Adhesive-backed cloth tape in contact with a fluorocarbon substrate was exposed to 4×10^6 rads. The bond produced was so strong that the bonded area was damaged when extreme force was used to try to break the bond. The method may also be used to restore adhesive strength after some bond strength is lost.

This work was done by Frank L. Bouquet of Caltech for **NASA's Jet Propulsion Laboratory**. *For further information, Circle 111 on the TSP Request Card.*
NPO-14995

Dewatering Peat With Activated Carbon

A proposed process should produce enough gas and carbon to sustain itself.

Because the moisture in peat is held as a collodial suspension and by hydrogen bonding, peat cannot be dewatered by conventional solid/liquid separation techniques alone. In a proposed process, a peat slurry would be dewatered to approximately 40 percent moisture content by mixing the slurry with activated carbon and then filtering with solid/liquid separation techniques. The activated carbon breaks the colloidal suspension, reduces the surface tension between the peat and water, and aids filtering. The process would produce, in a calciner, enough low-Btu gas to sustain itself and also produce the activated carbon from the peat.

This work was done by Naresh K. Rohatgi of Caltech for **NASA's Jet Propulsion Laboratory.** *For further information, Circle 112 on the TSP Request Card.*
NPO-15113

Improved Gas Seal for Electrolytic Cells

Breakage by differential thermal expansion is reduced.

Cells for the hot electrolysis of gases (to produce oxygen, for example) are improved by a design that reduces the vulnerability of the gas seals to breakage at the operating temperature of about 1000° C. In the new design, the electrolyte tube is lengthened so that the seal can be made outside the hot operating region. The inner and outer metal gas-flow tubes are both brazed to the metallized ceramic tube at the same axial position. To further restrain the differential thermal expansion of all three tubes, the outer tube is surrounded by a compression fitting at the joint.

This work was done by Robert Richter of Caltech for **NASA's Jet Propulsion Laboratory**. *For further information, Circle 109 on the TSP Request Card.*
NPO-15163

Life Sciences

Hardware, Techniques, and Processes

MiniBriefs

Acoustic Tooth Cleaner

An acoustically-energized water jet aids in plaque breakdown.

Langley Research Center, Hampton, Virginia

An acoustic tooth cleaner designed at Langley Research Center may help provide thorough daily dental cleaning to prevent calculous buildup. The technique will remove food particles and aid plaque breakdown with mild abrasive particles acoustically agitated in a water suspension by an acoustic wand.

Current mechanical brushing is not sufficient for cleaning between teeth and near the gum/tooth boundary. A water jet does wash away food particles in the mouth, but does not remove plaque. Furthermore, the high pressure generated by commercially-available water jets may damage gums, especially where gums have begun to separate from the tooth. Some acoustic techniques using cavitation have been developed for removing calculous deposits, but the power required for these scaling operations may be too high for safe daily home use.

The new technique uses a solution of water containing a mild abrasive, which is pumped through a tube joining a powerline to an acoustic wand inserted in the mouth. The wand itself incorporates an acoustic transducer (e.g., piezoelectric, magnetostrictive, or electromagnetic) to generate high-frequency acoustic waves.

As shown in the figure, the transducer is bonded to a ¼-wave impedance-matching plate with acoustic impedance Z(plate) such that

$$Z(\text{plate}) = \sqrt{Z(\text{transducer}) \times Z(\text{water})}$$

Z equals the product of the sound velocity times the density. The transducer is driven by an electrically shielded wire with the ¼-wave plate acting as a ground plane. The electrical signal is applied to the transducer through a suitable electrical impedance-matching network.

The ¼-wave plate is connected to a hollow, exponentially tapered cone, which acts as an amplitude amplifier when filled with water. The tube leads from the pump to the hollow cone through the ¼-wave plate. A small hole at the end of the cone reduces the waterflow rate.

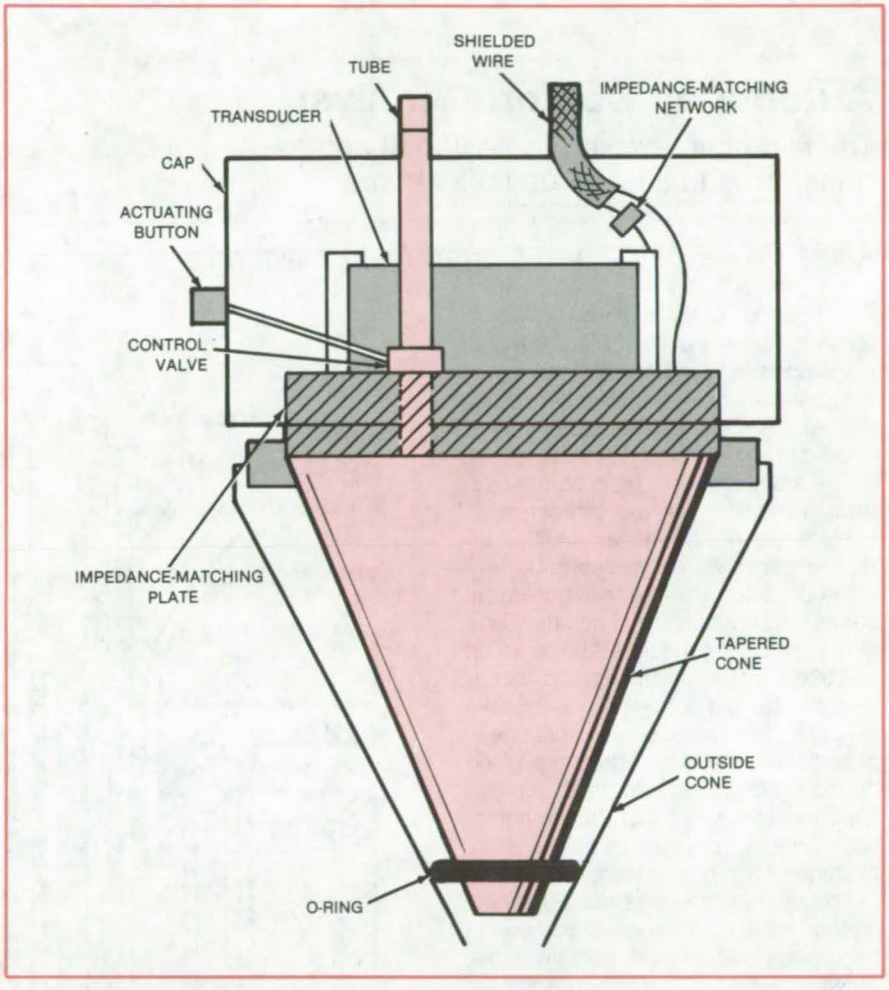

The **Acoustic Wand** includes an acoustic transducer, a ¼-wave plate, and a tapered cone. Together, these elements energize a solution of water containing a mild abrasive, which is injected into the mouth to help prevent calculous buildup.

For personal hygiene from user to user, an outside cone screws onto the amplifier base. An O-ring prevents water from filling between the cone and the amplifier. A hole at the end of the cone permits the water stream to pass out of the amplifier. An outside cap snaps over the transducer and seals the system and protects the user from electrical hazard.

The pump sends water and mild abrasive to the amplifier cone where the amplitude of the acoustic waves increases inversely to the amplifier diameter. (For acoustic wavelengths larger than twice the diameter of the cone, the amplifier gain equals the ratio of the large- and small-cone diameters.) At the exit hole, water with abrasive impinges on the teeth with the acoustic energy oscillating the abrasive particles. The vibrating particles tend to scrub the teeth clean and remove plaque and food particles.

A button opens and closes the liquid-flow control valve to turn the device on or off. Any transducer may be used to

(continued on next page)

drive the liquid cone with or without matching ¼-wave plates. Acoustic streaming may be used in place of a pump. Focusing transducers may be used to increase the acoustic amplitude.

The low-power, oscillatory nature of the acoustic waves will force the abrasive particles and water to remove food deposits and plaque without harmful cavitation. The more-complete dental cleaning will lead to a reduction in tooth decay and healthier gums. Clinical tests are planned to evaluate the efficacy and safety of this device.

This work was done by Joseph S. Heyman of **Langley Research Center.**

For further information, Circle 113 on the TSP Request Card.

This invention has been patented by NASA (U.S. Patent No. 4,331,422). Inquiries concerning nonexclusive or exclusive license for its commercial development should be addressed to the Patent Counsel, Langley Research Center [see page A5]. Refer to LAR-12471.

Automated Coliform Analysis

The hydrogen evolved by coliform bacteria is transferred to a separate measurement cell.

Ames Research Center, Moffett Field, California

A method for determining coliform-bacteria concentration in water samples is included in a prototype system that automatically monitors 15 water-quality characteristics. The complete system is housed in an 8- by 30-ft (2.4- by 9-m) van.

The concentration of coliform bacteria in water is an indicator of contamination and hence of the effectiveness of water treatment. Current methods determine the initial coliform-bacteria concentration in a water sample by measuring the time it takes for an electrode potential change to occur after the sample is placed in a cell containing a growth medium. The change in potential is caused by hydrogen evolved by the coliform bacteria as they grow. Unfortunately, there can also be potential changes caused by other non-hydrogen-evolving bacteria.

To separate these effects, the new method measures the electrode potential change both in a cell containing the growth medium and again in a similar cell containing a buffer solution to which the evolved hydrogen is vented and in which the hydrogen dissolves. In the second cell, any change in potential is due solely to the evolved hydrogen.

A cross-sectional view of one of the electroanalytical cells is shown in the figure. A combination electrode of the type commonly used to measure pH is used for the potential measurements. It includes a reference electrode enclosed within an electrically insulating jacket and an end-mounted platinum electrode that is wetted by the growth medium or buffer solution. (One suitable growth medium is autoclaved double-strength lauryl tryptose broth. One suitable buffer solution is 7 percent potassium phosphate.)

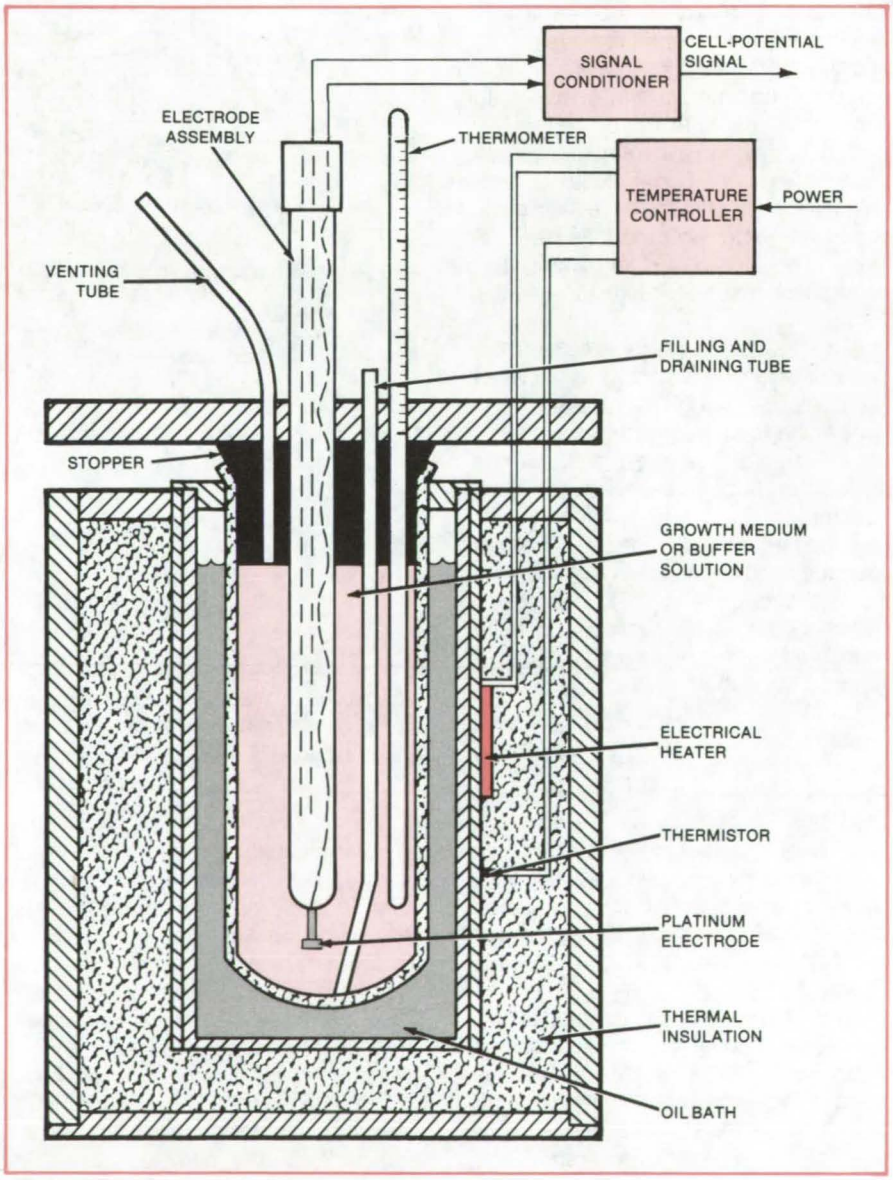

The **Electroanalytic Cell** is mounted in an insulated temperature-control bath that is cycled between a culturing temperature and a sterilizing temperature. The flow of materials into and out of the cell is controlled by electrically operated valves.

The sterilization of the cell between measurement cycles is done by flushing the cell first with nitric acid and then with hot deionized water. After the cell is filled with growth medium, it is heated to 85° C for one-half hour and then allowed to cool to a culturing temperature of either 35° or 44° C, depending on the type of coliform bacteria to be measured. The culturing period is terminated when a certain potential change has occured or when a specific interval has elapsed. (Representative values might be 200 mV and 14 hours, respectively.)

This work was done by Kenji Nishioka of **Ames Research Center** *and David Nibley, Eldon Jeffers, and Richard Brooks of The Boeing Co. For further information, Circle 114 on the TSP Request Card.*

Inquiries concerning rights for the commercial use of this invention should be addressed to the Patent Counsel, Ames Research Center *[see page A5].* *Refer to ARC-11322.*

Adjustable Walker for the Handicapped

The front legs adjust at the touch of a lever for use on stairs or ramps.

Langley Research Center, Hampton, Virginia

A walker for the handicapped has adjustable front legs for negotiating ramps and stairs. It is superior to conventional fixed-leg walkers, which are awkward to use on inclines or irregular surfaces. The user adjusts the two front legs as necessary simply by operating a lever located at the top of the walker.

As shown in the figure, the legs are spring-loaded at the top so that when the lever is depressed, the spring pushes the legs down. The legs are automatically locked in place when the lever is released, by a spring-loaded wheel similar to the balance wheel of a clock. A locking pin fitted to the spring-loaded wheel is forced into place to lock the legs in the desired position.

To shorten the legs, the user depresses the lever to release the locking mechanism and pushes downward until the legs are at the desired length. In this manner, the self-adjusting walker remains level regardless of the walking surface.

The walker can be fabricated from metal or from lightweight composites. A low-friction, high-polymer sleeve inside the upper sections and around the lower sections of the adjusting legs would enable the sections to move easily and would provide a tight fit. A connecting rod between the two locking mechanisms would allow both adjustable legs to move simultaneously, and the legs would be attached in a manner to ensure alinement with the locking pins at all times.

This work was done by Roland G. Kitts of **Langley Research Center.** *No further documentation is available.*
LAR-12990

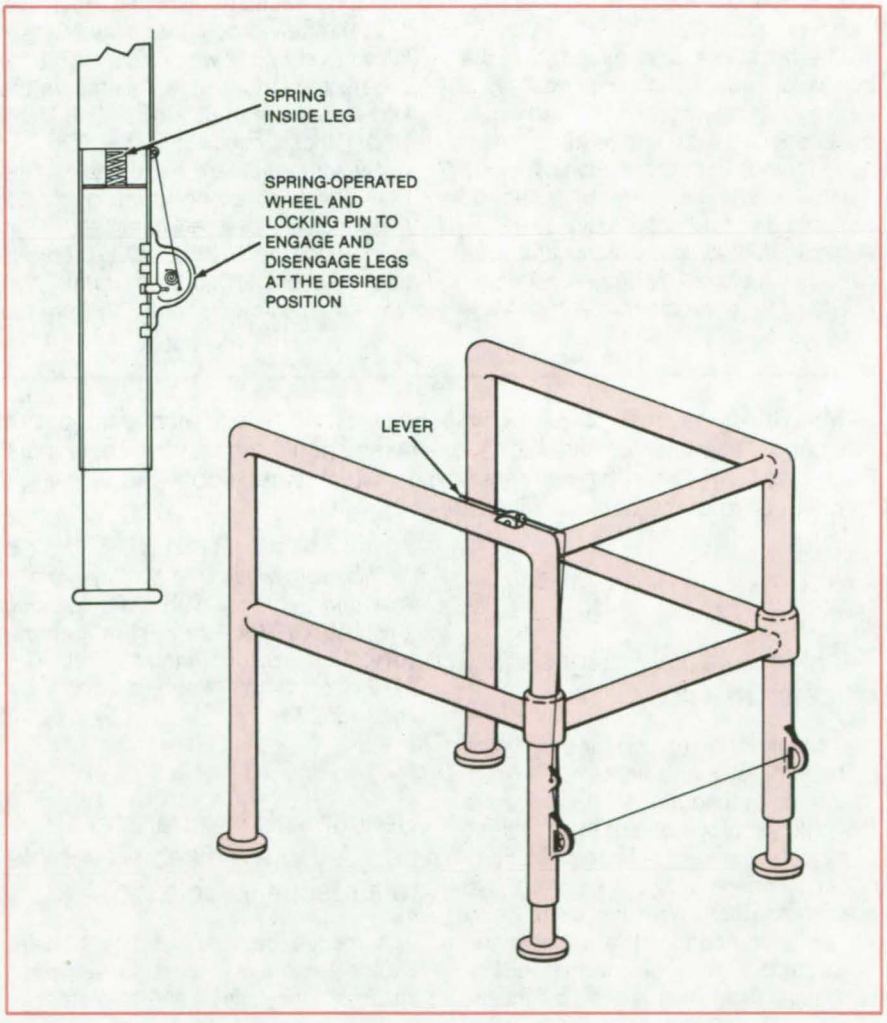

Spring-Loaded Legs Extend when a lever is depressed by the user. The legs lock in position when the lever is released. A lever can be mounted on either side of the walker or on both sides, so that the legs can be operated independently.

Removing Biostatic Agents From Fermentation Solutions

Liquid carbon dioxide is an inexpensive solvent.

NASA's Jet Propulsion Laboratory, Pasadena, California

An inexpensive process has been proposed for removing such poisons as furfural and related compounds from the fermentation baths of biomass hydrolysates. The new process is based on the use of liquid carbon dioxide as an extraction solvent. Liquid CO_2 is preferable to such other liquid solvents as ether or methylene chloride. These substances are expensive and are bacteriostatic in themselves so that they must be removed from the sugar solution before it can ferment.

The hydrolysis of hemicellulose, the polysaccharide found in plant cell walls in association with cellulose and lignin, by strong acid at temperatures near 100° C leads to the formation of sugars (pentoses and hexoses) that can be fermented into such liquid fuels as acetone, butanol, and ethanol and such gaseous fuels as hydrogen. Unfortunately, the byproducts of hydrolysis interfere with the action of fermenting bacteria. Prominent among these byproducts is furfural, which inhibits the fermentation bacteria of the genus *Clostridia*.

Removing furfural and its related compounds by conventional distillation does not solve the problem since the heat of distillation creates more of the offending substances as quickly as they are removed. Low-temperature distillation under vacuum is slow and expensive.

In the new process, liquefied CO_2 is introduced into a water solution of the sugars and furfural at room temperature and a pressure of 850 lb/in.^{2} (5.9 MPa). Under these conditions, the CO_2 and water form separate liquid phases, the CO_2 phase collecting at the bottom of the pressure vessel because of its greater density. The liquid CO_2 preferentially absorbs much of the furfural. Thus, when the liquid CO_2 is drawn from the vessel, a water solution of sugars with lower furfural content remains. Fermentation can then continue. When the pressure in the vessel is released, any CO_2 dissolved in the water escapes spontaneously as a gas. A small amount of CO_2 remaining in solution is not particularly harmful since CO_2 is not a strong bacterial inhibitor.

CO_2 is one of the cheapest industrial chemicals. Moreover, it is a byproduct of the production of hydrogen and other gases by fermentation. A well-designed system would be likely to generate enough CO_2 to make up for process losses, so that the extraction method could be highly economical.

This work was done by Eugene R. du Fresne of Caltech for **NASA's Jet Propulsion Laboratory.** *For further information, Circle 115 on the TSP Request Card.*
NPO-15806

MiniBriefs describe NASA innovations and reports in an abbreviated format. Readers desiring additional information on these items should request the Technical Support Packages (TSP's), available in most cases, which can be obtained by using the TSP Request Card at the back of this issue.

Computer Analysis of Eye Blood-Vessel Images

Technique rapidly diagnoses diabetes mellitus.

A computer technique for diagnosing diabetes mellitus automates a grid-scanning procedure previously done manually. Photographs of the "whites" of patients' eyes are scanned by a computerized image analyzer programed to quantify the density of the small blood vessels in the conjunctiva. Comparison with a data base of known normal and diabetic patients facilitates rapid diagnosis.

This work was done by Raymond J. Wall and Benjamin S. White of Caltech for **NASA's Jet Propulsion Laboratory.** *For further information, Circle 215 on the TSP Request Card.*
NPO-15527

Inflatable Rescue Capsules

Rescue spheres transfer people from a disabled vehicle to a rescue vehicle.

A rescue capsule used to transfer Shuttle personnel to a rescue vehicle in an emergency may have terrestrial or underwater applications. The container, an inflatable sphere, is constructed of gastight thermal-protective fabric to provide protection during the transfer. It is equipped with a self-contained air supply. The rescue capsules can be transferred between vehicles using tow lines. When not in use, the rescue spheres are deflated.

This work was done by James L. Baker of **Marshall Space Flight Center.** *For further information, Circle 116 on the TSP Request Card.*
MFS-25677

Mechanics

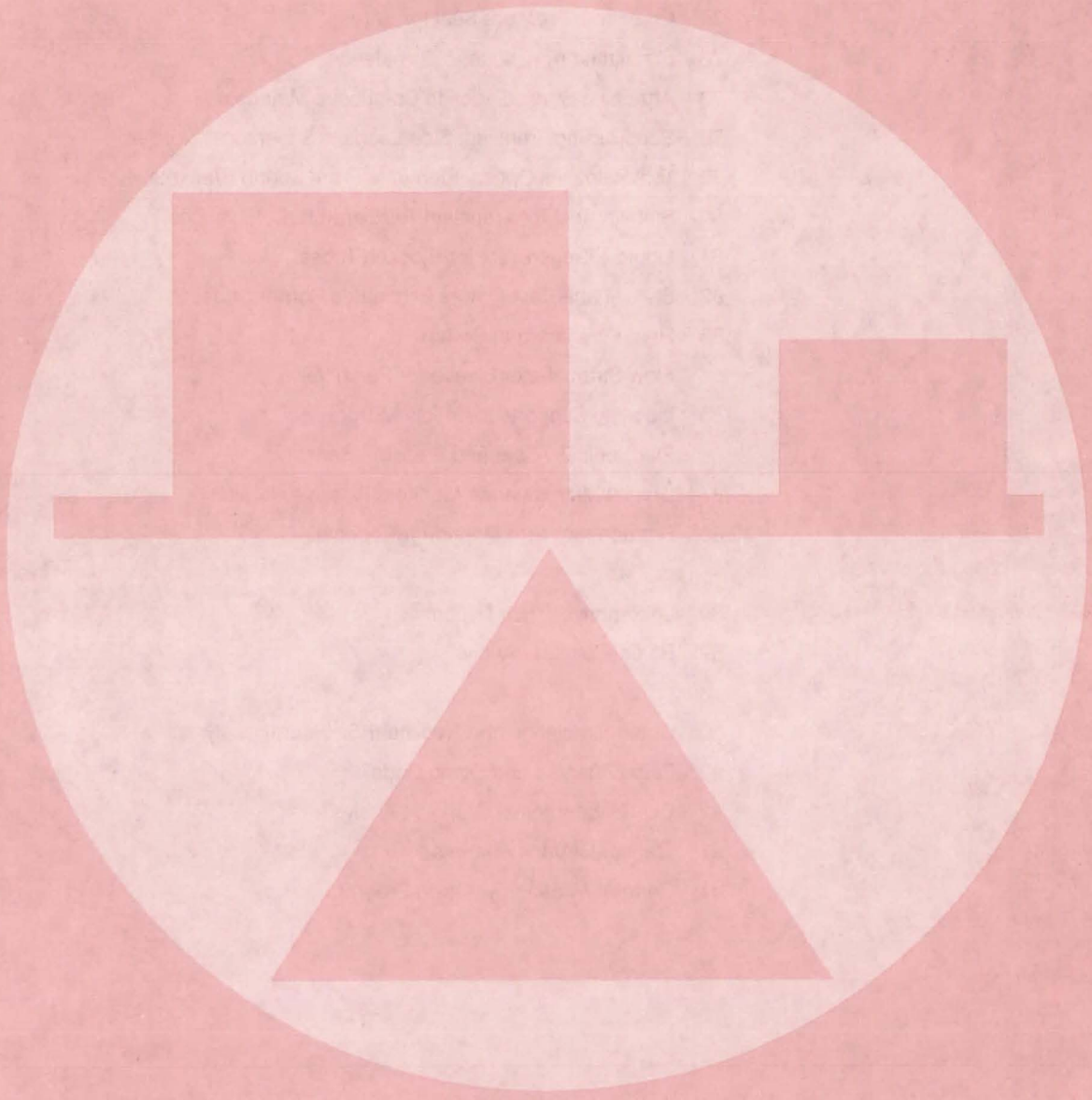

Hardware, Techniques, and Processes

Books and Reports

Computer Programs

MiniBriefs

Membrane Switches Check Seal Pressure

Door and hatch seals can be monitored electronically.

Lyndon B. Johnson Space Center, Houston, Texas

An array of flexible membrane switches can be used to indicate the closure of a seal. A switch membrane responds to the pressure exerted by a rigid surface on a compliant sealing medium and provides switch contacts that can be monitored electronically. The principle can be used to ensure the integrity of seals on refrigerator and oven doors, on weatherstripping, and on hatches on spacecraft, airplanes, and submarines.

A membrane switch includes three layers of polyester film bonded together (see figure). The top and bottom layers carry conductor pads and circuitry. The middle layer is a separator that provides 0.005 to 0.008 inch (0.13 to 0.20 mm) clearance between the switch contact pads.

The method of pressure sensing is particularly suitable for thin gaps. It is clean and provides fast "go/no-go" measurements. A membrane-switch array with a thickness of 0.020 inch (0.5 mm), for example, is thin enough to fit between the seal and seat of many closing devices. When the door is closed, the flexible seal presses the switch contacts together through the hole in the intervening membrane. A defective seal — that is, one that does not fully contact the sealing surface over its entire length — is indicated by the failure of one or more membrane switches to remain closed while the door is in its shut position.

The force required to close a switch depends on the cutout area in the separator at the site of the switch: The operating force varies inversely with the size of the cutout. The number of contact switches, their size and shape, and their position in the membrane are determined by the designer. An array of membrane switches can be designed to match the footprint of a seal, and with the array the sealing pressures at predetermined sites along the seal can be monitored simultaneously.

A simple circuit consisting of a battery, a current-limiting resistor, and a lamp or light-emitting diode (LED) can monitor the state of a membrane-switch array. The membrane switches are connected in series and placed under the seal. When all the switches are closed, the lamp or LED lights up, indicating that the requisite seal pressure has been realized at all switch positions.

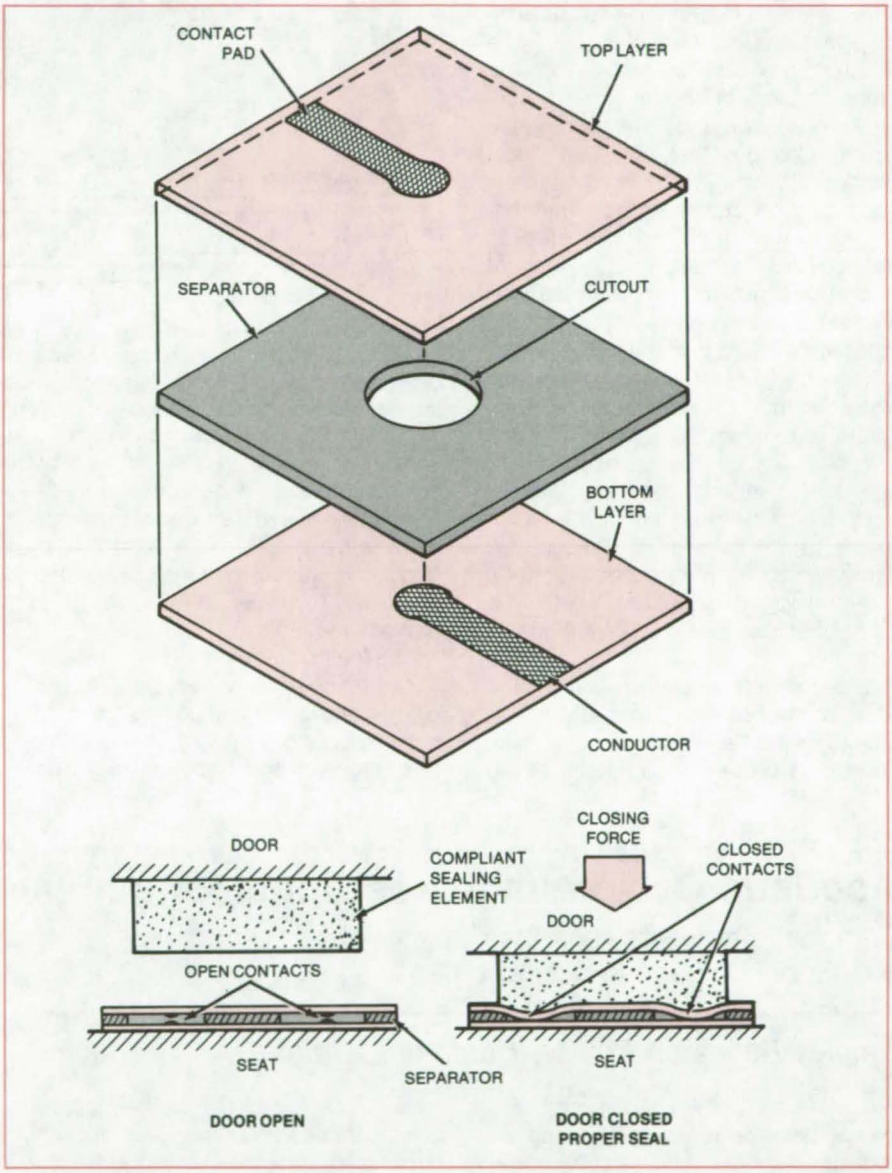

With Door Open (left) contacts of membrane switches are also open. With door closed (right) the contacts are closed — provided that an adequate seal exists.

This work was done by Philip J. Hodgetts, Fred H. Stuckenberg, and Edward T. Morrissey of Rockwell International Corp. for **Johnson Space Center.** *No further documentation is available.*

Inquiries concerning rights for the commercial use of this invention should be addressed to the Patent Counsel, Johnson Space Center [see page A5]. Refer to MSC-20468.

Eddy-Current Inspection of Narrow Metal Tubes

Changes in wall properties affect pickup-coil inductance.

Marshall Space Flight Center, Alabama

An inspection technique for narrow-bore metal tubing involves the use of a small internal eddy-current probe. The probe consists of one or a pair of copper-wire coils wound on a bobbin (see figure). Changes that affect electrical conductivity and magnetic properties, such as high strain, surface wear, or magnetic transitions, are detected as changes in coil inductance. The amount of change is determined by comparison with similar measurements on standard tubes with known properties.

The eddy-current technique is particularly useful for strain measurements where operating conditions or inaccessibility prevent the use of such conventional methods as X-ray diffraction, electrical-resistance measurements, strain gages, or holography. Typically, a coil of about 0.05-in. (1.3-mm) diameter would be inserted in a tube of about 0.08-in. (2-mm) inside diameter.

The coil can be excited and inductance measured simultaneously or sequentially at one or more frequencies, depending on the requirements of the specific measurement. For wear measurements, a differential-coil arrangement with two coils axially separated by about 0.15 in. (3.8 mm) may be needed. The coil response is viewed on a cathode-ray tube.

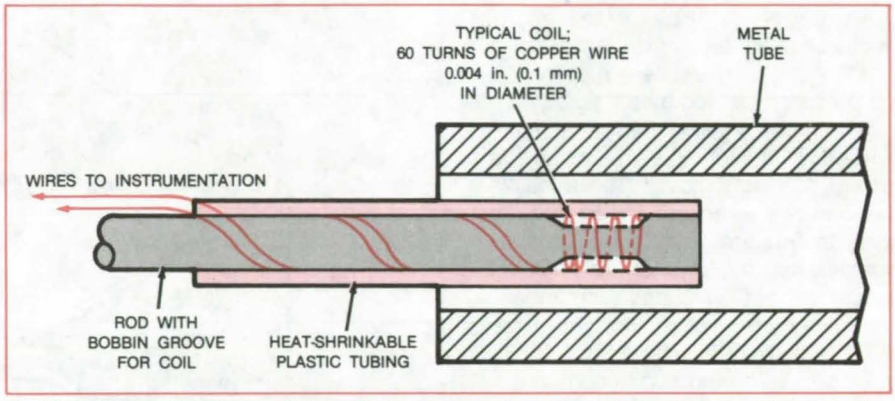

An **Eddy-Current Probe** consists of thin copper wire wrapped on a bobbin. The probe is small enough to pass through bends in the tube being measured.

The method requires experimentation to determine operating frequencies, amplitude and phase responses, and the null-response or standard-sample instrumentation settings. It is often necessary to minimize the instrument response to such features as fillets, brackets, or external welds that are not under investigation.

This work was done by Howard H. Ambrose, Roderic E. Kleint, and Kathleen E. Kirkham of Rockwell International Corp. for **Marshall Space Flight Center.** *For further information, Circle 117 on the TSP Request Card.*
MFS-19742

Acoustic Design Improves Composite Impact Resistance

Composite acoustic response to impact should be included in design criteria.

Langley Research Center, Hampton, Virginia

Improved tolerance of composites to impact damage is achieved using an acoustic response model to characterize the dynamics of the damage mechanism. The model is based on the assumption that in addition to the classical mechanical properties, such as interlaminar strength, buckling strength, and tensile and shear moduli, the damage mechanism depends on the acoustic properties of the composite material. Therefore, impact-tolerant design of a composite structure can be developed by placing proper emphasis on the acoustic response of the material.

While most previous attempts to improve impact tolerance of composites have included new materials, new fabrication techniques, and even novel structural geometries, they have not included the damage done by the acoustic shock wave generated by the impacting projectile. This new method considers the important aspect that the acoustic wave plays in impact damage and selects a process that significantly improves the impact tolerance of a material. The technique is based on Z (acoustic impedance), T (equivalent quarter-wave match), G (impedance gradient), and interface impedance matching.

When an impact occurs, a high-amplitude acoustic wave is launched from the point of contact. The acoustic wave velocity depends on the spatial strain field set up by the wave itself. This results in a shock-wave formation: a sharp gradient in strain with respect to position. As the wave propagates, the higher-amplitude lower frequency components undergo harmonic generation, shifting the propagating energy wave to higher frequencies. At some point, the energy lost by attenuation equals the energy harmonically generated from the propagating wave, and an equilibrium shock wave propagates at the strain-stiffened velocity.

A major damage mechanism occurs when the shock wave is reflected. This occurs either at a material boundary or within the material wherever the acous-

tic impedance Z of the material changes. A signficant strain gradient occurs at or near the reflecting boundary. If the gradient exceeds the material strength at that point, delamination, disbonding, or material failure occurs.

Using this acoustic model of the impact damage, several modifications to existing composite design will improve impact tolerance. The most straightforward design modification involves coupling a Z-match acoustic back layer of material to the back free boundary. This couples the acoustic energy out of the composite and reduces the high-strain gradient that would occur at the unmatched back layer. To match the acoustic impedance, the Z-match layer should have the impedance of the composite back face under shock loading.

For a practical material backing, the bulk back layer adds a significant weight penalty that may be prohibitive for some structures. For these examples, an acoustic back layer may be fabricated as a transmission or T-match layer. The T-match will couple shock-wave energy out of the composite in a bandwidth determined by the T layer or multiple T layer and the frequency spectra of the shock wave itself.

A third embodiment of the acoustic approach to improved shock tolerance is a gradient or G-match layer. The result of this approach is to diffuse the sharp of this approach is to diffuse the sharp reflection gradient into a smooth transition over a longer path. Thus the local gradient at any one point is reduced.

age can result in a more-impact-resistant composite structure. The correct physical model of the damage mechanism points to several possible acoustic back layers, Z-match, T-match, or G-match, which are applicable to the material or end-use parameters. In addition, interlaminar impedance mismatching can be reduced by this same technique.

This work was done by Joseph S. Heyman of **Langley Research Center.** *For further information, Circle 118 on the TSP Request Card.*

Inquiries concerning rights for the commercial use of this invention should be addressed to the Patent Counsel, Langley Research Center [see page A5]. Refer to LAR-12887.

Cryogenic Pressure Seal for Wires

A special fitting is filled with polyurethane.

Marshall Space Flight Center, Alabama

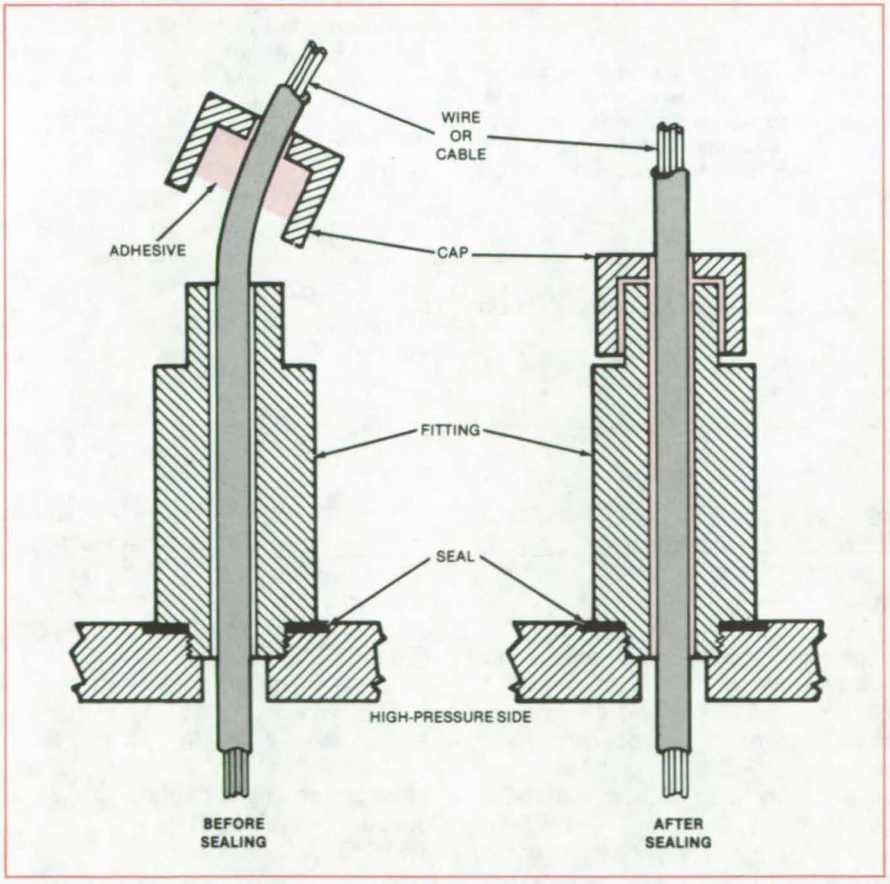

A **High-Pressure Seal** is formed by forcing polyurethane into the space surrounding the wire or cable in a special fitting.

Polyurethane is the sealant in a high-pressure feedthrough for use at cryogenic temperatures. A fitting filled with the sealant passes electrical leads through a wall between high- and low-pressure chambers. In the particular situation in which this technique was first used, the high-pressure chamber contained liquid hydrogen at 6,000 psi (40 MPa).

The wire or cable is routed through the fitting and then through a tightly fitting cap (see figure). The wire insulation is left intact. The cap is filled with the sealant and forced onto the fitting: This pushes the sealant into the fitting so that it seals the wire or cable in the fitting as well as in the cap.

The sealant is a two-part polyurethane (Uralite-3124 or equivalent). Other elastomers or polymers may work, depending on the pressure differential and the fluid to be contained.

This work was done by James J. Ciana of Rockwell International Corp. for **Marshall Space Flight Center.** *No further documentation is available.*
MFS-19668

Simulating Atmospheric Turbulence

Dimensionless time series for gusts and gradients have been calculated with a model.

Marshall Space Flight Center, Alabama

A mathematical model for atmospheric turbulence simulates instantaneous gusts and gust gradients along a flightpath. Developed to predict the effects of atmospheric turbulence in horizontal and near-horizontal flight during the return of the Space Shuttle, the model is also applicable to commercial aviation.

On the basis of the model, which is nondimensional and nonrecursive, dimensionless time series for both gusts and gust gradients were generated and stored on a set of magnetic tapes. The tapes represent atmospheric turbulence from ground level to an altitude of 10,000 meters.

The one-dimensional gust and gust-gradient spectral models were developed from three-dimensional Von Karman spectra integrated over finite limits based on the characteristic dimensions (length, width, and thickness) of the flight vehicle. The simulated time-dependent turbulence is treated as the output of a control system with a double-sided impulse-response function subject to an input of white noise. The impulse response to gusts and gust gradients is generated by the inverse Fourier transformation of a spectral density derived from the Von Karman spectrum for each axis. The dimensionless frequencies are related to the observable frequencies through scale factors involving characteristic dimensions of the aircraft and of the turbulence region.

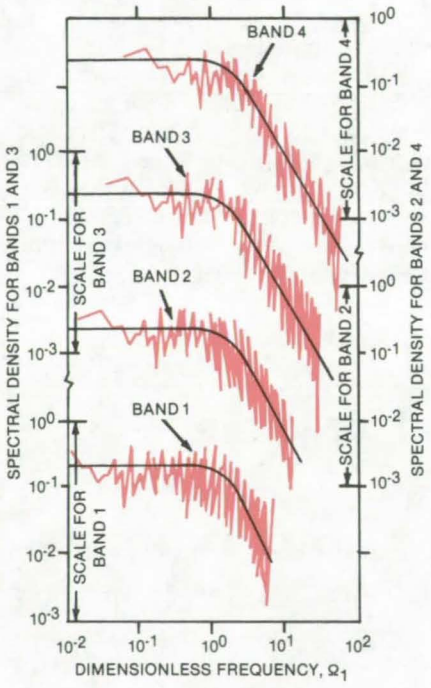

These **Single-Sided One-Dimensional Spectra** were obtained from Fourier analysis of simulated vertical gusts. Each of the four plots represents the spectrum in one of four altitude bands ranging from 0 to 10 km.

The new model differs from most other models in two important respects: It is nondimensional for greater generality, and it uses spectra with finite wave-number limits. The wave-number limits are calculated from the ratios of the integral scales of turbulence to the characteristic dimensions of the vehicle.

The data on the tapes have been subjected to spectral and statistical analyses (for example, see figure). The simulated gusts and gust gradients are normally distributed and have near-zero means. Furthermore, the standard deviation of each series is consistent with the theoretical energy content.

This work was done by Frank B. Tatom and S. Ray Smith of Engineering Analysis, Inc., for **Marshall Space Flight Center.** *For further information, Circle 119 on the TSP Request Card.*
MFS-25850

Attaching Strain Gages to Composite Materials

A polyurethane adhesive works well at liquid-nitrogen and ambient temperatures.

Marshall Space Flight Center, Alabama

A polyurethane adhesive bonds strain gages reliably to graphite/epoxy composites. The adhesive (Crest Product Corp. Epoxy 7450, or equivalent) is easy to apply, may be used over a wide temperature range (ambient to cryogenic), and is applied in a short time.

The area of the test sample to which the gage is to be bonded is first lightly buffed. Next, a thin film of adhesive recently mixed according to the manufacturer's specifications is applied to the buffed area and to the gage, and the gage and sample are joined. Finally, the adhesive is cured by letting the sample set at room temperature for 2 hours, followed by heating at 125° C for 20 minutes.

Tests on strain gages bonded to a composite with the polyurethane adhesive demonstrated the reliability of the attachment. The sample to which the strain gages were bonded were repeatedly cycled between room temperature (about 25° C) and liquid-nitrogen temperature (about −196° C). There was no evidence of the gages separating from the graphite/epoxy sample. Next, the samples were mounted on a fixture, submerged in liquid nitrogen, and tested in tension. Inspection of the samples after they were stressed at loads greater than 11,000 psi (7.6×10^7 N/m^2) at about −196° C revealed no change in bonding.

This work was done by Benjamin Penn, Johnny M. Clemons, F. E. Ledbetter III, and W. T. White of **Marshall Space Flight Center.** *No further documentation is available.*
MFS-25867

Suppressing Transient Side Loads in Supersonic Nozzles

Fins are added to the nozzle wall.

Marshall Space Flight Center, Alabama

Flow-separation instabilities due to overexpanded flow in supersonic nozzles and the consequent vibrational side loads are suppressed by axial fins equally spaced about the nozzle circumference. A local flow separation is confined to the region between a pair of fins.

The fins protrude from the nozzle wall near the exit (see figure) to a height that equals or exceeds the boundary-layer-momentum thickness. The fins may be made of beryllium/copper, for example, and brazed to the coolant tubes in the nozzle wall to form a good thermal and structural bond. Wall-surface friction added by the fins is compensated by the regenerative heat input to the coolant.

The transient-suppressing fins may be helpful in rocket nozzles, jet engines, gas turbines, laser nozzles, flow diffusers, flow separators, and other devices with supersonic flows. The usual way of coping with flow-separation side loads has been to strengthen the nozzle to withstand the vibrations. While this may be satisfactory in many cases, it increases the weight — a disadvantage in aircraft engines or other applications where weight is critical. On the other hand, the weight of a set of fins is less than the weight added by conventional nozzle stiffening.

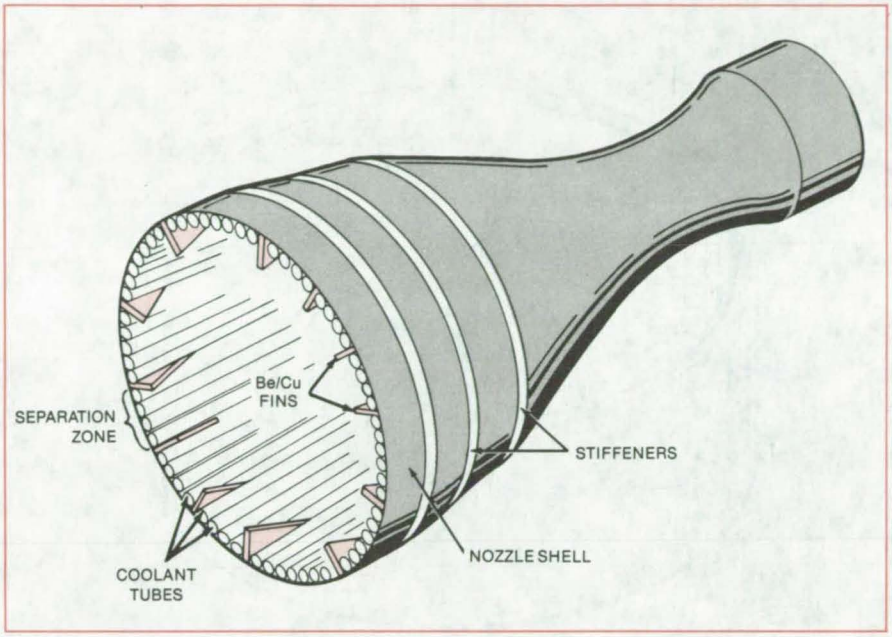

Fins Protrude From a Rocket-Nozzle Wall at equal intervals about the circumference. They inhibit the circumferential growth of local flow separations, thereby reducing sideways vibration of the nozzle.

This work was done by William R. Wagner of Rockwell International Corp. for **Marshall Space Flight Center.** *No further documentation is available. MFS-19769*

Tool Releases Optical Elements From Spring Brackets

Threaded hooks retract the bracket arms holding an element.

Goddard Space Flight Center, Greenbelt, Maryland

Using a new tool, one person can easily insert or remove an optical element (such as a prism or lens) from a spring holder or bracket with minimal risk of damage. Previously, pliers, wires, or even fingers were used to remove an element. However, these techniques often required two people and entailed some risk of damaging the optical element.

The brackets used to hold optical elements during testing prior to their final installation in an instrument usually have three or more clamping areas made of a springy or resilient material. In the example shown in the figure, the holder has three metal tabs formed by making right-angle bends in a flat piece of heat-treated beryllium/copper. Pins or detents on the tabs engage recesses in the sides of the optical element, preventing vibration from shifting or dislodging the element from its proper position.

(continued on next page)

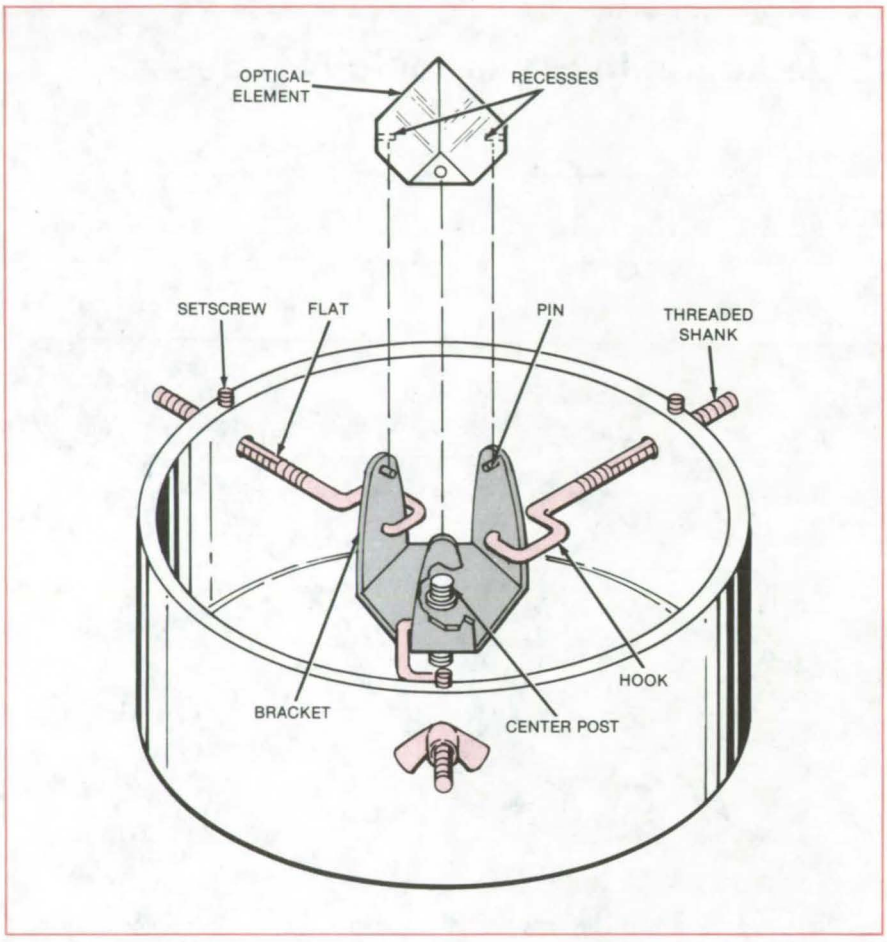

The **Optical-Element Release Tool** has hooks that retract the bracket tabs holding the optical element when the wingnuts are tightened. The setscrews on the ring may be used to prevent rotation of the hooks while inserting or removing the tool from the bracket or turning the thumbscrews.

The new tool uses three hooks with threaded shanks mounted in a ring-shaped holder to pull on the tabs to release the optical element. The bracket is slipped down into the tool and rotated slightly to engage the hooks on the tabs. For additional stability, the bracket may be centered in the tool by the engagement of a threaded tool center post with a matching threaded hole at the center of the bracket.

The hooks, which pass through clearance holes in the ring, are made to pull outward by turning wingnuts on the threaded shanks. The threaded portion of each hook is flattened on one side. Setscrews in the ring bear on the flat segments of the hooks to prevent rotation when the wingnuts are turned or while inserting or removing during retraction of the tabs.

This work was done by Jeffery S. Gum of **Goddard Space Flight Center.** *For further information, Circle 120 on the TSP Request Card.*

This invention is owned by NASA, and a patent application has been filed. Inquiries concerning nonexclusive or exclusive license for its commercial development should be addressed to the Patent Counsel, Goddard Space Flight Center *[see page A5].* *Refer to GSC-12794.*

Stability Test for Transient-Temperature Calculations

A graphical technique gives a rapid indication of stability or instability.

Marshall Space Flight Center, Alabama

A graphical test helps assure the numerical stability of calculations of transient temperature or diffusion in a composite medium. With the help of the test, the time increment is chosen small enough to keep the numerical error from growing out of bounds yet as large as possible within the stability limit to minimize the calculation time.

The test has been derived for the model shown in the figure, but can be adapted to other models as well. In this model, the medium may be homogeneous or divided into regions with different specific heats and heat conductivities. For simplicity, media interfaces lie along lines of rectangular grid points.

The equation for the flow of heat into the finite spatial element centered on a grid point is derived under the assumption of simple two-dimensional flow from the neighboring grid points. The resulting heat-balance equation expresses the temperature at a grid point during the next time step in terms of the present temperatures of that point and the neighboring points, the conductivities, the specific heats, the time increment Δt, and the x and y grid spacings (Δx and Δy, respectively).

The temperature $T_{ij}(n)$ of the grid point i,j at the nth time step as calculated by a computer will differ from the exact model value by an error $\delta_{ij}(n)$. In general $\delta_{ij}(n)$ is a complex quantity that can be expressed in the form

$$\delta_{ij}(n) = \xi^n e^{\hat{i}(i\beta\Delta x + j\gamma\Delta y)}$$

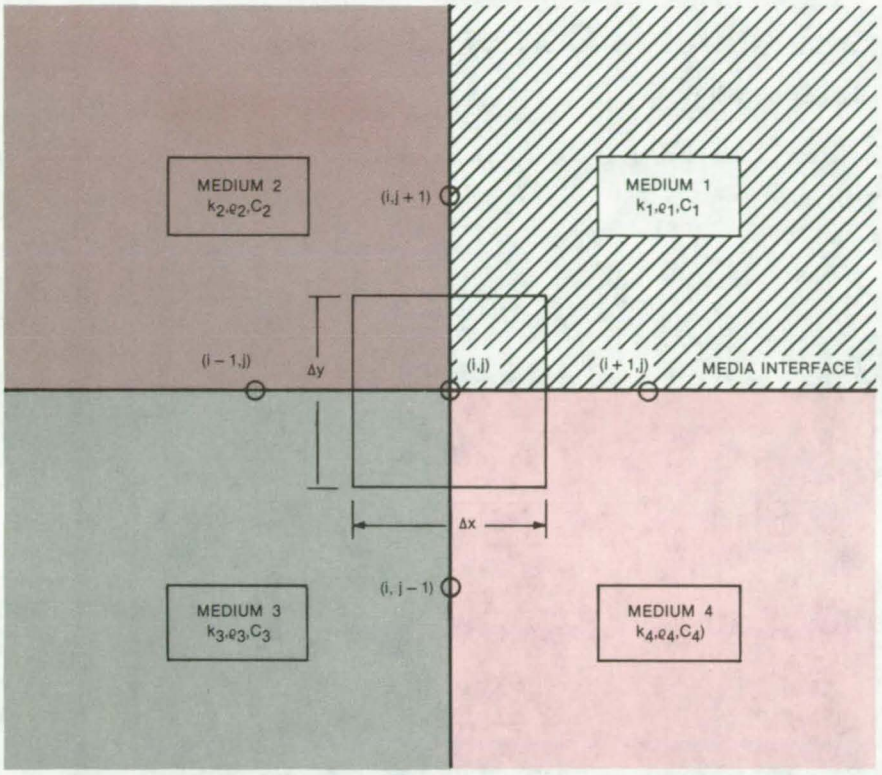

A **Rectangular Grid** forms the basis of a two-dimensional finite-difference model for heat conduction or other diffusionlike phenomena. The model enables the calculation of transient heat transfer among up to four different materials that meet at a grid point. The symbols k_i, ϱ_i, and C_i represent the heat conductivities, mass densities, and mass specific heats, respectively.

where β and γ are arbitrary free parameters. This term grows, remains constant in amplitude, or decays with time, depending on whether $|\xi|$ is greater than, equal to, or less than 1.

In the new procedure, an expression for ξ is obtained and each of the two arbitrary parameters is varied through small steps while the other is held constant. The result is a family of ellipses in the complex plane that graphically depict the envelope containing the possible values of ξ. If all points lie within the circle $|\xi| = 1$, then the stability condition is not violated. If any points lie outside $|\xi| = 1$, then numerical instability is likely to occur, and the time step must be diminished.

A computer plots the envelope quickly, and the operator determines by visual inspection whether the envelope lies within the stability circle. By trial and error the method quickly converges on a Δt that is as large as possible without causing numerical instability.

This work was done by Warren Campbell of **Marshall Space Flight Center.** *For further information, Circle 121 on the TSP Request Card.*
MFS-25803

Liquid-Nitrogen Test for Blocked Tubes

A simple method is based on retention of frost.

Marshall Space Flight Center, Alabama

A nondestructive test identifies an obstructed tube in an array of parallel tubes. The method is especially useful when the intake or exhaust ends of the tubes are obscured by a manifold or when the tubes are bent and no direct line of sight between intakes and exhausts exists. In such an array, conventional methods, such as inspection by X-rays, dye penetration, ultrasonics, or fluid flow, will not pinpoint individual blocked tubes. Applications of the new method include the inspection of rocket nozzles, solar panels, heat exchangers, boilers, heaters, water-feed systems, gaslines, and other flow systems having parallel legs.

A trickle of liquid nitrogen is allowed to flow through the tube array until the array accumulates a substantial formation of frost from moisture in the air. The liquid-nitrogen flow is then stopped, and warm air is introduced into the inlet manifold to heat the tubes in the array. The warm air flows readily through the unobstructed tubes and melts the frost. However, partially or completely plugged tubes will inhibit airflow and retain their frost for a longer time. Thus, tubes that are still frosted after others are defrosted are identified as obstructed tubes.

This work was done by William R. Wagner of Rockwell International Corp. for **Marshall Space Flight Center.** *No further documentation is available.*
MFS-19762

Shear-Panel Test Fixture Eliminates Corner Stresses

A new design eliminates corner stresses while maintaining uniform stress across the panel.

Langley Research Center, Hampton, Virginia

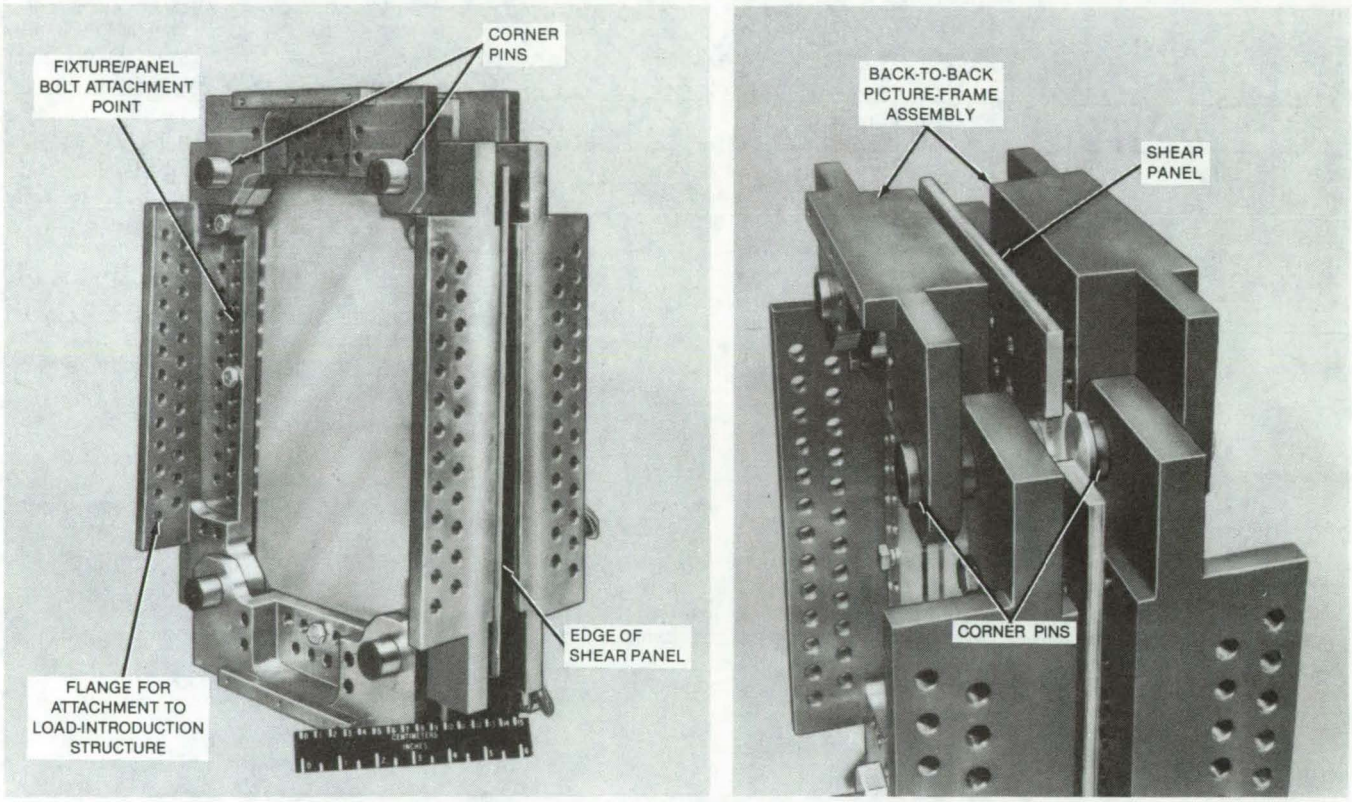

Figure 1. The new **Shear-Panel Test Fixture** includes eight frames and eight corner pins. The fixture is assembled in two halves with the shear panel sandwiched in between.

Fixtures for performing shear-panel tests include the biaxially-loaded picture frame and diagonal-tension, cantilever-beam, and three-point bending fixtures. All of these produce relatively-uniform shear-stress distribution in the center of the test panel but large normal and shear stresses in the corners. These corner stresses can cause non-shear-induced failures and erroneous test results. These test results, when applied to the design of built-up structures, lead to overly conservative designs resulting in heavier, less-fuel-efficient aircraft.

A new shear-panel test fixture is composed of eight frames and eight corner pins. The assembly is put together in two halves (picture frames) with the shear panel sandwiched between them (see Figure 1). The corner pins do not protrude through the panel. Their centers are located at the corners of the test panel. The location of the corner pins is critical in preventing large normal and shear stresses from building up in the corners of the test panel.

The panel and test fixture are assembled in the supporting structure (see Figure 2), which is bolted to the load platens of the test machine. Load is applied to one edge of the fixture while the opposite edge is restrained from moving. The edge where the load is applied is allowed to contract to eliminate binding of the fixtures and the introduction of extraneous loads into the fixtures and test specimens.

This test fixture can be used in testing machines other than the combined load/test machine shown. Supporting L's can be used for load introduction. Similarly, the diagonal tension and biaxially-loaded picture frames could also incorporate these new features. A detailed computer analysis of the new test fixture indicates that all of these load introduction techniques would produce similar results.

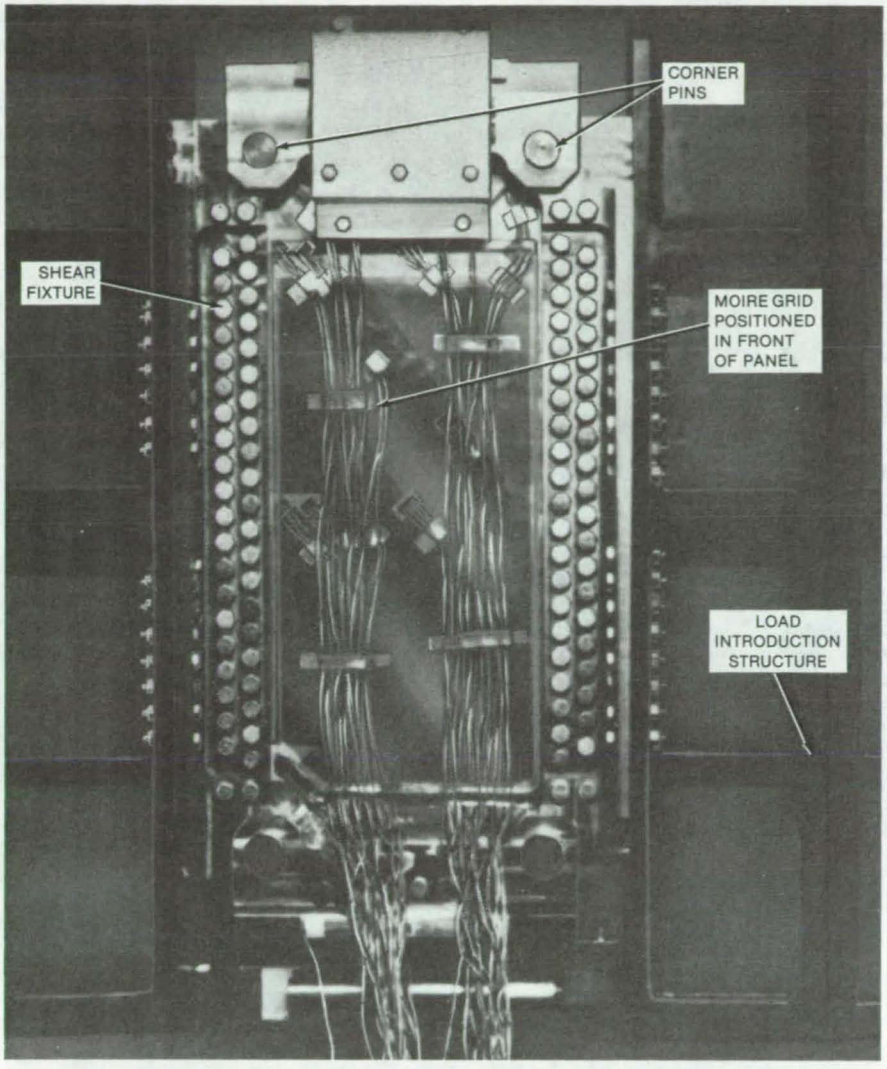

Figure 2. The **Fixture is Stressed in a Conventional Load-Test Machine.** One edge of the fixture is held stationary as load is applied to the other edge.

The shear-panel test fixture was originally designed for testing structural panels under a shear loading. Its features could be incorporated into a smaller fixture for determining the characteristic material properties, such as shear modulus, G, and shear-stress and strain ultimates, τ^{ult} and γ^{ult}, respectively. Other shear fixtures, such as the biaxially-loaded picture frame, are used to determine these material properties; but because of the introduction of large normal and shear stresses in the corners, the results are suspect.

The new shear-panel test fixture eliminates the large stresses in the corners while maintaining a uniform shear stress across the panel. Test results generated from the use of this fixture should result in a good data base for the design of efficient aircraft structures and other applications.

This work was done by James J. Kiss of **Langley Research Center** *and Gary L. Farley and Donald J. Baker of the U.S. Army Aviation Research and Development Command. For further information, Circle 122 on the TSP Request Card.*
LAR-12930

Heat-Pipe Thermal Switch

A new design isolates components from vibrations.

Goddard Space Flight Center, Greenbelt, Maryland

A new heat pipe lengthens to connect an object with a heat sink, then contracts when the heat sink is no longer needed. It was originally designed for cooling vibration-sensitive electronic components. The heat pipe isolates the components mechanically from the heat sink, except when cooling is actually required.

A flexible outer casing replaces the rigid pipe found in conventional heat pipes. When the working fluid begins to evaporate, the pressure buildup lengthens the casing until the heat-pipe condenser contacts the heat sink. This motion completes the conductive path, allowing heat to flow from the object to the heat sink. When the object has cooled sufficiently, the pressure decreases, and the casing contracts, again isolating the object from the heat sink.

As shown in the figure, the heat pipe consists of a bellows, a capillary, guide rods, a working fluid, a switch mount, and a contact plate. Heat from the body to be cooled is transferred to the switch

(continued on next page)

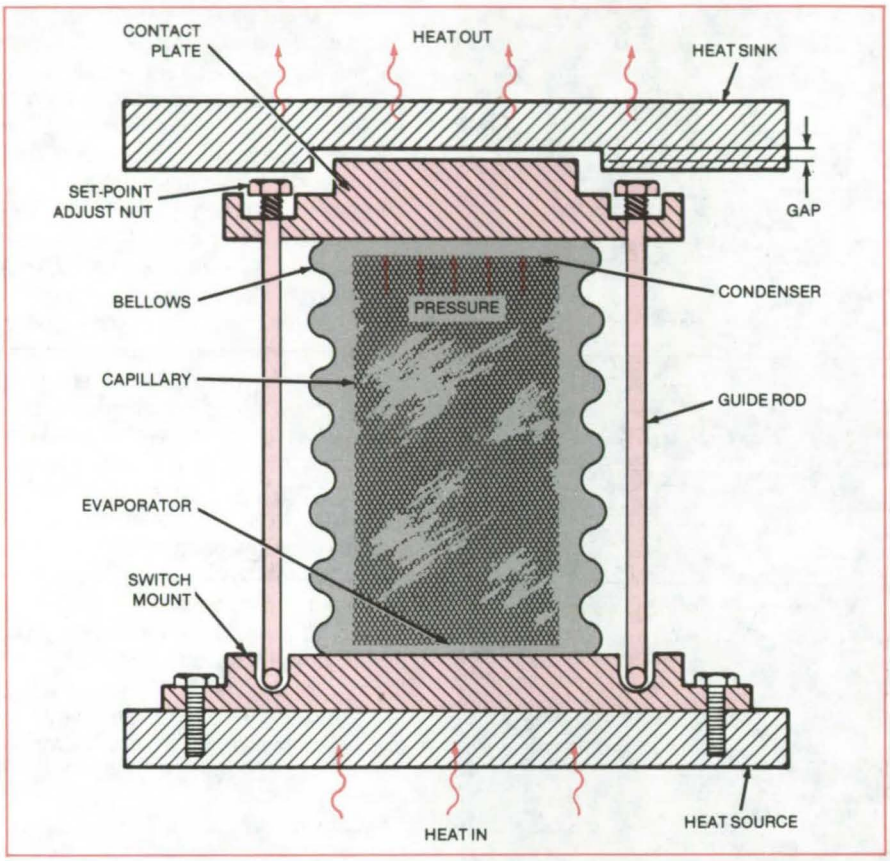

A Heat-Pipe Thermal Switch controls the temperature of the heat source. The ball-and-socket guide rods and the bellows allow relative motion of the source and its heat sink and protect the source from vibrations.

mount. Through conduction, it enters the liquid and turns it to vapor. The increasing vapor pressure within the pipe moves the contact plate upward until it touches the heat sink and begins to transfer heat. Liquid condensing at the top is returned by the capillary.

This work was done by Stanford Ollendorf of **Goddard Space Flight Center.** *For further information, Circle 123 on the TSP Request Card.*

This invention is owned by NASA, and a patent application has been filed. Inquiries concerning nonexclusive or exclusive license for its commercial development should be addressed to the Patent Counsel, Goddard Space Flight Center [see page A5]. *Refer to GSC-12644.*

Flow-Straightener Sleeve for Pump Valve

Vaned tube smooths the flow from a pump.

Marshall Space Flight Center, Alabama

A sleeve reduces turbulence in the high-pressure discharge from a pump. The fluid in the sleeve flows more uniformly than it would in an open pipe and generates less of the noise that is otherwise characteristic of turbulent flow. As a result, a valve downstream from the sleeve performs more reliably and quietly. The possibility of damage to internal valve parts from nonuniform, turbulent flow is greatly reduced. Valve life expectancy is also increased, and the time between overhauls can be extended.

The flow-straightening sleeve contains vanes in a modified honeycomb pattern (see figure). Each vane is a curved fluid-dynamic wing that helps to straighten and smooth out the flow of fluid passing over it. By increasing the structural rigidity of the sleeve, the vanes thereby help to damp out noise.

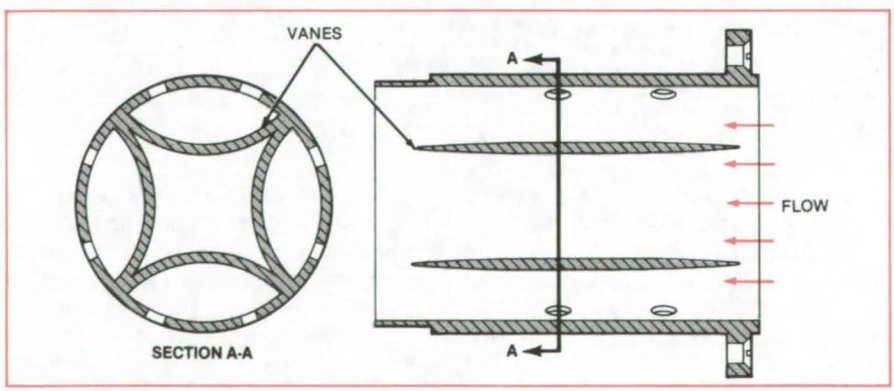

Transverse and Longitudinal Sections through the flow-straightening sleeve reveal the vanes.

This work was done by Jack Tolpen of Rockwell International Corp. for **Marshall Space Flight Center.** *For further information, Circle 124 on the TSP Request Card.*
MFS-19781

Isolating Supports for X-Ray Mirrors

Simple concept reduces effects of gravity, temperature, and magnetism.

Marshall Space Flight Center, Alabama

A concept for mounting paraboloidal and hyperboloidal mirrors and similar optical elements would help to isolate them from magnetic, gravitational, and temperature effects. The mounting scheme would allow inexpensive materials to be used — for example, high-thermal-expansion materials, such as aluminum, can be used to support a reflector instead of stainless steel or special low-thermal-expansion alloys.

In the new scheme, the reflector is supported by a single circumferential ring, which in turn is supported by a conical shell (see figure). The single ring is attached near the center of mass of the reflector.

The performance of the concept was predicted by finite-element structural analysis and optical-ray-trace analysis. Symmetric radial and circumferential deformations introduced into the ends of the support shell diminish exponentially with distance from the ends. The resulting deformations at the reflector/support juncture are therefore extremely small. In addition, axial forces that are introduced into the shell — whether by thermal effects or acceleration — cause an insignificant deformation in the reflector.

The concept was developed for supporting a mirror in an X-ray telescope. The support scheme would keep the mirror accurately alined, both in space and during testing on Earth. The scheme can be adapted to such terrestrial instruments as imaging devices and spectroscopes. With each optical element supported by a single circumferential ring, such instruments could operate with high efficiency and accuracy.

This work was done by Lester M. Cohen of the Smithsonian Astrophysical Observatory for **Marshall Space Flight Center.** *For further information, Circle 125 on the TSP Request Card.*
MFS-25904

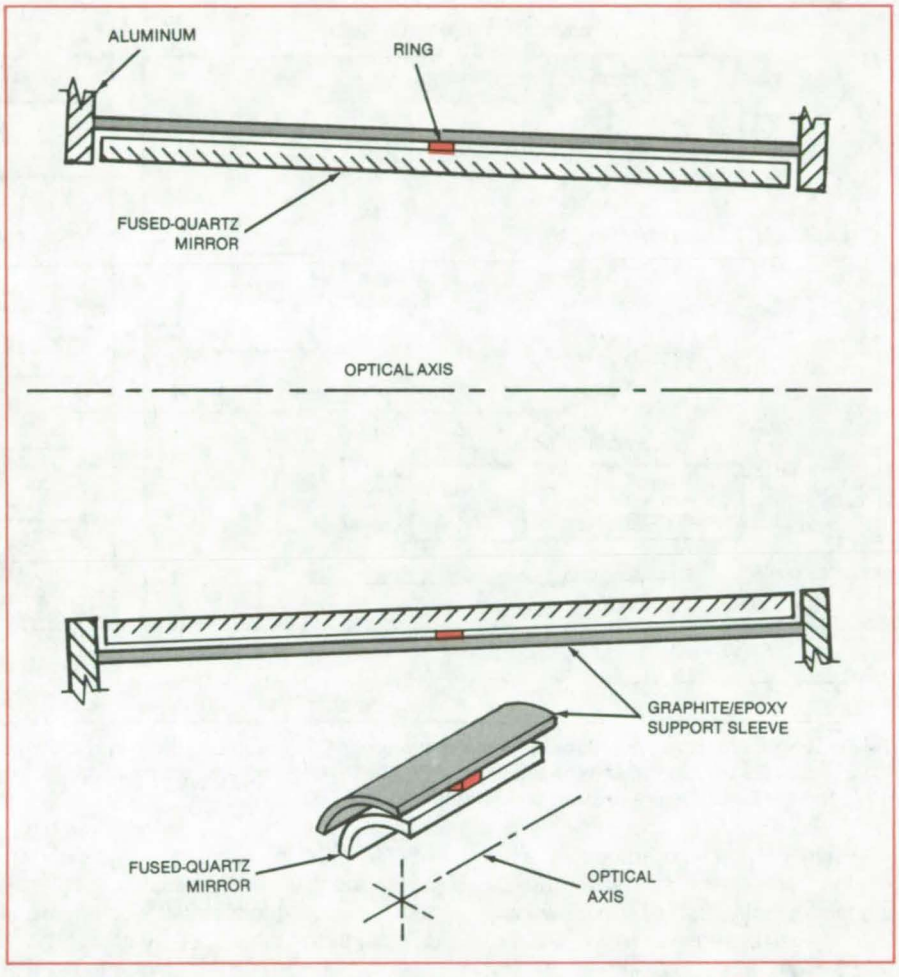

A **Single Circumferential Ring** supports a fused-quartz mirror in a high-resolution X-ray telescope.

Electronically-Scanned Pressure Sensors

Sensors do not have to be pneumatically switched.

Ames Research Center, Moffett Field, California

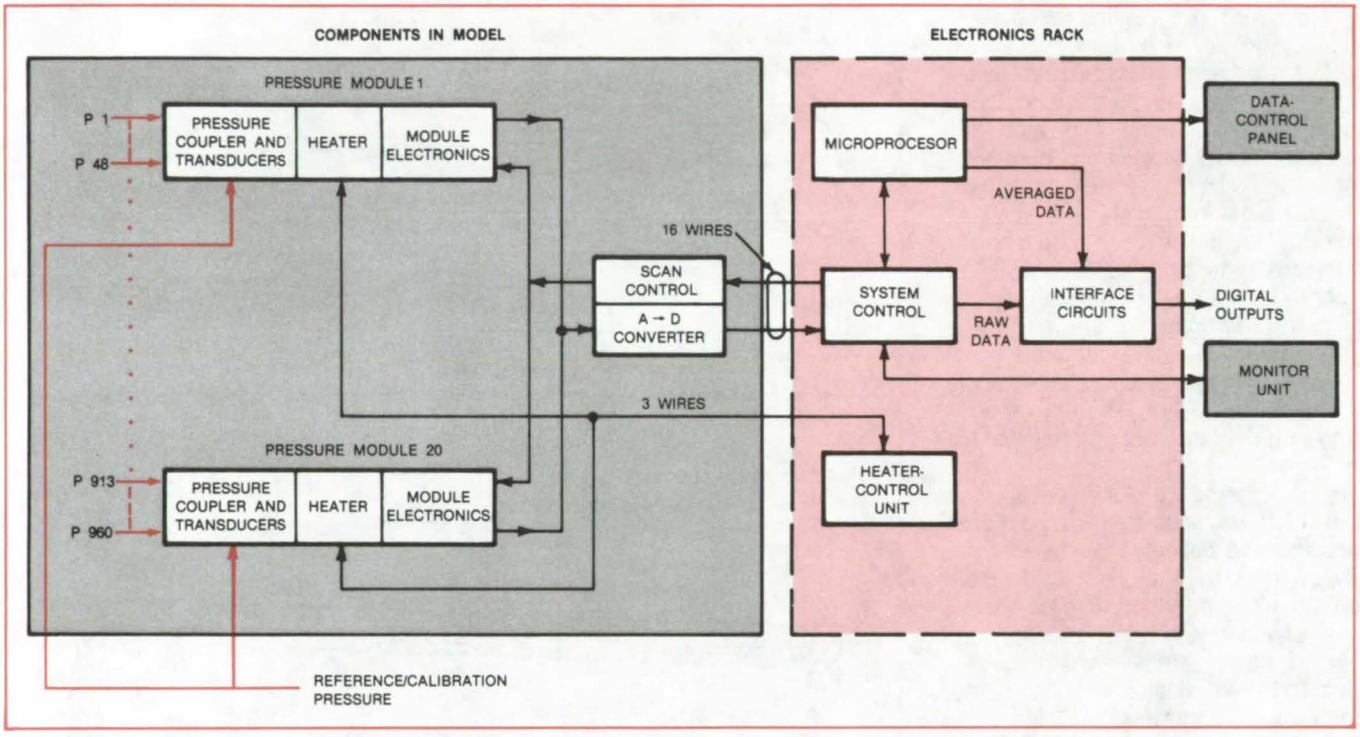

The **Electronic Pressure-Transducer Scanning System** is constructed in modular form. The pressure-transducer modules [2.3 by 1.0 by 0.9 in. (5.8 by 2.5 by 2.3 cm)] and the analog-to-digital-converter module [3.8 by 2.5 by 1.1 in. (9.7 by 6.4 by 2.8 cm)] are small enough to fit within the cavities of average-sized wind-tunnel models.

Arrays of pressure transducers (in a wind tunnel, for example) can be scanned electronically by a new continuous scan-based system. The system differs from earlier equipment in that pneumatic switching for measurements, zeroing, and recalibration during a test is unnecessary. All the switching is done electronically. The new system maintains a temperature-controlled environment within the sensor modules so that accuracy is maintained while the ambient temperature varies.

The main elements of the system are the pressure modules, an analog-to-digital converter, an electronics rack, a data-control panel, and a monitor (see figure). Besides pressure transducers, a pressure module contains a heating plate for temperature control and a multiplexer/amplifier for the transducer signals. A flat cable connects the modules to the analog-to-digital-converter module. The pressure modules and the analog-to-digital converter are sufficiently compact that they can be mounted in cavities in average-sized wind-tunnel models.

The system includes up to 20 pressure modules, each containing 48 transducers that convert pressure into an analog electrical signal. The 48 analog pressure signals are amplified and multiplexed onto the analog bus from within the module.

In the continuous process, the analog-to-digital converter transforms the pressure data on the analog bus into digital form, sampling each transducer output 80 times a second. The digitized pressure data are transmitted to the electronics rack where, under microprocessor control, they are averaged and converted into engineering units. The system keeps the module temperature constant within ±1° F (0.6° C). Pressure measurements are accurate within ±0.15 percent over a temperature range of 20° to 49° C. Pressure transducers can be replaced in the field.

The electronics rack containing the microprocessor, control circuits, and power supplies is placed outside the wind tunnel. The data-control panel and the monitor are usually placed in the wind-tunnel control room.

This work was done by Charles F. Coe, Gilbert T. Parra, and Ronald C. Kauffman of **Ames Research Center.** *For further information, Circle 126 on the TSP Request Card.*

Inquiries concerning rights for the commercial use of this invention should be addressed to the Patent Counsel, Ames Research Center [see page A5]. Refer to ARC-11361.

Crystal Microbalance Monitors Relative Humidity

Sensor could monitor water evaporation in industrial drying processes.

NASA's Jet Propulsion Laboratory, Pasadena, California

A moisture sensor made by modifying a quartz-crystal microbalance could measure the relative humidity of the ambient atmosphere near drying paper, food, textile fabrics, and pulp to optimize the water-drying portion of the processing cycle. Test data show excellent measuring capability for the technique.

When a thin layer of material is added to a surface of a shear-mode oscillating quartz crystal, the crystal resonant frequency decreases with increasing mass per unit area of the added material. With crystals operating in the resonant frequency range of 2 to 28 MHz, mass changes as small as 10^{-9} g/cm^2 are readily detectable. A hygroscopic coating added to the crystal surface makes it possible to detect moisture.

The quartz-crystal microbalance that was modified and tested contained two crystal elements. It was modified by coating the mass-sensing crystal with a solution containing 1 percent by weight of lithium fluoride, a hygroscopic coating. One element was shielded from the effects of mass accretion, and the mass-sensing element was left exposed. The difference frequency between the two elements, as measured by a frequency mixer circuit, is proportional only to the mass — in this case, water — accumulated on the mass-sensing element.

The characteristic curve of the modified microbalance is nearly linear (see figure) over a wide temperature range for the full relative-humidity range, 0 to 100 percent. The selected operating range of temperatures, 70° to 140° F (21° to 60° C), is fairly close to the exhaust temperatures of dryers used in industrial processing.

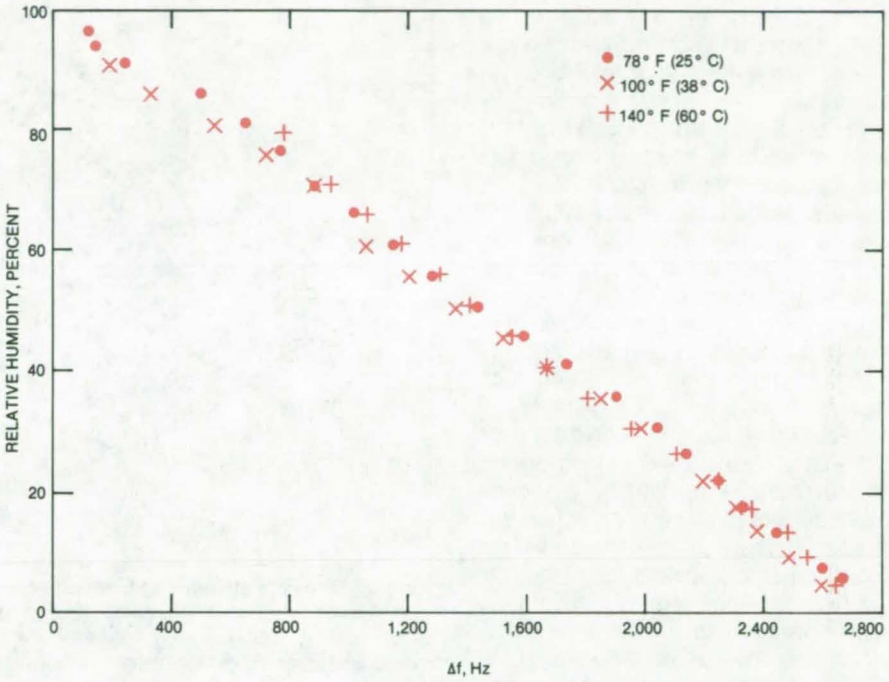

The **Measured Adsorption Isotherm** for the instrument is essentially linear over the entire range of relative humidity. Testing at each temperature setting takes less than half an hour for the full relative-humidity range, with an estimated frequency-response time of less than 10 seconds. The base frequency here is 9.332 MHz.

The instrument is calibrated onsite by using two small canisters: one containing a moisture-removing agent to simulate 0 percent relative humidity and one with a small amount of water to simulate 100 percent relative humidity. The sensitivity can be varied by using crystals of different resonant frequencies or by applying different amounts of coatings of lithium fluoride with varying solution concentration.

This work was done by Lien C. Yang of Caltech for **NASA's Jet Propulsion Laboratory.** *For further information, Circle 127 on the TSP Request Card.*
NPO-15493

Latch for Storage Cargo

Heavy cargo can be secured for storage by lightweight spherical latches originally developed for spacecraft payloads. Convex hemispherical latch elements attached to the cargo mate with concave latch elements secured to the cargo-bay floor. The elements automatically aline and engage with one another when the payload is moved into the storage position. The spherical shape of the latching elements distributes the cargo weight over a broad area.
(See page 97.)

Three-Fingered Robot Hand

A robot hand under development will perform rapid, small motions by human-like finger actions — independently of its manipulator arm. It will be attachable to many different manipulators without modifications to the arms. Like the fingers on the human hand, the robot-hand fingers can provide more than three contact areas since more than one segment per finger can contact an object.
(See page 99.)

Fabrication of Hollow Spheres

A "shell" generator produces gas-filled metal spheres at a rate of about 100 per second. The spheres can be filled with gas at a pressure as high as 2,000 psi. The process, which exploits the tendency of a liquid column to break up into droplets, would be suited for making targets for laser-fusion experiments.
(See page 138.)

Surface-Moisture Monitoring Technique

Technique would monitor the drying of continuous sheets of thin material.

NASA's Jet Propulsion Laboratory, Pasadena, California

The effect of moisture on a heated metal ribbon is the basis for a moisture sensor tested at NASA's Jet Propulsion Laboratory. Whereas the sensor described in the preceding article monitors ambient moisture, the new ribbon sensor measures the moisture in a solid material placed in contact with it. It therefore has possible applications in industrial production of sheet materials, such as paper and fabric.

One form of the new sensor is illustrated in Figure 1. A stainless-steel ribbon is mounted in a plastic roller, such that the ribbon is flush with the roller surface. Copper leads attached to the ends of the ribbon exit the roller along its axis.

The ribbon is excited by a square-wave current pulse, which heats it and raises its resistance. Contact with a moist material transfers heat from the ribbon, thus lowering its temperature and decreasing its resistance. This difference in resistance, before and immediately after contact with the material, is a measure of the moisture content.

The results of preliminary tests of the sensor are shown in Figure 2. Each of the tested materials was soaked in water and allowed to dry slowly in air. The materials were then pressed against the sensor surface. Water content was determined by weighing the material just prior to testing it.

The data show a dependence of the maximum voltage across the sample, and thus of the maximum resistance, on the moisture content of the materials placed in contact with the sensor. The voltage is measured by a Wheatstone-bridge circuit used for monitoring strain gages.

The tests showed that the resistance readings are not dependent on the pressure applied to the sensor to hold it in contact with the material. They also confirm that the sensor would have to be calibrated for each material tested.

This work was done by Lien C. Yang of Caltech for **NASA's Jet Propulsion Laboratory.** *For further information, Circle 128 on the TSP Request Card.*

This invention is owned by NASA, and a patent application has been filed. Inquiries concerning nonexclusive or exclusive license for its commercial development should be addressed to the Patent Counsel, NASA Resident Office-JPL [see page A5]. Refer to NPO-15494.

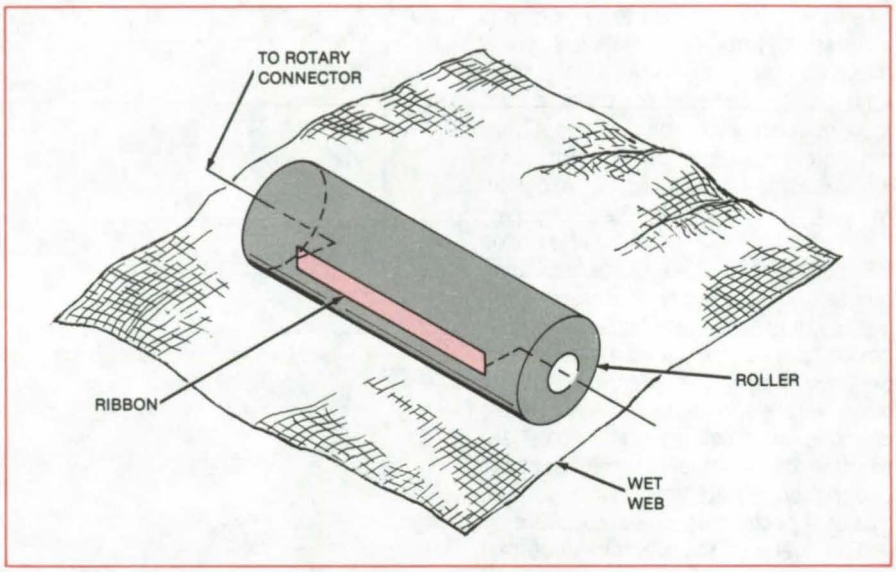

Figure 1. The **Ribbon Sensing Element** samples the moisture content of the web material during each rotation of the roller. The change in resistivity of the thermally and electrically conductive ribbon is the parameter used to measure the web moisture; the measurements are insensitive to ribbon contact pressure.

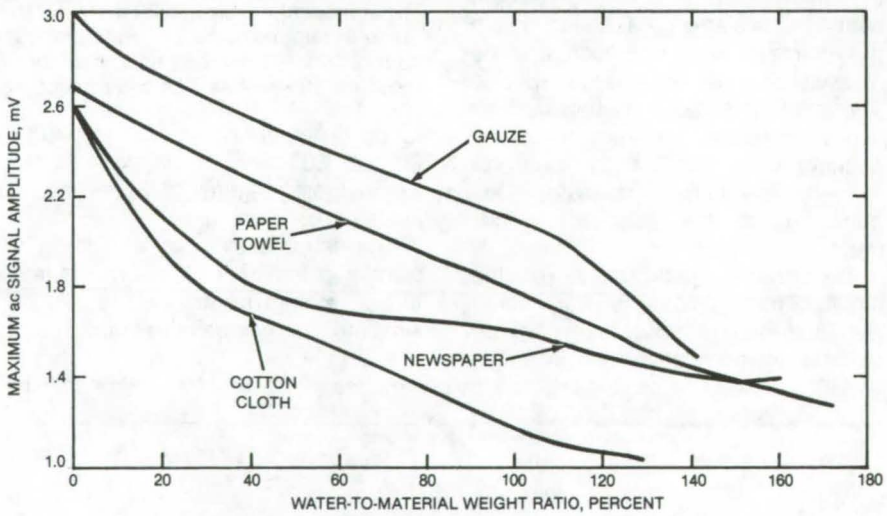

Figure 2. The **Correlation Between Measurement and Moisture Content** for several common materials is shown here. Each sample was soaked in water and dried slowly in air. Water content was determined by an accurate weighing of the samples before soaking and just prior to testing.

Books and Reports

These reports, studies, and handbooks are available from NASA as Technical Support Packages (TSP's) when a Request Card number is cited; otherwise they are available from the National Technical Information Service.

Locomotive Truck Dynamics

Commonly-used locomotive trucks were tested to study and improve ride safety.

The locomotive truck performs a number of essential functions: It damps the motion of the car body excited by rail imperfections, guards against derailment in the presence of lateral forces, transmits traction and braking force, and guides the car body around curves. In 1976, the Federal Railroad Administration and the National Aeronautics and Space Administration jointly initiated a program to study locomotive truck dynamics to improve operational safety. An 83-page final report summarizes the program and the truck and component tests.

A cross section of trucks commonly used on U.S. railroads was tested. Eight locomotive trucks — six three-axle trucks and two two-axle trucks — were tested, along with some key truck-suspension components. Each truck incorporated one of two basic suspension designs: standard and swing hanger. The difference in the designs is in the connection of the bolster, to which the car body is attached, to the frame. In the standard design, the bolster and frame are connected by compression springs; the swing hanger design uses a lateral pendulum suspension arrangement.

Test conditions measured either directly or indirectly the load-deflection characteristics representative of the 15 degrees of freedom that correspond to the relative motions of a truck. During testing, a fixture supported the truck wheels on slide plates that were restrained with hydraulic actuators to react wheel loads. The fixture could apply vertical, lateral, and longitudinal loads to the truck bolster center plate. The restraining actuators, on the wheel slide plates, also applied axle yaw forces. The testing and data acquisition were controlled by a microcomputer.

In addition to the locomotive truck tests, three component test programs investigated damping, stiffness, and energy-dissipation characteristics of key suspension components: rubber suspension pads, straight roller-bearing lateral bumpers, and shock absorbers and friction snubbers. A truck test-data summary appears in the appendix of the report; the sources of more detailed data are referenced in the report.

The testing procedures developed and the data collected have important applications to the railroad industry. One application is the derailment safety analysis of six-axle locomotives. The procedures can also be used to determine:

- Maximum safe operating speeds for various classes of track, based on locomotive dynamics;
- Critical track-geometry defects;
- Minimum track-strength requirements;
- Appropriate locomotive-maintenance standards;
- Derailment mechanisms;
- The relative importance of truck, track, and operational parameters to operational safety;
- The mechanical design of locomotive suspension components; and
- New and modified locomotive designs before introducing them into service.

A computer model was developed to simulate the nonlinear response of a locomotive to track-geometry defects and to evaluate safety measures. Track-geometry defects are specified by vertical, cross-level, or gage perturbations; and complex defects can be constructed by a superposition of defects. Wheel/rail interactions are modeled in detail. The model includes a nonlinear creep formulation and also simulates wheel flanging. In addition, constant coupler forces and windloads may be specified.

Two studies used the model: A parameter sensitivity analysis was performed to determine the relative importance of truck, track, and operational parameters to operational safety; and a comparative analysis was made of three different locomotives subjected to the same set of rail-geometry defects.

This work was done by Robert L. Berry and Frank E. Barone of Martin Marietta Corp. for **Marshall Space Flight Center.** *Further information may be found in NASA CR-81-577 [N82-28224/NSP], "Track Train Dynamics Analysis and Test Program: Locomotive Dynamic Characterization Summary" [$23]. A paper copy may be purchased [prepayment required] from the National Technical Information Service, Springfield, Virginia 22161. The report is also available on microfiche at no charge. To obtain a microfiche copy, Circle 129 on the TSP Request Card.*
MFS-25872

Radial-Cascade Analysis

Conformal mapping transforms a radial cascade to an axial cascade.

A report now available describes the analysis of pressure distributions on radial diffuser geometries within Space Shuttle main and preburner pumps. The analysis uses a modified version of the Douglas-Neumann (D-N) procedure for two-dimensional axial cascades.

Simply speaking, a cascade is a series of identical bodies equally spaced and identically oriented with respect to a circle or a line. In the radial-cascade method, the rotationally repeating structure is mapped into a linearly repeating structure that is then analyzed for two-dimensional axial flow in a rectangular geometry. The resulting solution is then transformed back into the radial plane. The conformal mapping chosen for this problem is between a logarithmic spiral in the physical plane and a straight line in the transformed plane.

D-N solves the fluid-flow problem by applying a source distribution of appropriate strength on the surface of the body in such a way that the flow normal to the surface is either zero or prescribed. When the boundary condition is applied, an integral equation in the source strength is obtained. To solve this equation the body surface is approximated by straight-line elements. Source strength is assumed constant along any one element, but varies from element to element.

To solve the general case of a lifting cascade at any angle of attack, "basic" flows are calculated and superimposed in such a way that the correct angle of attack is obtained, and the Kutta condi-

(continued on next page)

tion (relating to the matching of tangential velocities above and below the trailing edge) is satisfied. These basic flows are the following:

- Flow at zero angle of attack;
- Flow at 90° angle of attack; and
- Circulatory flow for each cascade.

The version of the D-N program used in the new radial-cascade program had been extended to calculate the flow about infinite two-dimensional lifting cascades. The program with its cascade modification calculates the velocity and pressure distribution normalized to average velocity, lift coefficient, and moment coefficient per cascade blade. The inlet and exit velocities and the cascade turning angle are also calculated.

The technique is rigorous in the sense that the exact solution is approached in the limit as the number of points describing the body goes to infinity. In a comparison of theoretical predictions with experimental results on a low-aspect-ratio axial-flow pump propeller, two-dimensional cascade theory proved superior to three-dimensional vortex theory.

This work was done by Sen Yih Meng of Rockwell International Corp. for **Marshall Space Flight Center.** *To obtain a copy of the report, Circle 130 on the TSP Request Card.*
MFS-19752

Computer Programs

These programs may be obtained at very reasonable cost from COSMIC, a facility sponsored by NASA to make new programs available to the public. For information on program price, size, and availability, circle the reference letter on the COSMIC Request Card in this issue.

Crash Simulation and Nonlinear Structural Analysis

Behavior of structures composed of trusses, frames, and membranes is modeled.

Crash simulation analysis is useful in developing an understanding of the multifaceted relationship between a complex structural configuration, such as an aircraft, and its response during a crash. Such an understanding can provide the basis for the crashworthy design of lightweight aircraft, better restraint systems, and efficient energy-absorption devices that may reduce passenger trauma.

ACTION (Analysis of Crash Transients in Inelastic and Geometrically Nonlinear Structures) is a special-purpose computer program that provides special modeling and evaluation processes for crash simulation and nonlinear structural analysis. ACTION can represent the material and geometric nonlinear behavior of a structure composed of truss, frame, and membrane elements. Although quite suitable for general nonlinear analysis, ACTION was primarily designed to analyze the response of vehicles crashing into a rigid or a deformable barrier.

The simulation is based on a discrete model of the structure using finite elements that respond plastically. A transient analysis of such a model yields the displacements, velocities, accelerations, internal loads, and stresses under time-varying loads that may cause complete failure of the structure. ACTION includes automatic control of discrete time error, the representation of rigid barrier impact with treatment of gapping and friction effects, program logic designed to minimize data transfers, and response data defining the allocation of stored and dissipated energies.

Input to the ACTION program consists of a set of data blocks for each problem. The number of data blocks included in any particular problem is dependent on the problem. Information that may be input through the data blocks includes data on joint coordinates, material, line elements, mass, initial conditions, function tables, forcing functions, terrain models, and guessed initial displacements. The output includes both printed data and data stored on peripheral storage units. The printed output includes an interpretation of the problem input, a detailed record of the time response of the structure, and diagnostic messages. Data stored on peripheral storage units may be used to restart an analysis or to plot the structural response.

The ACTION computer code is available in both CDC and IBM versions. The CDC version is written in FORTRAN IV for batch execution and has been implemented on a CDC CYBER 175 computer with a central-memory requirement of approximately 200K (octal) of 60-bit words. The IBM version is written in FORTRAN IV and Assembler for batch execution and has been implemented on an IBM 370-series computer with a central-memory requirement of approximately 560K of 8-bit bytes. The ACTION computer program was developed in 1980.

This program was written by Manohar P. Kamat of Virginia Polytechnic Institute and State University for **Langley Research Center.** *For further information, Circle A on the COSMIC Request Card.*
LAR-12926 and LAR-12927

Panel Analysis and Sizing Code

Program is of particular value in analyzing and sizing filamentary composite panels.

The Panel Analysis and Sizing code (PASCO) for the buckling and vibration analysis and sizing of prismatic structures having an arbitrary cross section is primarily intended for analyzing and sizing stiffened panels made of laminated orthotropic materials. It is of particular value in analyzing and sizing filamentary composite structures.

In the analysis mode, PASCO calculates laminate stiffnesses, lamina stresses and strains (including the effects of temperature and panel bending), buckling loads, vibration frequencies, and overall panel stiffness. In the sizing mode, PASCO adjusts panel sizing variables for a low-mass design that carries a set of specified loadings without exceeding the allowed buckling or material strength and that meets such other requirements as upper and lower bounds on sizing variables, upper and lower bounds on overall bending, extensional and shear stiffnesses, and lower bounds on vibration frequencies.

Because of their wide application in aerospace structures, stiffened panels having several identical bays are given special emphasis in PASCO; however, the only restriction on configuration modeling is that the structure is assumed to be prismatic. In addition, it is assumed that loads and temperatures do not vary along the length of a panel.

The panel cross section is composed of an arbitrary assemblage of thin, flat, rectangular plate elements that are connected together along their longitudinal edges. Each plate element consists of a balanced symmetric laminate of any number of layers of orthotropic material. Any group of element widths, layer thicknesses, and layer orientation angles may be selected as sizing variables. Substructuring is available to increase the efficiency of the analysis and to simplify the modeling of complicated structures.

PASCO is written in FORTRAN IV for batch execution. The program was developed in 1981 for a CDC CYBER 170-series computer and contains one subprogram written in COMPASS. It has a problem-dependent central-memory requirement of approximately 120K (octal) of 60-bit words. PASCO was adapted to the DEC VAX 11/780 computer in 1983.

This program was written by Melvin S. Anderson, W. Jefferson Stroud, Barbara J. Durling, Timothy R. Rau, Katherine W. Hennessy, and William H. Greene of **Langley Research Center** *and Christine G. Lotts of Kentron International, Inc. For further information, Circle B on the COSMIC Request Card.*
LAR-13004 and LAR-13164

QUICK Interactive Graphics Analysis

Cross-section and body-line plots are generated for error detection and analysis.

A FORTRAN 77 version of the QUICK Interactive Graphics Analysis program, QUIAGA, performs the same operations as its FORTRAN IV counterpart. A description of the FORTRAN IV version of QUIAGA appears in the article "Interactive Graphics Analysis for Aircraft Design" (LAR-12951) in *NASA Tech Briefs*, Vol. 7, No. 4 (Summer 1983), p. 437.

QUIAGA displays aircraft QUICK-geometry data to aid in the detection and analysis of errors. QUICK-geometry data can be used to generate a completely-analytical aircraft geometry description for finite-difference flow codes. A QUICK-geometry program is included in the COSMIC package for "Steady-State-Super/Hypersonic Inviscid Flow" (LAR-11891), *NASA Tech Briefs*, Vol. 2, No. 1 (Spring 1977), p. 124.

The QUIAGA program is written, in FORTRAN 77, for interactive execution and has been implemented on a Prime 750 computer. The program is designed for use with the Tektronix 4014 Computer Display Terminal supporting the Plot 10 graphics library. The QUIAGA program was developed in 1981.

This program was written by James C. Townsend of **Langley Research Center.** *For further information, Circle C on the COSMIC Request Card.*
LAR-12952

Transonic Airfoil Analysis

Program uses a fast iteration scheme for solving the transonic flow field around arbitrary airfoils.

The Transonic Airfoil Analysis Computer Code, TAIR, employs a fast, fully implicit algorithm to solve the conservative full-potential equation for the steady transonic flow field about an arbitrary airfoil immersed in a subsonic free stream. The full-potential formulation is considered exact under the assumptions of irrotational, isentropic, and inviscid flow. These assumptions are valid for a wide range of practical transonic flows typical of modern-aircraft cruise conditions. The primary features of TAIR include the following:

- A new fully-implicit iteration scheme that is many times faster than classical successive-line overrelaxation algorithms;
- A new reliable artificial density/spatial differencing scheme treating the conservative form of the full-potential equation; and
- A numerical mapping procedure capable of generating curvilinear, body-fitted finite-difference grids about arbitrary airfoil geometries.

Reliability, simplicity, and speed were emphasized during the development of TAIR. The reliability comes from the new algorithm employed and the implementation of effective convergence-monitoring logic. TAIR employs a "default mode" that simplifies code operation, especially by inexperienced users. It also includes many useful options, such as several airfoil-geometry input options, flexible user controls over program output, and a multiple-solution capability. The speed of TAIR is attributed to the new algorithm and the manner in which it has been implemented.

Input to TAIR consists of airfoil coordinates, free-stream mach number, angle-of-attack, flow-field convergence parameters, and geometric and grid convergence parameters. In the vast majority of cases, only airfoil coordinates, free-stream mach number, and angle-of-attack need to be specified by the user. The computer code will automatically choose appropriate values for all other parameters. Output from TAIR may include aerodynamic coefficients, the airfoil surface solution, convergence histories, and printer plots of mach number and density contour maps.

TAIR is written in FORTRAN IV for batch execution and has been implemented on a CDC 7600 computer with a central-memory requirement of approximately 155K (octal) of 60-bit words. Typical execution times range from 5 to 20 s per case. The TAIR program was developed from 1977 to 1981.

This program was written by Terry L. Holst and F. Carroll Dougherty of **Ames Research Center;** *Karen L. Gundy, Scott D. Thomas, Juanita Frick, and Alan Fernquist of Informatics, Inc.; and John Albert of the University of Santa Clara. For further information, Circle D on the COSMIC Request Card.*
ARC-11436

General Aviation Synthesis Program

Program performs the preliminary design of fixed-wing aircraft.

The General Aviation Synthesis Program GASP performs the configuration sizing and performance estimates associated with the preliminary phase of aircraft design. Emphasis is placed on fixed-wing aircraft with propulsion systems varying from a single piston engine with a fixed-pitch propeller through twin turboprop/turbofan systems used in business or transport aircraft.

(continued on next page)

GASP modules represent the various technical disciplines of design, integrated into a computational flow that accounts for the effects of interacting design variables. GASP determines configuration size, assesses aircraft performance and economics, and is useful in performing tradeoff and sensitivity studies. By utilizing GASP, the impact of various aircraft requirements and design factors may be studied systematically, with benefits measured in terms of overall aircraft performance and economics.

Six "technology" submodules perform the various independent studies required in the design of fixed wing aircraft. The six modules include geometry, aerodynamics, propulsion, weight and balance, mission analysis, and economics.

The geometry module calculates the dimensions of the synthesized aircraft components based on such input parameters as the number of passengers, aspect ratio, taper ratio, sweep angles, and the thickness of wing and tail surfaces. The aerodynamics module calculates the various lift and drag coefficients of the synthesized aircraft based on inputs concerning configuration geometry, flight conditions, and the type of high-lift device.

The propulsion module determines the engine size and performance for the synthesized aircraft. Cruise, takeoff, and climb requirements for the aircraft may be specified. This module can currently simulate turbojet, turbofan, turboprop, and reciprocating engines.

The weight and balance module accepts as input, payload, aircraft geometry, and weight trend coefficients for use in calculating component weights. Optional inputs provide for sizing tip tanks and balancing the aircraft for a specific center of gravity range. In the mission analysis module, the taxi, takeoff, climb, cruise, descent, and landing segments of a specified mission are analyzed to compute the total range. (Aircraft can be sized to meet a required range.) In the economics module, both the flyaway and operating costs are determined from estimated manufacturing and services costs.

The six technology modules are integrated into a single system by a control module. This integrated approach ensures that the results from each module contain the effect of design interactions among all the modules. Starting from a set of simple input quantities concerning aircraft type, size, and performance, the synthesis is extended to the point where all of the important aircraft characteristics are analyzed quantitatively.

GASP is written in FORTRAN IV for batch execution and has been implemented on a CDC 7600 Computer System. The basic program memory requirements are approximately 125K (octal) of 60-bit words. The program was developed in 1978 and is updated at regular intervals.

This program was written by T. L. Galloway, E. T. Schairer, J. V. Bowles, and M. H. Waters of **Ames Research Center.** *For further information, Circle E on the COSMIC Request Card.*
ARC-11434

MiniBriefs describe NASA innovations and reports in an abbreviated format. Readers desiring additional information on these items should request the Technical Support Packages (TSP's), available in most cases, which can be obtained by using the TSP Request Card at the back of this issue.

Monitoring the Thickness of Coal-Conversion Slag

Proposed technique adapts analogous ocean-floor-mapping technology.

Existing ocean-floor acoustic technology could be adapted for real-time monitoring of the thickness and viscosity of flowing slag in coal-conversion processing. The technique, known in marine applications as chirp sonar, involves timing the transmission of a shaped acoustic signal through an acoustical conductor and the return of the reflected signal from the slag surface.

The proposed sensor is a Y-shaped ceramic rod with the common end flush with the internal surface of the slag tap and the two branches bonded to electrostrictive driver and receiver crystals. The spread of frequencies in the processed return signals is an indicator of the thickness of the material on the tap end of the rod.

The acoustic signal, a linear frequency-modulated wave packet, would be repeated at intervals. The repetition rate would be as frequent as needed for continuous monitoring.

This work was done by John V. Walsh of Caltech for **NASA's Jet Propulsion Laboratory.** *For further information, Circle 131 on the TSP Request Card.*
NPO-15371

Measuring Coating Thickness

A gage measures the coating thickness in holes.

A gage for quickly determining the coating thickness in holes on a printed-circuit board could also be used to size small holes in other applications. The gage consists of a spring-loaded tapered probe, a dial indicator, and a pressure-sensitive audible alarm. It is calibrated by insertion of the probe into rings that have the maximum-allowable and average-allowable diameters. If the actual hole diameter is less than the diameter of the "maximum-allowable" calibrating ring, the coating thickness is considered acceptable.

This work was done by Alden Schaffer and Dallis Gates of Honeywell, Inc., for **Marshall Space Flight Center.** *For further information, Circle 132 on the TSP Request Card.*
MFS-25633

Self-Righting Objects

A book-shaped object always springs open with its "pages" upward.

A technique devised for righting small spacecraft after landing could possibly be applied terrestrially in transmitters for rescue beacons.

A device that must transmit after landing must be able to orient its antenna upward, independent of its landing orientation. This would be achieved by constructing the device in

the shape of a book with a hinged cover, the transmitter and antenna being inside as the "pages." Because of the flat shape of the book, it would tend to come to rest lying on one of its covers. Then a latch would release a spring, which would open the book; the antenna would then face upward no matter which cover the device had come to rest on when it landed.

This work was done by James D. Burke of Caltech for ***NASA's Jet Propulsion Laboratory.*** *For further information, Circle 133 on the TSP Request Card.*
NPO-15023

Predicting Thermal Conductivity

An empirical equation accurately predicts thermal conductivity in insulating materials.

An empirical equation predicts the thermal conductivity of composite insulators consisting of cellular, granular, or fibrous material embedded in a matrix of solid viscoelastic material. The thermal and physical properties are varied for use in different environments by changing the volume ratio of the components.

Calculations show a one-percent difference between the predicted and the experimental values of thermal conductivity. The equation may find application in designing custom insulators for particular environments.

This work was done by B. G. Penn, F. E. Ledbetter III, and J. M. Clemons of **Marshall Space Flight Center.** *For further information, Circle 134 on the TSP Request Card.*
MFS-25732

Passive Module for Cryogenic Refrigeration

It attaches to a cryostat cold plate to reduce the temperature below 0.3 K.

A refrigeration module with no moving parts attaches to the cold plate of a cryostat to reduce its temperature. The module includes an evaporation chamber, a condenser, and an adsorption pump. The evaporation chamber and adsorption pump are each connected to the condenser by low-thermal-conductivity tubes, and the module is thermally connected to the cold plate by a copper plate and copper rod.

In each refrigeration cycle, liquid helium III refrigerant is evaporated and the helium vapor is adsorbed by zeolite beads in the adsorption pump to reduce the vapor pressure in the module. Evaporation reduces the temperature below 0.3 K. The adsorbed helium is driven from the adsorption pump by a resistance heater and is condensed to replenish the liquid helium.

This work was done by Walter Brooks of **Ames Research Center** *and Peter Kittel of the National Research Council. For further information, Circle 135 on the TSP Research Center.*
ARC-11263

Determining Aircraft Altitude

Image motion and aircraft speed determine altitude.

The altitude of an aircraft could be determined rapidly from the comparison of digital pictures of the ground taken at different times or with different exposure times. The images would be recorded by a one-dimensional focal array of light-sensitive elements in a vertically oriented camera. A microprocessor would compute the altitude from the aircraft speed, the focal length of the camera, and the recorded image motion.

This work was done by Jean J. Lorre of Caltech for **NASA's Jet Propulsion Laboratory.** *For further information, Circle 136 on the TSP Request Card.*
NPO-15386

Determining Frost Depth and Density

A simple device determines frost density from the volume of the melted frost.

A quick determination of frost depth and density can be obtained without using cumbersome tools or calculations. A rectangular window comprising the base of a Z-shaped device is placed against a frost surface. Frost within the window is scraped into the container end of the device (the top of the Z). When the frost melts, the height of the water is determined from calibrated lines on this piece. The density of the frost is determined from a graph that compares frost thickness to the amount of water.

This work was done by Farouk Hunedi of **Marshall Space Flight Center.** *For further information, Circle 137 on the TSP Request Card.*

This invention is owned by NASA, and a patent application has been filed. Inquiries concerning nonexclusive or exclusive license for its commercial development should be addressed to the Patent Counsel, Marshall Space Flight Center *[see page A5].* *Refer to MFS-25754.*

Remotely-Adjustable Pressure-Control Valve

The simple, low-cost design resists leakage and clogging.

A hydraulic valve, designed for controlling a high-pressure fluid stream with a low-pressure gas or fluid, includes a free-floating cylindrical control piston. The piston consists of a large-diameter cylinder joined to a cylinder of smaller diameter. The diameter of the larger cylinder is exactly double that of the gas pipe.

With a gas blast against the larger cylinder, it is possible to regulate a high-pressure stream of up to 4,000 psi (276×10^5 N/m2) with a low-pressure gas of 500 to 1,000 psi (34.5×10^5 to 69×10^5 N/m^2). Small adjustments of the control pressure can be made remotely. The valve body and piston are easily machined.

This work was done by Ralph B. Morrow of Caltech for **NASA's Jet Propulsion Laboratory.** *For further information, Circle 138 on the TSP Request Card.*
NPO-15693

Rain and Dew Detector

Moisture between fingerlike electrodes actuates a simple alarm circuit.

A multifinger transducer actuates a simple circuit that sets off an alarm when moisture bridges the fingers. The detector could turn on caution signals automatically in traffic areas at the onset of dew or rain and in food drying, where excess moisture could damage the product.

(continued on next page)

The transducer is composed of interleaved copper fingers spaced apart about 0.8 mm; alternate fingers are connected in parallel to form the electrodes. The interleaved electrodes are the capacitance portion of an RC oscillator. Water droplets increase this capacitance, which causes the frequency to decrease. A frequency-to-voltage converter provides an analog-signal input to a Schmidt trigger circuit, and the setpoint of the Schmidt trigger allows adjustment of the alarm level. When the moisture dries out, the frequency increases and the alarm signal goes off.

This work was done by Eric G. Laue of Caltech for **NASA's Jet Propulsion Laboratory.** *For further information, Circle 139 on the TSP Request Card.*
NPO-15370

Modified Oscillograph for Impacting Composite Materials

A commercial instrument is modified to impart energy in a realistic manner.

A commercial oscillograph that imparts impact energy to elastomeric materials can be modified to perform the same function on composites. The instrument is modified to stabilize the faces of the composite and to impact a smaller area so that the energy is imparted in a more realistic manner — for example, as a blow that emulates the impact of a ball peen hammer.

The modified oscillograph can apply loads up to 400 psi (2.8×10^6 N/m^2) to the surface of a composite material. Composites can be tested to determine the level of impact energy that causes visually undetectable damage to the material.

This work was done by B. G. Penn, F. E. Ledbetter III, Johnny M. Clemons, J. G. Daniels, and W. T. White of **Marshall Space Flight Center.** *For further information, Circle 141 on the TSP Request Card.*

Inquiries concerning rights for the commercial use of this invention should be addressed to the Patent Counsel, Marshall Space Flight Center [see page A5]. *Refer to MFS-25901.*

Machinery

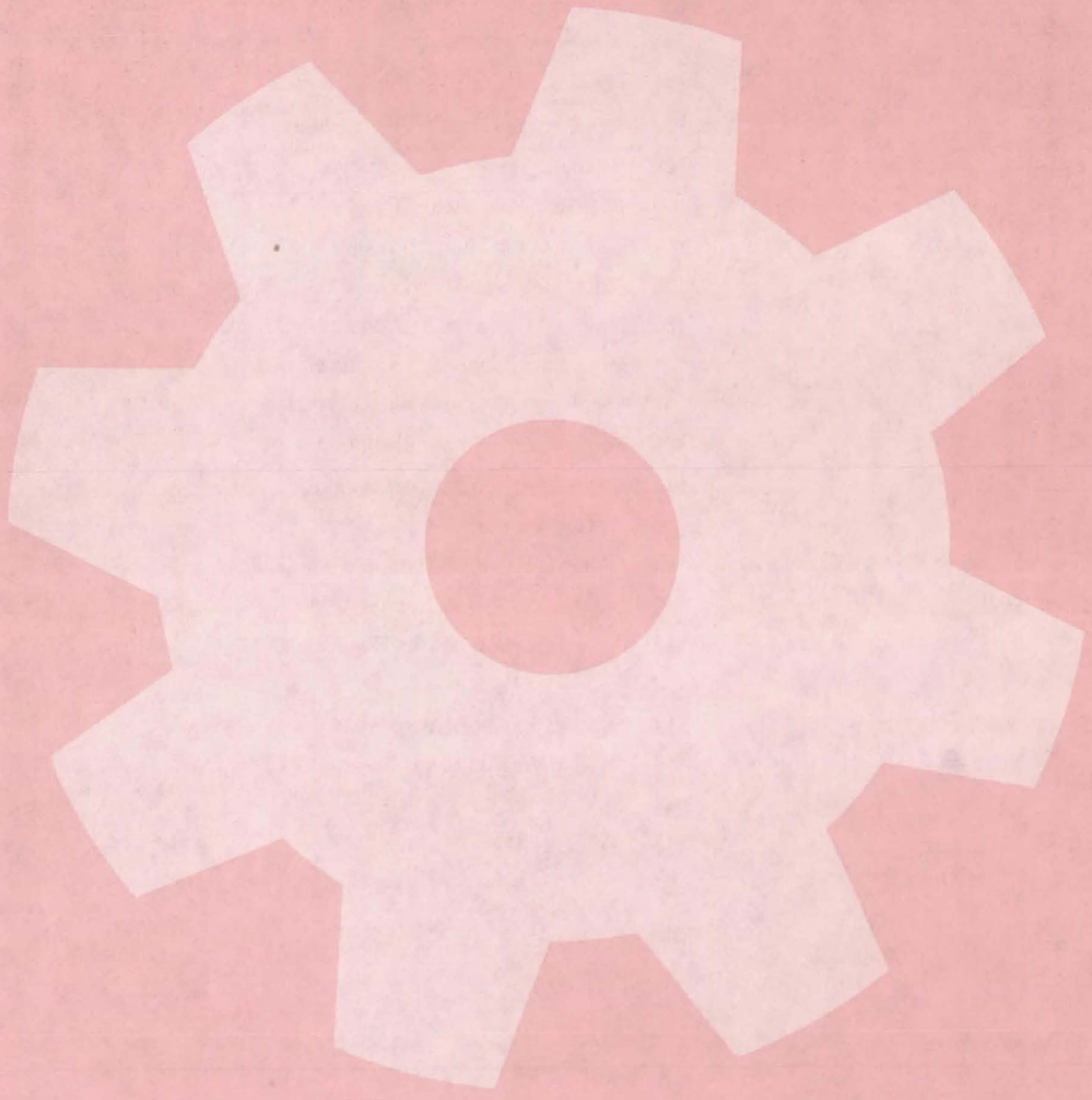

Hardware, Techniques, and Processes

Books and Reports

MiniBriefs

Latch for Stored Cargo

Spherical latch elements distribute the load over broad area.

Marshall Space Flight Center, Alabama

Heavy cargo can be secured for storage by lightweight spherical latches originally developed for spacecraft payloads. Convex hemispherical latch elements attached to the cargo mate with concave latch elements secured to the cargo-bay floor. The elements automatically aline and engage with one another when the payload is moved into the storage position. The spherical shape of the latching elements distributes the cargo weight over a broad surface so there are no "hotspots" when the cargo is secured.

Figure 1 illustrates the latch. Its original application was for securing a payload mounted on a gimbal or pivot, as shown; however, it could conceivably be adapted for other storage configurations.

The spherical latch elements are arranged on the platform and the payload so that they engage and couple when the cargo is moved into the storage position, gradually forcing alinement of the axes and coupling of the spherical latch elements.

Each of the latching assemblies is identical (see Figure 2). Each concave latch member is carried by a pivoted plate that is supported by standards welded to a supporting frame. A hole in one of the standards accepts a pin for locking the payload. A remote-controlled motor retracts and reinserts the locking pin.

When the payload is raised and undocked, the latches are automatically left in position for relatching and redocking the payload in the bay. The latch can be passive or active. If it is active, the concave latch member is driven to interlock with the convex member on the payload instead of passively alining and latching.

This work was done by Keith H. Clark of **Marshall Space Flight Center.** *For further information, Circle 142 on the TSP Request Card.*

This invention is owned by NASA, and a patent application has been filed. Inquiries concerning nonexclusive or exclusive license for its commercial development should be addressed to the Patent Counsel, Marshall Space Flight Center [see page A5]. Refer to MFS-25837.

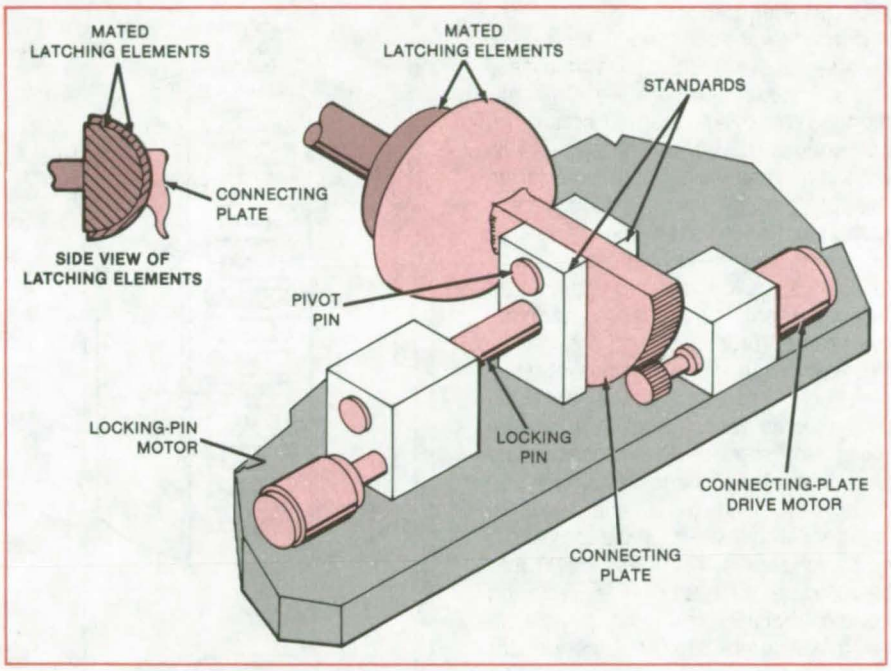

Figure 1. **Concave and Convex Latching Surfaces** couple with one another to secure the payload. A motor-driven pin locks the latch in place; and for an active latch, a second motor turns the connecting plate attached to the concave latch element.

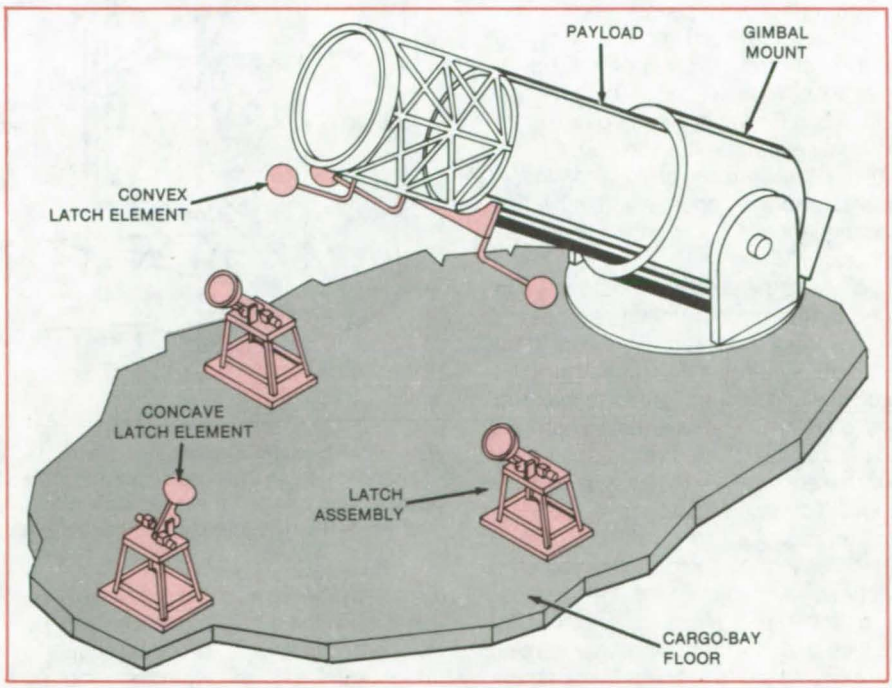

Figure 2. A **Set of Mating Spherical Latch Elements** is mounted on the payload and on the cargo-bay floor to lock the docked payload. Each concave latch element pivots on a plate that is attached to a supporting frame. After the payload is lifted from its retained position, the gimbal mount returns the payload to its stored position.

Variable-Conductance Heat-Transfer Module

Working lengths of heat pipes are electronically controlled.

Goddard Space Flight Center, Greenbelt, Maryland

Under electronic thermostatic control, a new variable-conductance heat-transfer apparatus maintains a process fluid at a steady temperature. Originally intended to provide thermal control for spaceborne material-processing systems, the system is expected to operate reliably for many years. The concept is adaptable to terrestrial instruments or processes in which atmospheres or fluids must be cooled and returned to the instruments or processes at fixed, lower temperatures.

The complete heat-transfer system includes the process module, the radiating module (see figure), and a controller (not shown). The process fluid flows from the process chamber, up through channels inside the heat exchangers, into headers at the tops of the heat exchangers, and back down into the process chamber. The radiating module includes radiator panels in which are embedded the condenser ends of several heat pipes. The evaporator ends of the heat pipes mate with the heat-exchanger panels of the process module.

The effective working length, and, therefore, the heat conductance, of each heat pipe is varied by electrically heating a reservoir at the condenser end. A gas (for example, nitrogen) in the reservoir expands when heated, thereby limiting the volume of the condenser available to the condensing fluid with a consequent reduction in the rate of heat transfer.

Power to the electrical heaters is supplied by the control unit in response to signals from temperature sensors in the headers. When the temperature of the process fluid about to return to the process chamber is above (below) the set point, the heater current is decreased (increased) to allow faster (slower) heat conduction to the radiators.

The modular construction enables rapid connection and disconnection and assures the isolation of the process fluid. The radiator can be removed for service or adjustment without disturbing the integrity of the process containment or the purity of the process fluid. If a process module must be repaired or replenished, the radiator module can be connected to another process module in the interim, thus reducing the required number and cost of radiator modules.

The volume above the process module and within the cylindrical radiator can be used for a module that could replenish and collect process fluid. This module, housing process-fluid pumps

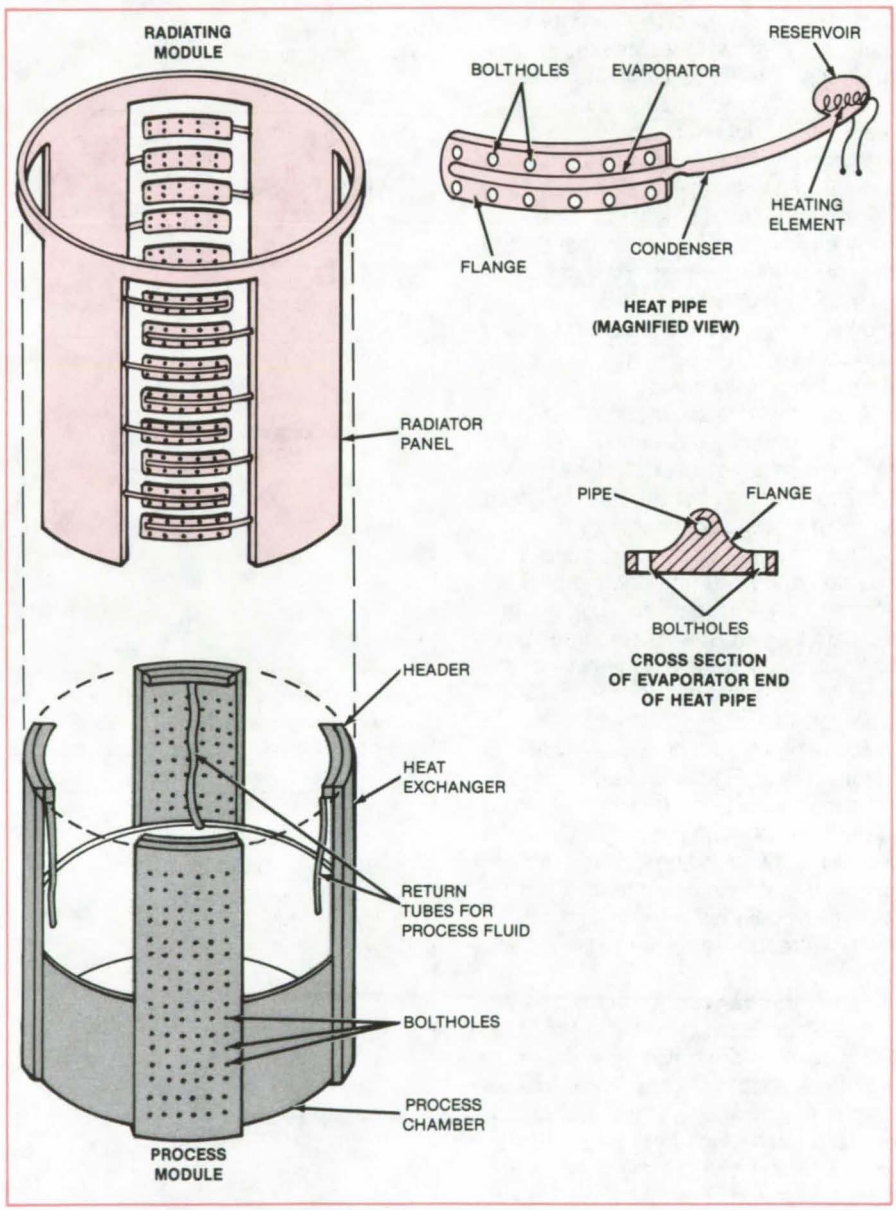

The **Heat-Transfer-System** is constructed in modular form for quick connection and disconnection and process isolation. The rate of heat transfer is controlled by electrical heaters that shorten the effective working lengths of the heat pipes. The concept is not limited to the right circular cylindrical shape illustrated here.

and fluid disconnects, could be replaced without disturbing the radiator.

This work was done by Dennis R. Hewitt of **Goddard Space Flight Center.** *For further information, Circle 143 on the TSP Request Card.*

This invention is owned by NASA, and a patent application has been filed. Inquiries concerning nonexclusive license for its commercial development should be addressed to the Patent Counsel, Goddard Space Flight Center [see page A5]. Refer to GSC-12771.

Three-Fingered Robot Hand

Mechanical joints and tendons resemble those of a human hand.

NASA's Jet Propulsion Laboratory, Pasadena, California

A robot hand under development will be able to perform rapid, small motions by humanlike finger actions — independently of its manipulator arm. It will be attachable to many different manipulators without modifications to the arms. The hand even has potential as a prosthesis for humans.

As shown in the figure, the hand employs three opposed fingers. Each has three joints and a cushioned tip on the outer segment. Each finger is controlled by four sheathed cables running to motors on the forearm. Forces and torques are measured and controlled by measuring the strain on pulley mountings.

The new hand eliminates some problems with previous designs. Its motor drives are on the forearm (rather than on the hand itself), where their weight and inertia impose no loads on the hand actuators. The drives are more easily accommodated on the forearm and have a much smaller effect on its response than they would if located on the hand.

The actuating cables, instead of running through the wrist-joint gimbals, run in sheaths alongside them. The ends of the cable sheaths are terminated at the base of the fingers, and the opposite ends are terminated at the drive housings, protecting the drive mechanisms from dirt. Because the cables do not pass through the wrist, they are not affected by the wrist geometry. This means that the arm and its controls can be treated as a "black box" in cable design and vice versa. The hand can be designed for use on many different arms and can be moved from one arm to another easily.

Finger torques and forces are sensed by strain gages on the cantilever supports of the cable sheaves. As a cable tightens, it bends a support and generates a proportional output from a strain-gage pair. The control system processes the data from all strain gages so that the individual joint torques and forces yield the requisite combined grasping and twisting forces. The drive motors use conventional output-shaft potentiometers and accelerometers to provide additional data for controlling the hand.

Like the fingers on the human hand, the robot-hand fingers can provide more than three contact areas since more than one segment per finger can contact an object. Thus, like the human hand, the robot hand can move objects about, twist them, and otherwise manipulate them by finger motion alone.

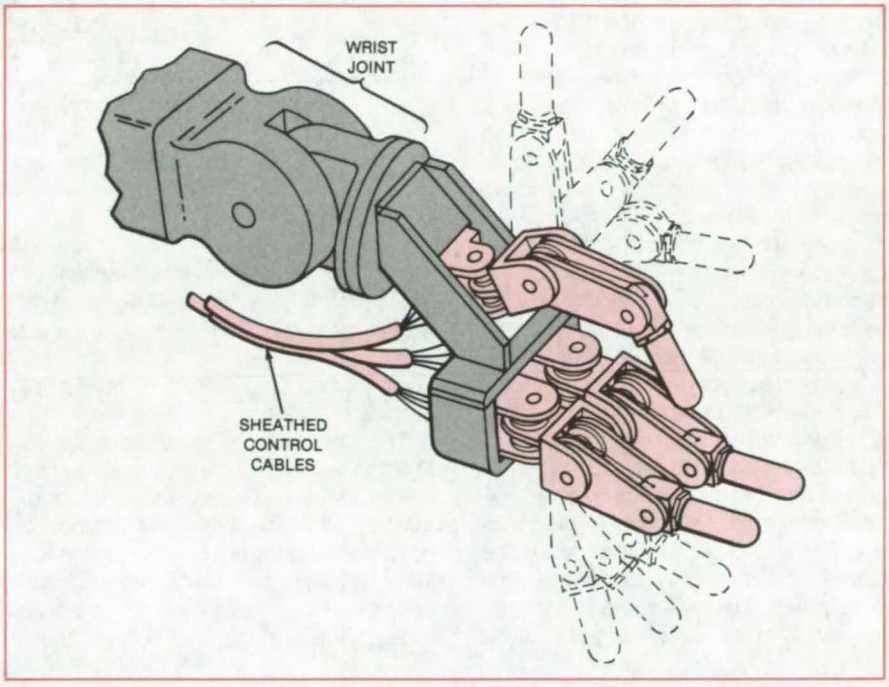

The **Robot Hand** has three "human-like" fingers. The "thumb" is at the top. The rounded tips of the fingers are covered with a resilient material that provides high friction for gripping. Although the full hand has yet to be tested, experiments with one finger have successfully tested the controls.

This work was done by Carl F. Ruoff and J. Kenneth Salisbury of Caltech for **NASA's Jet Propulsion Laboratory.** *For further information, Circle144 on the TSP Request Card.*

This invention is owned by NASA, and a patent application has been filed. Inquiries concerning nonexclusive or exclusive license for its commercial development should be addressed to the Patent Counsel, NASA Resident Office-JPL [see page A5]. Refer to NPO-15959.

Equations for Automotive-Transmission Performance

A curve-fitting procedure ensures high confidence levels.

NASA's Jet Propulsion Laboratory, Pasadena, California

A method for converting test data into equations that describe the performance of automotive transmissions can be used in the design and simulation of cars, trucks, and other vehicles. The equations are applicable to manual and automatic transmissions over a wide range of speed, torque, and efficiency.

Raw data obtained from transducers in transmission tests are used to generate equations for power loss as a function of transmission output speed and torque. The data are then subjected to a three-dimensional smoothing process to eliminate high-frequency noise. A three-dimensional least-squares curve-fitting algorithm is applied to the smoothed data. A linear, power-law, or exponential equation resulting from the least-squares fit is then compared with the calibrated and rounded power loss, output speed, and output torque; and a set of normalized errors is generated.

The mean and standard deviation are calculated for the normalized errors. Points with a normalized error probability less than the reciprocal of twice the number of data points are rejected. With these points discarded, the smoothing process and subsequent calculations are repeated until no further points are eliminated.

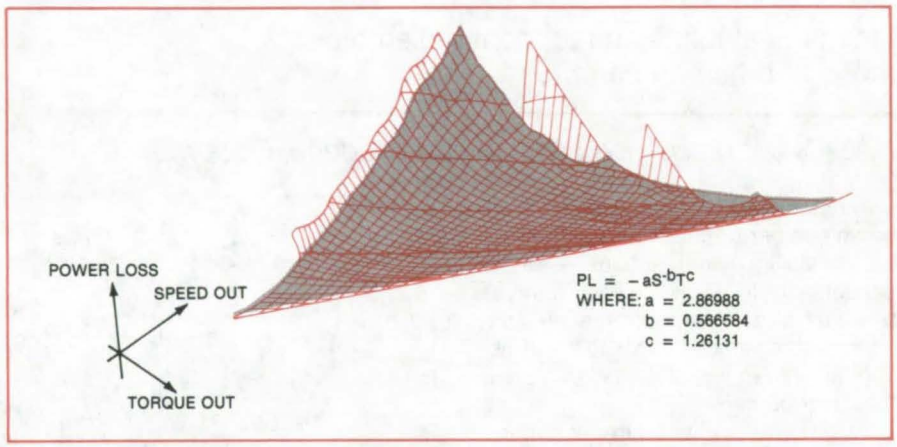

This **Three-Dimensional Plot** represents the performance of a small automatic transmission coasting in second gear. In the equation for the plot, PL is power loss, S is speed, and T is torque.

The four-speed manual transmission of a light utility vehicle was analyzed by this procedure. The synthesized equation of second gear was found to describe the data points to a confidence level of 99 percent. An automatic passenger-car transmission was also analyzed (see figure). The synthesized equation for coasting in second gear was found to describe the data to a confidence level of 85 percent.

This work was done by Seth Chazanoff, Martha B. Aston, and C. Phil Chapman of Caltech for **NASA's Jet Propulsion Laboratory.** *For further information, Circle 145 on the TSP Request Card.*
NPO-15825

Portable X-Y Scanner

Lightweight device uses just one drive motor for surface scanning.

Marshall Space Flight Center, Alabama

A portable scanner uses just one motor to drive a probe or other fixture in both the x and y directions. At NASA's Marshall Space Flight Center, it is used to move an eddy-current sensor over the surface of a metal plate; however, readers may find other applications for its unique features, which include low power consumption, light weight, and portability.

In the new scanner (see figure), a 12-volt motor drives a helical shaft. A saddle that holds the eddy-current detector engages the helix with a follower and is thereby moved along the x-scan path. As the follower reaches the end of the helix and its direction of motion is reversed, it strikes a cam gear that indexes the saddle one-sixteenth inch (1.6 mm) in the y direction.

An x scan over 8 inches (20.3 cm) occurs in 1.2 seconds. The y indexing occurs after every two scans in the x direction. Total travel in the y direction is 7.5 inches. Thus a plate 60 in.^{2} (387 cm^2) can be scanned in less than 4 minutes. The unit accommodates probes ranging in diameter from one-half to three-fourths inch (1.27 to 1.91 cm). The drive motor draws a current of 0.5 ampere at full load.

To use the scanner, the operator positions it over the plate to be inspected and installs the eddy-current probe in its normal test position, checking the distance of the probe face from the plate

surface. The operator slides the probe to the extreme y position opposite the motor. The operator then switches the unit on, and scanning begins. When scanning is complete, the operator turns the unit off and returns the probe to its starting position.

This work was done by George W. Kurtz and Ben F. Bankston of **Marshall Space Flight Center.** *For further information, Circle 146 on the TSP Request Card.*

This invention is owned by NASA, and a patent application has been filed. Inquiries concerning nonexclusive or exclusive license for its commercial development should be addressed to the Patent Counsel, Marshall Space Flight Center [see page A5]. *Refer to MFS-25687.*

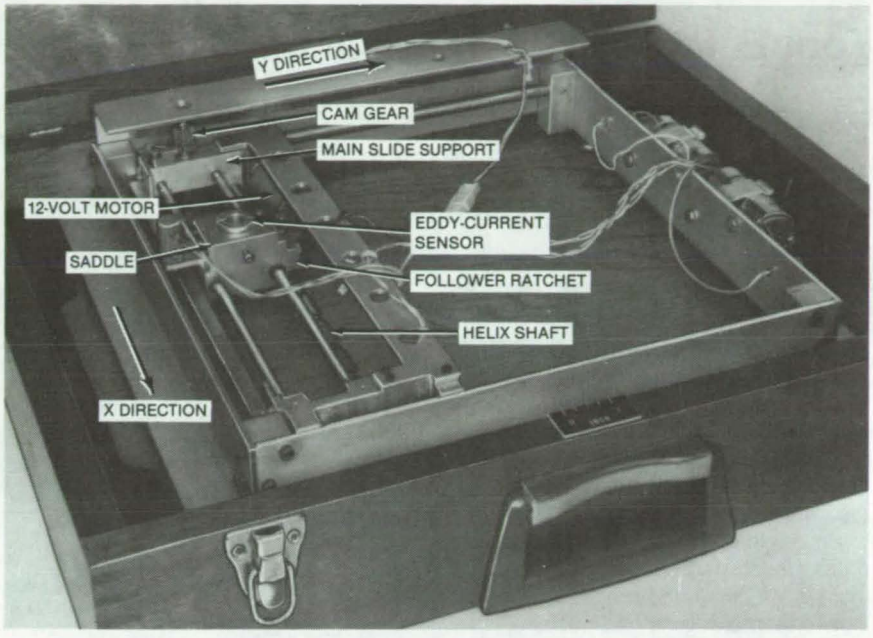

This **Electromechanical X-Y Scanner** is indexed in both x and y by a single motor. It is constructed of readily-available inexpensive parts.

Hole-Center Locating Tool

Tool alines the center of a new hole with that of an existing hole.

John F. Kennedy Space Center, Florida

A tool that resembles a C-clamp insures that the center of a newly drilled hole exactly matches the center of an existing hole. The tool requires no cumbersome measurements to insure this match. It can be used for field installations, where reference points may be unavailable or where the work area is cramped and not easily accessible with conventional tools. At Kennedy Space Center it is used to match drill holes on overhead support beams.

The tool (see the figure) consists of a three-sided frame with a rod end that can be slipped into the existing hole. A punch is located above this rod end. The material to be drilled slips between the two while bolts secure the device in place. The required hole center is marked by the punch.

The hole-center locating tool can be modified to fit into various hole sizes by machining different-diameter rod ends. The frame can be sized for the particular job at hand.

This work was done by Harry F. Senter of Boeing Services International for **Kennedy Space Center.** *No further documentation is available.*
KSC-11248

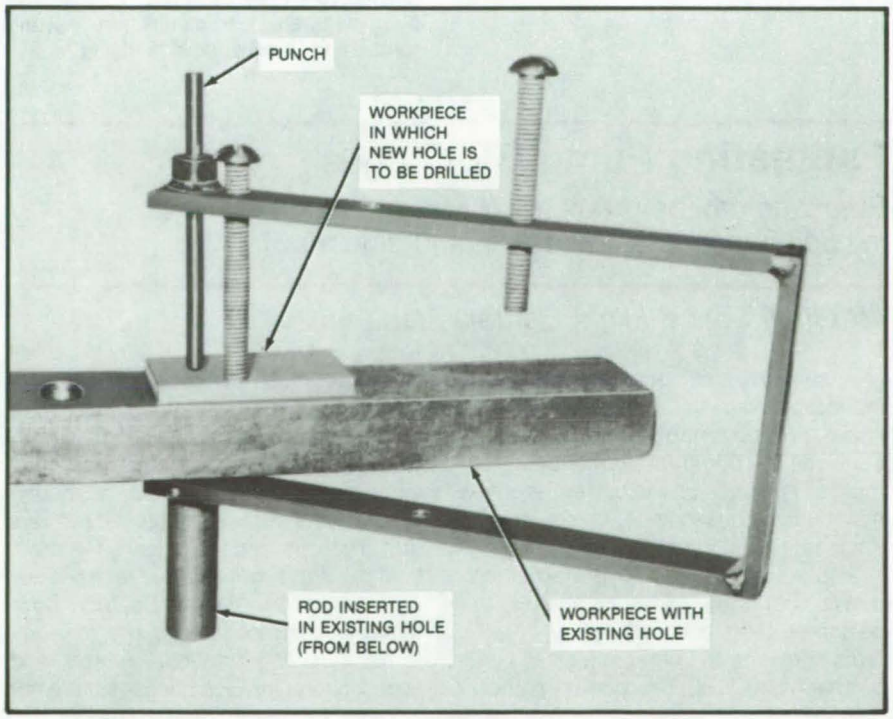

This **Tool Marks the Center** of a new hole to be drilled while the workpiece is in place. It is secured with bolts while the hole center is marked with a punch.

Tool Enlarges Hard-to-Reach Holes

Tool centers itself and cuts to a precise depth.

Marshall Space Flight Center, Alabama

A cutting tool makes it possible to enlarge valve seats or other orifices in hard-to-reach locations. The tool consists of a crosscut carbide bur; a sleeve that serves as a depth stop and pilot; a length of flexible, strong piano wire; and a standard drive socket (see figure). The parts are brazed together. The piano wire transmits torque and axial force to the cutting tool.

Before the cutting of an inaccessible orifice is started, the tool is used to machine a simulated orifice in a metal block. A mold is then made of the machined surfaces and is observed on a comparator. If the shape is correct, machining can proceed.

The user snakes the tool up the tube or other passage leading to the inaccessible orifice, attaches a small palm ratchet, and operates the ratchet several turns at a time, withdrawing the tool occasionally to relieve chip buildup. When the tool turns freely on its stop, it has cut to its full depth, and the job is complete. The user repeats these steps on the next orifice.

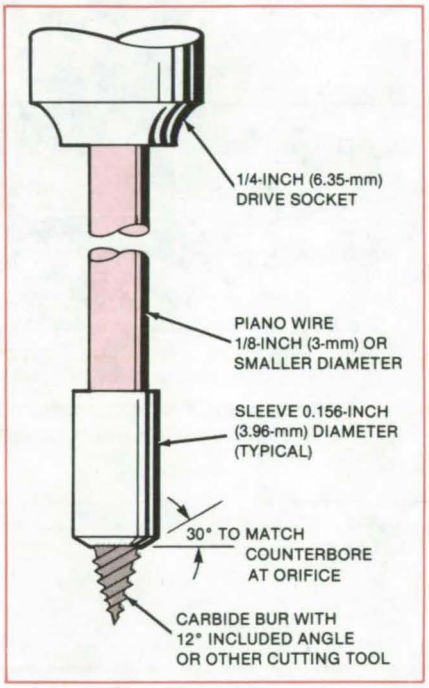

A **Flexible Shaft** allows a bur or ream to be snaked to an inaccessible location. The piano-wire shaft transmits the cutting torque and force without buckling.

Besides acting as a stop to ensure proper depth of the cut, the sleeve also serves to center the bur in the orifice counterbore. Instead of a bur, a drill or reamer can be attached to the tip of the tool.

This work was done by John P. Geddes of Rockwell International Corp. for **Marshall Space Flight Center.** *No further documentation is available.*
MFS-19789

Estimating Pump Blockage

Blockage can be predicted for all components, including inducers, impellers, and diffusers.

Marshall Space Flight Center, Alabama

A semiempirical approach for estimating blockage factors for pump passages improves the accuracy of calculations of pump performance. This method improves on the current estimation methods based solely on subjective engineering judgment.

A prediction of pump performance that is accurate enough for analysis or design requires a knowledge of the effects of blades and other objects in contact with the flow. The portion of flow blockage due to rotor and stator blades can be estimated from the blade thickness distribution. Unfortunately, a knowledge of blade geometry alone is inadequate when boundary-layer effects are present (as they always are). Theoretical calculation is not practical because boundary-layer theories are restricted to flat-plate or pipe flow. Moreover, complicated pump-flow patterns, including rotational effects and flow diffusing through passages, are not taken into account in current theoretical approaches.

The semiempirical approach involves an extrapolation of experimental data. It is based on tests of nonrotational, straight diffusers at a Reynolds number of 1.5×10^5. A plot of blockage versus diffusion factor is obtained from the test data and modified so that it can be applied to curved, rotational diffusers. The plot can also be corrected for flows with other Reynolds numbers by applying an

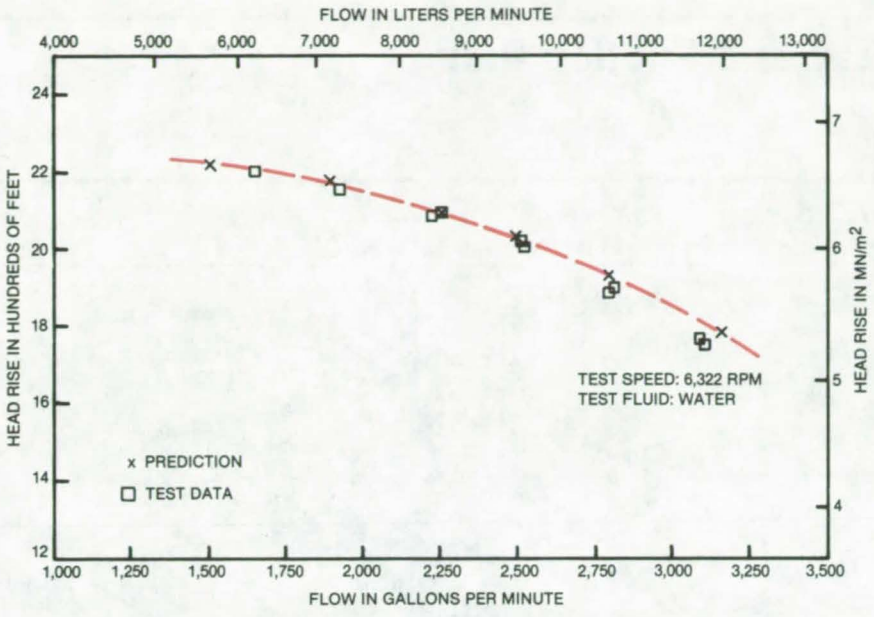

Pump Performance predicted by this semiempirical method shows excellent agreement with test results in the Space Shuttle main-engine high-pressure fuel turbopump. Comparisons of pump efficiency show equally good agreement of calculated values with experimental ones.

approximate scaling law for the dependence of the boundary-layer thickness on the Reynolds number.

A blockage distribution obtained by the semiempirical method was used in a centrifugal-pump-loss program for several Space Shuttle main-engine pumps. Suitable blockage values were obtained through iterative procedures; and the results indicate excellent agreement with test data (see figure) over a wide range of flow rates, with the exception of separated flows.

This work was done by Wei Chung Chen and Sen Yih Meng of Rockwell International Corp. for **Marshall Space Flight Center.** *For further information, Circle 147 on the TSP Request Card.*
MFS-19763

Wire Retrieves Broken Pin

A safety wire retains the pieces of a broken tool.

Marshall Space Flight Center, Alabama

A solid pin that could not be redesigned to prevent breakage was instead redesigned to permit easy retrieval of the broken pieces. In the new version, the pin retains the same outside dimensions, but the inside is hollow (see figure) so that a safety wire can be strung through it. A metal bead is brazed or welded onto the end of the wire at the tip of the pin. Should the pin break, the pieces are removed from the hole by pulling on the wire.

Applying this idea to a solid pin used in a NASA liquid-oxygen system lowered costs by avoiding the delays previously associated with fishing out the pieces of the broken tool. The safety-wire concept is suitable for other pins that are subject to deflection or breakage.

This work was done by Glenn H. Burow of Rockwell International Corp. for **Marshall Space Flight Center.** *No further documentation is available.*
MFS-19768

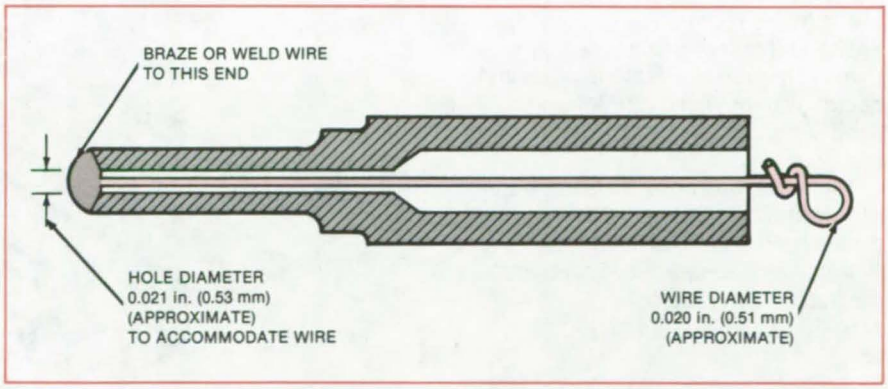

A **Retrieval Wire** running through the shaft of a tool can be used to pull pieces of the tool out of a hole, should the tool break during use. The wire and hole sizes shown here are only typical.

Control-Chain Safety Tray and Friction Pull

A sprinkler-system control chain is stored above a suspended ceiling.

Lyndon B. Johnson Space Center, Houston, Texas

A tray mounted above a suspended ceiling keeps a sprinkler-system control chain safely out of the way of pedestrian traffic below (see figure); yet when needed, the loop of chain that hangs through the slot in the tray may be reached easily by using a fireman's hook, a short stepladder, or a chair, or even simply by jumping up to grasp the chain. The slot in the tray is made of two strips of neoprene that are stiff enough to keep the chain from falling freely but flexible enough to permit the chain to be pulled through when needed.

The safety tray was originally designed to solve a problem in a computer room. The chain operates a sprinkler-system cutoff valve located several feet above a suspended ceiling. To minimize equipment damage, the valve should be closed as soon as possible after the fire is extinguished. That precludes taking the time to climb up to close the valve directly; but if the chain used to operate the valve from floor level were simply to be left hanging, it would be a hazard to pedestrian traffic in the room.

The safety tray provides a tidy solution to the problem. Such a safety tray could also be used for infrequently-used control chains on vents and dampers.

This work was done by Gene Hajdik of **Johnson Space Center** *and Charles R. Peek of Pan American World Airways, Inc. No further documentation is available.*
MSC-20401

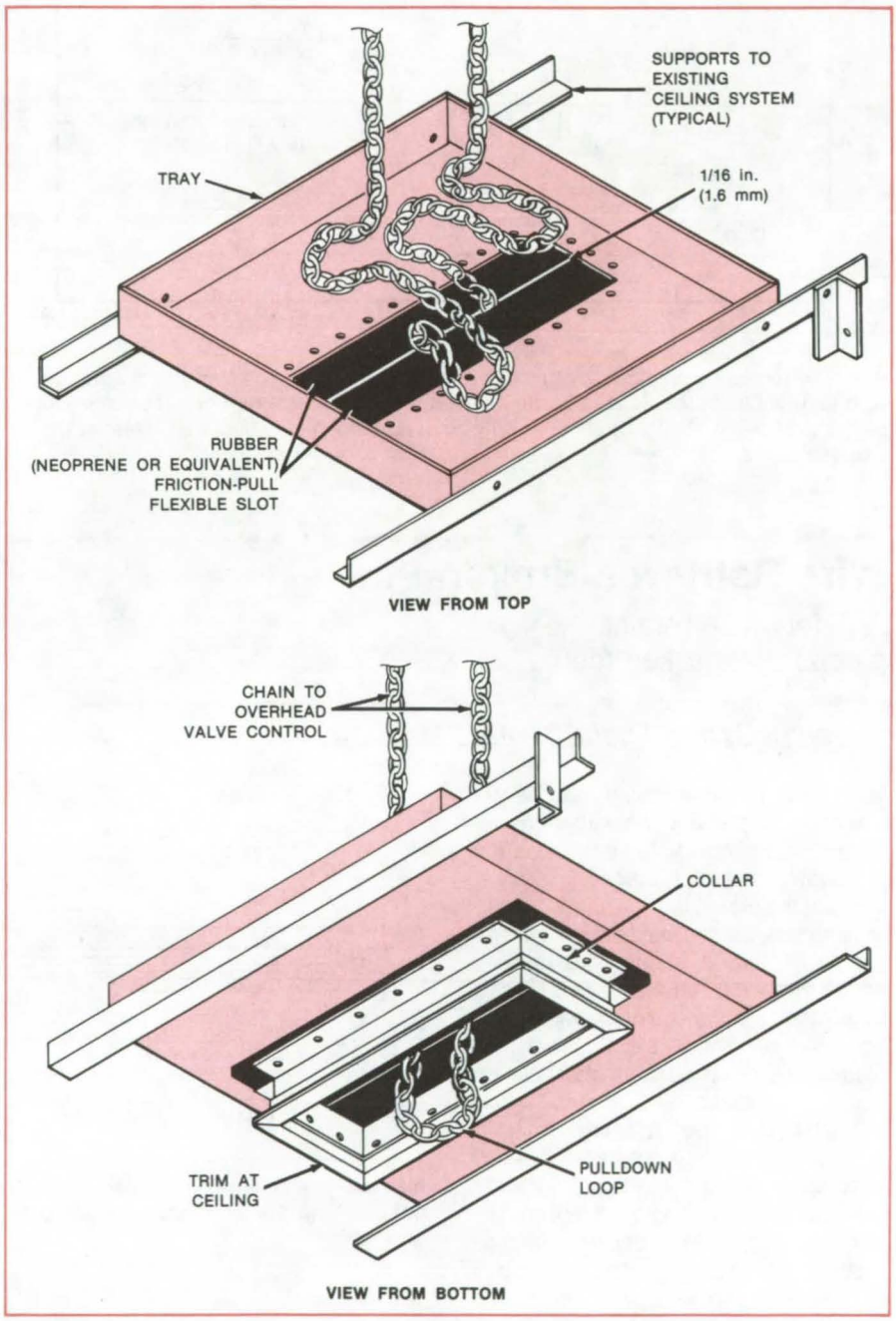

The **Control-Chain Safety Tray** stores a portion of a control chain out of the way above a suspended ceiling. A loop of the chain is left hanging below the slot so that the chain can be pulled down from below the ceiling.

Automated Coal-Mine Shuttle Car

A cable-guided car would increase efficiency in underground coal mines.

NASA's Jet Propulsion Laboratory, Pasadena, California

An automated coal-carrying car would be guided by a cable stapled to the mine floor. Under the control of a computer, the car would run between the working face of a coal mine and a conveyor where it would be unloaded.

The proposed unmanned vehicle shown in the figure would contain storage batteries in its side panels for driving traction motors located in the wheels. The batteries can be recharged during inactive periods or might be slid out as a unit and replaced by a fresh battery bank. An onboard generator could charge the batteries as the car operates.

The guide-wire system could employ the phase-sensitive characteristics of the guidance system described in "Phase-Sensing Guidance for Wire-Following Vehicles" (NPO-15341) on page 139 of *NASA Tech Briefs*, Vol. 7, No. 2. The optical collision-avoidance system, described in "Focal-Plane-Array Optical Proximity Sensors" (NPO-15155) on page 259 of *NASA Tech Briefs*, Vol. 7, No. 3, could be used for collision avoidance.

A typical car would have six wheels, with four wheels used for steering. Because of limitations on tire load-carrying capacity and on floor loading in mines with soft clay or mud floors, car capacity would be 3½ tons (3,200 kg) maximum as compared to that of 5 to 10 tons (4,500 to 9,000 kg) and higher for standard track-mounted cars. However, the automated cars would have a shorter turnaround time.

The flexible guide wires would be easily and quickly laid out and changed. Cars could be moved on and off a branch by signal codes, using different carrier frequencies for each path or car, or by signal multiplexing. The central computer would keep track of the location and heading of each car.

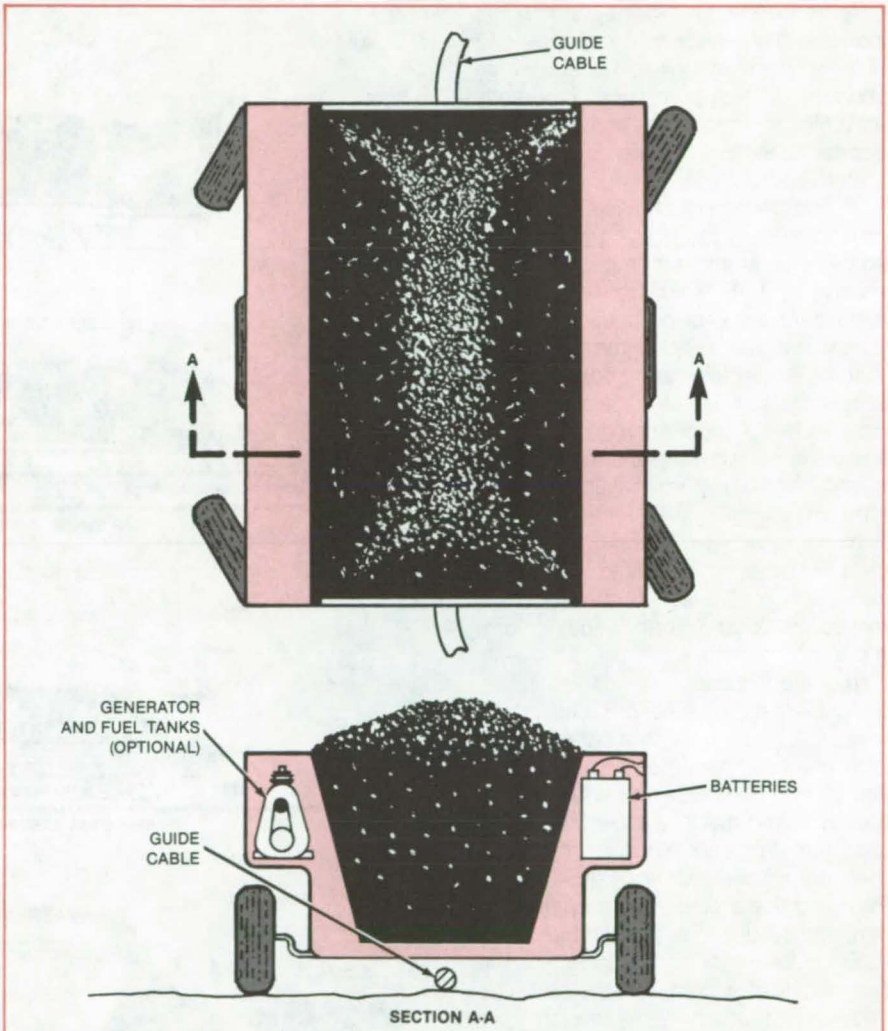

The **Cable-Guided Shuttle Car** would contain a bank of storage batteries in its side panels for driving traction motors that would be best located in the wheels.

At the output conveyor, the cars can be dumped automatically, using technology now in wide use for dumping train cars. Dumping may be by trapdoors in the floors or by tilting and opening end doors.

This work was done by Earl R. Collins, Jr., of Caltech for **NASA's Jet Propulsion Laboratory.** *For further information, Circle 148 on the TSP Request Card.*

NPO-15850

Shuttle-Car System for Continuous Mining

Buffer storage catches the coal production between loadings.

NASA's Jet Propulsion Laboratory, Pasadena, California

A proposed shuttle-car system would increase the rate of coal transport and allow a mining machine to operate continuously. The system is not inherently restricted to coal mining and may prove economical for hauling other solid materials.

In a conventional shuttle-car system, production has to be stopped while an empty car is moved into position to receive coal. To minimize stopping time, extra cars are kept on hand so that an empty one is ready to move into the loading position as soon as the preceding car is full. These features contribute to higher production cost since the shuttle cars and their drivers spend much of the time waiting between load cycles.

In the new system, coal from a conveyor is fed continuously to a telescoping reservoir. The end of the conveyor moves back and forth under microprocessor control to insure an evenly distributed full load.

As the reservoir is filled, the tailgate of a car is let down, and the car is moved into place under the reservoir (see figure). When the reservoir is full, its endgate is pulled away to allow the coal to slide into the car. Hydraulic cylinders then retract the reservoir sections out from under the coal, thus dropping the coal a short distance into the car.

Once the reservoir is unloaded, the car tailgate is closed, and the reservoir endgate is reattached. As the car pulls away, the reservoir is reextended to full length, all the while catching the uninterrupted flow of coal from the conveyor.

This work was done by Earl R. Collins, Jr., of Caltech for **NASA's Jet Propulsion Laboratory.** *For further information, Circle 149 on the TSP Request Card.*

This invention is owned by NASA, and a patent application has been filed. Inquiries concerning nonexclusive or exclusive license for its commercial development should be addressed to the Patent Counsel, NASA Resident Office-JPL [see page A5]. Refer to NPO-15949.

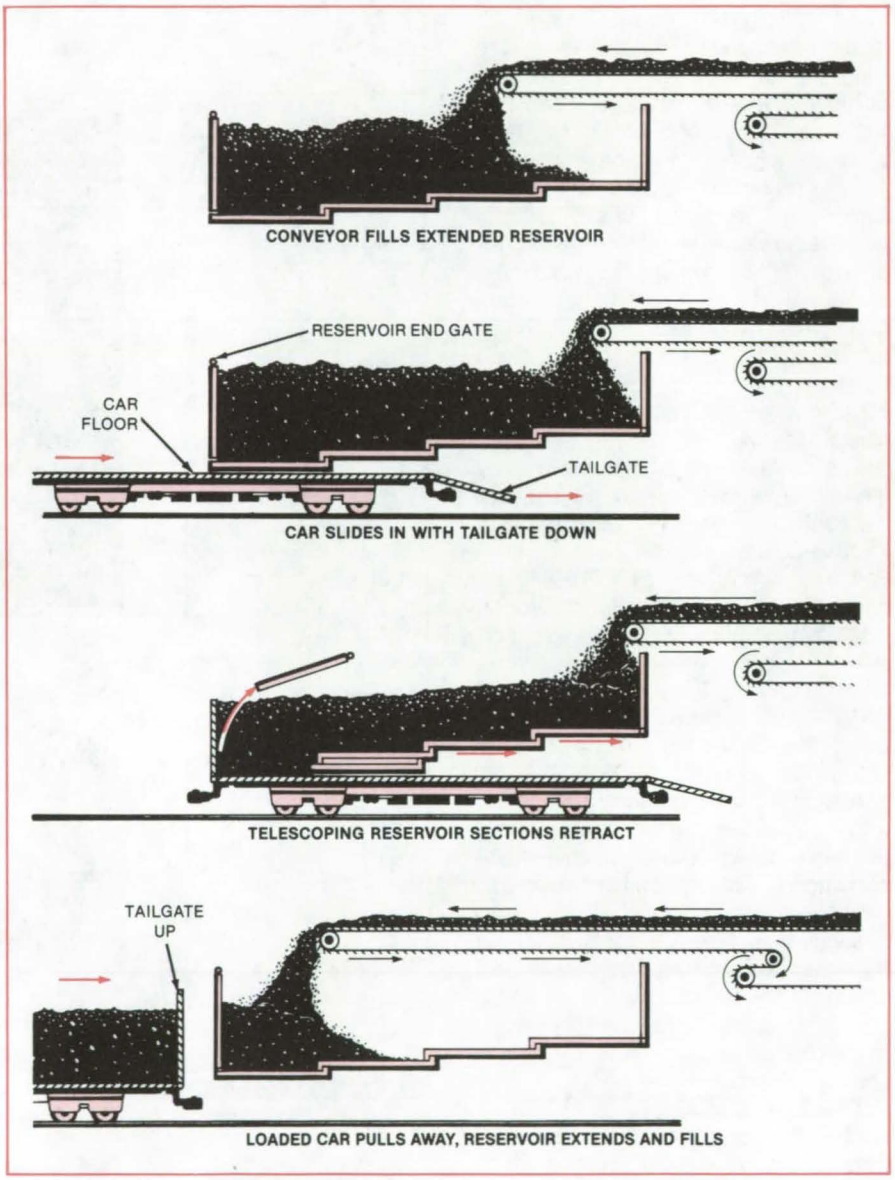

The **Telescoping Reservoir** is filled continuously. With its tailgate down, the shuttle car slides into place along the sides and bottom of the reservoir. The reservoir retracts along the inside of the car and out through the tailgate, leaving the coal behind in the car.

Mechanical Coal-Face Fracturer

Radial points on a proposed drill bit would take advantage of the natural fracture planes of the coal.

NASA's Jet Propulsion Laboratory, Pasadena, California

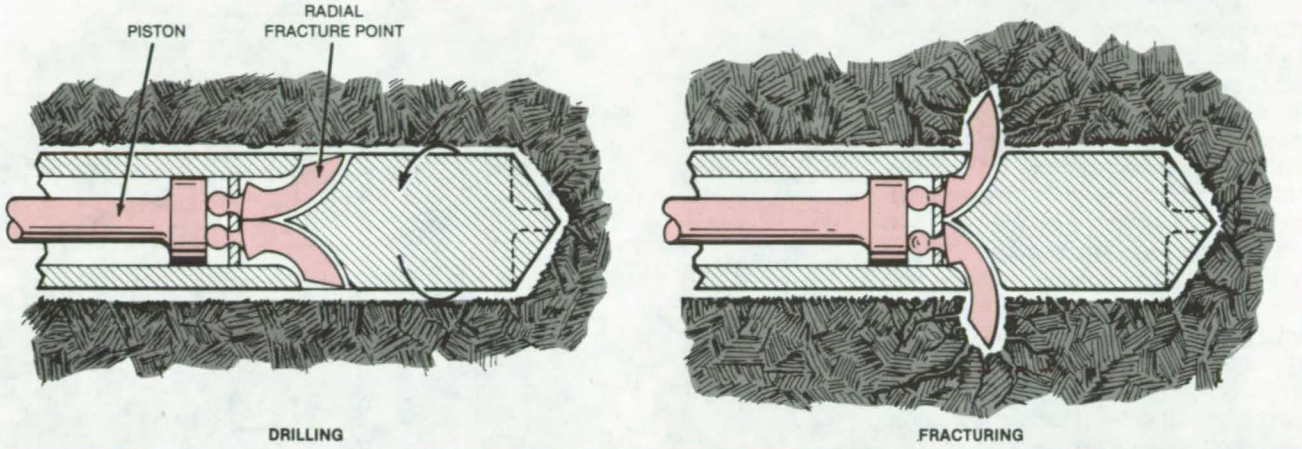

The **Radial Fracture Points** are retracted during drilling and impacted by the piston to fracture the coal once drilling halts. A group of bits is attached to an array of pneumatic drivers to fracture a large area of coal face.

A modified drill bit proposed for mining coal would include a group of impact-driven points to fracture and breakup a coal face. The modified bit would take advantage of available drill machines that sink as many as 12 holes into the working face at one time. Conventionally, the coal is broken up by mechanically sawing it or by loading the holes with blasting powder. The points, however, would shatter the coal face by impacting the natural fracture planes of the coal.

A bit with radial fracture points is shown in the figure. Depending on the fracture-point size and the fracture characteristics of the coal, there may be as many as eight fracture points to a bit. A piston within the hollow drill shank retains the ball ends of the fracture points.

During drilling, the inner piston is retracted so that the fracture points do not project out of the drill tube. However, when the proper hole depth is reached, drilling is stopped; and the end of the rod attached to the piston is impacted, driving the fracture points radially outward into the coal face. This fractures the coal, and the pieces fall away from the face.

Depending on drill spacing, fracture-point volume, and coal characteristics, fracturing may occur after one heavy impact or after several impacts. For deeper drilling, a second set of fracture points could be deployed farther back along the drill shaft. After coal fracture, the rod is retracted, and the drill and assembly are ready for drilling into the face again.

This work was done by Earl R. Collins, Jr., of Caltech for **NASA's Jet Propulsion Laboratory.** *For further information, Circle 150 on the TSP Request Card.*

NPO-15847

Shock Mounting for Heavy Machines

Elastomeric bearings eliminate extraneous forces.

Marshall Space Flight Center, Alabama

A shock mounting originally developed for rocket engines under test might be used as a support for heavy machines, bridges, or towers. The new mounting replaces older supports used for Space Shuttle engine tests, which were carved out of 5,000-lb (2,300-kg) blocks of high-alloy steel. The old design was more expensive, and sometimes failed during engine proof testing.

In a static test fixture for measuring the thrust of a rocket motor, the motor is supported by two flexure elements — one forward and one aft. The forward support isolates the thrust from extraneous forces and impresses the thrust on load cells, which measure its magnitude.

(continued on next page)

An adapter transmits the thrust of the rocket to the load cells through the new support (see figure). The main body of the support is a rectangular steel block having two trunnions extending from its side faces. A boss, centrally located on an end face of the main block, fits into the adapter.

A cylindrical elastomeric bearing is installed on each trunnion. Each bearing comprises concentric, rigid, hollow cylinders of successively larger diameter, separated from each other by layers of elastomer to which they are bonded. The outer elastomer layer of each bearing is bonded inside a circular hole in an outer casing — a square steel block. Each casing is supported by a flat elastomeric bearing composed of steel shims stacked alternately with layers of elastomer to which the shims are bonded. The vertical side of each casing opposite the rocket motor bears against a pair of load cells.

The cylindrical elastomeric bearings are compliant with extraneous forces in a vertical plane, and the flat elastomeric bearing is compliant with those in a horizontal plane. Thus, such forces will not interfere with measurements of axial and side thrusts.

This work was done by Arnold R. Thompson of Thiokol Corp. for **Marshall Space Flight Center.** *No further documentation is available.*
MFS-25888

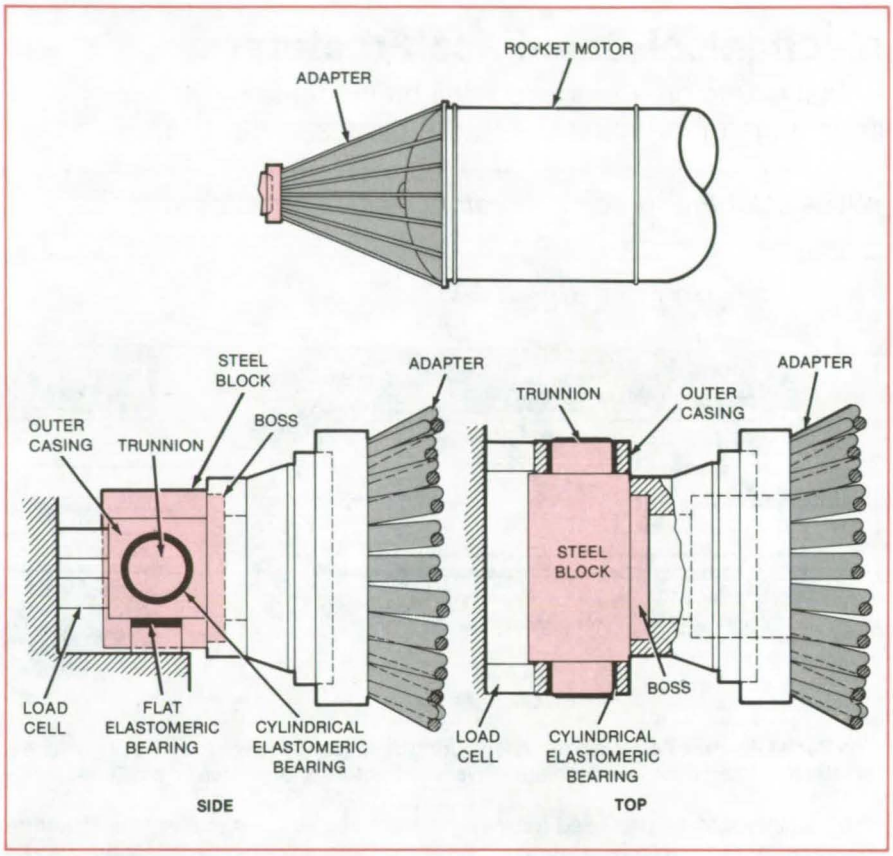

Rocket Thrust Is Transmitted from the motor to the load cells via a support that absorbs extraneous forces so that they do not affect the accuracy of thrust measurements. The adapter is a spoked cone that fits over the forward end of the rocket motor.

Reciprocating Linear Electric Motor

Features include structural simplicity and good force/displacement characteristics.

Goddard Space Flight Center, Greenbelt, Maryland

A new approach to the design of reciprocating electric motors promises to improve performance while eliminating some of the deficiencies of earlier versions. The new motors are constructed in a simple, rugged cylindrical configuration. Originally intended to provide drivers for long-lived Stirling-cycle cryogenic refrigerators, the concept may also have less exotic applications, such as fuel pumps.

As shown in the figure, a nonmagnetic yoke attached to a shaft holds two ring-shaped permanent magnets that are radially polarized in opposite directions. The assembly of magnets, yoke, and shaft is free to move axially. The shaft slides in a housing while the yoke and magnets move in a cylindrical gap between inner and outer cylindrical ferromagnetic cores.

Four electromagnet coils are attached to the ferromagnetic cores, with one coil just inside and one just outside each permanent magnet. The coils are electrically connected in series. The current in both coils associated with one magnet is in the same azimuthal direction, while the current in both coils associated with the other magnet is in the azimuthal direction opposite that of the first magnet.

Since the coils are placed in both the inner-diameter and outer-diameter air-gaps of the magnet rings, the radial-force instability caused by the magnetic attraction between magnets and cores is substantially reduced. Long-life conventional bearings or reduced-size magnetic bearings are then feasible to employ.

The azimuthal current interacts with the radial permanent-magnet field to produce an axial force. In the case of the figure, the shaft is pushed to the right. The coils are longer than the magnets.

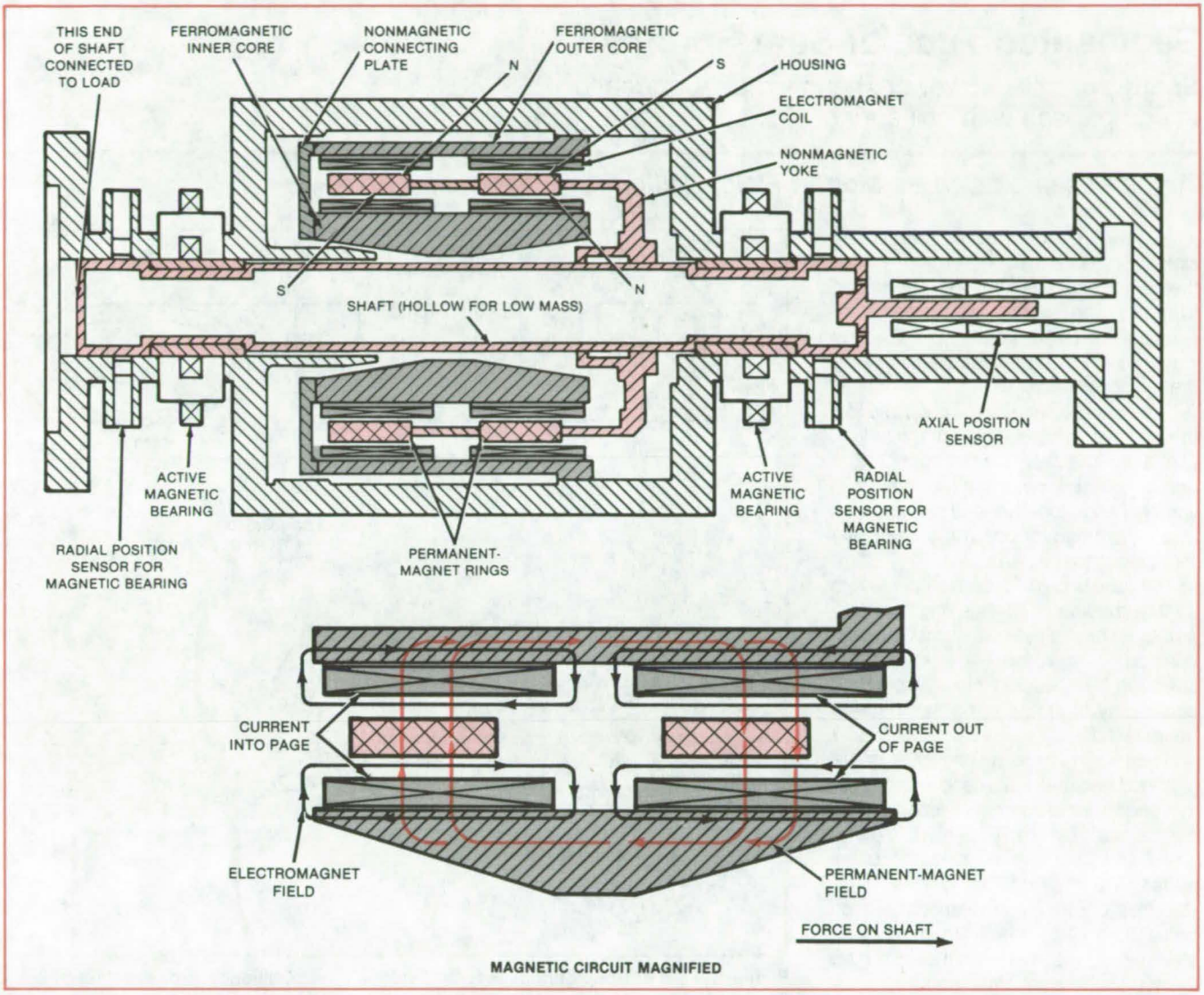

The **Reciprocating Motor** has simple, rugged construction, relatively low reciprocating weight, improved power delivery, and improved force control. In addition, wear can be reduced by the use of magnetic bearings.

Provided that the magnets remain within the axial region defined by the coils, the permanent-magnet field will intersect the same number of coil turns, and the force will remain nearly proportional to the electric current only, varying minimally with axial position. The total available nearly-constant-force stroke length is roughly the difference in length between the coils and magnets.

Another advantage of using four coils and two magnet rings over previous motor designs is the exceptional linearity with current. The motor force is directly proportional to current even for high currents. As one magnet ring loads magnetically, the other unloads, thereby keeping the average flux density in the coils constant. This is a decided advantage in closed-loop servosystems.

The placement of the coils in the stationary portion eliminates the need for flexible wires to the armature. The breakage of these wires was a persistent source of failure in earlier reciprocating motors of the loudspeaker-voice-coil type. The cylindrical core shape prevents variations in the permanent-magnet flux path that would otherwise cause axial bias forces, thereby interfering with the armature displacement. The low armature mass decreases the overall reciprocating mass, thus permitting the delivery of more power than is available from comparable heavier units.

To reduce wear and assure long life, the shaft can be supported by active magnetic bearings instead of sliding on conventional dry lubricated bearings. A linear variable-differential transformer may be placed at the unloaded shaft end to sense the axial position. The position information may be used to control the motor; for example, to enforce the sinusoidal reciprocating motion required for ideal Stirling-cooler operation.

This work was done by Michael P. Goldowsky of U.S. Philips Corp. for **Goddard Space Flight Center.** *For further information, Circle 151 on the TSP Request Card.*

This invention is owned by NASA, and a patent application has been filed. Inquiries concerning nonexclusive or exclusive license for its commercial development should be addressed to the Patent Counsel, Goddard Space Flight Center [see page A5]. Refer to GSC-12773.

Segmented Tubular Seat Springs

Springs promise lower cost and simpler fabrication in comparison with coil springs.

Ames Research Center, Moffett Field, California

A new type of tubular spring may simplify the construction of and reduce the cost of seat cushions in vehicles and furniture. The springs are formed from elliptical tubes by cutting most of the way through on planes perpendicular to the cylindrical axis.

The hoops formed by the cuts (see Figure 1) give independent spring action, somewhat like separate coil springs. The part of the tube not cut through holds a line of springs together and serves as an attachment pad for bonding or fastening the springs to the pan.

The tube is cut to a convenient length so that the line of springs might, for example, extend all the way across a seat cushion. This simplifies cushion construction by reducing the number and complexity of spring parts that have to be installed.

Several variations are possible in the methods and materials used to fabricate the spring tubes. For example, a tube can be made by simply rolling up a metal sheet and leaving the inner and outer edges loose (that is, not welded, soldered, or otherwise seamed). Springs could also be made from thin-walled steel tubing that is first annealed, then formed to the elliptical shape, then cut, and finally retempered to restore springiness. Tubes could also be formed from composite materials by wrapping the impregnated reinforcing fabric ("prepreg") around a mandrel of the desired elliptical cross section, then subjecting the material to the usual curing cycle. Cushioning made of selected composite materials may serve as suitable replacements for polyurethane foams in seat and mattress applications where potential flammability and the formation of toxic fumes are of concern.

Inside a line of main springs, a line of smaller bottoming springs could be installed by bonding a smaller tube inside the main tube before or after cutting. Figure 2 shows a seat cushion in cross section with main and bottoming springs.

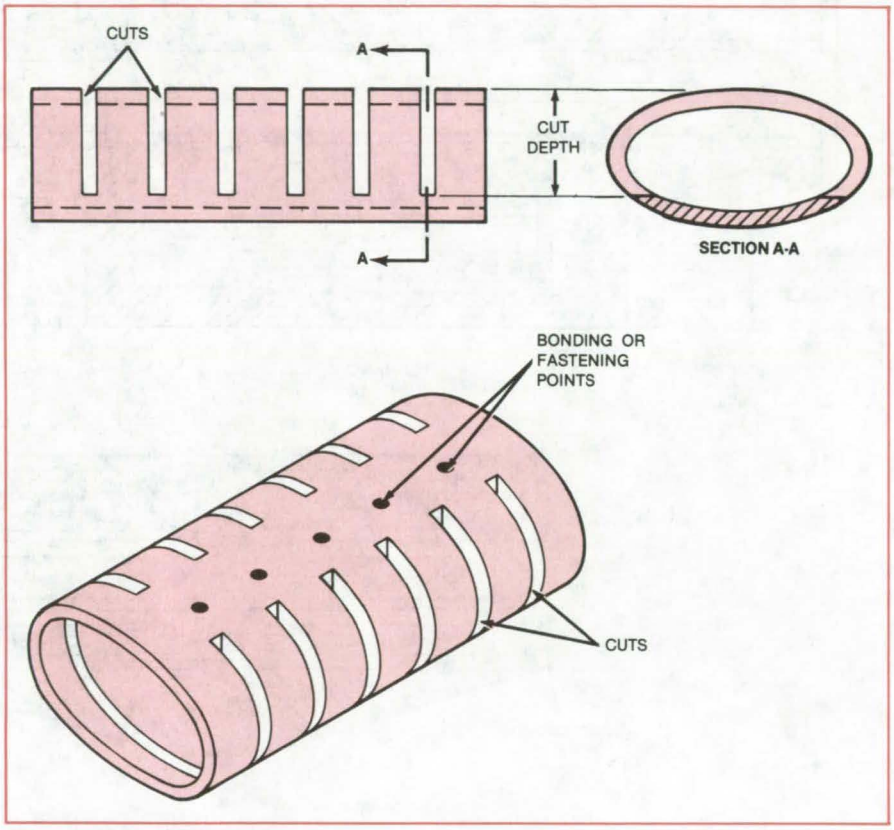

Figure 1. **A Set of Hoop Springs** is formed from a tube of elliiptical cross section by cutting most of the way through the tube at numerous planes perpendicular to the axis. The tube can be made by a variety of methods and in a variety of materials, the choice depending on considerations of cost, weight, fire retardancy, and mechanical properties.

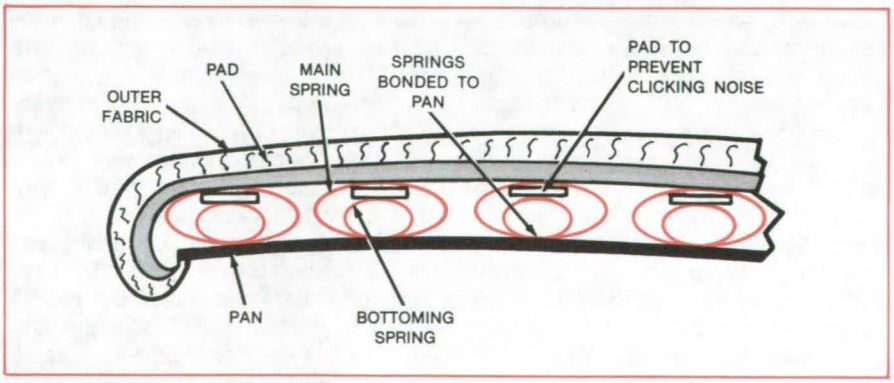

Figure 2. **A Low-Cost Seat Cushion** is made with rows of hoop springs. This view is a cross section along the spring axes.

The new segmented tubular springs would probably be more limited than coil springs in such characteristics as spring travel, spring rate, and preload capability. Nevertheless, the low cost and ease of fabrication may be overriding considerations. There is still a great deal of design flexibility: The major- and minor-axis dimensions, tube-wall thickness, cut width, cut spacing, cut depth, tube material, and fabrication methods are all design parameters that can be varied to meet the technical, safety, and cost requirements of a particular application.

This work was done by Leonard A. Haslim of **Ames Research Center.** *For further information, Circle 152 on the TSP Request Card.*
ARC-11349

Air Guide for Sheet-Metal Grinder

Tool attachment reduces heat distortion of the sheet.

Marshall Space Flight Center, Alabama

A small trough attached to a hand-held grinder directs cooling air to the grinding wheel and workpiece. The cooling air reduces thermal distortion of the workpiece due to localized frictional heating. It is particularly useful when grinding sheet metal.

When a high-speed hand-held grinder is used to smooth the surface of a thin sheet of metal [0.025 inch (0.6 mm) or less], considerable distortion of the sheet can occur. The material can bubble or warp, and the grinder then removes material unevenly; yet sheet flatness may be essential.

The attachment alters the direction of airflow from a port on the motor housing. The flow created by the fanlike action of the rotating motor cools the sheet metal. It thus reduces or eliminates the need to slow down grinding or to temporarily stop grinding to allow the sheet to cool.

This work was done by Todd Heermann of Rockwell International Corp. for **Marshall Space Flight Center.** *No further documentation is available.*
MFS-19788

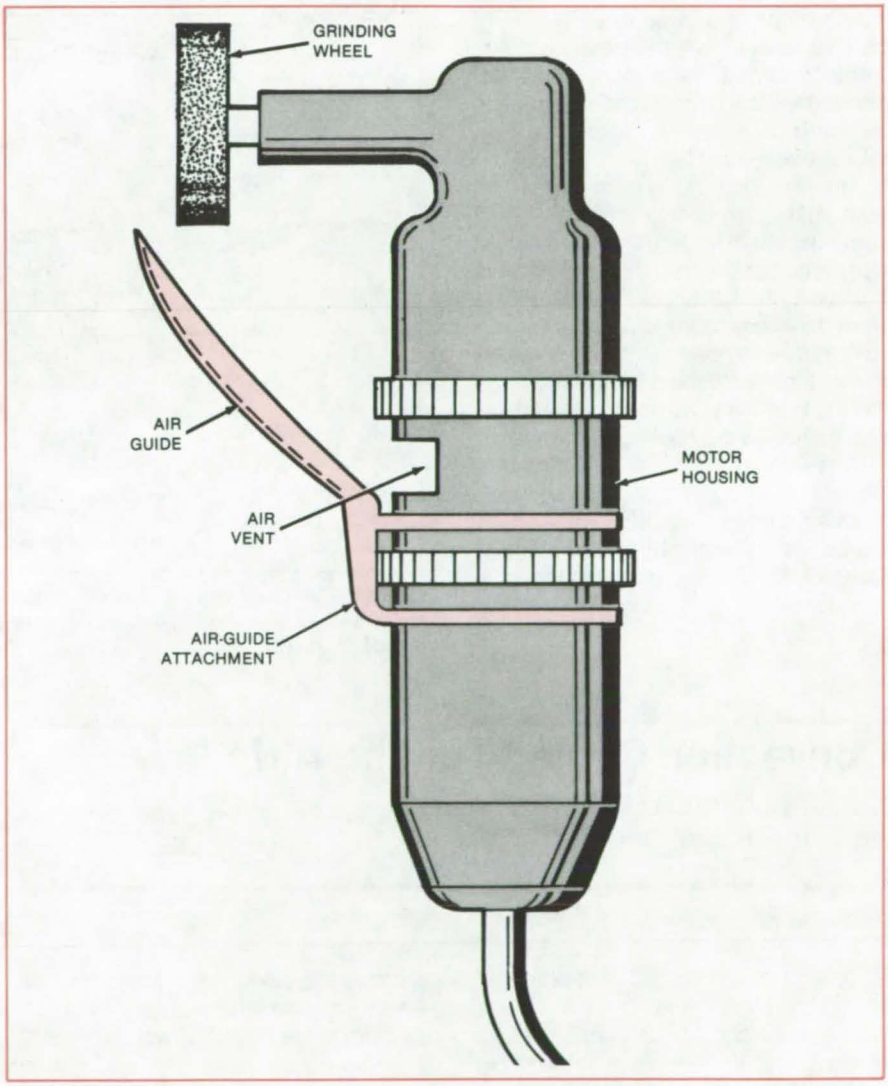

An **Air-Guide Attachment** directs air from a grinder motor to the grinding wheel and the metal sheet being ground.

Metering Baffle for Turbine-Blade Cooling

Mixing losses due to excessive film cooling are reduced.

Marshall Space Flight Center, Alabama

A scheme for cooling turbine airfoils involves a series of rows of small holes through which a gas or liquid is injected at the airfoil surface. The resulting surface-film flow keeps the airfoil cool enough to operate in high-heat, high-pressure turbines.

The interior of the airfoil is hollow (see figure) and serves as a passage for the cooling fluid. The flow to each row of holes is governed by a metering baffle inside the airfoil. The amount of obstruction to the flow in each baffle section is set by drilling several holes of a particular diameter.

The metering baffle is needed to insure against excessive film cooling and the consequent mixing losses that would degrade turbine efficiency. This is because the smallest holes running from the inside to the outside of the airfoil that can be made by present manufacturing techniques are too large to provide the correct amount of obstruction to the cooling flow.

This work was done by Robert Moore, Donald E. Paulus, and Thomas S. Rackley of Pratt & Whitney Aircraft Group for **Marshall Space Flight Center.** *No further documentation is available.*
MFS-25849

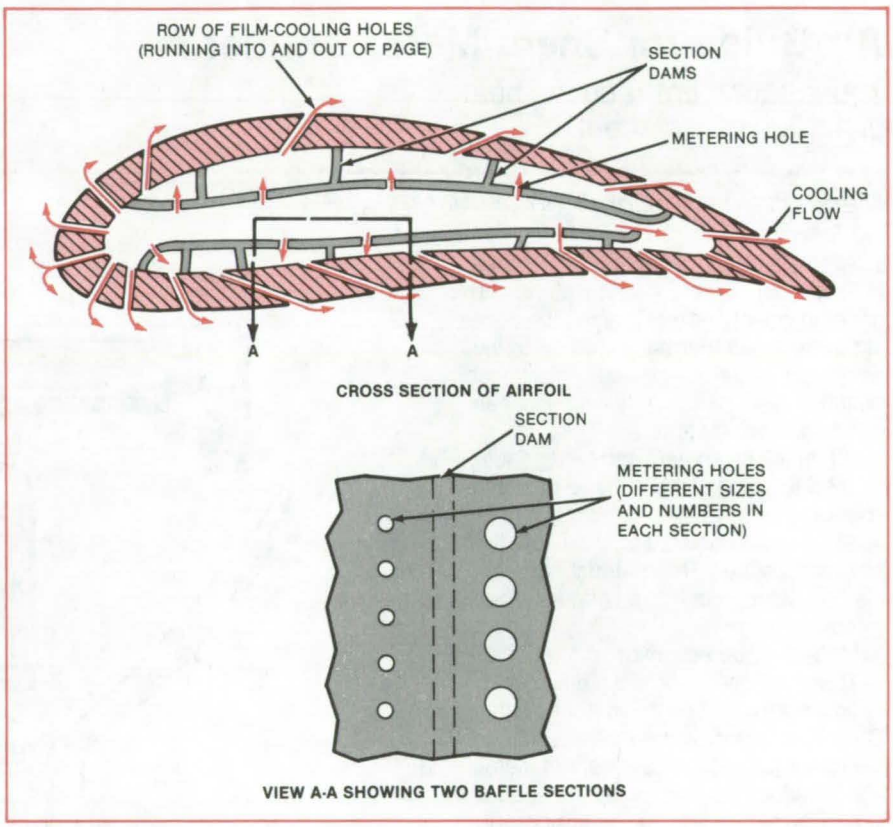

A **Turbine Blade or Vane Is Cooled** by gas or liquid flowing through holes to the exterior airfoil surface. A metering baffle inside the airfoil controls the flow to each row of cooling holes.

Convection-Cooled Turbine Airfoils

Coolant channels close to surface ensure efficient heat transfer.

Marshall Space Flight Center, Alabama

Cooling fluid flows just under the skin of turbine blades and vanes in a new fabrication technique. Because the flow is so close to the hot gases at the blade surface, heat is removed more effectively, and thermal stresses in the interior parts of the blade are greatly reduced. As a result, the turbines are expected to perform more dependably.

The coolant passages are cut by photoengraving or machining into the outside surface of a cast or forged turbine airfoil (see figure). The passages are then filled with a removable material such as wax, and an outside skin is applied overall — by electroforming or sputtering, for example. A heat-resistant, high-conductivity metal such

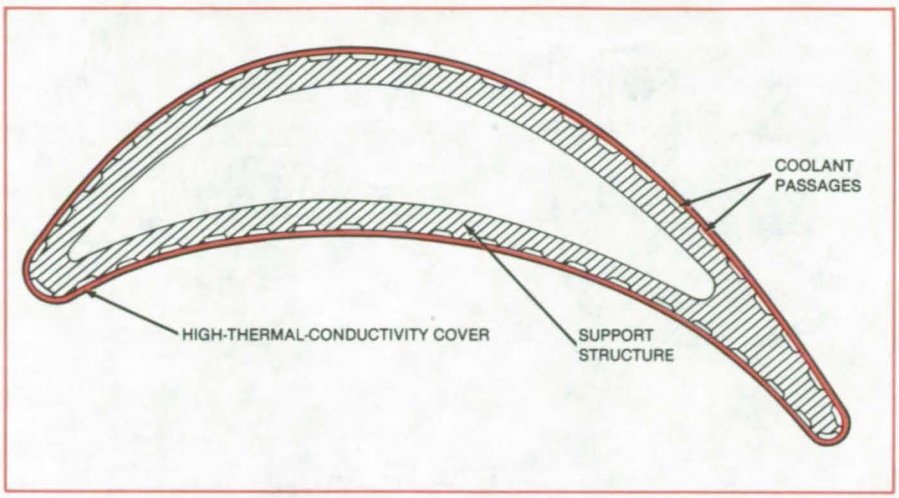

An **Advanced Convection-Cooled Airfoil** consists essentially of a metal cover on a grooved support structure. The grooves form coolant passages that may be oriented in any direction.

as nickel makes a good skin. After the cover material is applied, the filler material is removed from the coolant passages that then form a conduit for a heat-transfer fluid.

This work was done by Donald E. Paulus of Pratt & Whitney Aircraft Group for **Marshall Space Flight Center.** *No further documentation is available.*
MFS-25848

Antivortex Inlet Ribs for Fluid Seals

Instability in rotating machinery is reduced.

Marshall Space Flight Center, Alabama

Flow-straightening ribs in the inlets of annular-cross-section fluid pressure seals have proved successful in reducing turbine-rotor instability. The ribs are easy to manufacture and are usually easy to install in existing equipment.

Like a film of lubricating fluid in a journal bearing (see Figure 1), the working fluid in such a pressure seal produces spring forces that tend to recenter the rotor when it is in an eccentric position and damping forces that help to suppress vibrations. Destabilizing forces are also present, however: These forces tend to decenter the rotor and increase vibrations, posibly causing the rotor to break the lubricating film and damage itself and the stator.

The destabilizing forces are minimized when the azimuthal component of the flow in the seal consists only of the azimuthal component of Couette (viscous laminar) flow that is induced by the motion of the rotor. This requires that the fluid enter the seal axially, with little or no azimuthal velocity component.

(continued on next page)

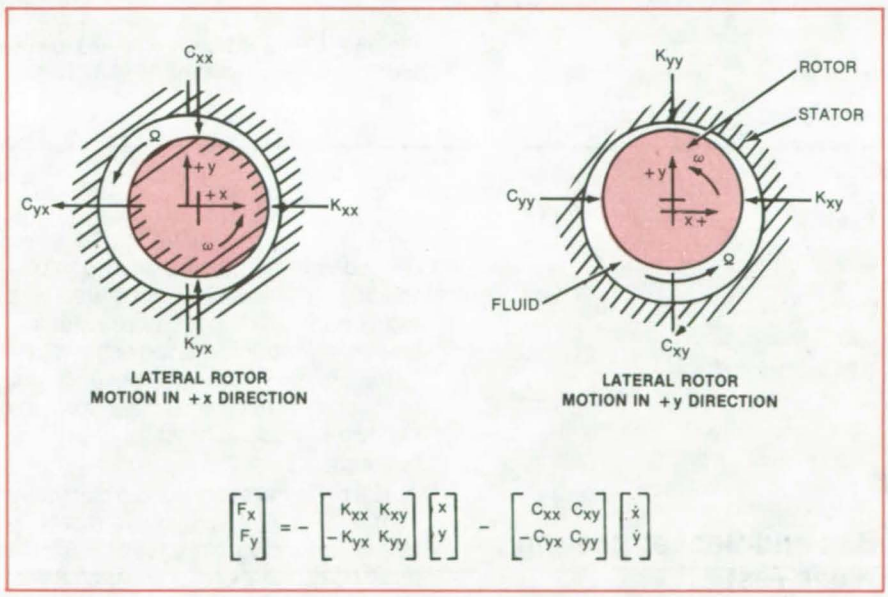

Figure 1. An **Annular Fluid Pressure Seal** exerts forces F_x and F_y on the rotor. The cross-coupling terms (those with subscripts xy and yx) represent destabilizing forces. These tend to increase when the flow entering the seal is not purely axial.

The use of flow-straightening vanes or ribs to suppress unwanted transverse velocity components is well known in other applications. In Figure 2, a set of inlet ribs suppresses the turbine swirl so that the fluid is forced to approach the seal radially, then axially. In tests with one turbopump employing this configuration, 480-Hz nonsynchronous vibrations were suppressed, resulting in an increase in the stability-threshold speed from 30,150 rpm to at least 30,600 rpm. The rib concept may offer a relatively inexpensive solution to some lateral-instability problems in many other systems with rotating pressure seals.

This work was done by Wei-Chung Chen, Robert F. Beatty, and Eugene D. Jackson of Rockwell International Corp. for **Marshall Space Flight Center.** *For further information, Circle 153 on the TSP Request Card.*
MFS-19793

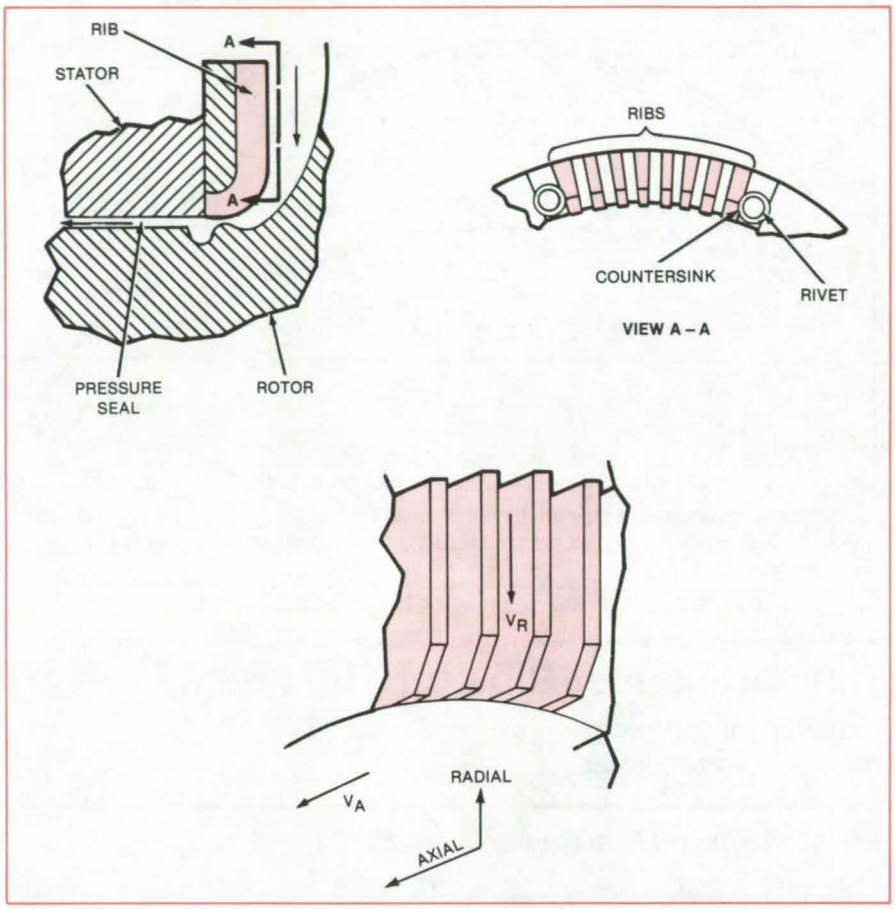

Figure 2. A **Ring of Ribs** is fastened to the existing stator in a turbopump pressure-seal inlet. The ribs suppress the swirl in the flow entering the seal.

Books and Reports

These reports, studies, and handbooks are available from NASA as Technical Support Packages (TSP's) when a Request Card number is cited; otherwise they are available from the National Technical Information Service.

Ball-and-Socket-Bearing Wear Test

Service life under severe load was measured.

A series of experiments to measure the wear life of a spherical bearing is summarized in a brief report. The experiments were required because adequate wear data were not available in the literature. In particular, it was desired to establish clearance, contour, finish, and lubricant parameters for a highly-loaded, compact, plain spherical bearing. This information should be useful in the design of bearings for helicopter control linkages, business machines, nuclear reactors, and rotor bearings.

The balls and sockets, with diameters near 1.09 in. (2.77 cm), were machine-lapped to a profile tolerance of ±0.0001 in. (0.0025 mm) and a finish of 8 μin. (0.2 μm), arithmetic average. Ceramic-bonded MoS_2 dry lubricant was applied to both the ball-and-socket-bearing surfaces in layers 0.0004 to 0.0006 in. (0.010 to 0.015 mm) thick. Several different diametral clearances were tried, ranging from +0.00274 in. (+0.070 mm) to an interference fit of −0.00315 in. (−0.080 mm).

In the testing apparatus, the spherical bearing was squeezed between two sockets. A splined shaft was placed through the center of the ball so that the ball could be cycled back and forth through the desired angular range. The sockets were pressed against the ball by a force of 22,000 lb (98 kN) to produce the intended loading of 50,000 psi (350 MN/m^2). Frictional moments and temperature were continuously monitored at the bearing surfaces to spot the onset of bearing deterioration.

Under load, the coefficients of static and dynamic friction were 0.008 and 0.007, respectively. At each bearing clearance, tests were run both with gimbal-angle cycles of ±10.5° and ±0.25° at the rate of 30 and 1,200 cycles/min, respectively. The bearings with all clearances performed equally well under all test conditions. The small-angle tests resulted in high-luster bearing finish after more than 137,000 cycles. The large-angle tests resulted in

a high-luster finish after 11,000 cycles.

This work was done by William G. Graham of Rockwell International Corp. for **Marshall Space Flight Center.** *To obtain a copy of the report, Circle 154 on the TSP Request Card.*
MFS-19737

Bearing Wear in Large Thermal Gradients

Spring preloading is important.

A report presents the results of a study of bearing distress resulting from a malfunction of the spring-preloading arrangements. In particular, the study examined the effect of thermal growth on wear depth of a bearing. Such growth occurs in large thermal gradients and can cause eventual lockup of the bearing cartridge. The report considers bearing-failure modes, the relationship between growth and wear, maximum stresses as a function of load, and the effect of thermal growth on spring-load deflections. The study was conducted to extend the life of the Space Shuttle main engine, but should also be of interest to engineers and students of bearing design.

According to the study, metallic wear can easily be a source of enlargement of the contact zone between the ball and the races. This wear is a result of poor lubrication and can cause movement of the preload spring. Thermal growth in the bearing contributes to this wear but probably not extensively.

As loads are increased in a bearing, high fatigue-inducing shear stresses are generated. The depth of the stresses is about 0.1 to 0.2 mm. Since fatigue occurs in a region rather than at a fixed depth, the failure depth could be as much as 0.28 mm for an 8,000-lb (35,580-N) load.

In the particular configuration studied, the preload springs appear to operate satisfactorily at a temperature differential of about 100° C. At temperature differentials in the 100° to 150° C range, however, the springs bottom out, and high loads are developed in the bearing. The conclusion is that more attention should be given to allowable spring movement after assembly.

This work was done by J. W. Kannel of Battelle Columbus Laboratories for **Marshall Space Flight Center.** *To obtain a copy of the report, "Evaluation of Bearing Mounting Design and Excessive Wear Phenomena," Circle 155 on the TSP Request Card.*
MFS-25879

MiniBriefs describe NASA innovations and reports in an abbreviated format. Readers desiring additional information on these items should request the Technical Support Packages (TSP's), available in most cases, which can be obtained by using the TSP Request Card at the back of this issue.

Clamp for Attaching Equipment to an I-Beam

A quick-connect/disconnect clamp is applied without tools or significant force.

A quick-connect/disconnect clamp attaches instruments or equipment to an I-beam, or similar flanged structures, without the use of tools or much force. Equipment can be temporarily mounted, regardless of the orientation of the I-beam, and then can be removed quickly or secured to another location on the beam, without any modification to the beam.

The equipment to be mounted is attached to one face of the clamp baseplate, for example, by bolts. Hinged locks on the baseplate secure the clamp to the I-beam. A pressure pad on the baseplate keeps the clamp from slipping.

This work was done by Keith H. Clark of **Marshall Space Flight Center.** *For further information, Circle 156 on the TSP Request Card.*

This invention is owned by NASA, and a patent application has been filed. Inquiries concerning nonexclusive or exclusive license for its commercial development should be addressed to the Patent Counsel, Marshall Space Flight Center [see page A5]. *Refer to MFS-25510.*

Continuous Mining Machine

A proposed miner would have maneuverable cutting drums.

A proposed mining machine would contain two maneuverable drums for cutting coal and rock intrusions in the coal seam. The axes of the drums may be individually tilted from vertical to horizontal and moved up and down and from side to side for efficient cutting without having to reposition the mining machine. The machine would cut wide and narrow passages and high or shallow passages by sweeping the drum across the seam face. When a rock intrusion is encountered, the drums would be individually managed to undercut and overcut the intrusion or to cut along the sides of the intrusion before attacking it directly to break it down.

This work was done by Thomas Knurovsky and Julius Kiskis of Caltech for **NASA's Jet Propulsion Laboratory.** *For further information, Circle 157 on the TSP Request Card.*
NPO-15164

Roof Support Near Coal-Mining Face

Support and conveyors would be combined into a single efficient unit that improves safety.

As coal is taken from a working face, conveyors must be moved forward toward the face to pick up the coal cut by the mining machine. After the conveyors move forward, roof-support sections are moved forward.

Hydraulically-powered legs mounted on crawlers and carrying sections of conveyors are proposed that would provide roof support close to the working face and above the workspace at all times. Each section would contain three vertical hydraulic rams mounted on a common crawler base. A forward exten-

(continued on next page)

sion, containing a hydraulic cylinder with a 2-foot (0.6-m) stroke would bring a cantilevered support section right up to the working face. Conveyor sections are located between the forward ram and the two rearward rams, just above the crawler base.

This work was done by Thomas Knurovsky, Julius P. Kiskis, and Gilbert Siegel of Caltech for **NASA's Jet Propulsion Laboratory.** *For further information, Circle 158 on the TSP Request Card.*
NPO-15165

Bidirectional Continuous Coal Miner

As the miner moves forward and backward, the cutting drums pivot to cut in the direction of travel.

A continuous-mining machine would cut coal in both directions of travel, eliminating the downtime caused by retreating across the face to start a new cut. The proposed miner, which is a variation of a longwall miner, carries a pair of side-saddle cutting drums that rotate in opposite directions; hydraulic elevators on the crawler adjust the drums for different seam thicknesses.

At the end of a coal-cutting pass, the miner maneuvers to initiate a return pass. Because of its very short turn radius, the miner maneuvers easily in, but needs a shearer-like start in moving toward the entrance. The miner applies equal power and speed in both face directions. Each return requires a repositioning of the drums, which is promptly achieved with hydraulics.

This work was done by Thomas Knurovsky, Julius P. Kiskis, and Jack Harris of Caltech for **NASA's Jet Propulsion Laboratory.** *For further information, Circle 159 on the TSP Request Card.*
NPO-15166

Miner for Cutting Entry Passages in Coal Seams

A pilot drum opens a coal seam to its full height and two shearing drums broaden it to full entry width.

A coal mining machine is proposed that would cut a swath wider than itself and would cut entry passages into a coal seam in one pass. The forward end of the miner carries a set of three cutting drums: a wide horizontal cutting drum in the center, which can be swept up and down the full height of a coal seam, and two vertical shearing drums that flank the center drum to cut a full-width entry in one pass. As the cut progresses, the crawler tracks keep the mining machine moving forward.

This work was done by Thomas Knurovsky and Julius Kiskis of Caltech for **NASA's Jet Propulsion Laboratory.** *For further information, Circle 160 on the TSP Request Card.*
NPO-15167

Drilling Holes on a Large Bolt Circle

A centering plate allows precise adjustment.

A special machine tool creates a circle of holes that are spaced and bored to an accuracy of a few thousandths of an inch. It includes a milling machine head mounted on a swivel base that can be moved readily to the hole locations. The base is equipped with four leveling bolts and an adjustable journal block, which holds the boring bar in position.

The tool was built for finish-boring holes to a diameter of 2.875 in. (7.302 cm). The holes were drilled through steel 5½ inches (13.97 cm) thick on a 39.5-inch (100.33 cm) bolt circle. The holes had been previously rough-drilled by a magnetic-base drill, which could not maintain dimensions within the required tolerance.

This work was done by Robert A. Hibdon of Boeing Services International for **Kennedy Space Center.** *For further information, Circle 161 on the TSP Request Card.*
KSC-11115

Tool for Taking Clay Impressions

Profiles of parts are transferred for measurement.

Clay impressions of small parts are taken with a tool consisting of a hollow tube closed at one end. Slots at the other end admit the part a short distance into the tube.

The tube is filled with clay protruding beyond the slots. It is then pressed against the part so that the part slides into the bottom of the slot, displacing the clay as it goes. The displaced clay forces an equivalent amount of clay out through holes and other gaps, thereby relieving the pressure and preventing clay springback that would distort the impression. The clay impression could be used to make a silicone rubber mold for subsequent examination.

This work was done by R. S. Duncan of Rockwell International Corp. for **Marshall Space Flight Center**. *For further information, Circle 162 on the TSP Request Card.*
MFS-19728

Tool for Tightening Bolts With Knurled Heads

A modified clamp transfers a torque to the bolthead.

A readily-available spring-loaded clamp can be modified so that it can transfer a measured torque to a bolt with a knurled head. The modified clamp holds the bolthead in its jaw while torque is applied through it. Normally, the bolt is secured finger-tight and no tools are needed.

The clamp is modified to apply additional pressure to secure the clamp to the bolthead and to hold the shortened shaft of a hexagonal socket head so that torque can be applied by a standard torque wrench. Plastic tips on the clamp protect the bolthead finish.

This work was done by Jack G. Smith and William A. Wall of **Marshall Space Flight Center.** *For further information, Circle 163 on the TSP Request Card.*
MFS-25694

Damping Seals for Turbomachinery

Seals perform a dual function while permitting higher speeds.

Seals with rough surfaces are proposed for stabilizing shaft motion and preventing leakage along the shaft in machines such as turbopumps. Ordinarily such seals contribute to instability at higher shaft rotational speeds; with rough surfaces on the seals, however, this effect is eliminated.

The dynamic and static parameters of seals with rough surfaces have been analyzed, and it has been shown that shaft stability and leakage are controllable in the presence of high roughness. Although experimental verification is needed, the proposed seals are simple and should be readily applicable to turbomachinery. Speed limits could be raised and bearing life extended, thus avoiding costly shutdowns.

This work was done by George L. von Pragenau of **Marshall Space Flight Center**. *For further information, Circle 164 on the TSP Request Card.*
MFS-25834

Controlling Sanding Depth

A mounting fixture for a rotary sander ensures a uniform finish.

A sander mounted on a traversing mechanism is moved toward or away from the workpiece by a screw drive. The depth of sanding and the position of the sander on the work is therefore reliably controlled.

The sander is useful for surface cleaning of out-of-round parts. It prevents them from being oversanded and thin surface layers from being sanded through — problems that could arise if sanding depth were controlled manually. It can also be used for finishing flat parts with linear contours and for controlled repair of pores and pits. The sander is an adaptation of a small air-driven grinder.

This work was done by Cecil E. Flowers of Rockwell International Corp. for **Marshall Space Flight Center.** *For further information, Circle 165 on the TSP Request Card.*
MFS-19713

Measuring Recessed Pins

A sleeve-and-rod-tool measures distances in blind locations.

A new tool makes distance measurements in nearly inaccessible locations. It was developed for measuring the small distance from the top of a pin to the body holding it. The pin is 0.136 inch (3.45 mm) in diameter and the body is 0.184 inch (4.67 mm) in diameter. The body is recessed in a reamed hole 0.30 inch (7.62 mm) in diameter: Therefore the pin-to-body distance cannot be observed directly.

The tool consists of a sliding sleeve on a central rod. The sleeve fits in the reamed hole and contacts the top surface of the body. The central rod contacts the top surface of the pin. The sleeve and rod are equal in length and long enough to extend out of the hole. Thus, the relationship of the top surfaces of the pin and body is transferred to the top surfaces of the rod and sleeve, where it can be seen.

This work was done by C. Kostas and W. Parker of Rockwell International Corp. for **Marshall Space Flight Center.** *For further information, Circle 166 on the TSP Request Card.*
MFS-19673

Lock for Tube Fittings

Covers for the fitting nuts engage to secure the fittings.

An attachment for the nuts of tube fittings locks the fittings securely. The attachment includes covers for the nut on the tube fitting and the nut on the boss fitting. Serrations within the two covers engage so that they mate and lock; this in turn locks the tube fitting.

To disengage the nut covers, the tube-fitting cover is pulled away from its mating nut cover. The nut covers can be adapted to any type of tube fitting.

This work was done by Leopold A. Hein and William N. Myers of **Marshall Space Flight Center.** *For further information, Circle 167 on the TSP Request Card.*

Inquiries concerning rights for the commercial use of this invention should be addressed to the Patent Counsel, Marshall Space Flight Center [see page A5]. *Refer to MFS-25964.*

Test-Bench Dynamometer

It would simulate programs for electric/hybrid vehicle design.

A proposed test bench would confirm the operating characteristics of motors and drive mechanisms. Originally proposed for testing simulation models for future electric/hybrid vehicles, the test bench would be fabricated from available materials and would include a 20-hp dc motor with appropriate controls, a loading system made up of a conventional automotive transmission, and a 20-kW alternator. Air bearings would be used in the drive motor and alternator/transmission mounts.

Basic electronic instrumentation would include standard load-cell bridges and excitation sources, commercial laboratory counters for speed measurements, a variable-voltage high-current power source for the drive motor, and a resistance-load bank for the alternator.

This work was done by Gerald S. Perkins of Caltech for **NASA's Jet Propulsion Laboratory.** *For further information, Circle 168 on the TSP Request Card.*
NPO-15084

Bearing Measuring Fixture

Tool increases accuracy and reduces labor.

A tool serves an accurate base for making critical measurements of large bearings such as those in turbopumps. The tool is a U-shaped bar 7 inches (17.8 centimeters) long. It is bolted to the lower bearing housing on two of the studs that hold the bearing assembly together. A technician takes the bearing measurements with a depth micrometer through a slot in the tool.

Previously, two technicians were needed for the measurements. One held a bar against the lower bearing housing while the other took the measurement. Since only one-half of one side of the micrometer would fit on the bar, the procedure was awkward and difficult.

This work was done by Willo D. Mason of Rockwell International Corp. for **Marshall Space Flight Center.** *For further information, Circle 169 on the TSP Request Card.*
MFS-19315

Stripper for Cables of Any Cross Section

Shoulders prevent penetration any deeper than intended.

A new wire stripper removes the insulation from cables with noncircular cross sections, as well as circular cross sections. The cutting blade extends from its holder far enough to cut the insulation but not the wire beneath the insulation. The blade exposure is adjustable for insulating jackets of different thicknesses.

To strip a wire, it is pressed against the projecting edge of the blade and rotated to score the insulation, which can then be slid off. The shoulders of the blade-holder support the cable and prevent penetration any deeper than intended.

This work was done by James O. Lonborg of Caltech for **NASA's Jet Propulsion Laboratory.** *For further information, Circle 170 on the TSP Request Card.*
NPO-15631

Staging Two-Phase Turbines

Turbine efficiency is 70 percent with staging as compared to 63 percent without staging.

A staging method solves the problem of friction loss and low efficiency of two-phase (liquid/gas) flow in turbines by using high blade-tip speeds in the first stage and progressively lower tip speeds in succeeding stages. The relative velocity between the liquid and the turbine blades and the accompanying friction drag are thereby reduced. Even if all of the relative velocity between the liquid and the turbine blades is dissipated in friction, the new staging method would still keep the turbine efficiency high.

This work was done by David G. Elliott of Caltech for **NASA's Jet Propulsion Laboratory.** *For further information, Circle 171 on the TSP Request Card.*

This invention is owned by NASA, and a patent application has been filed. Inquiries concerning nonexclusive or exclusive license for its commercial development should be addessed to the Patent Counsel, NASA Resident Office-JPL *[see page A5].* *Refer to NPO-15037.*

Low-Contamination Vibrating Feeder for Silicon Chips

Making the trough top surface out of semiconductor-grade silicon would reduce contamination.

Vibratory feeding is a method of controlling the flow of small oddly shaped particles. It is proposed that the top surface of the vibrating trough of a hopper for silicon chips be made of semiconductor-grade silicon. Although the trough will suffer some erosion from impact with the silicon chips, it will only introduce silicon (rather than a foreign material) into the feed. The technique could be applied to other materials that require contamination control by feeding the material through vibrating troughs topped by that particular material.

Silicon cannot be formed readily into the bowls used in vibratory feeders. However, slabs of silicon cut from standard polycrystalline rods can be assembled into a trough by bonding the slabs with epoxy to a thin aluminum trough and mounting the trough to the vibrator with aluminum ribs.

This work was done by Brian H. Mackintosh of Mobil Tyco Solar Energy Corp. for **NASA's Jet Propulsion Laboratory.** *For further information, Circle 172 on the TSP Request Card.*
NPO-15128

Self-Locating Latch

A latch locates fittings without using electronic sensors.

A new latch secures a fitting without displacing the fitting and without regard to where on the latch the fitting makes its initial contact. The new latch is driven by a motor through a differential. When one of the moving jaws encounters the fitting, the differential senses the resistance and transfers power to the other jaw. After both jaws close, the motor is shut off to secure the fitting. The latch is purely mechanical, and requires no electronic sensors.

This work was done by John Gibson and John Calvert of **Marshall Space Flight Center.** *For further information, Circle 173 on the TSP Request Card.*

This invention is owned by NASA, and a patent application has been filed. Inquiries concerning nonexclusive or exclusive license for its commercial development should be addressed to the Patent Counsel, Marshall Space Flight Center *[see page A5].* *Refer to MFS-25956.*

Torque-Wrench Extension Arm

Chain-link pulleys transmit torque to hard-to-reach fasteners.

A torque-wrench extension arm makes it possible to apply a torque to a bolt, screw, or nut that is inaccessible to conventional wreches or is in areas where a wrench cannot be manipulated. It could be used in narrow pockets and behind panels and walls.

Torque is transmitted along a chain-link pulley attached to two sprockets, all contained within a long narrow hollow housing. A shaft attached to one sprocket receives the input torque from a conventional torque wrench. The torque is transmitted by the pulley to the other sprocket, where a female socket is attached. The female socket fits over the hexagonal head of the bolt, screw, or nut to be tightened. A periscope accessory could be added to simplify locating the inaccessible fastener components.

This work was done by Thomas J. Pacala, Donald D. Trujillo, and James B. Laudenslager of Caltech for **NASA's Jet Propulsion Laboratory.** *For further information, Circle 174 on the TSP Request Card.*
NPO-15495

Fabrication Technology

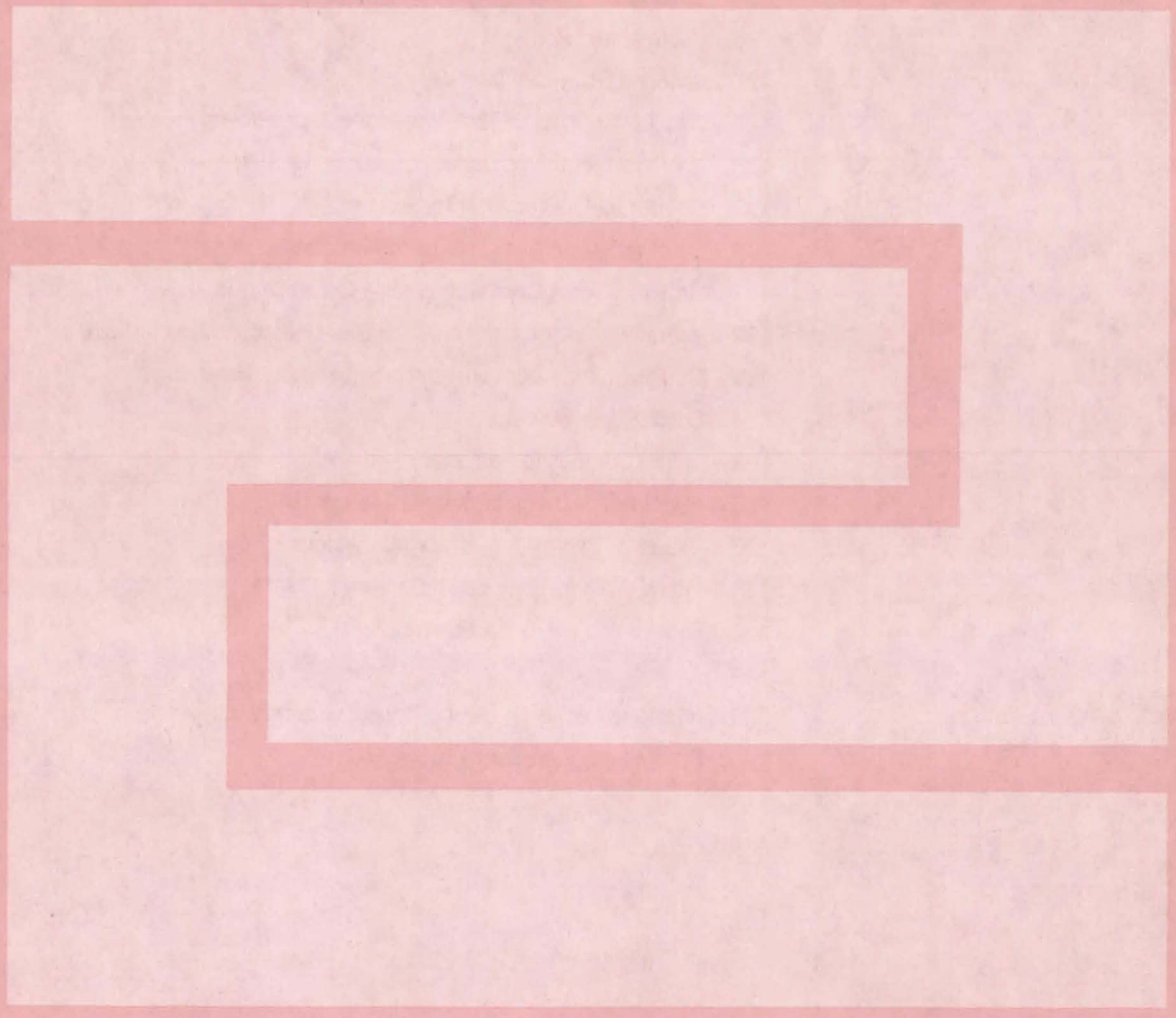

Hardware, Techniques, and Processes

Books and Reports

MiniBriefs

Lightweight Metal Mirrors

Two "eggcrate" halves are brazed together.

Goddard Space Flight Center, Greenbelt, Maryland

Flat mirrors fabricated by a new process are less than half the weight of previous constructions. The new design is a nearly symmetrical version of the "eggcrate" structure that is often used when fabricating large, lightweight reflectors.

A mirror of the new type (see Figure 1) is made from two plates of beryllium. Pockets are machined into each plate, leaving a face sheet on the nonmachined surface and thin walls between the pockets. About 85 percent of the material is removed from the original solid plates. (CAUTION: Beryllium is toxic. Designers may prefer to consider the use of other materials wherever weight is less critical.)

Figure 2 shows a cross section of a mirror of the new type. The two machined halves are brazed together in an oven with 1100 aluminum alloy as the brazing material. Since the brazing surfaces are located at the centroid of the cross section, differential thermal expansion (bimetallic effect) between the structural and brazing materials will cause little bending if any, and the mirror will remain flat over a range of temperatures.

Some care must be taken to prevent the brazing alloy from flowing down onto the back of the face sheet, or else the bimetallic effect will slightly distort the mirror when it is taken to different temperatures. This distortion can manifest itself as a deviation of the overall mirror surface from flatness or as a "print-through" of the wall pattern that gives a quilted surface.

To produce an adequate braze fillet, a ledge is machined into the top of the wall in the back half of the mirror. Alternatively, a "splitter" plate (fabricated by photoetching) can be used in place of the machined ledge, but does result in twice as many braze joints (one on each side of the splitter plate).

(continued on next page)

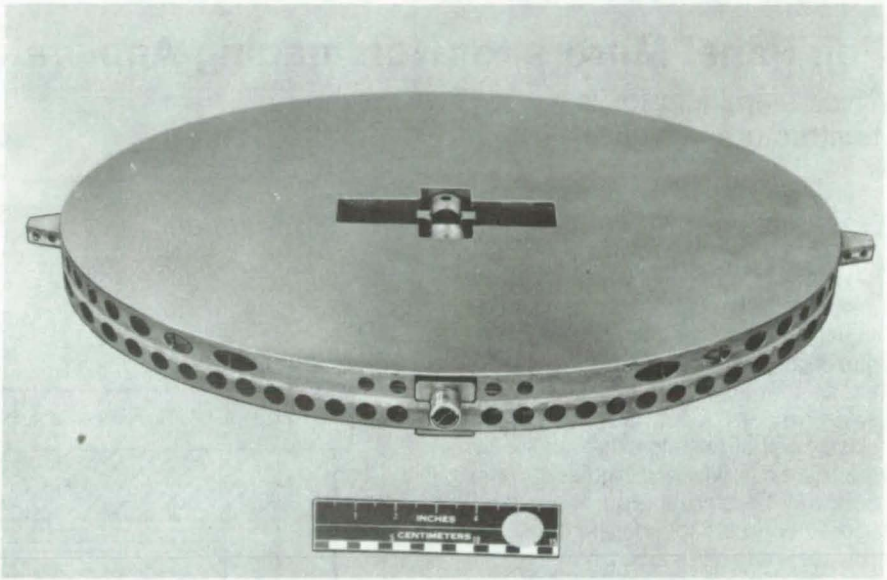

Figure 1. **Lightweight Flat Mirrors** are fabricated by machining pockets in two plates of beryllium, and then brazing the machined halves together. The mirror shown is less than half the weight of the same mirror made by the previous design.

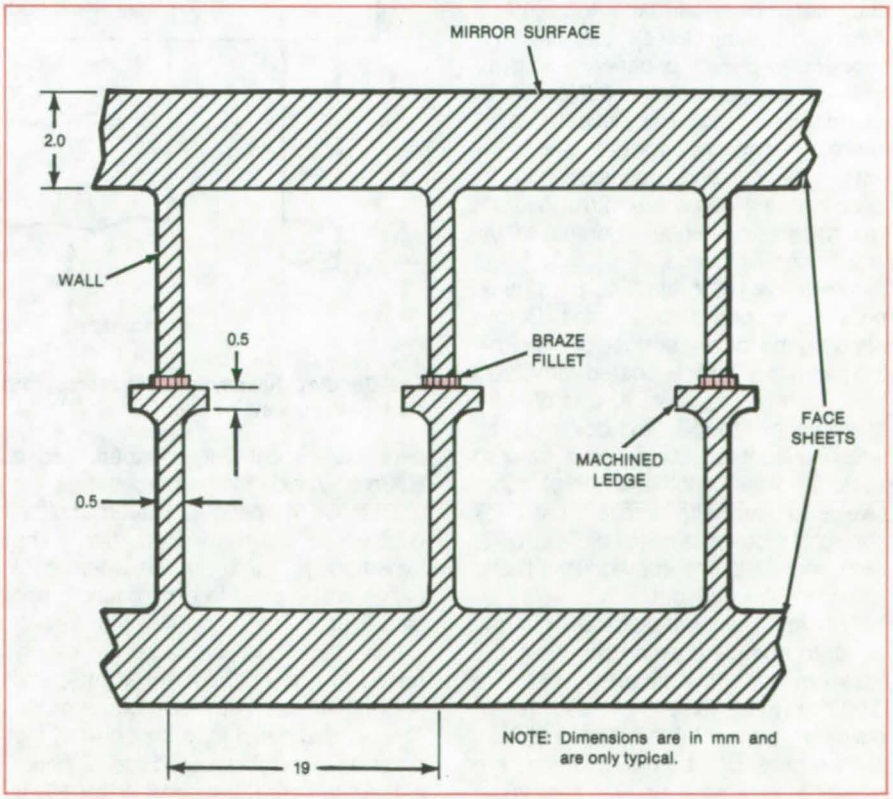

Figure 2. A **Mirror Is Fabricated** from two machined halves, using the well-known "eggcrate" configuration. The brazing surface is at the middle to minimize the bimetallic effect.

The bimetallic effect is further minimized by thermal cycling to relieve the residual brazing stresses. In addition, care must be taken to account for stress relief caused by mirror polishing and thermal distortions caused by thermal cycling before and after polishing.

Flat mirrors of the new type were made with a thickness of 4 cm, elliptical profiles of 53 by 41 cm, and masses of 2 kg. The same mirrors made by the previous design would have masses of 5.2 kg.

This work was done by E. Gossett and P. Winslow of Hughes Aircraft Co. for **Goddard Space Flight Center.** *For further information, Circle 175 on the TSP Request Card.*
GSC-12743

Foil Panel Mirrors for Nonimaging Applications

Thick aluminum foil is glued to structural panels.

Goddard Space Flight Center, Greenbelt, Maryland

Large, durable, lightweight mirrors are made by bonding thick aluminum foil to honeycomb panels or other rigid, flat backings. Such mirrors are suitable for use as infrared shields, telescope doors, solar-furnace doors, advertising displays, or other reflectors that require low thermal emissivity and high specularity but do not require the precise surface figure necessary for imaging. If fabrication costs can be reduced, heliostat mirrors may be added to the list of applications.

Fabrication by the new technique avoids the expense of custom polishing the metal panel surface to a mirror finish. In many cases the finish of moderately-priced commercially available foil is superior to that achievable by custom polishing. The critical item is therefore not the surface finish but rather the bonding process, since the process determines the mirror flatness and the environmental extremes that the mirror can withstand.

The foil is 0.005 in. (0.13 mm) thick, polished on one or both sides. Before applying the foil, the surface of the backing panel is first roller-coated with 0.003 in. (0.08 mm) of adhesive. One ply of a glass scrim fabric is laid down on the adhesive-coated surface, with care to avoid wrinkles. Another layer of adhesive is applied with a roller, just thick enough to cover the fabric. The foil is then applied to the impregnated fabric with the shiny side out.

The foil must be pressed onto the panel to complete assembly. First, the foil is covered with a clean polyimide film 0.002 in. (0.05 mm) thick, and then a polyvinyl chloride (PVC) film 0.020 in. (0.51 mm) thick. The first two films are rolled flat to remove air, with care taken to avoid deformation of the foil.) Both polymer films are then removed, the perimeter is carefully cleaned, and a clean polyimide film is placed over the foil. Under the panel is placed another 0.020-in. (0.51-mm) PVC film. The assembly is then put between caul plates and placed in a hydraulic press (see figure).

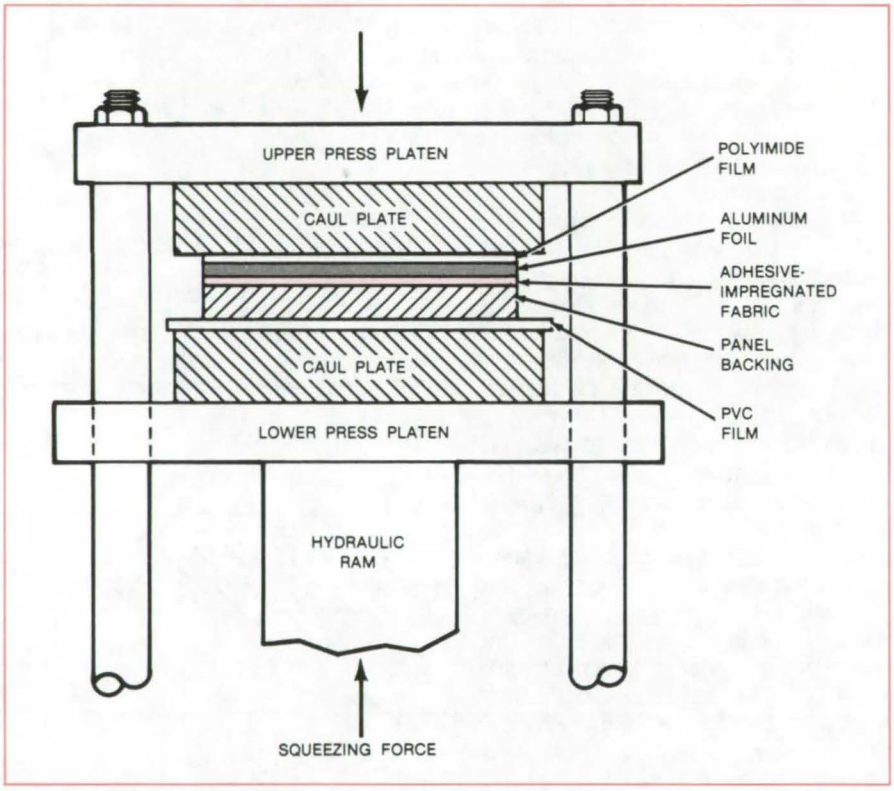

The Bonding Assembly is squeezed in a hydraulic press along with protective and cushioning sheets of plastic.

The hydraulic pressure is slowly raised to about 20 psi (14 kN/m^2) and held for 4 hours at room temperature. The bonded panel is removed from the pressing assembly, cured for 12 hours at room temperature, and then cured for 72 hours at 60° C.

A mirror fabricated by this technique tolerated a temperature range of −100° to +60° C in a vacuum. The performance characteristics were as follows: total integrated solar scatter, less than 2 percent; surface waviness, less than 1°; hemispherical emissivity at 25° C, less than 0.025; and solar absorptance, less than 0.15.

This work was done by D. J. Kuyper and A. A. Castillo of Hughes Aircraft Co. for **Goddard Space Flight Center.** *For further information, Circle 176 on the TSP Request Card.*
GSC-12751

Handling Fixture for Solar-Cell Arrays

Thin cells can be processed and stored safely.

NASA's Jet Propulsion Laboratory, Pasadena, California

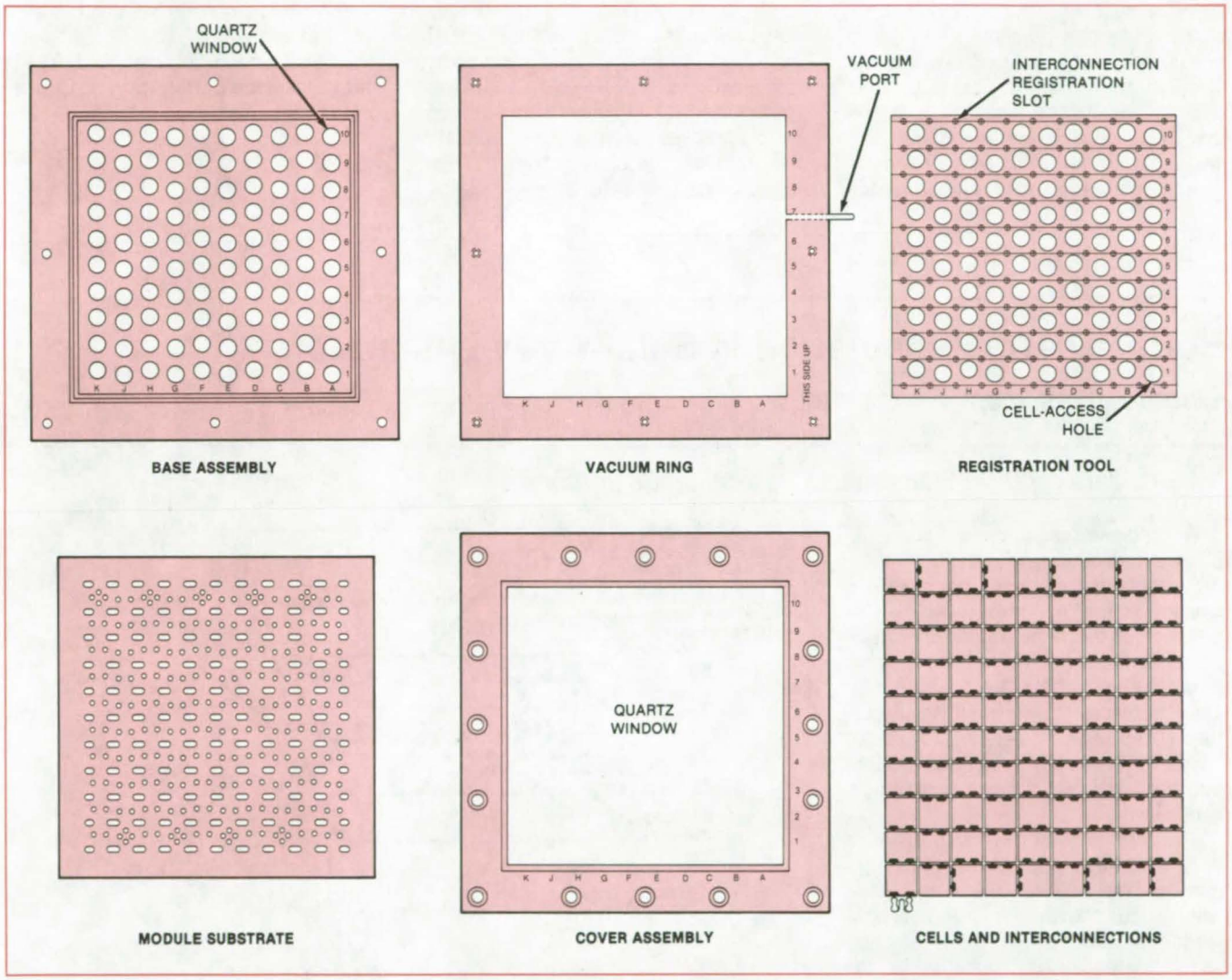

These **Major Parts of the Handling Fixture** hold components of solar-cell-array modules safely, yet allow the assembly process to proceed without interference. The fixture can be used with or without an internal vacuum.

A concept for handling photovoltaic cells would allow many such cells to be held in a fixture for support and protection during production, transport, and storage. Since the concept would allow the handling of thin, relatively-fragile cells, it offers potential for savings in silicon material and in cost.

The fixture comprises a registration tool, a vacuum ring, a base, a cover, and a handling cover (see figure). Cell components would be assembled by conventional bonding processes, in air or in vacuum. Welding can be done by parallel-gap or laser techniques, for example. Manual or automatic soldering can be done by parallel-gap, laser, soldering-iron, induction, infrared, or oven methods.

The registration tool supports and restrains the module substrate, interconnection layer, cells, and covers during fabrication. Each component is handled separately only once — as it is loaded into the tool in proper sequence. From that time on, the registration tool provides support and access to components for processing, inspection, testing, and other operations.

The registration tool is a plate having access holes and spring-loaded spacers. The holes provide access for bonding the interconnection layer and substrate to the cell backs. The spacers provide a matrix of slots into which the cells are loaded, and they position and hold

(continued on next page)

the interconnection layer in registration with the electrical contacts on the cells. The spring loading on the spacers ensures that the components are held securely with uniform pressure. The registration tool is adaptable to any combination of cell thickness and diameter, substrate, superstrate, interconnection configuration, and bonding method foreseen at present.

The base is a machined frame with mounting holes, quartz windows, and a vacuum seal. When the base is mated with the registration tool, its quartz windows are coplanar with the module surface. The quartz windows provide a mounting surface and a view of the back of each cell. They also pass laser light to the interior of the fixture for laser bonding in vacuum.

The vacuum ring provides a vacuum port to the interior of the fixture. It can be attached to either the cover assembly or base assembly depending on whether the back or the front of the module is being worked on.

The cover consists of a quartz window bonded to an aluminum frame that includes vacuum seals, mounting bolts, and spacer bolts. The cover can be moved inward and outward, as required by the process steps, without breaking the vacuum. The spacer bolts provide legs on which the fixture rests while the back of the module is being processed.

The handling cover is a rigid transparent sheet that attaches to the registration tool. It is used when the fixture and its contents are stored or transported. It has recessed edges so that the borders of substrates can be joined to form complete panels without removal of the cover.

This work was done by Paul A. Dillard and Donald W. Higbee of Lockheed Missiles & Space Co., Inc., for **NASA's Jet Propulsion Laboratory.** *For further information, Circle 177 on the TSP Request Card.*
NPO-15908

Better Thermal Insulation in Solar-Array Laminators

Glass marbles improve temperature control.

NASA's Jet Propulsion Laboratory, Pasadena, California

A modified vacuum laminator for photovoltaic solar arrays includes thermal insulation made of conventional glass marbles. The marbles serve as insulation for the temperature control of a lamination process at cure temperatures as high as 350° F (175° C). They replace the original insulation made of an asbestos cement. The use of standard insulation materials for this purpose would have been much more expensive.

The laminator shown in the figure uses a resistive strip heater as an inexpensive heat source. The strip heater with an autotransformer power supply replaces tungsten-filament lamps, which were originally located in the lower chamber.

The previous insulation caused problems due to heat loss. The controller temperature set point had to be adjusted manually to prevent the temperature of the laminant adhesive/encapsulant from overshooting.

The glass-marble thermal insulation resulted in improved temperature control and a balanced thermal load below and above the strip heater. The marbles provide both support and thermal insulation.

This work was done by Dale R. Burger and John F. Knox of Caltech for **NASA's Jet Propulsion Laboratory.** *For further information, Circle 178 on the TSP Request Card.*
NPO-15925

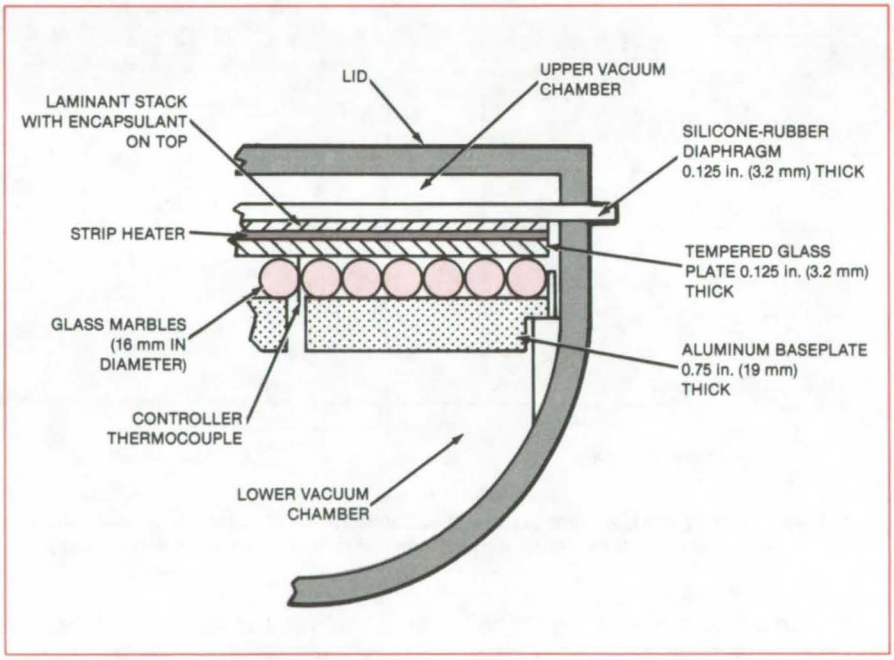

The new **Solar-Array Laminator** includes a mechanically-stiff, large-area thermal insulation made of glass marbles simply sorted to measure 16 mm (± 0.13 mm) in diameter. The marbles support a tempered glass plate under a load of 14.7 psi (101.3×10^3 N/m^2). The improved thermal insulation also reduces the volume of the vacuum chamber, resulting in reduced pumpdown times and energy savings.

Edge Supports for Photovoltaic Modules

Mounting strips are patterned after glazing gaskets.

NASA's Jet Propulsion Laboratory, Pasadena, California

New, easy-to-install supports for rooftop solar modules (see Figure 1) consist of extruded rubber mullions with locking zippers. The supports can be cut to length with a utility knife and installed without special tools. They are adaptable to many different roof configurations.

The mullions are installed along the roof slant at a separation of 4 ft (1.22 m) between centers. They are secured to the roofing surface by an adhesive or by mechanical grippers that mate with undercut slots (see Figure 2). After a string of modules is placed in the throats of two adjacent mullions, solid rubber extrusions (the locking zippers) are forced into slots in the top mullion surfaces.

For fire safety, the mounting throat is positioned so that the bottom of the photovoltaic module rests no more than 0.5 in. (13 mm) above the roofing surface. Furthermore, as shown in Figure 1, the modules in a vertical string do not butt up against each other but instead are deliberately kept at least 0.375 in. (10 mm) apart. This scheme allows thermal expansion and convective cooling of the modules while providing intermediate vents and sufficient flow impediment to slow down fire propagation in what otherwise would be a dangerous chimney running along the whole roof from bottom to top.

Wires, cables, and electrical connectors can be molded in the mullions or installed later. At the ends of the roof or array, mullions can be extruded with one cavity closed. The closed cavity can be used as a conduit for wires or pipes or as a pipe for cooling fluid.

This work was done by Timothy J. Maloney of AIA Research Corp. for **NASA's Jet Propulsion Laboratory.** *For further information, Circle 179 on the TSP Request Card.*
NPO-15740

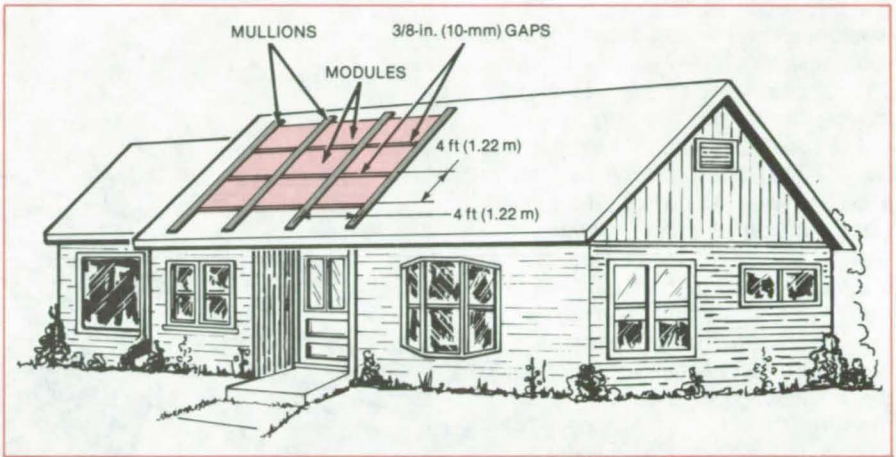

Figure 1. **Modules Are Mounted With Gaps Between Them** to thwart the chimney effect that could be a fire hazard.

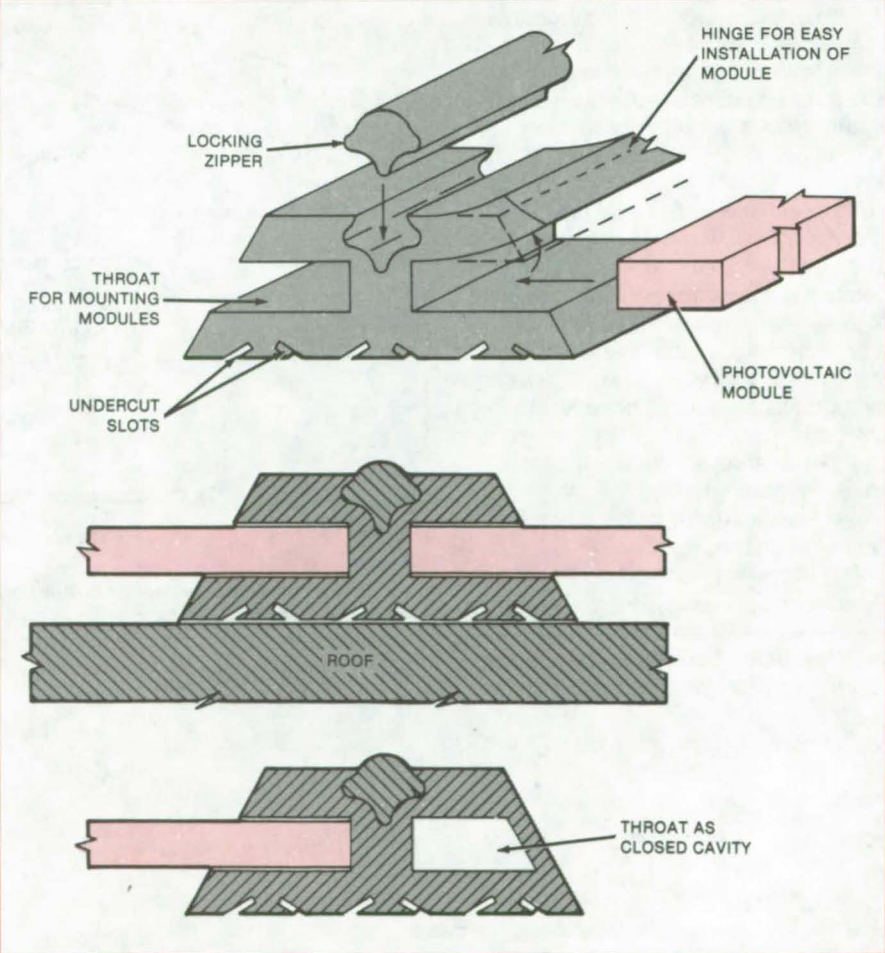

Figure 2. **Extruded Mullions** of a heat- and ultraviolet-resistant rubber are installed on rooftops to grip the edges of solar photovoltaic modules.

Photovoltaic Roofs

Solar cells would perform two functions: waterproofing the roof and generating electricity.

NASA's Jet Propulsion Laboratory, Pasadena, California

A proposed rooftop photovoltaic array would serve as a watertight south-facing roof, replacing shingles, tar, and gravel. The concept would thus reduce the cost of a residential solar-cell array.

The modules are stacked in overlapping fashion like ordinary shingles to allow rainwater to run off. The east-to-west (horizontal) seam between two solar-cell modules is sealed as an overlapping joint (see figure). The rear side of an L-shaped rubber extrusion on the upper overlapping module is covered with a tacky adhesive that bonds to the inactive glass area of the lower module, forming a secondary seal against water leakage at the joint.

The north-to-south joint (running along the roof slant) between two modules is sealed by clamping P-shaped rubber extrusions in a roll-formed steel channel section. The sections of each channel are assembled on the roof in a tongue-and-groove fashion so that leakage water drains from one channel section to another, finally discharging at the eaves.

Thus, water is prevented from leaking into the house by three distinct sealing or drainoff mechanisms. The first line of defense is the compression of the bulb of the P-seal between the vertical wall of a channel section and the underside of the clamping strip. Any water leaking through this seal drains directly into the channel interior and flows from one channel to another until it reaches the eaves. Finally, the leg of the P-seal prevents water from leaking over the top flat of the channel section.

This work was done by Robert W. Drummond, Jr., and Neal F. Shepard, Jr., of General Electric Co. for **NASA's Jet Propulsion Laboratory.** *For further information, Circle 180 on the TSP Request Card.*
NPO-15881

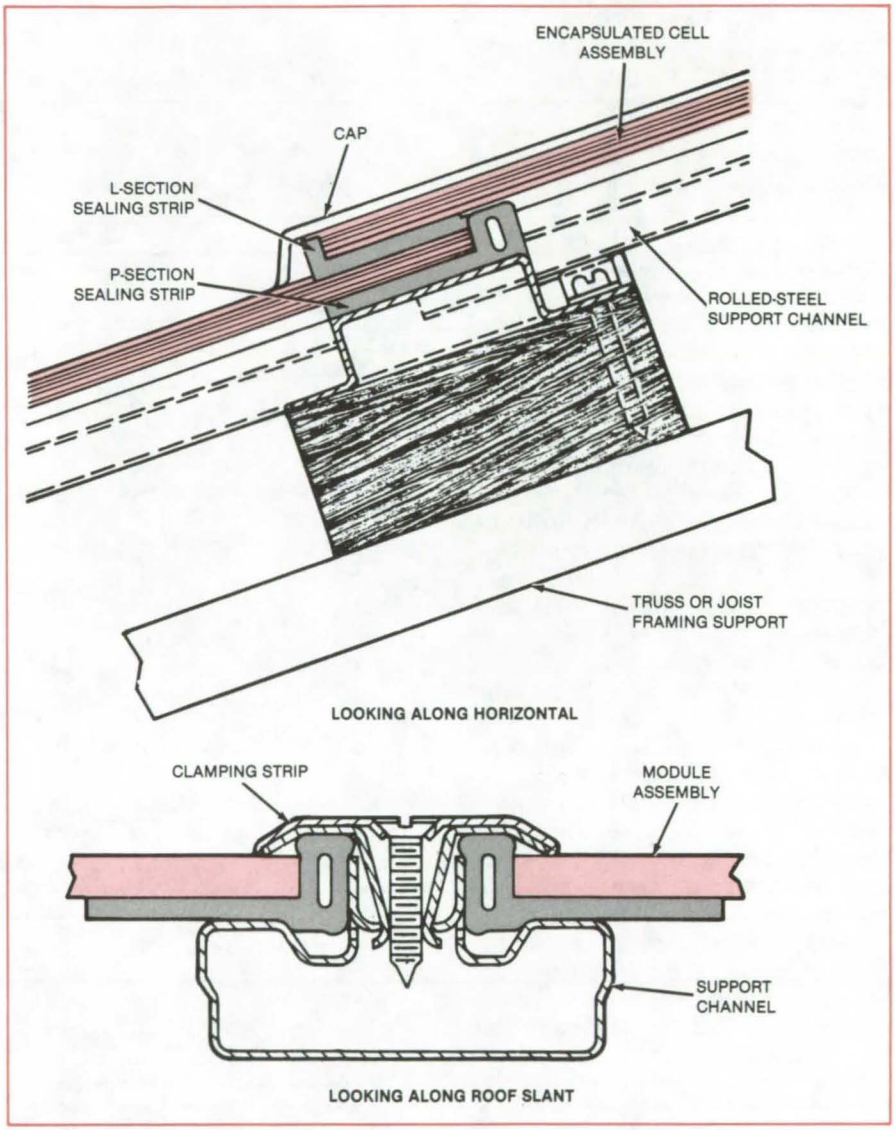

Sections Through Horizontal and Slanting Joints show how overlapping modules are sealed by L-section rubber strips and side-by-side modules are sealed by P-section strips. Water seeping through the seals of the slanting joints drains along the channels.

Labeling Solar-Cell Modules

A photocopying machine produces a durable identification label.

NASA's Jet Propulsion Laboratory, Pasadena, California

Solar-cell arrays can be labeled by using a standard electrostatic copying machine. The process has been used for double-glass photovoltaic-cell modules (see figure), in which a matrix of cells is sandwiched between thin, flexible glass mats and covered above and below by protective sheets of glass. The label contains such information as manufacturer, model number, voltage and power ratings, and serial number. It may also contain an electrical-shock hazard warning and an identification of positive and negative terminals.

The glass mats are loaded in the copying machine instead of paper. They are run through the machine in the conventional way. The label is copied on each mat. Since the toner used in the electrostatic copying process is carbon black, the label resists fading on exposure to Sunlight. At any rate, exposure to light is minimal because the label is on the back, or shaded, side of the module.

The cells and glass mats are laminated within the cover glass as in the present manufacturing process. The label is visible through the rear cover, which protects it from the environment.

A master label is drawn and photocopied on each module. At the same time, serial numbers are indexed in sequence and photocopied on the module, either by manually rotatable dials or by an electrically activated counter.

The new labeling method saves the expense of procuring and applying conventional labels. It produces a label that will last as long as the module and cannot fall off or be altered. The label does not shade any valuable solar-exposure area. Moreover, the technique readily allows changes in label configuration, location, and size, within the limits of the copying machine.

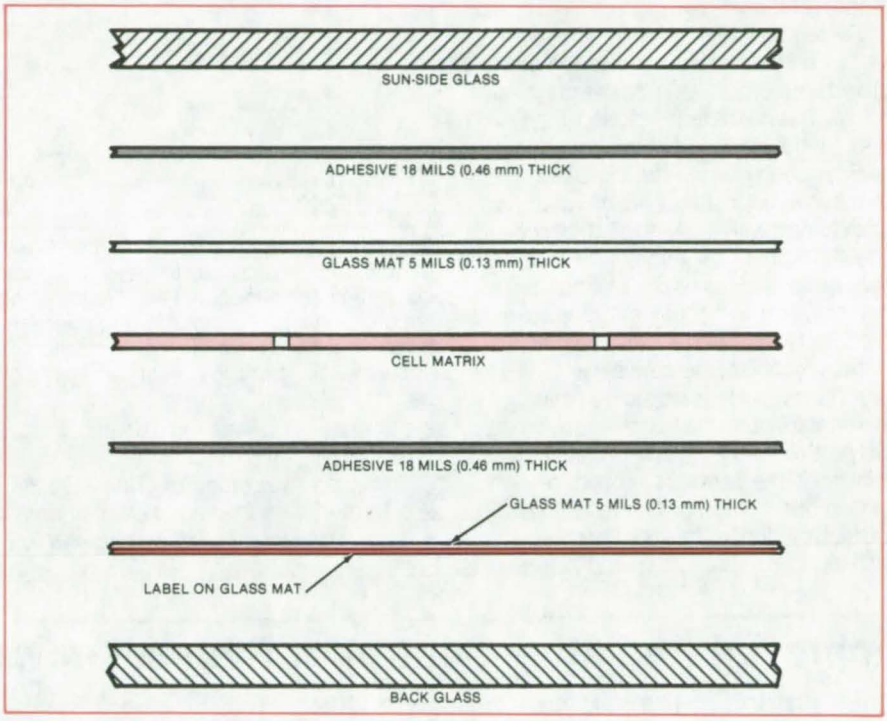

Photocopied on a Glass Mat, an identification label is protected from damage by the back glass plate of a photocell module. The label should endure for the 20-year expected lifetime of the module.

This work was done by Edwin G. Watson and Peter J. Coyle of RCA Corp. for **NASA's Jet Propulsion Laboratory.** *For further information, Circle 181 on the TSP Request Card.*
NPO-15997

Oscillating-Crucible Technique for Silicon Growth

Technique would yield better mixing of impurities and superior-quality crystals

NASA's Jet Propulsion Laboratory, Pasadena, California

Crystalline silicon obtained by unidirectional-solidification would be significantly improved by accelerated rotation of the growth crucible and seed. In the proposed technique, the accelerated motion stirs the melt, which reduces temperature gradients and decreases the boundary layer for the diffusion of impurities near the growing surface. The results would be better mixing of impurities into the melt, a decrease in the tendency for dendritic growth or cellular growth, and crystals with low dislocation density. Accelerated/decelerated crucible rotation has been applied with success to solution growth and Czochralski growth, resulting in large crystals of superior quality.

(continued on next page)

Three directional-solidification techniques are seed Bridgman, heat-exchanger, and fast-freezing casting. In these configurations, convection and fluid flow are insignificant. Consequently, the crystal growth obtained by these techniques is limited by dislocations and grain boundaries, which limit solar-cell efficiencies from such crystals to 10 to 12 percent, maximum.

To remedy the defects, the melt is stirred by the oscillatory rotation of the growth crucible, as illustrated in the figure. The crucible is accelerated from rest to 20 rpm and then decelerated back through rest to rotation speed of 20 rpm in the opposite direction, and then back to rest with a period of 10 seconds. The sinusoidal oscillation of the crucible generates an out-of-phase rotation of the melt. The part of the melt close to the crucible wall follows changes in the state of motion of the crucible with only a slight delay; when the crucible rotation is momentarily stopped or even reversed, the part of the melt away from the wall continues the previous motion, or nonmotion due to inertia. The resulting pattern of motion is one of slippage and shear around the rotation axis and is an effective stirring mechanism.

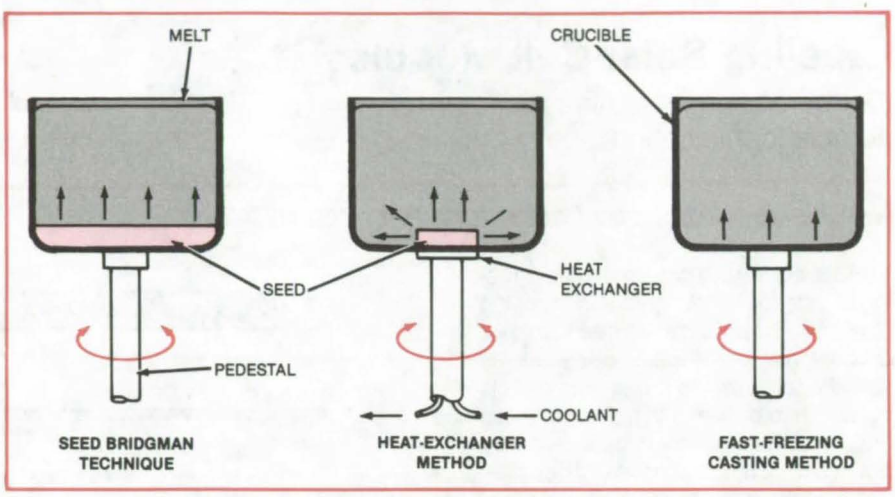

The **Three Directional-Solidification Growth Techniques** rely primarily on a vertical temperature gradient to achieve the thermal conditions necessary for the control of nucleation and directional solidification. Without oscillations, convection and fluid flow are insignificant, so that the addition of rotational acceleration of the crucible in this modified technique is the major contributor to homogenizing the melt temperature. The arrows within the crucibles show the direction of crystal growth or freezing.

This work was done by Taher Daud and Katherine A. Dumas of Caltech and K. M. Kim, Guenter H. Schwuttke, and P. Smetana of IBM Corp. for **NASA's Jet Propulsion Laboratory.** *For further information, Circle 182 on the TSP Request Card.*
NPO-15938

Improved Radiative Control of Ribbon Growth

Shield modifications enhance growth rate while reducing silicon oxide formation.

NASA's Jet Propulsion Laboratory, Pasadena, California

Improvements in an apparatus for growing dendritic-web silicon crystals increase the growth rate and reduce the formation of silicon oxide. Both the crucible lid and the radiation shields were modified.

In the growth apparatus, the significant heat-loss mechanism is thermal radiation. The radiation shields control the temperature distribution in the web and in the melt by modifying the radiation field where the web is crystallizing. The temperature distribution in turn determines both the growth speed and the thermal stresses in the crystal.

Part (a) of the figure shows a cross section through the region of crystal growth: This region lies in the center of the crucible shown in (b). The arrows indicate directions of net radiation flow away from the melt and ribbon. The radiation field impinging on the melt and ribbon comprises three components, which, in order of decreasing temperature, are radiation from within the cavity, from the lid and radiation shields, and from the cooler ambient region above the shields. The process is controlled by adjusting the proportion of these three components in the total radiation field.

Part (b) shows the view from the top of the apparatus. The induction-heating coil surrounding the crucible and susceptor heats the melt. The crucible contains molten silicon. To replace the silicon drawn off as ribbon, pellets of silicon are added through the feed hole.

To help keep the crucible temperature uniform when this relatively cold silicon is added, an adjustable heat shield was added around the feed end of the crucible. It reduces the radiative heat loss by whatever amount is required for a given silicon feed rate. The shield position is adjusted up or down to control the temperature.

A similar adjustable shield was added to the other end of the apparatus. The adjustable shields "fine tunes" the temperature during a run.

Parts (c) and (d) each show a cross-sectional view and half of a top view of two successive states of development of the multilayer radiation shield surrounding the crystal web. The configuration in (c) gave particularly good results. The crucible lid and the radiation shields were made of molybdenum.

Two modifications of (c) were found to improve the process. The first modification was the addition of a 0.5-mm-thick shield on top of the three shields shown.

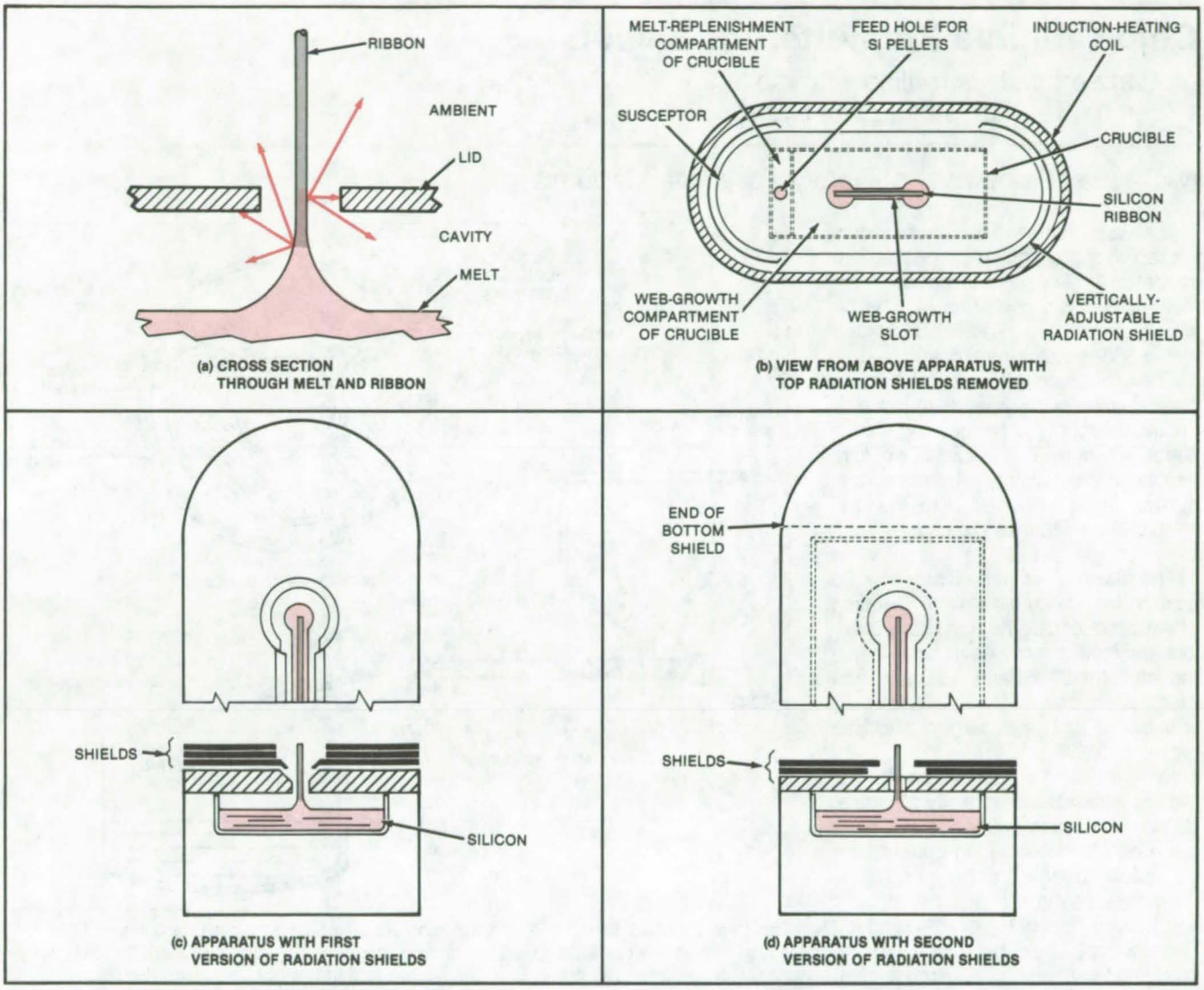

The **Control of Dendritic-Web Crystal Growth** requires precise control of the web temperature profile. This is achieved by using a series of thermal-radiation shields to control the thermal-radiation field in the region where the melt is solidifying onto the crystal ribbon being pulled from the melt.

This lowered the effective temperature of the top shield as seen by the web growing above it. Unfortunately, this shield warped badly with long use and changed the thermal properties.

The second modification, which had many of the thermal properties of the first, involved a slitted shield as the top-most member shown in (c). A shield with a continuous periphery as shown couples to the heating-coil field and thus runs hotter than might otherwise be expected. Slits were cut 1.5 mm wide and 13 mm long at intervals of 13 mm around the periphery. In one case where the solid shield had operated at 955° C, a slitted shield operated at 879° C under conditions otherwise identical.

The revised radiation-shield system (d) was designed to increase the heat loss from the ribbon to increase ribbon-growth rate. In this configuration, the crucible lid was about 3 to 4 mm thick with multiple radiation shields. If the lid were thinner, the heat loss to the surroundings would be higher. Although thin lids result in faster growth, they are cooler at the growth slot and accumulate deposits of the silicon oxide, which evaporates from the melt. These deposits cause problems by either falling into and contaminating the melt or by obstructing the growth slot.

Additional heat shields increase the lid temperature, but are, in turn, fouled by oxide. It has been found that having at least a 4-mm spacing between the lid and the first shield changes the gas flow in the system so that oxide accumulation is not a significant problem.

This work was done by J. P. McHugh, R. G. Seidensticker, and Marie E. Skutch of Westinghouse Electric Corp. for **NASA's Jet Propulsion Laboratory.** *For further information, Circle 183 on the TSP Request Card.*
NPO-15916, 17, and 18

Cold-Crucible Premelter for Silicon

A quartz crucible is refilled with molten silicon between crystal-growth cycles.

NASA's Jet Propulsion Laboratory, Pasadena, California

The system shown in the figure allows the replenishment of the silicon melt in a crystal puller. The heart of the replenishment system is a cold crucible in which silicon chunks are heated and melted with a 500-kHz electromagnetic field.

The cold crucible consists of a water-cooled, silver-plated boat surrounded by an induction coil. The coil induces a secondary current in the silver coating, heating it only slightly. The secondary current in turn couples with the preheated silicon chunks and causes them to melt.

The silicon is not contaminated by the cold crucible because a slight levitation effect, produced by the high fields, cushions the melt, preventing it from wetting the cold metal surface. Liquid silicon runs along the slightly-inclined cold crucible and is discharged into the growth crucible.

By allowing for replenishment, the system expands the capacity of crystal pullers. The crystal puller does not have to be cooled down during growth, and the quartz growth crucible can be reused, resulting in a higher productivity and a lower cost of the crystal product. The concept could be applied to the crystal growth of other materials that are sufficiently conductive and difficult to keep free of contamination by the container walls at the temperature of operation.

This work was done by R. L. Lane of Kayex Corp. for **NASA's Jet Propulsion Laboratory.** *For further information, Circle 184 on the TSP Request Card.*
NPO-16050

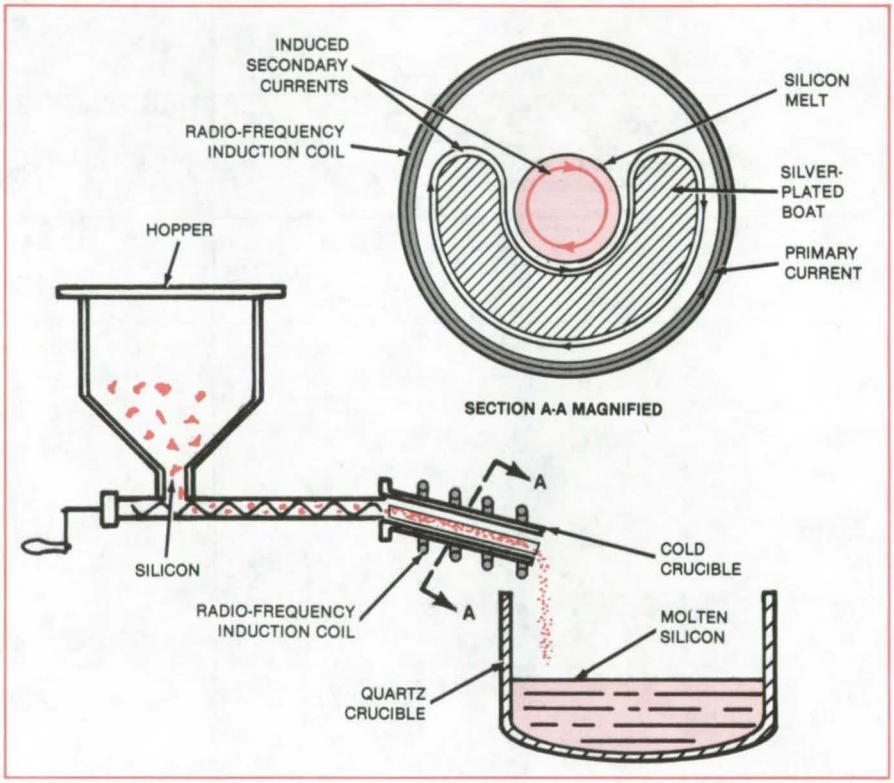

The Cold Crucible consists of a water-cooled, silver-plated boat in a 500-kHz field. Induced secondary currents cause the preheated chunks of silicon to melt. The magnetic repulsion between the currents in the silicon and in the boat prevents the silicon from touching the boat.

Starting Silicon-Ribbon Growth Automatically

A programable two-channel controller reproduces standardized growth conditions.

NASA's Jet Propulsion Laboratory, Pasadena, California

A semiautomatic system developed by a NASA contractor starts the growth of silicon sheets more reliably than systems with purely manual control. The system uses a commercial programable process controller to ensure that the pulling speed and temperature are varied reproducibly during the crucial initial stage of growth. Once growth has been established and is proceeding normally, the controller relinquishes control of the growth furnace and can then be used to initiate growth in another furnace.

Starting the growth of a silicon-crystal sheet involves a sequence of temperature and speed changes over a period of several minutes. When control is exercised manually, success in producing consistent high-quality ribbon starts depends largely on the skill of the furnace operator, particularly the operator's ability to reproduce the sequence on the basis of subjective observation.

Programed control offers important advantages over manual control. It can start wide sheets of silicon repeatedly, it yields high-quality crystals reproducibly, and it is less demanding of operator skill and training.

The profiles of desirable furnace temperature and pulling speed during growth initiation have been established experimentally and consist of a series of constant levels and linear increases or decreases with time (see figure). Voltages or currents representing these profiles can be obtained readily from a process controller.

This system uses a commercial two-channel process controller. The output voltage in each channel is independently programed as a sequence of constant values and linear increases or decreases. One channel is programed to supply the control voltage for the speed-control circuitry while the other channel supplies the control voltage for the temperature control. Once the growth-initiation sequence is stored in the two channels of the controller it can be called forth at the touch of a button.

After crystal growth has been initiated, a local nonprogramable automatic or manual control circuit takes over. To make a smooth transition to local control, it is necessary to set the control voltages in the local controller to those of the programable controller at the time of transition. This is done manually with the aid of simple interface circuits.

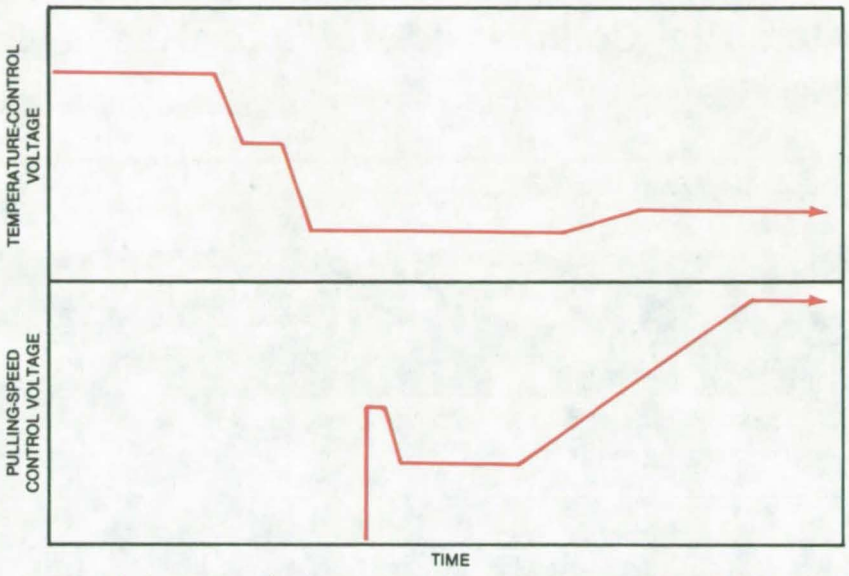

Control Signals for starting sheet-crystal growth consist of ramps (during which a signal changes linearly from one value to another over a preset time interval) and soaks (during which a signal remains constant). The ramps and soaks for the best temperature and pulling speed are determined by experimentation.

This work was done by J. P. McHugh of Westinghouse Electric Corp. for **NASA's Jet Propulsion Laboratory.** *For further information, Circle 185 on the TSP Request Card.*
NPO-15919

Growing Single-Crystal Sheets by Controlled Cooling

Immersed heating and cooling elements would establish the desired temperature gradients.

NASA's Jet Propulsion Laboratory, Pasadena, California

The conventional Czochralski method of pulling a crystal from a melt of its own composition that is encapsulated by a layer of molten boric oxide may produce crystal defects because of extreme temperature gradients occurring during the growth cycle.

A proposed method envisions the use of a high-pressure, Czochralski crystal-growth apparatus as is presently employed to grow gallium arsenide and gallium phosphide but modified to accept deep crucibles so that deep layers of encapsulant can be used, plus X-ray or an optical or sonic-imaging system to observe the growth of the crystal submerged in the encapsulant.

Temperature sensors and heating or cooling elements with closed-loop temperature controls are ordinarily part of the crystal-growth system for maintaining the proper melt temperature. Similar temperature controls attached to submersible elements in the encapsulating fluid would tailor the thermal gradients in the growing crystal. A proper distribution of heating and cooling elements in the encapsulating liquid could also roughly impose a preferred shape on the growing ingot.

The proposed method would be especially applicable to the horizontal growth of ribbons of compound semiconductors. The growth would be at the interface of the melt and an upper encapsulating liquid and would be controlled by cooling of the upper liquid. Seeding through the upper encapsulating liquid induces the sheet to grow as a single crystal, and continuous pulling grows long ribbons. The same advantages accrue as in the Czochralski growth, but the process is more material-efficient and the product is in a ready-to-use form.

This method is expected to reduce crystal defects and loss of one of the crystal constituents by selective vaporization until the crystal has cooled and become stable.

This work was done by Andrew D. Morrison of Caltech for **NASA's Jet Propulsion Laboratory.** *For further information, Circle 186 on the TSP Request Card.*

This invention is owned by NASA, and a patent application has been filed. Inquiries concerning nonexclusive or exclusive license for its commercial development should be addressed to the Patent Counsel, NASA Resident Office-JPL [see page A5]. Refer to NPO-15800 and NPO-15827.

Interstitial Collimating Holes for Gas-Levitation Microfurnace

Spaces between small rods direct gas flow.

Marshall Space Flight Center, Alabama

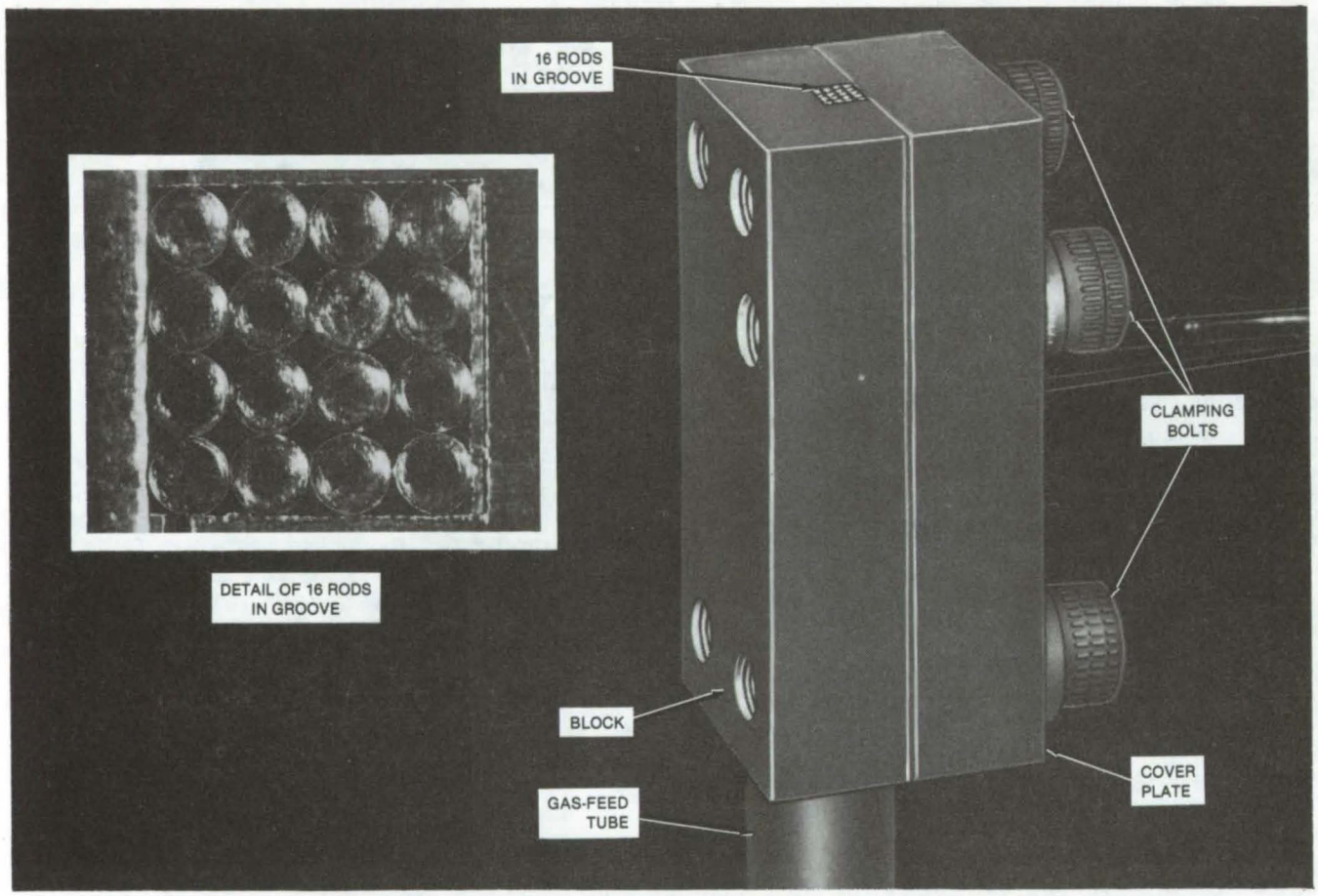

Figure 1. **Wires or Thin Rods Are Clamped** in a square array in a precise, square groove. The spaces between the wires are long, thin, parallel channels that direct the flow of gas.

The flow-collimating head for a gas-levitating microfurnace is fabricated by a precise yet relatively inexpensive method. The head straightens the flow of gas and renders it laminar by directing it along the spaces between thin, parallel, packed rods or wires.

For stable levitation, parallel collimating holes must have small diameters and length-to-diameter ratios of 10 or more. Most small-hole-forming techniques are either too expensive in small production quantities or else limited to length-to-diameter ratios of about 3, as in the case of drilling. Most techniques provide round holes, but the holes do not have to be round to straighten the flow.

In the new technique, a block is milled to form a square-cross-section groove of the size required for the tight square-array packing of the rods or wires. In this case, 16 rods of 0.020-in. (0.51-mm) diameter and 1/2-in. (13-mm) length are used. After being cut to length and deburred, the rods are laid in the groove so that one end is flush with an end of the block. A cover plate is bolted on the side to enclose the groove and clamp the rods in place. A tube is attached to the block to feed the gas to the plenum on the inside ends of the rods. The completed head is shown in Figure 1.

The effective diameter of an interstitial space is about half the wire diameter. With the dimensions cited above, this gives an effective length-to-diameter ratio of 50. Such a high ratio results in a well-formed laminar flow that contributes to stable levitation (see Figure 2).

The technique is clearly applicable to a wide variety of array dimensions, array shapes, and hole sizes. The principal advantage is that it enables the fabrication of arrays of high-length-to-diameter-ratio holes with ordinary machine-shop equipment. With little additional effort, the

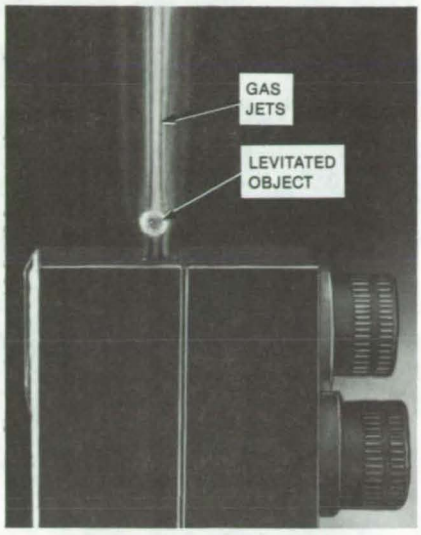

Figure 2. A **Small Spheroid Is Levitated** by the flow of gas out of the collimating head.

technique can be extended to such hard-to-machine refractory metals as tungsten and molybdenum.

This work was done by Stanley A. Dunn, Elmer G. Paquette, E. C. Ethridge, and J. L. Johnson of Bjorksten Research Laboratories, Inc., for **Marshall Space Flight Center.** *No further documentation is available.*

This invention is owned by NASA, and a patent application has been filed. Inquiries concerning nonexclusive or exclusive license for its commercial development should be addressed to the Patent Counsel, Marshall Space Flight Center [see page A5]. Refer to MFS-25829.

Off-Resonance Acoustic Levitation Without Rotation

Orthogonal acoustic-levitation modes are excited at slightly different frequencies to control rotation.

NASA's Jet Propulsion Laboratory, Pasadena, California

Laboratory tests have demonstrated that the rotation of an object in a square-cross-section acoustic-levitation chamber is stopped by detuning the two orthogonal (x and y) excitation drivers in the plane of the square cross section. The detuning can be done using the fundamental degenerate modes or the odd harmonic modes.

When the acoustic levitating field includes two orthogonal modes at the same frequency, the levitated object rotates at a rate dependent on the local phase shift between the two modes. The high temperatures necessary for some applications can introduce uncontrolled phase shifts in the x and y acoustic waveguides, causing uncontrolled rotation. The off-resonance method eliminates unwanted rotation and allows controlled rotation when desired.

To suppress the circulating acoustic field that causes rotation, the x and y driving frequencies must be separated. Since the x- and y-mode resonance frequencies are the same (or nearly the same), this means that either or both acoustic drivers must be operated away

(continued on next page)

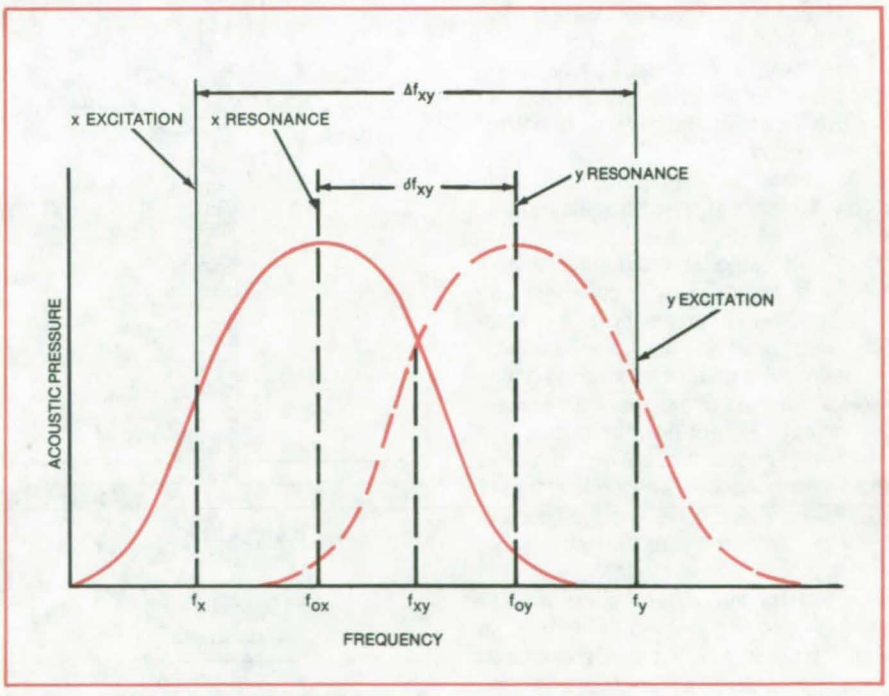

These **Resonance Curves** illustrate the principle of operation for x- and y-axis acoustic modes having nearly the same fundamental resonance frequencies. The x mode is excited at a frequency slightly below that of the x resonance, and the y mode is excited an equal amount above the frequency of the y resonance.

from the resonance frequency. The problem is, therefore, to operate with enough frequency difference to stop rotation but close enough to resonance so that adequate acoustic pressure is generated in the chamber.

The imperfect construction of the apparatus can be exploited to permit off-resonance operation closer to resonance than would be possible with a perfect chamber. The x and y resonance frequencies of a typical square-cross-section chamber differ by a few hertz. Suppose, for example, that the fundamental x and y resonance frequencies differ by δf_{xy} and that the desired excitation frequency separation is Δf_{xy} (see figure). The frequency of the y oscillator is raised by $\Delta f_{xy}/2$ while that of the x oscillator is lowered by $\Delta f_{xy}/2$ from the central frequency f_{xy}. Even though the modes then differ in frequency by Δf_{xy}, they are both $\delta f_{xy}/2$ closer to resonance than they would be if they had the same resonance frequency.

It is possible to apply the same principle to operation at frequencies near odd harmonics of the two modes and to take advantage of acoustically generated harmonics. For example, a large resonance-peak frequency separation δf_{x3y} may be attainable in a given system when the fundamental x and the third-harmonic y modes are employed.

The principle was demonstrated with a levitated foamed-polystyrene ball. Rotation was stopped by raising the x driving frequency and lowering the y driving frequency by 12 Hz each in a system with resonant frequencies of 1,138.6 and 1,137 Hz, respectively. The frequency shifts needed to stop rotation corresponded to about the half-power points of the acoustic-pressure-versus-frequency resonance curves.

This work was done by Martin B. Barmatz and James L. Allen of Caltech for **NASA's Jet Propulsion Laboratory.** *For further information, Circle 187 on the TSP Request Card.*
NPO-15634

Sonic-Pump Levitator

An audiospeaker drives the gas and rapidly responds to corrective signals.

Marshall Space Flight Center, Alabama

A pressure transducer for a gas levitator responds rapidly to computer-generated corrective signals to position a levitated object accurately for containerless processing. The levitating gas is driven by an audiospeaker. The speaker intensity, and hence the height of levitation, is controlled by adjusting the power to the speaker. Speaker response time is on the order of a tenth of a millisecond.

As shown in the figure, the transducer, which is termed "a sonic pump," consists of an audiospeaker sealed to a plate perforated at the center with a tubular duct that leads to columnar outlets. The speaker drives the array of outlets with sinusoidal or other periodic pressure to behave as a rectifying or unidirectional fluid pump that can levitate an object. Except in the region immediately above the outlets, the flow from the transducer is essentially free of return and intake flows and the flow stability is comparable to that obtainable with a steady flow of levitating gas.

In general, the power requirements to produce the same levitation increases with the volume of the space enclosed over the speaker cone. The enclosed space between the outlets and the speaker thermally insulates the speaker from the rest of the levitator so that off-the-shelf speakers can be used safely in high-temperature levitating conditions.

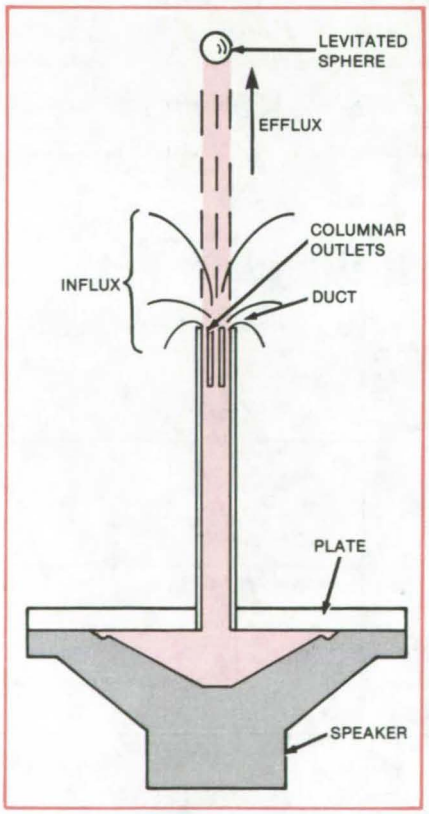

An **Audiospeaker** drives the gas through the plate opening and columnar outlets to levitate the sphere. The exhaust flow is dominated by the gas momentum and is essentially parallel to the axis of the outlets.

In tests, a prototype sonic pump, which contained a 4-inch (10-cm) 10-watt speaker, stably levitated a 600-micron solid-glass sphere. The face of the speaker was covered with a flat steel plate one-eighth inch (3.2 mm) in thickness, through the center of which connection to the gas outlets was made by a brass tube one-fourth inch (6.4 mm) in diameter and 2.75 inches (7.0 cm) long. Levitation often could be initiated simply by raising the intensity of the sound signal. For lateral-displacement control, six 1-1/2-inch (3.8-cm) 0.1-watt speakers also were tested successfully. With appropriate scaling up of the hardware, the sonic pump could function as a levitator for containerless processing of more massive specimens of higher densities and of different materials.

This work was done by Stanley A. Dunn, Alan R. Pomplun, E. C. Ethridge, and J. L. Johnson, of Bjorksten Research Laboratories, Inc., for **Marshall Space Flight Center.** *For further information, Circle 188 on the TSP Request Card.*

This invention is owned by NASA, and a patent application has been filed. Inquiries concerning nonexclusive or exclusive license for its commercial development should be addressed to the Patent Counsel, Marshall Space Flight Center [see page A5]. Refer to MFS-25828.

In Situ Composite Fastener

Fasteners are installed prior to curing.

Langley Research Center, Hampton, Virginia

The in situ composite fastener provides a low-cost alternative method of point fastening composite components. It would be used in lieu of mechanical fasteners or stitching.

When composite components are fabricated, the stiffeners are usually co-cured or secondarily bonded to the skin. Because the bond integrity between stiffener and skin is uncertain, mechanical fasteners or stitching with thread are used to provide additional strength. Another recently developed technique, called tufting, injects a fiber tow or yarn through the thickness of the laminate that, when cured, results in a three-dimensional weave. Mechanical fasteners are expensive, require specification and inventory, and are costly to install. Stitching becomes questionable when considering large, built-up structures, such as stiffened aircraft-fuselage sections.

The in situ composite fastener can be a polymeric, graphite, glass, or metallic thread; a pin; or a staple (see figure). The selected fastener is pressed through the thickness of the composite component while the composite is in the prepreg or B-stage state. This is a distinct advantage over conventional fastening techniques in that the parts are not removed from the mold to install a fastener. Since the parts are not yet cured, local damage as a result of fastener installation is minimized. If a fastener is incorrectly located, it can be removed and another one installed with minimum damage. Once each component is fastened and cured, the in situ fastener becomes an integral part of the structure without cut fibers or abrupt load-transfer discontinuity. Fastening pattern, tensile strength, fastener diameter, and load-transfer efficiency are factors influencing the required fastener strength.

This technique can be used around cutouts to prevent the free edges from delaminating. As with stitching, the in situ composite fasteners can be installed over areas that are highly susceptible to low-energy impact damage to reduce impact-precipitated failures. The in situ composite fastener provides a variety of pattern possibilities not available with other inexpensive application methods. In addition, it is anticipated that its application to large structures can be readily automated.

Results of lap-shear tests employing different in situ fasteners have shown a 20- to 45-percent improvement in lap-shear strength. Further tests are being conducted to expand this data base. Selected fastening concepts will undergo further evaluation through stiffened-shear-panel tests.

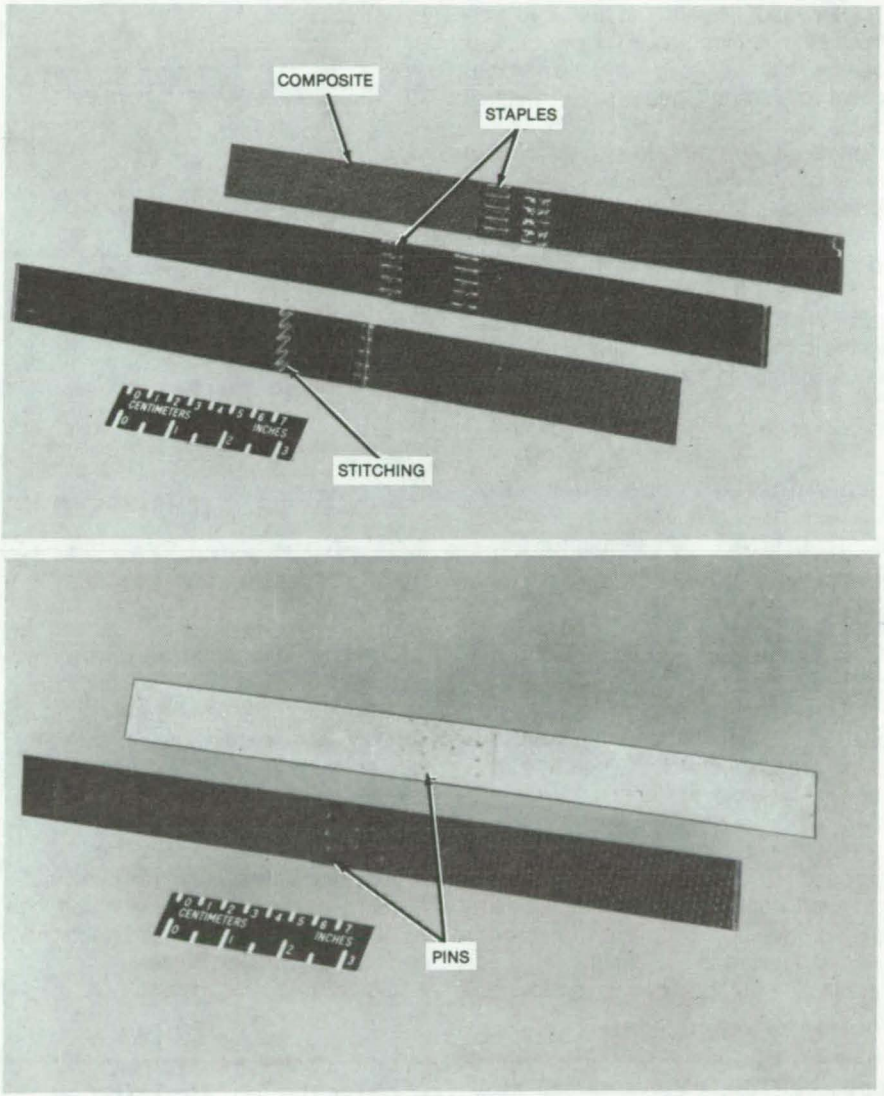

Fasteners may vary from simple pins and staples to more-complex box weaves and other appropriate patterns.

This work was done by William T. Freeman, Jr., and William S. Jones of **Langley Research Center** *and Gary L. Farley of the U.S. Army Aviation Research and Development Command. No further documentation is available.*

This invention is owned by NASA, and a patent application has been filed. Inquiries concerning nonexclusive or exclusive license for its commercial development should be addressed to the Patent Counsel, Langley Research Center [see page A5]. Refer to LAR-12939

Repairing Damaged Power-Cable Insulation

Simple method saves time, money, and material.

John F. Kennedy Space Center, Florida

Damaged insulation at bulkhead terminations of underground power cables can be repaired inexpensively while the cable remains in place. Using standard cable-splicing and cable-termination techniques, the method results in new terminations with a safety factor equal to that of any portion of the cable.

Cable-insulation failures resulting in electrical breakdown at terminations can occur if the insulation is damaged by heat during formation of a wipe joint in the cable sheath. Whereas the previous solution in such cases was to replace the entire section of cable, in the new method, the cable remains in place while new insulation is applied to the damaged portion. Unless the conductors are damaged with pits or peaks from high arcing, the new method gives a completely satisfactory repair.

A typical three-conductor power-cable bulkhead termination with an insulation failure is shown in Figure 1. To begin the repair, the new ferrule is cut to the size of the new lead sleeve to be applied (see Figure 2); and the bulkhead wires are disconnected when it is dismantled. The old ferrule and sheath are then removed along a sufficient length of cable until undamaged insulation is exposed. The damaged insulation is removed from the conductors. New insulation (oil-packed varnish cambric tape) is applied to the conductors, and termination compound is used to fill the void. The repaired cable section is covered with the new lead sleeve. The sleeve is then finished to the cable sheath and to the ferrule according to factory specifications, using standard lead solder wipes. The lead sleeve, new ferrule, insulation paper, and termination compound could be sold in kits suited for the various cable sizes.

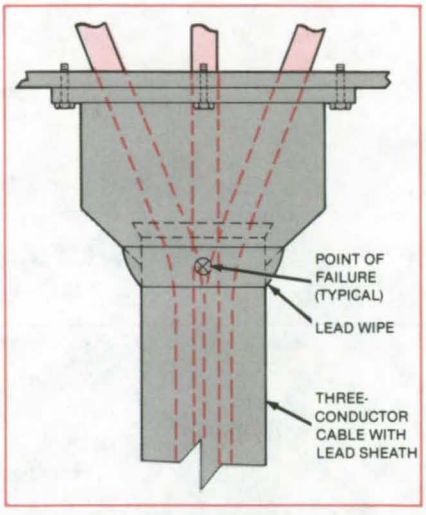

Figure 1. The insulation in a **Bulkhead Power-Cable Termination** can fail in the vicinity of the lead solder wipe.

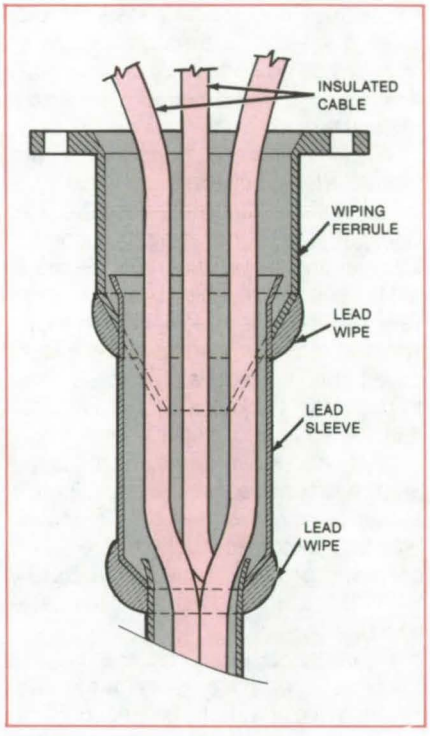

Figure 2. **Repair of the Cable Termination** includes the installation of new insulation, a void-filling compound, a new sleeve, and a new wiping ferrule. The new joint is finished with a standard lead solder wipe.

This work was done by Grover E. Baker of Boeing Services International for **Kennedy Space Center.** *No further documentation is available.*
KSC-11206

Growing Crystals for Infrared Detectors

Unidirectional solidification yields bulk crystals with compositional homogeneity.

Marshall Space Flight Center, Alabama

A new process produces $Hg_{1-x}Cd_xTe$ ingots with radial compositional homogeneity suitable for fabricating infrared detectors. The process which uses a stationary growth ampoule and a furnace that moves in one direction, is expected to be useful for the crystal growth of other materials with similar thermophysical properties.

The $Hg_{1-x}Cd_xTe$ ($0 \leq x \leq 1$) alloy system is preferred for many infrared applications because its properties are uniquely suited to both the detection of infrared radiation and the requirements for fabricating junction devices. HgTe and CdTe are completely miscible in all proportions and form a direct band-gap semiconductor alloy system for which the energy band gap increases approximately linearly from -0.3 to 1.6 eV as the mole fraction of CdTe increases

from 0 to 1. Consequently, the spectral response of HgCdTe can be compositionally tuned between 0.8 and 50 μm to tailor a detector for maximum performance at a given wavelength. However, segregation during solidification, high volatility of one of the components, and strain fields associated with large temperature gradients make the preparation of homogeneous, high-quality, bulk crystals of $Hg_{1-x}Cd_xTe$ very difficult using conventional methods.

In the new process the $Hg_{1-x}Cd_xTe$ alloys are prepared by reacting 99.9999-percent-pure elemental constituents in sealed, evacuated, fused-quartz tubing. The end of the tubing where solidification begins is tapered to a point to enhance the probability of single-crystal growth. A quartz rod is fused directly to the tapered end of the ampoule to position the ampoule on a quartz pedestal inside the growth furnace. The ampoules are loaded with precisely weighed amounts of Hg, Cd, and Te. Following loading, the ampoules are sealed, and the alloys are cast in a rocking furnace.

The precast alloys are regrown by unidirectional solidification (Bridgman-Stockbarger method) in the growth apparatus shown in the figure. The ampoule is initially positioned in the upper zone and remains stationary during the growth process. The furnace assembly travels vertically so that the crystal grows progressively upward from the bottom tapered end of the ampoule.

Separately controlled furnaces are used for the hot (upper) and cold (lower) zones. Each furnace is provided with a heat-pipe isothermal furnace liner to provide two well-defined heated zones. The hot-zone heat pipe is sodium-charged, and the cold-zone heat pipe is either sodium- or mercury-charged, depending on the temperature requirements.

The heat pipes are separated by a heat barrier that must provide the necessary thermal isolation between the heated zones. Within this restriction the barrier thickness is chosen to be as small as possible, typically less than 4 mm, so that the maximum thermal gradient is obtained. The circular opening in the barrier is the minimum sufficient for physical clearance around the ampoule wall. Temperature gradients sufficient to prevent constitutional supercooling in the melt are obtained in all cases.

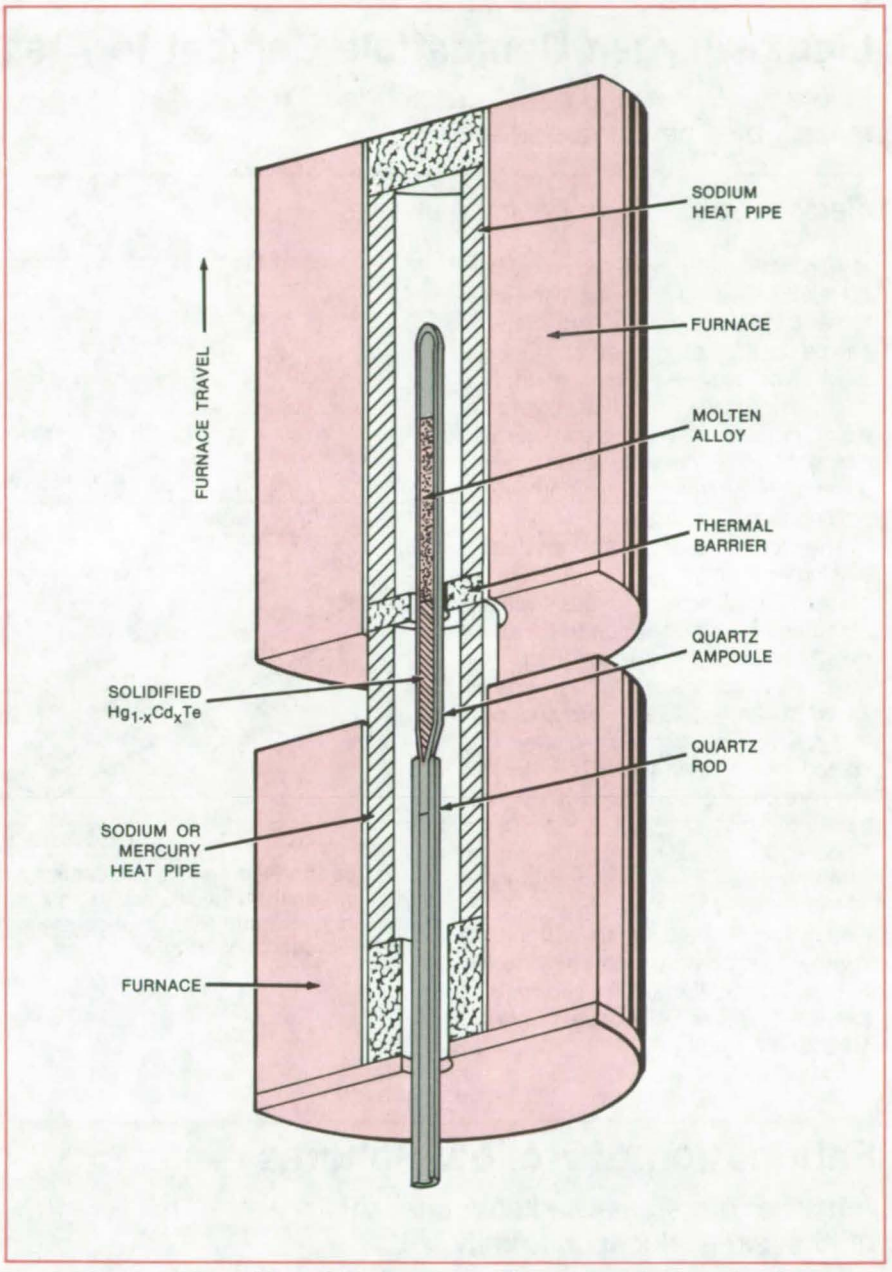

The Unidirectional Crystal-Growth Furnace Assembly travels vertically so that the crystal grows upward from the bottom tapered end of the ampoule. Separately controlled furnaces are used for the hot (upper) and cold (lower) zones.

This work was done by Sandor L. Lehoczky and Frank R. Szofran of McDonnell Douglas Corp. for **Marshall Space Flight Center.** *For further information, Circle 189 on the TSP Request Card.*

This invention is owned by NASA, and a patent application has been filed. Inquiries concerning nonexclusive or exclusive license for its commercial development should be addressed to the Patent Counsel, Marshall Space Flight Center [see page A5]. Refer to MFS-25786.

Liquid-Oxygen-Compatible Cement for Gaskets

Fluoroelastomer and metal are bonded reliably by a new procedure.

Marshall Space Flight Center, Alabama

A procedure using a liquid-oxygen-compatible adhesive bonds Viton elastomer (or equivalent) parts to metal. It can be used to seal gaskets and O-rings, as in its original NASA application, or it might be used to splice layers of elastomer to form non-standard-sized O-rings. Another possible use is to apply a protective, liquid-oxygen-compatible coating to metal parts.

The procedure employs a liquid fluoroelastomer cement [Pelmor PLV2000HS cement (or equivalent)] that is available commercially. The surface to be joined must be clean and roughened. Two coats of adhesive are applied and allowed to air-dry until they are no longer tacky. The pieces are positioned and placed in a vacuum bag (see figure). They are cured at 150° F (66° C) for one-half hour, then at 250° F (121° C) for 7 hours. The pieces remain in a vacuum until they return to room temperature.

This work was done by Norris L. Elmore and Bruce C. Neale of Rockwell International Corp. for **Marshall Space Flight Center.** *For further information, Circle 190 on the TSP Request Card.*
MFS-19797

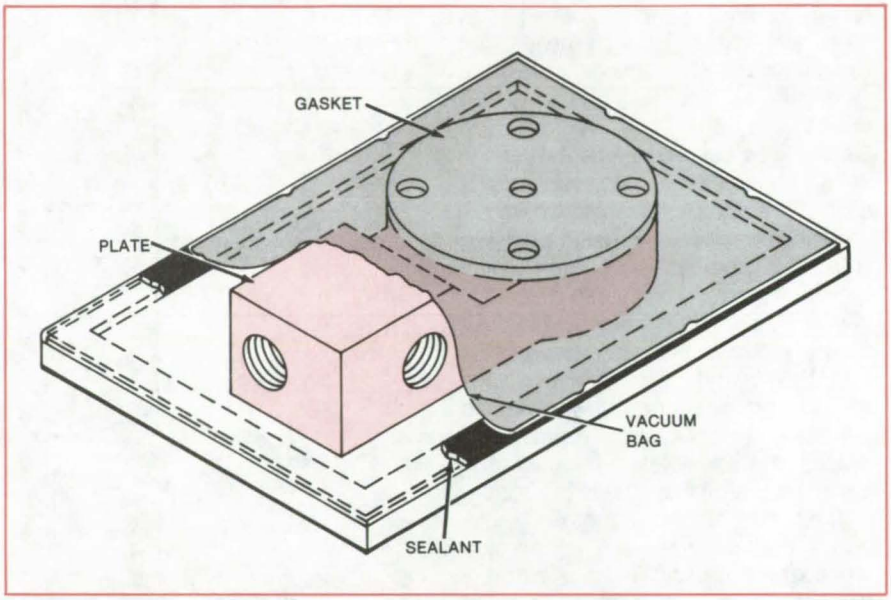

To Cure the Fluoroelastomer Cement, the metal plate/gasket assembly is placed in a vacuum bag that is evacuated to a minimum vacuum of 27 inches (69 cm) of mercury. The vacuum is maintained throughout the heating process and until the assembly returns to ambient room temperature.

Fabrication of Hollow Spheres

A nozzle forms gas-filled spherical shells of high dimensional uniformity.

NASA's Jet Propulsion Laboratory, Pasadena, California

An improved apparatus forms uniform gas-filled spheres. The apparatus contains a nozzle through which a liquid and a gas flow simultaneously, with the liquid becoming the constituent material of the shell wall. The design exploits and optimizes the inherent tendency of a liquid column or filament to breakup into droplets, which are hollow in the present case.

The nozzle shown in the figure includes a reservoir for the liquid, which is molten metal, polymer or the like; and it incorporates an annular opening at the bottom. There, a flow of liquid surrounds the flow of gas and forms a hollow, cylindrical jet. The pressure of the liquid just above the orifice is varied to control the liquid flow velocity, either by changing the liquid height in the container or by varying the pressure of a "blanket" gas above the free surface of the liquid. The flow of the filler gas is adjusted by passing the gas through a restriction, such as a needle valve or a capillary tube.

Shells are formed spontaneously at a predictable rate and with uniform dimensions as the materials issue from the

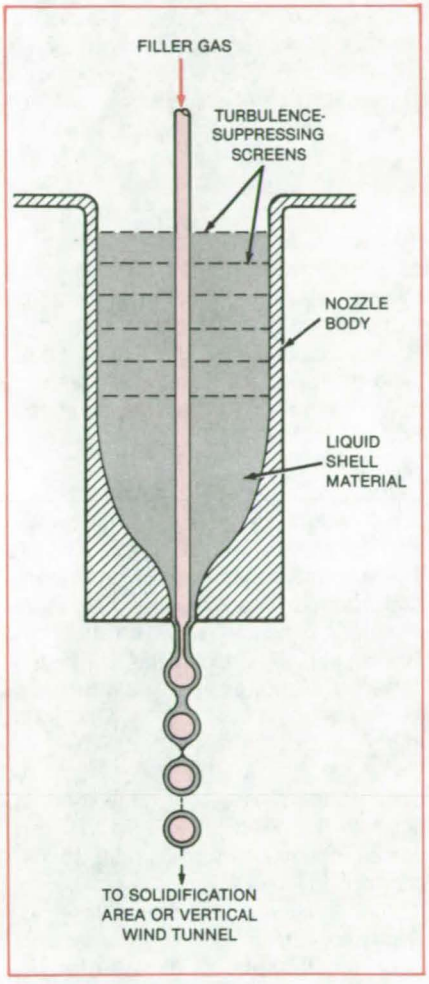

This **Hollow-Sphere Shell Generator** produces gas-filled metal spheres at a rate of about 100 per second with repeatability in all dimensions. The spheres can be filled with gas at a pressure as high as 2,000 psi (13.8 MPa). The process would be well suited for making targets for laser fusion experiments.

nozzle. The surface tension of the liquid causes the hollow gas-filled liquid stream to pinch off. The stream constricts into an all-liquid filament, then breaks altogether, releasing the spheroid below. A new pinching-off cycle then begins in the liquid/gas stream above. Hollow spheroids are thus repeatedly formed at a rate equal to the frequency of the pinching-off oscillations.

Prior to solidification of the liquid, aerodynamic forces on freely falling shells produce a distortion of the exterior surface and a decentering of the interior one. When shells of high precision are required, the nozzle flow is directed downward into a vertical wind tunnel contoured to produce a downward acceleration of air equal to the acceleration of gravity. The spheroid then experiences no relative air motion and no drag, allowing surface tension alone to determine the shape.

Under optimal conditions, neither a crossflow airstream nor any pinchoff mechanism is needed to close off the individual shells, and no leakage of filler gas or loss of liquid occurs. The liquid must be of a material that solidifies rapidly, such as by freezing or by chemical reaction, during the fall.

The outer diameter of a shell depends principally on the size of the orifice. There is a linear relationship between the two, with the shells being approximately twice the diameter of the nozzle opening. A measure of control of the wall thickness can be exercised by adjusting the annular gap and the liquid pressure.

This work was done by James M. Kendall, Jr., of Caltech for **NASA's Jet Propulsion Laboratory.** *For further information, Circle 191 on the TSP Request Card.*
NPO-15798

Silicon Nitride Antireflection Coatings for Photovoltaic Cells

Antireflection coatings that increase the efficiency of silicon solar cells are formed by the plasma-enhanced chemical-vapor deposition of silicon nitride coatings. The silicon nitride is deposited in layers, the refractive index of which decreases with distance away from the cell/coating interface. The changing index of refraction allows adjustment of the spectral transmittance for the wavelengths at which the cell is most efficient. The average conversion efficiency of solar cells was increased from 8.84 to 12.63 percent.
(See page 55.)

Air Guide for Sheet-Metal Grinder

A small trough attached to a hand-held grinder directs cooling air from a portion of the motor housing to the grinding wheel and workpiece. It is particularly useful when grinding sheet metal. The cooling air reduces thermal distortion of the workpiece due to localized frictional heating. The flow created by the fanlike action of the rotating motor cools the sheet metal. It thus reduces or eliminates the need to slow down grinding, or temporarily stop grinding, to allow the sheet to cool.
(See page 111.)

Books and Reports

These reports, studies, and handbooks are available from NASA as Technical Support Packages (TSP's) when a Request Card number is cited; otherwise they are available from the National Technical Information Service.

Interface Instability During Crystal Growth

Nonequilibrium effects are examined.

The final report on a study of solute segregation and interface stability during crystal growth describes a new theoretical model for crystal growth from a melt. The report also describes experiments in crystal growth by controlled-gradient freezing and by pulling from the melt (Czochralski growth).

The theoretical model introduces a new interface-field term to account for previously-neglected chemical and physical phenomena in the vicinity of the growth interface. This term is particularly important in calculating the change in chemical potential due to variations in local molecular configurations with position relative to that of the interface: The chemical potential of an atom in the interface region is different from the potential in either the bulk solute or the bulk liquid phase and is affected not only by spatial variations in chemical composition but also by local inhomogeneities in stress, electrostatic poten-

(continued on next page)

tial, and magnetic potential. As a result, the stability of the growth interface is affected, and the spatial distribution of the solute or solutes involves concentrations markedly different from the equilibrium values.

The experimental portion of the study focuses on $CsCdCl_3$ as the material of choice for study since it can be crystallized by the Czochralski method or by gradient freezing, and its melting point is low enough to permit direct visual observation of crystal growth. The material was doped with $CoCl_2$ for solute-redistribution studies. The liquidus slope, specific heat, heat of fusion, density, and viscosity were measured to test the theory experimentally for the interface stability of $CsCd_{1-x}Co_xCl_3$. An attempt to measure thermal diffusivity did not succeed.

The density or distribution of the cobalt doping in liquid and solid $CsCd_{1-x}Co_xCl_3$ was measured via the absorption of light from a 10-mW He/Ne laser. The absorption-versus-density calibration was done with samples having known values of x. Distribution data differed greatly, depending on whether crystals were grown by gradient freezing or pulling from the melt. This indicates that in either one or both cases, there is a large difference from equilibrium.

Studies of interface shape and the breakdown of stable growth revealed a sensitivity of the interface curvature to the cobalt concentration in the liquid. This effect has been neglected in previous studies and is believed to be due to radiation absorption in the liquid.

This work was done by W. A. Tiller, R. S. Feigelson, and Dennis Elwell of Stanford University for **Marshall Space Flight Center.** *To obtain a copy of the report, "Direct Observation of Interface Instability During Crystal Growth," Circle 192 on the TSP Request Card.*
MFS-25841

Erectable Space-Construction Fixture

A computer-controlled fixture would be deployed on the Space Shuttle to manufacture structures.

A concept for an erectable space-construction fixture is described in a report that is now available. The proposed fixture would combine all the equipment required for construction of the framework for a space platform into a single compact work station. Almost all aspects of assembly and fabrication would be automated. During use the fixture would be deployed from the Space Shuttle. The astronauts' role would be to monitor the machine and perform functions beyond its capability.

The fixture would employ a beam fabrication machine to construct triangular lightweight truss members. It would also move the fabrication machine to three positions on a yoke for truss fabrication. The fixture would also automatically install cross-bracing cables and data and power cables. In addition, it would move the completed platform members to their final positions. After forming joints, the fixture would proof-load them to verify sound construction.

The fixture would comprise a basic fabrication and assembly fixture with yoke and roller supports which would grip beams after they were fabricated and cut from the beam-building machine. Centrally located in the yoke would be a removable cross-bridge with a rotating head, which would accept several construction devices, including a beam builder and an extra-vehicular-activity work station.

The rotating-head concept makes minimal electrical power demands for illumination and TV services while maximizing use of the Shuttle remote-manipulating system for handling and installing components. The fixture would be largely automated and would be controlled remotely by astronauts in the Space Shuttle or in other support spacecraft.

The major item of removable equipment would be the central cross-structure/rotary-head complex, to which the beam positioner, the wire-laying reel, and the astronaut-maneuvering arm with "cherry picker" would be attached. The station would have solar arrays and batteries for power and would function as an active satellite controllable from the ground.

Design goals for the fixture would include platform assembly in the shortest possible time and minimizing fuel and power requirements of support spacecraft.

This work was done by Russell R. Thompson of Rockwell International Corp. for **Johnson Space Center.** *To obtain a copy of the report, Circle 193 on the TSP Request Card.*

Inquiries concerning rights for the commercial use of the technology described in this report should be addressed to the Patent Counsel, Johnson Space Center [see page A5]. Refer to MSC-20259

MiniBriefs describe NASA innovations and reports in an abbreviated format. Readers desiring additional information on these items should request the Technical Support Packages (TSP's), available in most cases, which can be obtained by using the TSP Request Card at the back of this issue.

Rapid Circuit Breadboarding

The cost of a one-of-a-kind circuit board would be reduced.

One-of-a-kind circuits can be assembled quickly by using a prototyping board (Protoboard, or equivalent) in conjunction with a copper-clad circuit board that has the same hole pattern. The circuit board would be placed over the prototyping board before any electronic components or wires are inserted. After testing and verification of the circuit, the circuit board would be lifted with the components remaining in place. With a retainer placed over the components, the board would then be inverted and the components soldered in place. Thus, the need for removal and reinsertion of the electronic components is avoided.

This work was done by Edwin C. Ethridge of **Marshall Space Flight Center.** *No further documentation is available.*

Inquiries concerning rights for the commercial use of this invention should be addressed to the Patent Counsel, Marshall Space Flight Center [see page A5]. Refer to MFS-25761.

Improved Silicon-Growth Chamber

Improvements include a better transport mechanism and a better trough heater.

A silicon-growth technique, based on coating ceramic substrates with a thin layer of molten silicon that solidifies to form a polycrystalline film, was modified to produce solar-cell quality silicon sheet.

The modification includes a new transport mechanism that uses a series of graphite rollers to move the substrate in and out of the coating chamber, and a longer trough heater. Coatings 300 μm thick were produced at pull speeds of 0.25 cm/s. Cells fabricated from these sheets reached photovoltaic conversion efficiencies up to 9.7 percent on 5 cm^2 cells.

This work was done by J. Don Heaps and J. David Zook of Honeywell, Inc., for **NASA's Jet Propulsion Laboratory.** *For further information, Circle 194 on the TSP Request Card.*
NPO-15237

Growing Single Crystals From Low-Purity Silicon

The heat exchanger method continuously moves impurities to the outside of the growth interface.

Large single crystals of silicon can be grown from inexpensive metallurgical-grade silicon (i.e., purity of 98 to 99 percent) by the heat exchanger method. In this method, the silicon is heated in a crucible to above its melting point, and the melted silicon is then solidified by extracting heat from the bottom of the crucible by means of a heat exchanger. As solidification proceeds, the impurities are pushed out in front of the solid/liquid interface, so they end up in the last region to solidify — that is, at the upper surface and at the crucible walls. These exterior surfaces are easily cropped off, leaving a large single crystal. Solar cells with efficiencies greater than 12 percent have been made from crystals grown by the heat exchanger method.

This work was done by Frederick Schmid of Crystal Systems, Inc., for **NASA's Jet Propulsion Laboratory.** *For further information, Circle 195 on the TSP Request Card.*
NPO-15538

Melt-Level Sensing in Silicon-Web Growth

The shift of a laser beam reflected from the melt surface is sensed by a position detector.

A laser beam is reflected from a silicon-melt surface onto a position detector to monitor melt level during web growth. With this method, silicon-web production could be increased by synchronizing silicon melt replenishment with the web growth rate.

The light beam is directed at an angle of about 45° onto the melt surface from which it is reflected through a lens onto a commercial solid-state position detector. The vertical movement of the melt level produces a shift of the light-beam position, which is sensed by the position detector. Sensing the level of a silicon melt with a laser beam has been used previously for continuous Czochralski growth of silicon ribbon.

This work was done by Charles S. Duncan, Marie E. Skutch, and Kennith B. Steinbruegge of Westinghouse Electric Corp. for **NASA's Jet Propulsion Laboratory.** *For further information, Circle 196 on the TSP Request Card.*
NPO-15356

Proposed Technique of Crystal-Ribbon Growth

Two filaments protruding from a silicon melt would guide sheet growth.

In a proposed technique for silicon-crystal-ribbon growth from a crucible, two inert wettable filaments are dipped into a silicon melt to guide the growth of the silicon sheet. The filaments are clamped in place and tilted slightly away from each other, and a seed ribbon is lowered into contact with the melt to establish menisci between the filaments.

Ribbon thickness is controlled by conventional edge-supported pulling and cooling, which would complete the ribbon growth, with attention given to melt replenishment and the control of melt level.

Alternatively, two permanent guide filaments could be welded to the bottom of the crucible, or two inert wettable sheets could be attached to the crucible walls with their tops protruding from the melt surface.

This work was done by Jay W. Thornhill of Caltech for **NASA's Jet Propulsion Laboratory.** *For further information, Circle 197 on the TSP Request Card.*

This invention is owned by NASA, and a patent application has been filed. Inquiries concerning nonexclusive or exclusive license for its commercial development should be addressed to the Patent Counsel, NASA Resident Office-JPL [see page A5]. Refer to NPO-15629.

Shield Boosts Silicon-Growth Rate

Simple device aids removal of heat from solidified crystal and retention of heat in the melt.

A radiation shield permits faster growth — by 20 percent — of single-crystal silicon from molten silicon by producing sharper thermal gradients near the growth front. The shield therefore reduces the cost of growing silicon for solar cells and other components.

The shield is a smooth cone-shaped sheet of molybdenum, polished to increase its reflectivity. The smaller opening of the cone is positioned near the melt surface. The cone reflects heat radiation from the crucible wall into the melt, maintaining the temperature of the melt and preventing it from cooling and from thereby creating unwanted crystals. Heat from the solidifying material is reflected upward and away, thereby cooling the solid and allowing it to be withdrawn more rapidly.

This work was done by R. L. Lane of Kayex Corp. for Caltech and ***NASA's Jet Propulsion Laboratory.*** *For further information, Circle 198 on the TSP Request Card.*
NPO-16049

Low-Cost GaAs Solar Cells

A silicon substrate lowers cost and increases efficiency.

A single-crystal gallium arsenide (GaAs) solar cell can be produced at greatly reduced cost by replacing the GaAs wafer substrate with a silicon substrate. These GaAs solar cells can be more effective than Si solar cells in hybrid photovoltaic/thermal systems

with operating temperatures as high as 200° C. The increased efficiency and decreased mass of these cells results in a smaller solar array for a given power output and reduces the required supporting structures.

Germanium or a silicon/germanium alloy interlayer is deposited on the silicon substrate. A recrystallization process is used on this surface to produce a high-quality surface upon which the GaAs crystal will be grown. This growth can be accomplished by vapor deposition. These GaAs layers can then be processed into solar cells.

This work was done by Richard J. Stirn and John Scott-Monck of Caltech for **NASA's Jet Propulsion Laboratory.** *For further information, Circle 199 on the TSP Request Card.*

Inquiries concerning rights for the commercial use of this invention should be addressed to the Patent Counsel, NASA Resident Office-JPL [see page A5]. Refer to NPO-14914 and NPO-14931.

Preventing Moisture Damage To Solar Panels

A proposed encapsulant would dissociate water into gas.

Encapsuating photovoltaic solar cells with a polysulfonated membrane would prevent moisture damage to the cells. The membrane would prevent retention of moisture on the solar panels by dissociating any moisture into gaseous hydrogen and oxygen. The gases would escape through vents before damage can occur.

The membrane dissociates water when an electrical potential is applied to opposite faces of the membrane. This potential is available from the panel itself as long as the solar cells are irradiated. In darkness, the electrical potential for the membrane can be supplied by an alternate source.

This work was done by Eric G. Laue of Caltech for **NASA's Jet Propulsion Laboratory.** *For further information, Circle 200 on the TSP Request Card.*
NPO-15481

Quenching Alloys in Containerless Processing

Gas quenching would be combined with magnetic levitation.

Magnetic levitation and gas quenching are combined in a proposed method to melt and rapidly solidify alloys without contacting the container walls. This containerless-processing method would reduce contamination during the production of high-purity alloys and could, because of rapid cooling, produce alloys with fine-grain structure and possibly glassy structures. This method could be used to develop new carbides for drill bits, high-strength high-ductility structured steels, and new high-strength superplastic alloys.

In the method, an alloy 3 to 4 mm in diameter is melted in a miniature magnetic coil. Argon or another low-heat-conducting gas suppresses electrical breakdown and vaporization. When the valve opens on the helium or hydrogen quench gas, the pressure within the housing quickly rises from 25 torr (0.3×10^4 N/m^2) to about 400 torr (5.3×10^4 N/m^2) to rapidly cool the sample.

This work was done by William A. Oran of **Marshall Space Flight Center.** *For further information, Circle 201 on the TSP Request Card.*

This invention is owned by NASA, and a patent application has been filed. Inquiries concerning nonexclusive or exclusive license for its commercial development should be addressed to the Patent Counsel, Marshall Space Flight Center [see page A5]. Refer to MFS-25305.

Containerless-Processing Module

Specimens are melted, manipulated, and solidified without contact.

A proposal is made for a high-temperature, containerless-processing module that positions and melts molten glass or metal without contact with the container wall. The fluid masses are manipulated, stirred, and controlled by acoustic forces. The module provides photographic monitoring and transfer of the solidified specimens to storage bins.

The module heats specimens to temperatures up to 1,450° C. Samples between 0.5 and 2.5 centimeters in diameter can be accommodated. It can provide atmospheres of nitrogen, carbon dioxide, argon, or helium for experiments. The module consists of 12 subsystems: experiment chamber, sample handler, electronics, servomechanism, thermal control, acoustic manipulation, optical sensors and sources, spot heating, mechanical unit, bubble injection, instrumentation, and data-management hardware.

This work was done by Taylor G. Wang, Martin B. Barmatz, Frederick R. Chamberlain, Melvin A. Hagan, Richard C. Heyser, Harvey H. Horiuchi, James H. Kurashita, Jaroslav K. Lamgmaier, Robert L. Robinson, Ronald P. Salazar, and Charles L. Youngberg of Caltech for **NASA's Jet Propulsion Laboratory.** *For further information, Circle 202 on the TSP Request Card.*
NPO-14932

Value-Engineering Review for Numerical Control

A systematic value-engineering review can increase production efficiency.

When selecting parts for conversion from conventional machining to numerical control, a value-engineering review can be performed for every part to identify potential changes to the part design that will result in increased production efficiency. Any item considered for conversion to numerical control can be subjected to a value-engineering review. This approach has been used with success by production engineers for the Space Shuttle.

This work was done by Jerry L. Warner of Rockwell International Corp. for **Marshall Space Flight Center.** *No further documentation is available.*
MFS-19664

Checking Weld Composition

Inconel® 718 alloy welds are tested for the presence of filler metals.

Electrolytic etching can determine whether certain iron/nickel alloys are welded with sufficient quantities of the desired filler metal. For Inconel® 718 alloy, weld beads are abrasively cleaned and then electrolytically etched with a 15 percent by weight hypophosphite solution for 5 seconds at 20 Vdc. After etching, the operator observes whether a yellowish film has accumulated on the weld. If no yellowish deposit is detected, the filler metal is mostly Inconel® 718 alloy. If the yellow deposit is present, a filler containing tungsten, molybdenum, or cobalt may be present.

(Inconel® is a registered trademark of the Inco family of companies.)

This work was done by Marston D. Robertson and Steven M. Collier of Rockwell International Corp. for **Marshall Space Flight Center.** *For further information, Circle 203 on the TSP Request Card.*
MFS-19628

Adhesive Removal From Protective Clothing

An electric eraser removes butyl cement from protective coveralls.

The protective coveralls worn by handlers of hypergolic propellants often become soiled with butyl cement. Usually this cement is removed using medical tongue depressors as scrapers — a long and tedious procedure.

An efficient alternative is to use a conventional rotary electric eraser. The erasing tip is applied at about 3,600 rpm. The speed of the rotation varies with the pressure applied by the operator. Too much pressure simply stalls the eraser without damaging the fabric. The method can be used to remove other adhesives from different surfaces.

This work was done by D.R. Prather of The Bendix Corp. for **Kennedy Space Center.** *No further documentation is available.*
KSC-11017

Portable Plating System

A 30-gallon system is transported on a mobile cart.

A plating system mounted on a portable cart includes a 30-gallon (23.5-liter) electrolyte tank, a filter pump, heaters, replenishing anodes, plating rectifiers, and a tank rectifier to continuously remove contaminants. A dropout relay in line with the plating rectifiers and the filter pump prevents plating in case of accidental interruptions in the current flow. The previous plating system was not portable. In addition, heater control in that system presented safety hazards.

This work was done by Randolph Flores of Rockwell International Corp. for **Marshall Space Flight Center.** *For further information, Circle 204 on the TSP Request Card.*
MFS-19631

Repairing Defective Welds

Welds are reinforced by electrodeposition.

Welds that cannot be reworked because of their limited accessibility or material-annealing considerations can be reinforced by electrodeposition. The procedure may be of interest for nuclear reactor construction.

A plastic container is placed around the weld area to be repaired and filled with an electrolytic metallic solution. An electrode fitted in the container directs the ionized metal to the area to be plated. The type of plating solution used depends on the parent metal and the structural requirements of the joint.

This work was done by T. Adams of Rockwell International Corp. for **Marshall Space Flight Center.** *For further information, Circle 205 on the TSP Request Card.*

Inquiries concerning rights for the commercial use of this invention should be addressed to the Patent Counsel, Marshall Space Flight Center [see page A5]. Refer to MFS-19618.

Wicking Coating for Heat Pipes

Grooves in a porous coating are produced by flame-spraying over a wire mesh.

A "wicking" for the inside of heat pipes and heat-storage canisters can be formed by flame-spraying a porous coating over a wire mesh placed on the surface to be treated. When the mesh is removed, the wicking remains, consisting of many small channels in the surface coating. The method should be less expensive than permanently spot-welding a wire mesh, the technique currently used. It also can be used on nonmetallic surfaces, whereas spot-welding cannot.

This work was done by Wayne Kent Minnich of General Electric Co. for **NASA's Jet Propulsion Laboratory.** *For further information, Circle 206 on the TSP Request Card.*
NPO-15212

Decoupling a Reflecting Layer From Its Support Structure

Proposed mounting isolates the main support through intermediate flexural supports.

A proposed mounting would decouple the thermal distortions of a reflective surface so that they are not transmitted to the support structure. The reflecting layer consists of aluminum reflecting tiles attached to the support structure by flexural mountings that bend and twist to accommodate the thermal expansion of the tiles.

Each flexural support consists of three components: one attached to the

main support structure, one attached to the reflective tile — both are tangentially stiff and one or both are radially soft — and a support pin that holds the other two components together. There are three flexural supports for each tile. The mounting technique would be useful in microwave-antenna reflectors.

This work was done by Robert M. Bamford of Caltech for **NASA's Jet Propulsion Laboratory.** *For further information, Circle 140 on the TSP Request Card.*
NPO-15346

Sealant Applicator for Fastener Heads

It dispenses sealant, either manually or automatically, in predetermined amounts.

An applicator encapsulates the heads of fasteners with a measured shot of sealant to protect them from corrosive environments. The applicator meters, mixes, and dispenses the sealant. It can be operated manually or automatically and could be operated by a robot. The manner of operation is changed by switches.

The sealant resin and catalyst, initially kept separate, are pumped into a three-inlet valve, passed to a mixer and hose, and then to a gun with a tip customized for the particular fastener-head size and shape. One of the valve inlets is attached to a tank of solvent so that the valve and all downstream components can be flushed.

This work was done by Max H. Sharpe, Charles H. Jackson, Joe D. Lambert, Charles E. Henderson, and William E. Norton of **Marshall Space Flight Center.** *No further documentation is available.*
MFS-25922

Mathematics and Information Sciences

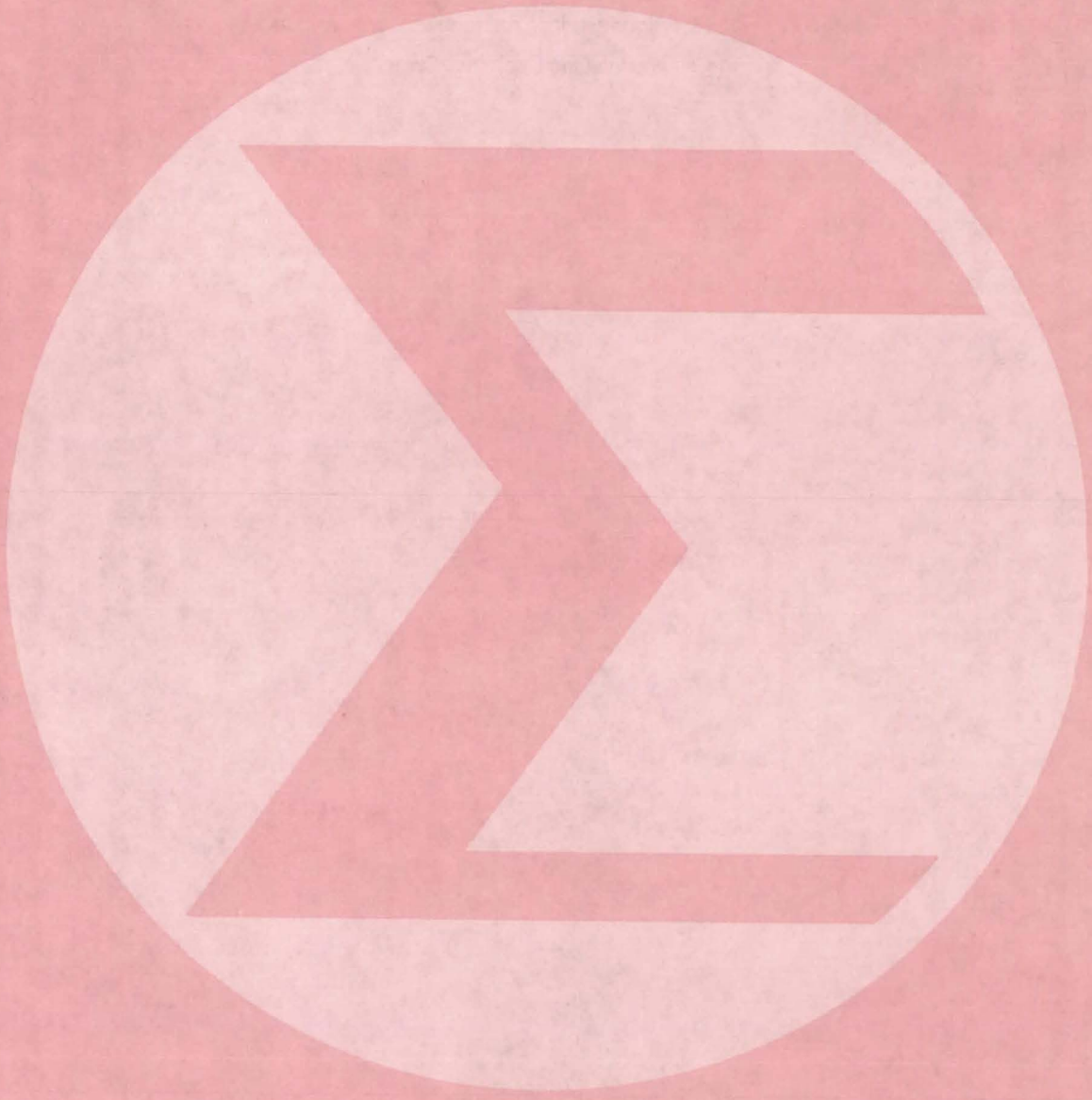

Processing of Synthetic-Aperture-Radar Data

Ambiguous data are combined to permit fast-transform convolution.

NASA's Jet Propulsion Laboratory, Pasadena, California

Range migration in the two-dimensional ensemble of range-correlated synthetic-aperture-radar (SAR) data prevents the direct application of frequency-domain or other fast-transform convolution algorithms. The problem occurs because the successive data traces from targets at a constant slant range are not colinear. Colinearity of the successive translations of the reference vector found in the signal to be processed is an essential requirement for transform domain convolution. Thus, a processor is needed to apply a "steamroller" algorithm to flatten the azimuth-vs.-range migration.

To overcome this problem, a new data processor was designed, such that the two-dimensional ensemble of range-correlated SAR data is stored in memory and extracted in a format for which the azimuth data are colinear. With this new processor, the effect of range migration is removed, and the data have a single one-dimensional linear form, so that they can be subjected to any desired form of fast-transform convolution.

The new method involves the following steps:

1. Condensing R rows of data in one column of memory by addition into one vector (colinear),
2. Multiplying by a transform of a normal correlation function,
3. Inverse transforming,
4. Reprocessing in range, and
5. Detecting.

The data selector successively selects R rows of data for input to the adder. In this manner the slant-range data are combined in such a way that they have the format of a single one-dimensional vector.

Figure 1a shows how the slant range may vary for successive azimuth samples of a radar image pixel. This is the succession of "fishbone" data traces that cannot be stored in any single slant-range bin due to the range migration effect. Figure 1b is the idealized constant-slant-range azimuth pixel data for a single range bin. Note that adjacent azimuth samples are at a constant-slant-range value.

(continued on next page)

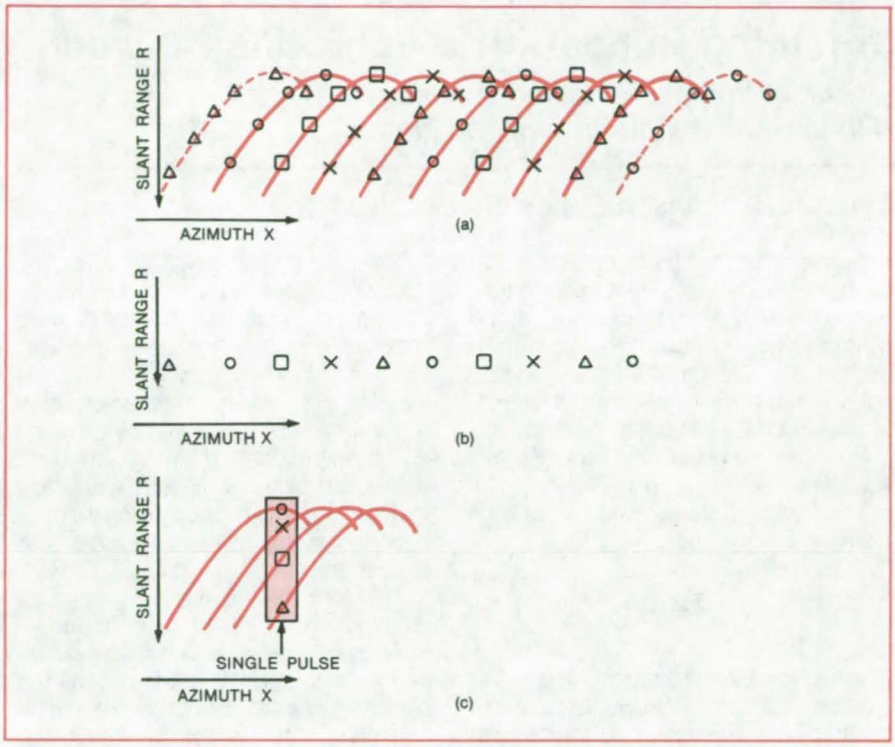

Figure 1. **Synthetic-Aperture-Radar Data** for a single range value are shown in their natural format as they migrate through different range bins in (a) and in the ideal desired format in (b). The coherent combination of range-correlated echoes from a single pulse is shown in (c).

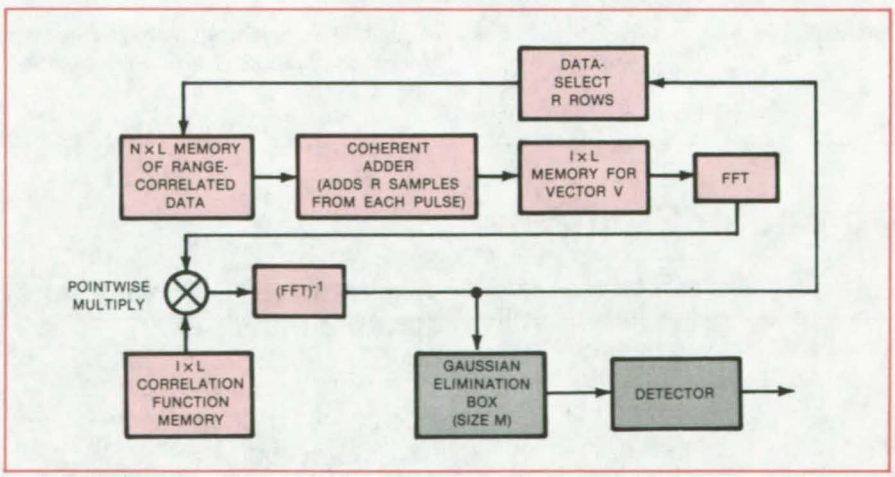

Figure 2. The **SAR "Steamroller" Algorithm** can be implemented in either hardware or software. Range-correlated SAR data are recorded in a two-dimensional N × L memory. The data-select circuit picks out R rows of data within one column, and the first R entries are coherently added. This procedure is performed for every entry in the memory. Next, a fast Fourier transform (FFT) is used, after which the output vector is multiplied pointwise with a transform of a normal correlation function. An inverse FFT is then performed. To eliminate smearing of range bin limits, a Gaussian elimination function is connected to the output of the inverse FFT.

Figure 1c illustrates the new method of coherently combining the values of the ambiguous data by coherent addition of values concurrent with an enabling pulse (K). All points in the vertical rectangle are to be coherently added and placed in position K of a single, flat colinear combination of the respective fishbones. The resulting azimuth vector may then be subjected to any desired form of fast-transform convolution. Figure 2 is a block diagram of the new procedure.

This work was done by Alan E. Di Cenzo of Caltech for **NASA's Jet Propulsion Laboratory.** *For further information, Circle 208 on the TSP Request Card.*
NPO-15316

Obtaining Runge-Kutta Solutions Between Time Steps

A new interpolation method is used with existing Runge-Kutta algorithms.

Lyndon B. Johnson Space Center, Houston, Texas

Scaled interpolation algorithms have been developed for use with third- through fifth-order Runge-Kutta algorithms. The interpolation algorithm evaluates a solution at an intermediate point within an integration step. Only a few additional computations are required to produce the intermediate solution data.

The Runge-Kutta method for solving the differential equation

$$dy/dt = f(y,t)$$

is a highly-efficient numerical approximation method. Although its calculations are more complicated than those of other methods for solving differential equations, fewer calculations are required. The Runge-Kutta method provides an accurate solution with larger time steps than are allowable in other methods.

The method can lose its advantages, however, if the time step has to be decreased to obtain solutions at more closely spaced times than are demanded purely by accuracy. In computer-aided process control, for example, controller settings sometimes may be needed more frequently than accuracy requires. In orbital calculations, time steps that are too large may occasionally miss important moments like the apogee and the perigee.

The form of the interpolating algorithm resembles that of the main Runge-Kutta algorithm with which it is used. The derivative of f(y,t) is evaluated at the same intermediate points as in the main algorithm, plus one or two additional points. The coefficients of the derivatives in the Runge-Kutta sum are calculated for the desired fractional portion, σh of the full time step h (where $0 \leqslant \sigma \leqslant 1$).

By making slight adjustments in the integration step sizes when necessary, any point within an integration interval can be made to coincide with a chosen σ and the coefficients taken from sets that have been precalculated for various prechosen σ values. If the required data-output point is not known in advance or if a dense output is required within a given step, the scaled algorithms may be used to formulate an interpolating polynomial for data determination or may be used with an iterative procedure to reach the required output point with only a minor loss of efficiency.

This work was done by M. Kathleen Horn of **Johnson Space Center.** *Further information may be found in NASA TM-58239 [N82-21967/NSP], "Sealed Runge-Kutta Algorithms for Treating the Problem of Dense Output" [$11.50]. A copy may be purchased [prepayment required] from the National Technical Information Service, Springfield, Virginia 22161.*
MSC-20404

Computer Programs

These programs may be obtained at very reasonable cost from COSMIC, a facility sponsored by NASA to make new programs available to the public. For information on program price, size, and availability, circle the reference letter on the COSMIC Request Card in this issue.

Algorithm for Constructing Contour Plots

Contours are constructed from a set of irregularly distributed points.

A general computer algorithm has been developed for the construction of contour plots. The modular algorithm can be modified for special applications.

The algorithm accepts as input data values at a set of points irregularly distributed over a plane. The algorithm is based on an interpolation scheme in which the points in the plane are connected by straight-line segments to form a set of triangles.

The data are smoothed using a least-squares fit to a bivariate polynomial. Interpolation along the edges of the triangles is performed to construct the contours, using the bivariable polynomial if data smoothing is performed. Once the contour points have been located, the contour is drawn.

This program is written in FORTRAN IV for batch execution and has been implemented on an IBM 360-series com-

puter with a central-memory requirement of approximately 100K of 8-bit bytes. The algorithm was developed in 1981.

This program was written by Wayne Johnson of **Ames Research Center** *and Fred Silva of Informatics, Inc. For further information, Circle F on the COSMIC Request Card.*
ARC-11441

Hidden-Line Computer Code

A new, efficient solution minimizes run time.

The requirement for computer-generated perspective projections of three-dimensional objects has escalated significantly in recent years. Drawings that show visible and hidden lines are relatively easy to generate. However, in most situations it is desirable to generate drawings from which the hidden lines have been "removed" so that the renderings have no ambiguities of perspective that could be misinterpreted by the viewer. Unfortunately, the task of generating such drawings represents a major computing effort using the commonly available algorithms.

A new solution to the hidden-line problem is incorporated into the Hidden-Line Computer Code. Historically, solutions to the hidden-line problem have had inherent limitations, among the most significant being that the computer execution time grows as the square of the number of elements. Most are also restricted by environmental limitations. The solution employed in this program does not assume any environmental limitations. Furthermore, it determines the visibility of an entire line segment just by choosing only a few points on that line, thus providing a basis for a rapid algorithm.

The new approach is based on a proved theorem, which provides a formal basis for assuring generality and rapid execution. The theorem does not directly address the nuisance of square-law growth. However, analysis of the algorithm shows that it tends to avoid the square-law growth, and rigorous testing has verified that the algorithm tends to enjoy almost linear growth.

Input to the Hidden-Line Computer Code consists of either line segments or planar polygons. The polygons can be n-sided, concave or convex, and can have concave or convex holes. The user also identifies the perspective from which the drawing is to be produced. The program currently generates plotted output for a CALCOMP plotting system but could be readily adapted to other plotting systems.

The program is written in FORTRAN IV for batch execution and has been implemented on a CDC 6000-series computer with a central-memory requirement of approximately 62K (octal) of 60-bit words. The code should be readily adaptable to any computer supporting FORTRAN IV and any X-Y graphics system. The program was developed in 1982.

This program was written by David R. Hedgley, Jr., of Dryden Flight Research Facility for **Ames Research Center.** *For further information, Circle G on the COSMIC Request Card.*
ARC-11446

MiniBriefs describe NASA innovations and reports in an abbreviated format. Readers desiring additional information on these items should request the Technical Support Packages (TSP's), available in most cases, which can be obtained by using the TSP Request Card at the back of this issue.

Flow Chart for Management

Planner's attention is focused on the full requirements for each stage of a project.

A flow chart management tool presents organizational/staffing relationships, resource requirements and time-dependent product-activity relationships on a single chart. The flow chart focuses a planner's attention on the full requirements for each stage of a project and presents visual reminders that every element must be considered together with the interrelationships within each stage and the interface between stages.

The flow chart uses four basic symbols to define a specific task, or stage, of a project. A brief description of the activity to be performed is placed in the upper box. The product of this stage is designated in the box below, and usually represents the output of that activity; when it would aid in planning, the box can be divided in half to include input and output descriptions. The third box down designates the people involved by listing the organizational responsibility or names or titles of staff. The bottom box lists tools or resources. To avoid visual overload, annotations are presented on a separate sheet, keyed to each stage by symbols.

This work was done by Kristine A. Blom of Caltech for **NASA's Jet Propulsion Laboratory.** *For further information, Circle 209 on the TSP Request Card.*
NPO-15014

Three-Level Control of Manipulators

Hierarchical control yields fast response.

A concept for control of remote manipulators is based on a three-level hierarchy that allows complex tasks to be performed in real time. The scheme was developed for interactive human/computer control with sensory feedback.

The hierarchical structure allows control data to be processed in parallel. It can thus quickly handle the immense amounts of data involved in sensory feedback (position of the end effector, its proximity to targets, and force and torque exerted by it).

At the lowest level in the hierarchy, simple actions and commands are executed (for example, "move a robot hand

(continued on next page)

one incremental step"). At the second level, composite actions and commands are handled ("shift the hand from A to B"). At the third and highest level, complex actions and commands are carried out ("bring the specified object").

This work was done by Robin L. Zawacki and Marko I. Vuskovic of Caltech for **NASA's Jet Propulsion Laboratory.** *For further information, Circle 210 on the TSP Request Card.*
NPO-15048

Control of Self-Replicating Systems

Three concepts are proposed for system management and control.

A proposed addition to a model for self-replicating systems includes concepts for three hierarchical levels of management and control. The concepts are: (1) an internal system for autonomous management and control, (2) a separate system for environment monitoring, and (3) an optional intelligent system that would be required in especially chaotic environments.

The autonomous system manages and controls all internal systems by comparing them with a programed global model. The external system responds to external situations and events through stored programs to maintain the functions of the system in a changing environment. The intelligent system responds by making decisions and solving problems in novel situations that cannot be preprogramed.

This work was done by Georg von Tiesenhausen of **Marshall Space Flight Center.** *For further information, Circle 211 on the TSP Request Card.*
MFS-25865

Training Simulator for Fire Management

Users manipulate resources in practicing fire-control strategy.

Management of people and equipment at a fire can be practiced on a simulator that consists of readily-available hardware and NASA-developed software. Users (generally fireground commanders) manipulate resource information that is displayed on two separate monitors, as computer-generated messages and computer-controlled fire scenes. The "decision tree" used to write the software is available as part of the Technical Support Package for this article, although a program listing is not.

Three modules comprise the simulator software. The introduction module sets the scene and informs the user of the main areas of concern: search and rescue, property conservation, resource utilization, and communications. The main-program module displays a menu of several choices offered to the user. Only when the simulator reaches a protected or out-of-control situation is the end-logic module activated to present the user with the results of the decisions made during the main program.

This work was done by Kenneth A. Smith, Ricardo C. Rodriguez, Joseph L. Randolph, and Richard T. Howard of **Marshall Space Flight Center.** *For further information, Circle 212 on the TSP Request Card.*
MFS-25898

Generating Random Number Pairs

An algorithm generates pairs drawn from a bivariate normal distribution.

An algorithm generates random numbers drawn from a bivariate normal distribution with any desired values of the two means, two standard deviations, and correlation coefficient. A sequence of pairs of random numbers uniformly distributed between 0 and 1 are transformed by scale-factor multiplications and rotations to obtain a sequence of random number pairs that are bivariate normally distributed. The only accuracy limitations are in the quality of the input sequence of uniformly-distributed random numbers and in the ability of a computer to perform exact calculations. The algorithm is a special case of a general method for generating sequences of random n-vectors drawn from a multivariate normal distribution with any desired covariance matrix.

This work was done by C. Warren Campbell of **Marshall Space Flight Center.** *For further information, Circle 213 on the TSP Request Card.*
MFS-27039

SUBJECT INDEX

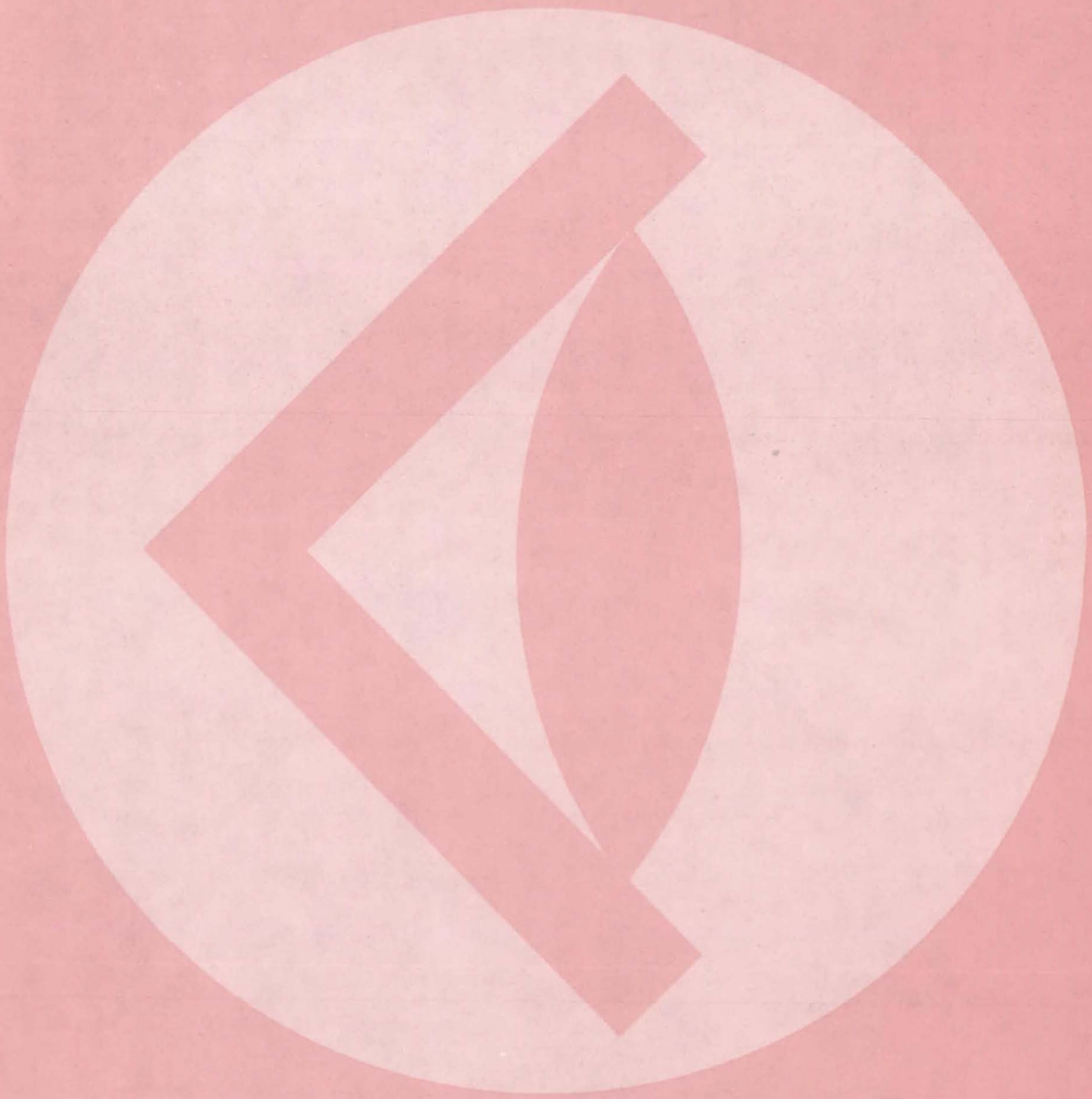

National Aeronautics and
Space Administration

Washington, D.C.
20546

THIRD-CLASS BULK

25th Anniversary
1958-1983

NASA

Gas tanks at a New Jersey powerplant are filled with hydrogen from an onsite electrolysis system that evolved from NASA fuel-cell technology. Filling from the onsite system is considerably more efficient than filling from supplies delivered by tube trailer. [*See the bottom of page A1.*]